PhD Thesis

Recursive Vesicle Reproduction System Coupled with Enzymatic Cascade Reactions: Toward Synthetic Minimal Cell

（酵素カスケード反応と連携した再帰的なベシクルの自己生産システム：
人工ミニマルセルに向けて）

Minoru Kurisu

Department of Physics
Graduate School of Science
Tohoku University

2021
(令和 3 年)

-Design of Synthetic Minimal Cell-

"Rather than trying to define life precisely,
biologists concentrate on deepening their understanding of life by studying living things."

————"Life," the *World Book Encyclopedia*

"What I cannot create, I do not understand."

————————Richard P. Feynman

Chapter 1

Introduction

1.1 Living System

Although life sciences have not reached a consensus of the definition of “living” state, living systems are often characterized by three major components; gene, metabolism, and reproduction [Alberts et al. 2015]. Living systems have information polymers such as DNA to encode amino acid sequences, i.e., proteins, to catalyse metabolic reactions in the cell. The metabolism system is the very complex chemical reaction network inside a cell, which synthesize the components of the system based on the genetic information and sustain the system in a steady state by incorporating energy and ingredients from the environment and by excreting the waste from the system. By using gene and metabolism, living systems show reproduction that is recursive growth and division cycles of the system. Regardless of the extraordinary diversity of living things, any living systems we know work with the above principles.

Recent molecular biology is revealing the essential molecular pathways to realize such behaviors of living systems. For example, to reveal the minimal biological set, there have been investigations to extract essential genes maintaining the living system [Koonin 2000; Xu et al. 2011; Hutchison et al. 2016; Breuer et al. 2019]. Focusing on the investigations by Xu et al., they defined an essential gene as whether loss of the gene is lethal or not, and they identified approximately 250 essential genes for one of the simplest known bacteria, *Streptococcus sanguinis* [Xu et al. 2011]. The identified essential genes are associated with only three basic categories of biological functions (**Figs.1-1-1(a) and (b)**). First one is “energy currency production domain”, which involves the synthesis of energy currency molecules such as ATP by using glucose taken in from the environment (grey **Fig.1-1-1(a)** or orange region **Fig.1-1-1(b)**). Second one is “processing of genetic information domain”, which replicates DNA (the polymer encoding genetic information) and synthesizes proteins (the functional molecules in biological systems) via RNA (green region). Third one is “maintenance of the cell membrane domain”, in which proteins catalyze the synthesis of membrane molecules from byproducts of the energy currency production domain by using energy currency molecules (blue region). Finally, membrane molecules are incorporated into the cell membrane, resulting in the membrane growth and cell division. This is how the whole cellular systems realize reproduction.

Living systems are unique molecular systems which differ from ordinary condensed

matter physics systems in many aspects. From the viewpoint of physical science, living systems are composed of the molecular assembly called “soft matter”, such as biopolymers (DNA, RNA, and protein) and biomembranes. Concerning to each component of living system, their underlying physics is becoming clearer such as seen in DNA conformation [Manghi & Destainville 2016; Wang et al. 2017], protein folding [Praprotnik et al. 2008; Zuckerman 2010], and membrane deformation [Israelachvili 2011; Lipowski 2020]. However, there is still a huge gap of complexity between today’s soft matter physics studies and living systems. Therefore, one can say that one of the ultimate goals of (soft matter) physics is to overcome the gap and to understand the physical basis bridging non-living and living forms of matter.

Figure 1-1-1. Essential pathways inside a cell.

(a) Deduced essential pathways based on the analysis of the essential genes of the bacterium *S. sanguinis*. The pathways are associated with three domains indicated by different colors as follows; energy currency production domain (grey), processing of genetic information domain (green), and maintenance of the cell membrane domain (blue). Reprinted with permission from Xu, P. et al. *Sci. Rep.* **1**, 125 (2011) © 2011 Springer Nature.

(b) Further simplified scheme representing essential pathways in (a), which focus only on the selected biological components. The colored regions represent energy currency production domain (red), processing of genetic information domain (green), and maintenance of the cell membrane domain (blue).

a

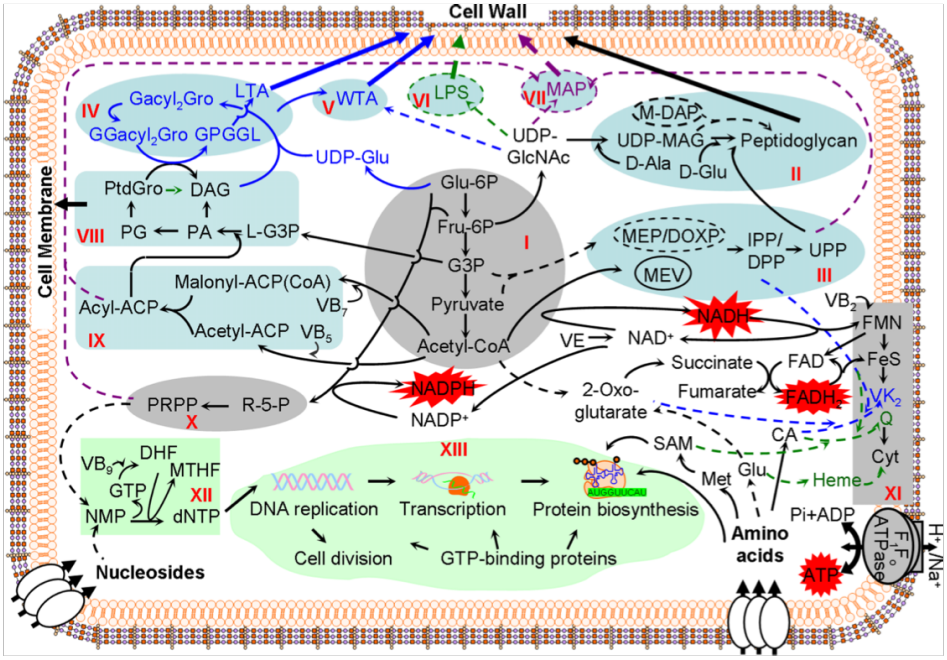
Cell Wall
Cell Membrane
Gacyl2Gro
GGacyl2Gro GPGGL
LTA
WTA
LPS
MAP
UDP-Glu
UDP-GlcNAc
M-DAP
UDP-MAG
D-Ala
D-Glu
Peptidoglycan
PtdGro
DAG
PG
PA
L-G3P
Glu-6P
Fru-6P
G3P
Pyruvate
Acetyl-CoA
MEP/DOXP
IPP/DPP
UPP
MEV
Malonyl-ACP(CoA)
Acyl-ACP
Acetyl-ACP
VB7
VB5
NADH
NAD+
VE
VB2
FMN
FAD
FeS
Succinate
Fumarate
FADH2
VK2
Q
Cyt
2-Oxo-glutarate
NADPH
NADP+
PRPP
R-5-P
SAM
CA
Met
Glu
Heme
VB9
DHF
MTHF
GTP
NMP
dNTP
DNA replication
Transcription
Protein biosynthesis
Cell division
GTP-binding proteins
Amino acids
Pi+ADP
ATP
Nucleosides
H+/Na+

b

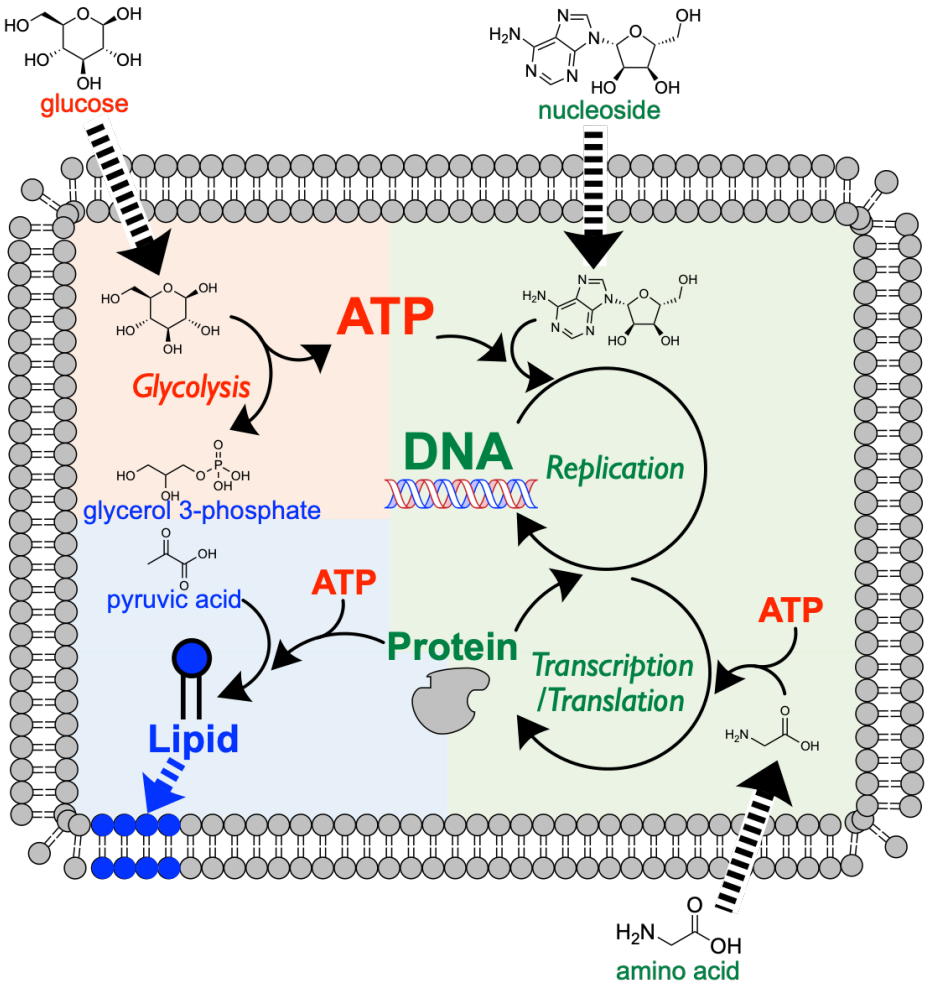
glucose
nucleoside
ATP
Glycolysis
glycerol 3-phosphate
pyruvic acid
DNA
Replication
Protein
Transcription
/Translation
Lipid
amino acid

1.2 Protocell / Minimal Cell

1.2.1 Introduction to Protocell and Minimal Cell

Based on the understanding of living systems from recent molecular biology studies, one of the promising approaches to understand origins of living systems is actually constructing the simplest forms of cell-like system [Szostak et al. 2001], called “protocell” or “minimal cell”. They are the concepts of the intermediate system bridging non-living soft matter assembly and complex living system as the model living system (**Fig.1-2-1**). Although there are various terminologies in this field, I use the term “protocell” for the prebiotic ancestor of living things which can evolve to the today’s biological systems on the earth. On the other hand, I use the term “minimal cell” for the literally the simplest form of living systems regardless of whether such systems may actually exist in the prebiotic era or not. According to the overview of living system (**Fig.1-1-1**), with the extreme simplification, one can say that living system is the sustainable and autonomous system that synthesizes information polymer and membrane (compartment) for the reproduction of the system. Then, the key for the construction of protocell and minimal cell system should lie in (i) origins or designs of information polymer of the system, (ii) construction of metabolic network to replicate information polymer and synthesize membrane molecules, and (iii) recursive growth and division of membrane compartments. When we could develop such non-equilibrium chemical compartment systems that show reproduction coupled with above three properties, one might call them “living” systems. However, despite various theoretical and experimental trials, such simplest living systems have not been achieved (yet). In this section, I will review the previous works on the origins of living systems in the context of protocell / minimal cell.

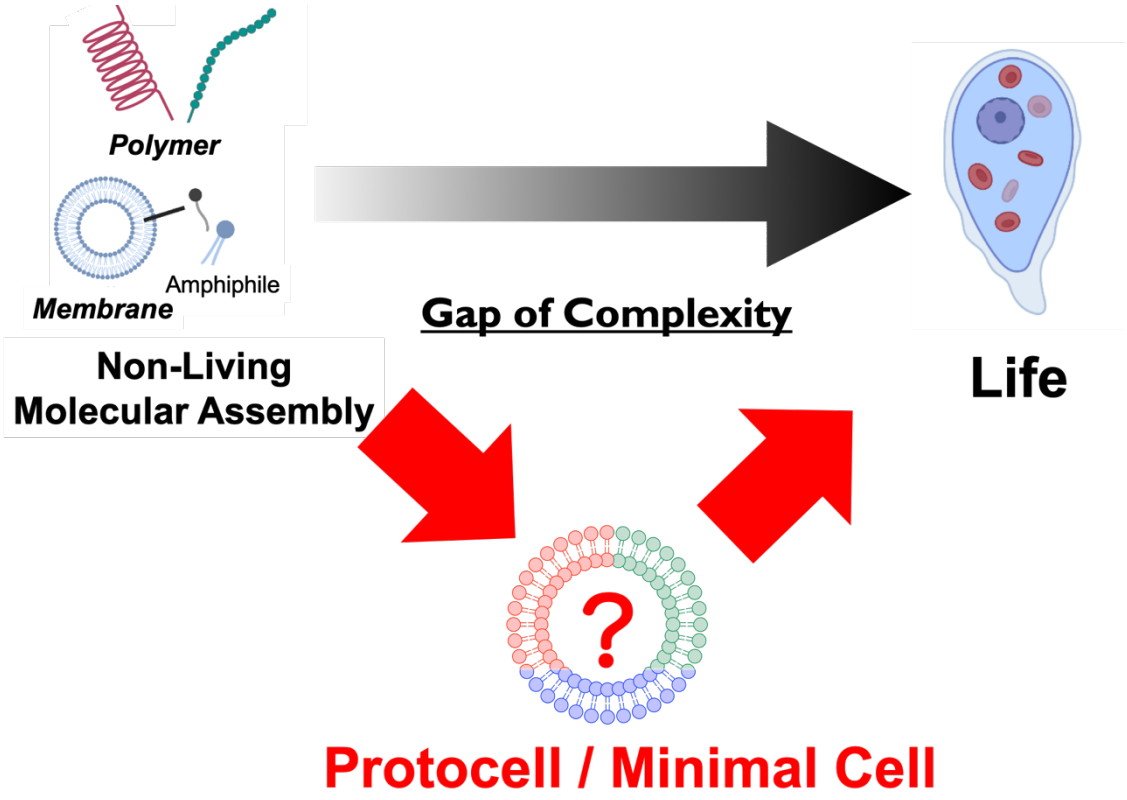

Figure 1-2-1. Schematic explanation of the concept of protocell and minimal cell. To understand what bridges non-living molecular assemblies and complex living systems, one of the promising approaches is to work on the simplest cellular systems.

1.2.2 Ganti's Chemoton

"Chemoton" (short for *"chemical automaton"*) proposed by Gánti (**Fig.1-2-2**) is one of the pioneering models in the approaches to extract the essence of living systems [Gánti 1975 & 2003]. This model considers the simplest form of a cell, in which three autocatalytic cycles are integrated inside a membrane closure: a metabolic cycle, a genetic cycle, and a membrane cycle [Griesemer 2015; Bich & Green 2018; Tanaka 2002]. Here, ingredients (X_A) taken in from the environment are converted into membrane precursor molecules (T') through intermediates (A_i) in the metabolic cycle ("*metabolism*"), and waste molecules (Y) are excreted. In the genetic cycle ("*information*"), the genetic polymer (pV_n) is template-replicated, and simultaneously, the membrane precursor molecule (R) is synthesized from the product (V') of the metabolic cycle. In the membrane cycle ("*structural closure*"), the membrane molecule T is synthesized from T' and R, which is then supplied to the membrane to realize the reproduction of the system. Please note that the catalytic relationship inside the system is not shown in the scheme. The overview of the essential pathways of the living system in **Fig.1-1-1(b)** is conceptually reproduced in this model, which tried extracting the essence of living systems by eliminating the specificities of biological molecules.

We should note some requirements for the formation of reaction networks such as shown in **Fig.1-2-2**. First, reaction products must have mutual catalytic relationships (requirements for "autocatalytic sets") and the reaction paths must have been connected to close the reaction network (*i.e.*, "percolation transition") [Kauffman 1986 & 1993]. In particular, the evolution of such reaction networks is called as "reflexively autocatalytic food-generated networks (RAFs)" in which each reaction is catalyzed by a molecule within the network, and each molecule is produced from a set of food sources [Hordijk & Steel 2004; Xavier et al. 2020]. Second, from the viewpoint of experimental construction, chemoton is difficult to be constructed as it is since there is no consideration on trans-membrane molecular traffic (*i.e.*, transport protein, endocytosis and exocytosis). The continuous inflow and outflow of molecules which keeps the system non-equilibrium inside closure is one of the biggest difficulties for the construction of protocell / minimal cell system.

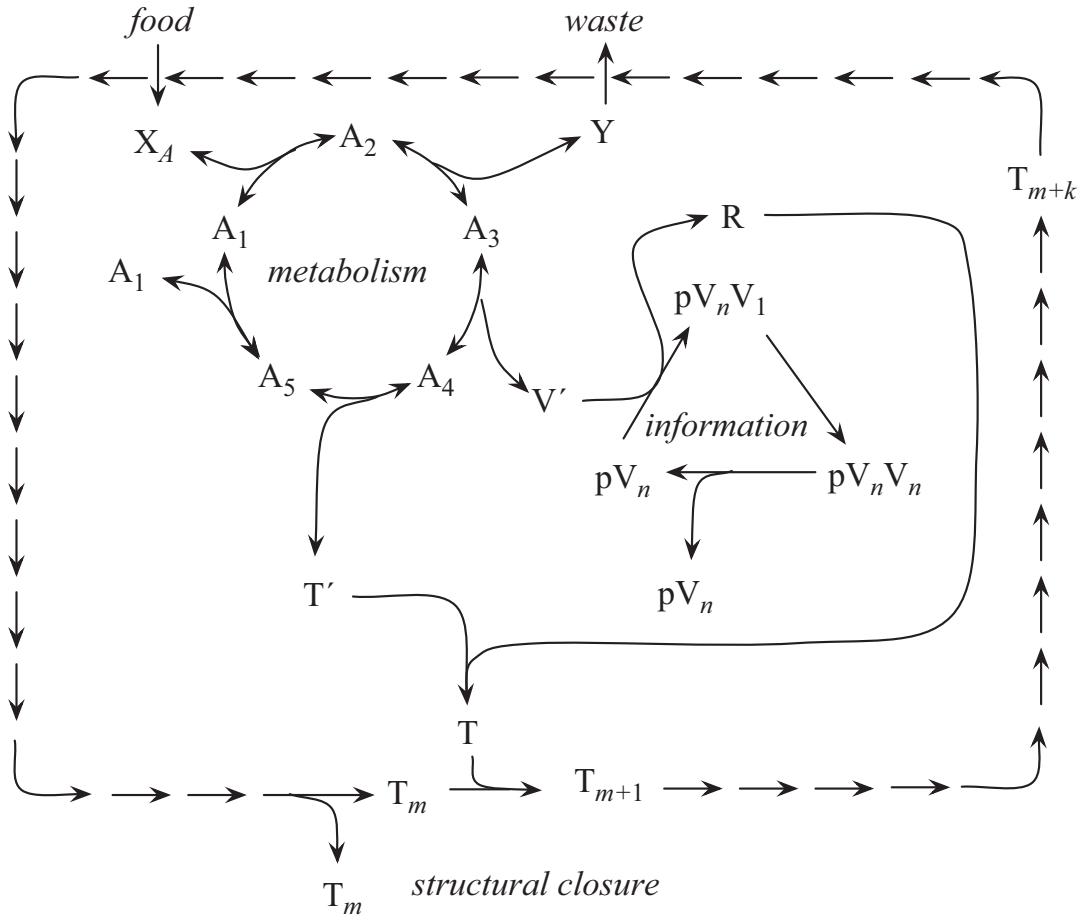

Figure 1-2-2. Chemoton proposed by Gánti [Gánti 1975 & 2003]. All arrows represent chemical reactions (material causation), reversible in the case of double-headed arrows, otherwise irreversible. The catalytic activities of the system are not shown in this scheme. Reprinted with permission from Letelier, J. et al. *J. Theor. Biol.* **286**, 100-113 (2011) © 2011 Elsevier Ltd.

1.2.3 RNA World Hypothesis

In the biological approaches, RNA world hypothesis has been investigated as the mainstream of the origins of life research [Crick 1968; Gilbert 1986; Higgs & Lehman 2015]. This hypothesis suggests that a set of self-replicating RNAs have appeared as the starting point of biological system in the Hadean eon. In contemporary biological systems, genetic information (genotype), functions and structures (phenotype) are assigned to different biopolymers, DNA and proteins, respectively. When we consider the origins of such a system (central dogma), the information polymer DNA is difficult to be replicated without the help of catalytic activities of proteins. At the same time, functional molecules proteins cannot succeed their structural information to the next generations without DNA, *i.e.,* there is a chicken-or-egg problem. However, concerning to the potentials as the first prebiotic systems, nucleic acids can form the complementary base pairing between the strands having equivalent sequence information, which has the potential of heredity and evolution. In contrast, even though proteins with 20 amino acids sequence can perform various functions, proteins lack a replication mechanism equivalent to the complementary paring of nucleic acids, which is the limitation of proteins [Neveu et al. 2013; Higgs & Lehman 2015; Tanaka 2002]. RNA is nucleic acid which can work as information polymer to keep sequence information of DNA and can bridges the translation process from DNA to proteins. Coupled with the experimental finding that a specific RNA also functions as an enzyme (ribozyme) [Kruger et al. 1982], that a specific RNA can catalyze RNA polymerization [Johnston et al. 2001], and that a specific set of RNAs can catalyze each other's replication [Lincoln & Joyce 2009], self-replicating RNA sets have been considered as the origins of today's biological systems on the primitive earth (RNA world hypothesis).

Various reaction schemes have been proposed for the prebiotic synthesis of nucleobases, nucleotides, and RNA from ingredients existed in the Hadean eon [Pressman et al. 2015; Patel et al. 2015; Joyce & Szostak 2018; Becker et al. 2019; Kim et al. 2020 & 2021]. In addition, the requirements to enable such reaction conditions and the possible mechanisms for primitive RNAs to evolve have been discussed from many aspects as follows: the "concentration problem" for precursors to react [Zubey 2000; Braun & Libchaber 2002], the possible places on the primitive Earth (such as mineral and ice surfaces [Wächtershäuser 1988; Ferris 2002; Attwater et al. 2013] and hydrothermal vents [Martin et al. 2008; Baaske et al. 2007; Kreysing et al. 2015]), the "error catastrophe problem" that prevents replication error [Eigen & Schuster 1977, 1978(a)(b) & 2012; Toyabe & Braun 2019], the evolution of RNA based on the fittest landscape concept [De

Visser & Krug 2014] from theoretical [Kauffman & Levin 1987; Kauffman & Weinberger 1989] and experimental point of view [Athavale et al. 2014; Pressman et al. 2019]. The future challenge of RNA world hypothesis is to link the chemical requirements to synthesize RNA in the prebiotic conditions and physical requirements for RNA to act as information polymers that can evolve [Kim et al. 2020 & 2021].

1.2.3 Previous Works on Protocell / Minimal Cell

While RNA world hypothesis may shed light on how the first "biological molecules" appeared and evolved, the scenario for how the first "living system" could emerge on the earth is a mystery. At least, for the emergence of cellular structures, such hypothetical RNA replication systems should be coupled with membrane compartments. Focusing on primitive membrane compartments, one simple scenario for the possible coupling between prebiotic molecules and membrane compartments is as follows. Amino acids, peptides [van der Gulik et al. 2009; Parker et al. 2011; Rodriguez-Garcia et al. 2015; Pascal & Chen 2019], and primitive membrane molecules (fatty acids) [Allen & Ponnamperuma 1967; Mccollom et al. 1999; Rushdi & Simoneit 2001; Patel et al. 2015; Mißbach et al. 2018; Joshi et al. 2021] were synthesized in high temperature geochemical niches. Such primitive biomolecules coexisted in the primordial soup, and the primitive membrane molecules self-assembled to form aggregates, including vesicles [Walde 2006; Hanczyc & Monnard 2016]. With the help of amino acids and peptides in the primordial soup, the vesicles underwent growth and division by incorporating membrane molecules [Monnard & Deamer 2002; Chen & Walde 2010; Black et al. 2013; Black & Blosser 2016; Cornell et al. 2019]. This is the scenario currently supposed to explain the reproduction of membrane compartments in the primordial soup. However, when we consider the role of RNA molecules in this scenario, it is still difficult to understand how RNA and catalytic proteins were linked in metabolic reaction systems to promote the membrane molecule synthesis. Although the evolution of RNA from ribozymes that catalyzes RNA replications [Johnston et al. 2001; Lincoln & Joyce 2009] to ribozymes that also work as enzymes for membrane molecules seems a plausible answer, the synthesis of membrane molecules is realized by sophisticated reaction pathways, which seems peptides and proteins made of 20 chemically different amino acids are more suitable than RNA molecules made of four chemically different bases. Therefore, following the RNA world hypothesis, ribozymes that catalyze tRNA aminoacylation [Lee

et al. 2000] and peptide synthesis [Sun et al. 2002] must have emerged at some stages to link RNA and proteins. Finally, such RNA-mediated protein synthesis system might have eventually developed to a metabolic network as shown in the chemoton model (**Fig.1-2-2**), whereby some proteins molecules would act as catalysts for the membrane molecule synthesis in the scheme [Hayden et al. 2008; Noller 2012; Bissette & Fletcher 2013; Lancet et al. 2018].

In the context of emergence of the first cell, Szostak, Bartel, and Luisi published the seminal paper "Synthesizing Life" at the very beginning of this century [Szostak et al. 2001]. They pointed out the importance of bottom-up construction of the simplest form of a cell to deepen our understanding on the essence and origins of living systems. They proposed a design of protocell consisting of RNA replicase (a ribozyme) as information polymer and vesicle (membrane closure) as compartment, and the replication of genetic polymer is encapsulated and linked to the vesicle reproduction system (**Fig.1-2-3**). Stimulated by this paper, various approaches attempting to synthesize a cell have been taken with the aim of making progress in understanding the origins of living systems, as summarized in the following reviews [Chen & Walde 2010; Stano & Luisi 2010; Stano et al. 2011; Noireaux et al. 2011; Walde et al. 2014; Blain & Szostak 2014; Pressman et al. 2015; Rasmussen et al. 2016; Deamer 2017; Schwille et al. 2018; Imai & Walde 2019; Ghosh et al. 2021; Gaut & Adamala 2021; Podolsky & Devaraj 2021].

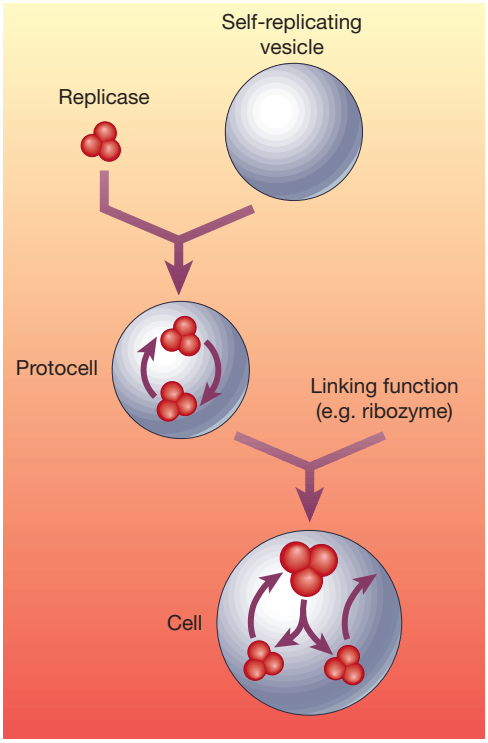

Figure 1-2-3. Outline of proposed pathway for the synthesis of protocell. Reprinted with permission from Szostak, J. W. et al. *Nature* **409**, 387-390 (2001) © 2001 Macmillan Magazines Ltd.

Growth of Vesicle Membrane.

In the following, I will briefly summarize the experimental studies aiming at the construction of protocell and minimal cell, especially the studies working on the realization of reproduction systems. In the approaches to reproduction system, the traditional approaches have been trying to equip the vesicles with various chemical mechanisms and nucleic acids which are required for vesicle reproductions. The one of the most popular approaches is the construction of vesicle membrane growth system, by the incorporation of existing membrane molecules or by the synthesis of new membrane molecules. The common strategy for the incorporation is to generate the flux of membrane molecules from the environment to vesicle membrane by using the chemical potential difference (see also section 2.4.2). In the case of fatty acids that are supposed first amphiphiles on the primitive earth [Deamer 1985; Monnard & Deamer 2002], the vesicle growth is triggered by the changes of the surrounding environment (such as pH) which modifies the degree of dissociation of their carboxyl group [Morigaki et al. 2003; Morigaki & Walde 2007]. For example, while p*K*a (acid dissociation constant) values of a free carboxylic acid monomer is typically 4 to 5 [Smith & Tanford 1973], the values of fatty acids located in vesicle membrane are apparently 7 to 9 due to the local proton condensation on anionic vesicle surfaces [Haines 1983]. In addition, fatty acids molecules change their preferable aggregation states according to the ratio of protonated and deprotonated molecules such as micelle with deprotonated molecules and vesicles with half deprotonated and half protonated molecules. Therefore, by adding fatty acid micelles in high pH solution toward the fatty acid vesicle suspension with a pH around p*K*a (~7-9), pH drop of the supplied micelles solution induces a flux of fatty acid molecules to the vesicle membrane, which results in the vesicle membrane growth [Morigaki et al. 2003; Chen & Szostak 2004(a); Zhu & Szostak 2009]. The chemical potential of membrane molecules can be modified in a different way, for example, some additives which have the affinity with membrane molecules induce vesicle membrane growth. Hanczyc et al. reported that the clay mineral montmorillonite accelerated the uptake of fatty acid micelles into vesicle membrane when the clay particles were encapsulated or associated to fatty acid vesicles, which implies the importance of mineral particles in the emergence of protocell on the primitive Earth [Hanczyc et al. 2003]. Adamala & Szostak showed another example with fatty acid vesicles and dipeptides, in which the specific hydrophobic dipeptide promoted the incorporation of fatty acid micelles into fatty acid vesicles and succeeding vesicle growth when the dipeptide was embedded in vesicle membranes [Adamala & Szostak 2013].

In parallel with the attempts to vesicle growth by incorporation, researchers have also

worked on another major approach which synthesizes membrane molecules for vesicle growth. The first experimental demonstration used the hydrolysis of oleic anhydride for the growth of oleic acid vesicles [Walde et al. 1994; Wick et al. 1995]. Here the externally supplied oleic anhydride molecules was hydrolyzed to produce new oleic acid molecules, resulting in the membrane growth and division of oleic acid vesicles. We should also note a well-designed chemical system for the synthesis of membrane molecules *within* the vesicle constructed by Sugawara's group [Takakura et al. 2003 & 2004; Toyota 2008; Matsuo et al. 2019]. They formed the vesicles with artificially designed membrane molecules (V) (**Fig.1-2-4(a)**). The bola-amphiphile (V*) is a precursor molecule which contains two polar headgroups connected by a hydrophobic linker with an imine bond. Hydrolysis of this bond is catalyzed by the catalyst (C), which results in the formation of V and an electrolyte E. Therefore, when the precursors V* is supplied to the suspension of vesicles composed of V and C, V* is hydrolyzed within the vesicle membrane embedding C, and then newly formed V is incorporated into membrane and E is released to bulk solution. They observed the vesicle growth and division as shown in **Fig.1-2-4(b)**. This system uses catabolism type reaction (*i.e.,* decomposition of ingredients), however, the Devaraj's group recently developed various anabolism type systems (*i.e.,* synthesis from ingredients) that mimic the phospholipid synthesis process of contemporary cellular life, where phospholipids with two hydrophobic tails are synthesized by combining an acyl donor and lysophosphatidic acids (LPA) [Podolsky & Devaraj 2021; Vance & Devaraj 2021]. They first worked on the addition of the second hydrophobic tail to the single-tail phospholipids (**Fig.1-2-5(a)**) [Hardy et al. 2015]. In this system, the synthesis of copper catalyst within the vesicle membrane (A) and the synthesis of a phospholipid within the vesicle membrane (B) take place at the same time (C). As a result, the lipid synthesis caused the membrane growth of the pre-existing vesicles (D). They realized the vesicle growth *without* pre-existing vesicles (*i.e., de novo* vesicle formation) in the different system [Brea et al. 2014 & 2017; Liu et al. 2020], and furthermore, they showed a synthetic mimic of the actual phospholipid synthesis process inside biological systems (**Fig.1-2-5(b)**) [Bhattacharya et al. 2019]. The highly reactive intermediate doecanoyl-AMP (1) was synthesized by reacting dodecanoic acid (DDA) with ATP in the presence of the enzyme FadD10. Dodecanoyl-AMP (1) reacted with an amine-functionalized lysolipids (2) to form phospholipids (3), resulting in the vesicle membrane growth. Devaraj's group also succeeded in synthesizing phospholipids by using enzymes, fatty acyl CoA ligase (FACL) [Bhattacharya et al. 2021]. Such anabolism type membrane growth system was also reported by Toyota's group [Castro et al. 2019].

We do not look into the detail here, but researchers also have worked on the third

choice for membrane growth: the fusion of vesicles [Ivanov et al. 2019] from theoretical [(surface charge) Tatulian 1983; Morini et al. 2015; Chibowski & Szcześ 2016; (fusion process) Lipowsky et al. 2020; Jahn & Grubmüller 2002; Tamm et al. 2003; Shillcock & Lipowsky 2005; Grafmüller et al. 2009; (lipid reorder) Kuzmin et al. 2001] and experimental approaches [(cationic & anionic vesicles) Caschera et al. 2010; Sunami et al. 2010; Suzuki et al. 2012; Lira et al. 2019; (anchored DNA) Heuvingh et al. 2004; Dreher et al. 2021; (ligand mediated) Haluska et al. 2006; (tension induced) Tanaka et al. 2004; Ikari et al. 2015; Deshpande et al. 2019; Cordomí et al. 2008]. All in all, the designs of vesicle membrane growth mechanisms are highly challenging but the indispensable aspect of protocell / minimal cell since the fate of all reactions and components will depend on the future of their reaction field, *i.e.,* death or proliferation. For the other aspects of vesicle reproduction; deformation, division, and volume inflation of vesicles, see the introduction of chapter 5.

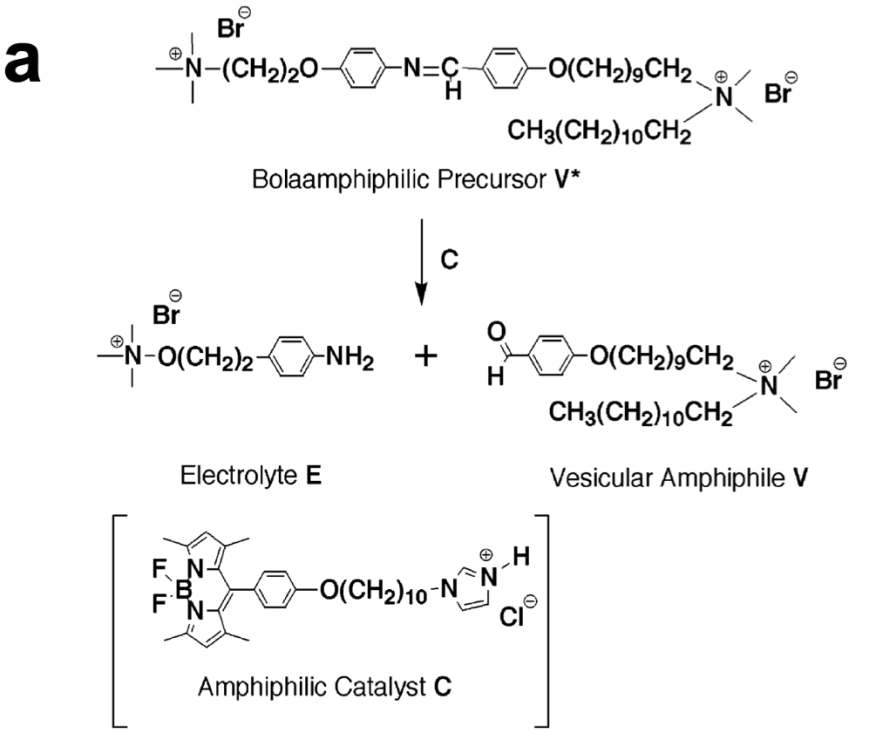

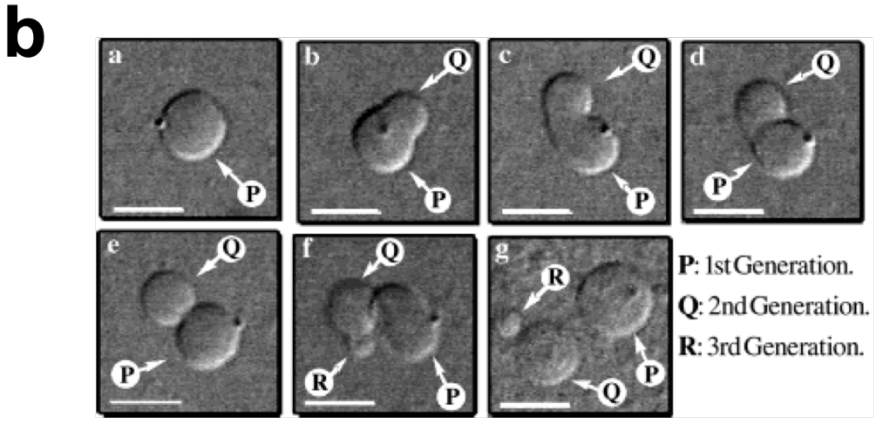

Figure 1-2-4. Vesicle growth system designed by Sugawara's group.
(**a**) Reaction scheme of the vesicle reproduction. The membrane molecule (V) and electrolyte (E) are formed by the hydrolysis of the membrane precursor (V*) by the catalyst (C) anchored within the vesicle membrane.
(**b**) Microscopy images of the morphological changes of the vesicles composed of V and C induced by the reaction in (**a**). (a – g) are obtained at different times after mixing the vesicle dispersion (V and C) and precursor solution (V*). Scale bar: 10 μm. Reprinted with permission from Takakura, K. et al. *Langmuir* **20**, 3832 - 3834 (2004) © 2004 American Chemical Society.

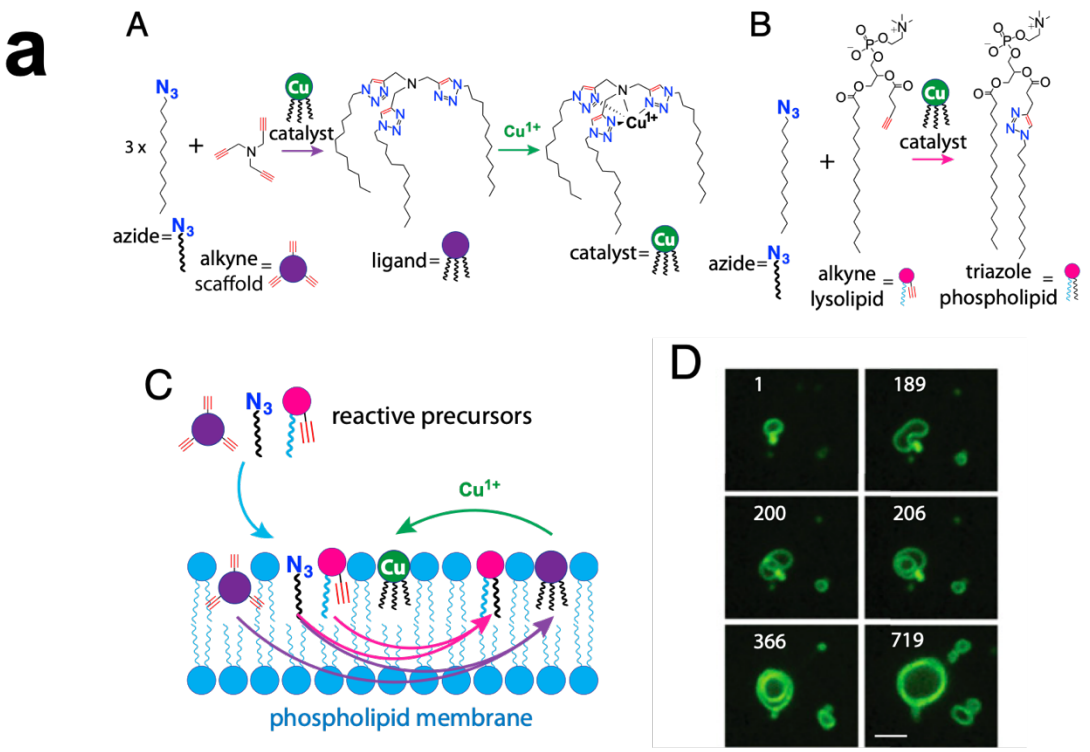
a
A
3 x
catalyst
Cu1+
azide=
alkyne =
scaffold
ligand=
catalyst=
B
azide=
catalyst
alkyne =
lysolipid
triazole
phospholipid =
C
reactive precursors
Cu1+
phospholipid membrane
D
1
189
200
206
366
719

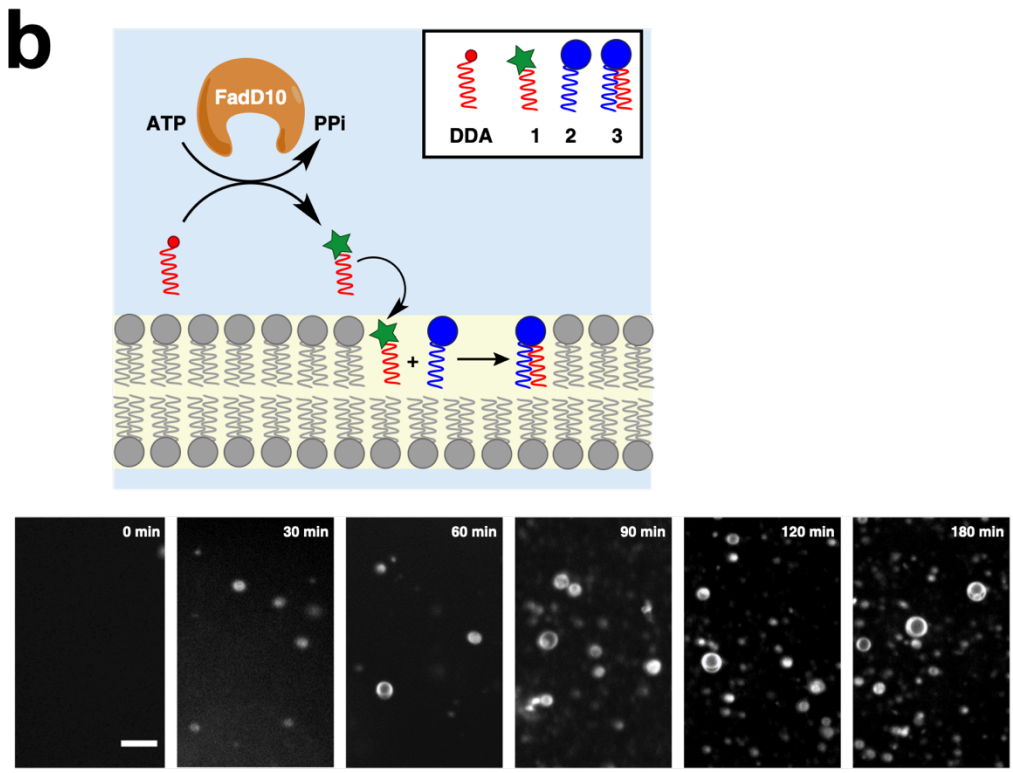
b
FadD10
ATP
PPi
DDA
1
2
3
0 min
30 min
60 min
90 min
120 min
180 min

Figure 1-2-5. Two vesicle growth systems designed by Devaraj's group.
(a) Phospholipids synthesis by the addition of a hydrophobic chain to a single-tail phospholipid coupled with self-reproducing catalyst. (A) The ligand tris-(lauryl triazole) amine (TLTA) was synthesized by combining a tripropargylamine scaffold (alkyne scaffold) with 1-azidododecane (azide). TLTA can bind Cu^{1+} ions to form a catalytic complex (catalyst). This copper complex catalyzes the synthesis of a new ligand from azide and alkyne scaffold, which, upon metalation, produces additional catalytic molecules. (B) The copper complex also catalyzes the formation of a triazole phospholipid from azide and an alkyne modified lysolipid. (C) Membrane-embedded catalysts act on azide and alkyne reactive precursors, synthesizing additional phospholipid and oligotriazole ligands. (D) Lipid synthesis-mediated growth results in an increase in membrane surface area and volume of multilamellar vesicles. Time scale: minutes, scale bar: 3 μm. Reprinted with permission from Hardy, M.D. et al. *PNAS* **112**, 8187-8192 (2014) © 2014 National Academy of Sciences.

(b) De novo formation of phospholipid membranes based on adenylate chemistry. (Upper) Scheme for a phospholipid synthesis pathway. First, reactive lipid precursors, dodecanoic acid (DDA), are converted to dodecanoyl-AMP (**1**) through enzyme FadD10, and then chemoselective reaction of (**1**) and amine-functionalized lysolipids (**2**) produces phospholipids (**3**). (Lower) Time series of confocal microscopy images of de novo phospholipid (**3**) vesicle formation which result from the incubation of an aqueous solution of DDA, (**2**), ATP, FadD10 at 37˚C. Scale bar: 10 mm. Reprinted from open access journal, Bhattacharya, A. et al. *Nature Commun.* **10**, 1-8 (2019).

Information Polymer of Vesicles.

The vesicle reproduction systems have been developed by various research groups, however, in order to actually construct protocell or minimal cell system as the simplest form of "living" system, the vesicle reproduction system must be loaded the information polymer. In this context, encapsulation of DNA or RNA replication system is not sufficient. Information polymers should encode the information for reproduction of the system and for replication of themselves, and then the information should be decoded to reproduce the system [Szostak et al. 2001; Noireaux et al. 2011; Neumann 1951]. In the case of any contemporary living systems we know, the synthesis of membrane molecules is catalyzed by functional molecules proteins (enzymes), and the information of all proteins (sequence information of amino acids) are encoded in the base sequence of DNA via RNA (*i.e.,* central dogma). Then, for the understanding of the key processes which enable the reproduction of protocell or minimal cell system, one plausible approach is to reconstruct a minimal reaction pathway from glucose to lipids (**Fig.1-1-1(b)**) by using proteins expressed by DNA in a vesicle. This approach was first attempted by synthesizing PC (phosphatidylcholine) lipids in PC vesicles with four enzymes of the salvage pathway for PC synthesis, G3P-AT (*sn*-glycerol-3-phosphate acyltransferase), LPA-AT (l-acyl-*sn*-glycerol-3-phosphate acyltransferase), PA-P (phosphatidate phosphatase), and CDPC-PT (cytidinediphosphocholine phosphocholinetransferase) [Schmidli et al. 1991]. After that, Kuruma et al. succeeded in synthesizing two of those enzymes, G3P-AT and LPA-AT, inside lipid vesicles [Kuruma et al. 2009] by using a totally reconstructed cell-free protein expression system (Protein synthesis Using Recombinant Elements, PURE) [Shimizu et al. 2001]. In the other several approaches, the vesicle growth was achieved by synthesizing various phospholipid within a vesicle from glycerol-3-phosohate (G3P) and acyl-CoA [Scott et al. 2016; Exterkate et al. 2018; Blanken et al. 2020] (**Fig.1-2-6(a)**). By using PURE system, the model plasmid, pGEMM7Δpsd, was expressed within giant vesicles to produce glycerol 3-phosphate acyltransferase (G3P-AT (=PlsB)), lysophosphatidic acid acyltransferase (LPA-AT (=PlsC)), cytidine diphosohatediacylglycerol synthase (CDsA), and phosphatidylserine synthase (PssA). Then, PssA catalyzed the formation of PS (phosphatidylserine) lipids from G3P and acyl-CoA. The PS lipids synthesized in the vesicle membrane bind to the green fluorescent dye in the external solution, then the accumulation of green fluorescence indicates the synthesis of DOPS lipids from oleoyl-CoA (**Fig.1-2-6(b)**) [Blanken et al. 2020]. Concerning to fatty acids system, although the formation of vesicles from the synthesized fatty acids are difficult, the reconstruction of a pathway which converts glucose to fatty acids *in vivo* was achieved for decanoic acid, lauric acid, myristic

acid, and palmitic acid by using 30 purified proteins expressed from *E. coli* DNA [Yu et al. 2011; Liu et al. 2017].

In other approaches, artificially designed non-natural vesicle reproduction systems were developed. The aim of this type of works does not lie in the simplification of present biological cells, but lies in the extraction of universal key features of any possible living systems by designing the simplest form of a cell which is only conceptually related to the biological ones. The main focus in this approach is to prepare vesicle reproduction systems of any type, where vesicle reproduction is coupled to an information polymer in a simple way. Sugawara's group performed the pioneering works in this field [Kurihara et al. 2011]. The experimental setup such as vesicle compositions and precursors was the generally same as the one shown in **Fig.1-2-4**. The only difference was that the giant vesicles encapsulated DNA amplification system. Then, the vesicles again showed growth and division after the supply of precursor molecules of vesicle membrane, and the encapsulated DNA was amplified by the PCR technique (**Fig.1-2-7**). The amplified DNA was succeeded to be encapsulated in daughter vesicles, and in particular, the amplification of DNA was observed to accelerate the division of the giant vesicles. This means that replication of the encapsulated information polymer (DNA) was linked to the reproduction of the vesicles through an interplay between anionic DNA and the cationic vesicle membrane, which demonstrated the dependence of the vesicle division mode and the DNA length [Matsuo et al. 2019]. Although the DNA in this system did not encode the information for producing membrane molecules, this system was further developed to a recursive proliferation system, where the vesicles were fed with the ingredients by pH-induced vesicle fusion process, and then shifted to the reproduction and replication process [Kurihara et al. 2015].

I have briefly reviewed the history of previous protocell / minimal cell researches and picked up some milestone achievements. Please note that there was more or less the author's personal opinion, and I have just focused on the studies related to the construction of reproduction system. Except the aim of reproduction, researchers have worked on the containment of various biological molecules in vesicles and induced characteristic behaviors by using vesicles.

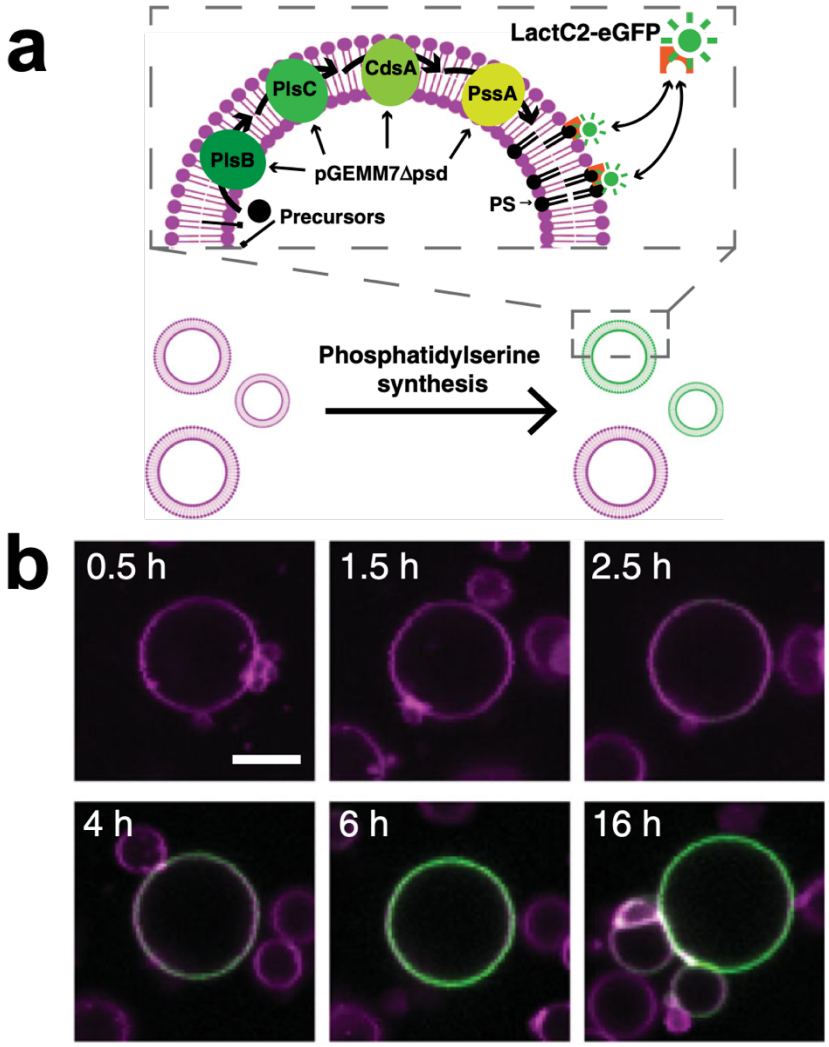

Figure 1-2-6. Membrane growth by genetically controlled phospholipid synthesis.
(**a**) Scheme of phosphatidylserine (PS) lipids synthesis from acyl-CoA and G3P coupled with gene expression. PS-producing enzymes (PlsB, PlsC, CdsA, and PssA) encoded in a synthetic minigenome (pGEMM7Δpsd) are cell-free expressed within giant unilamellar vesicles. The vesicles were prepared with DOPC, DOPE, DOPG, cardiolipid, DPPE-Texas Red, and DSPE-PEG-biotin. The PS in the membrane binds to the fluorescent reporter LactC2-eGFP, resulting in accumulated GFP signal in PS-enriched liposomes.
(**b**) Time-lapse confocal microscopy images of a giant vesicles exhibiting increasing LactC2-eGFP signal. Scale bar: 5 mm.
Reprinted from open access article, Blanken, D. et al., *Nature Commun.,***11**: 4317 (2020).

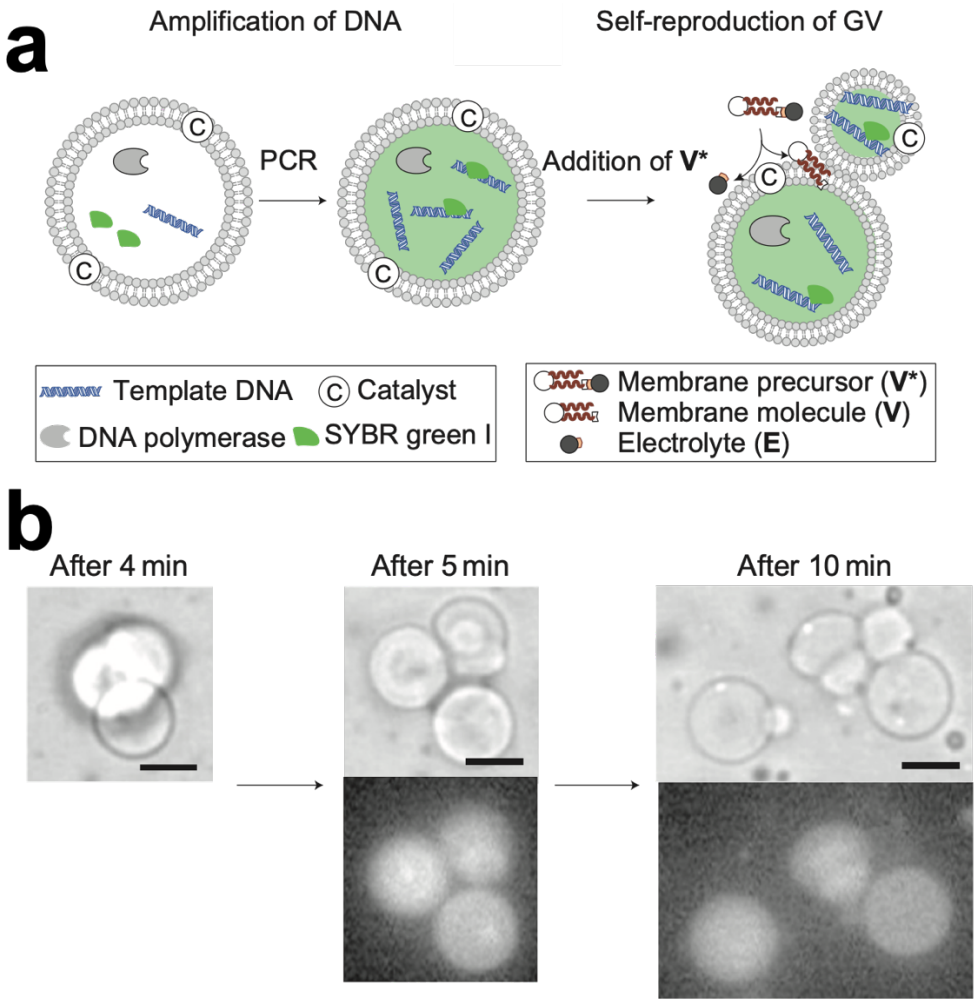

Figure 1-2-7. Vesicle reproduction coupled with DNA amplification.
(a) Scheme for the link between DNA amplification and self-reproduction of giant vesicles composed of the amphiphile V and its precursor V* (see also **Fig.1-2-4**). DNA is amplified within a vesicle containing PCR reagents (template DNA, primers, fluorescent tag SYBR Green I, deoxynucleoside triphosphates, DNA polymerase, and Mg^{2+}). Vesicle self-reproduction is induced by adding membrane precursor V*. Addition of V* produces membrane molecules (V) and electrolytes (E) through hydrolysis catalyzed by membrane-embedded catalyst (C). Adhesion of the amplified DNA to the inner leaflet accelerates vesicle growth and division.
(b) (top panels) Microscopy images of morphological changes of DNA-amplified vesicles after the addition of V*. (bottom panels) Partition of DNA was detected using fluorescence microscopy. Scale bars: 10 μm.
Reprinted with permission from Kurihara, K. et al., *Nature Chem.*,**3**, 775 - 781 (2011)
© 2011 Springer Nature.

1.3 Design of Minimal Cell in This Thesis

My biggest interest lies in the universal laws of physics and chemistry which allow the emergence of "living" system from non-living molecular assemblies. The biological systems driven by the central dogma as shown in **Fig.1-1-1** is the one particular solution to realize a living state, but it will be difficult to extract the universal laws on the any possible living states from them. Some of the biological principles might be universal to any possible living systems, on the other hand, some other biological principles might be just the requirements to use particular molecules in particular environments. Above all, the gap of complexity between simple soft matter assembly and complex living system hinders the approaches from physical sciences. One of the promising approaches for this is to explore possible simplest living systems based on the constructive approaches. However, to the best of my knowledge on the coupling between information polymer and vesicles, they have used biological information polymer, DNA, as we reviewed above. DNA is highly sophisticated information polymer that encodes varieties of functional polymer structures (proteins), at the same time, DNA requires us to load the complex expression mechanisms to the system. In the context of artificial cells and molecular robotics, such complex but well-organized molecular system will be welcomed. In contrast, when we consider the emergence of living systems and the simplest form of any possible living systems, the introduction of DNA as an information polymer might confuse us by unwanted particular biological requirements. Therefore, in this thesis, I do not use DNA as information polymer, and I will show my originally designed reproduction system consisting of artificial information polymer and vesicles. Based on the knowledge of soft matter physics and chemistry, the reproduction system is designed to conceptually mimic the key features of biological systems. I call the reproduction system as "synthetic minimal cell" in this thesis in order to distinguish it from conventional protocell and minimal cell design based on the biological mechanism.

Here I introduce the design of my synthetic minimal cell system (**Fig.1-3-1**). The synthetic minimal cell system artificially reproduces the three major characteristics of biological systems as I reviewed in section 1.1; (i) artificial information polymer which codes the information of the vesicle membrane, (ii) simple and artificial metabolism system which links the three essential reaction domains, and (iii) vesicle reproduction cycles that is the recursive membrane growth, deformation, division, and volume inflation.

The center scheme in **Fig.1-3-1** represents the artificial metabolism system of the synthetic minimal cell, where each symbol represents a reaction component, and bold arrows indicating inward represent the supply of ingredients close to the vesicle

composed of AOT molecules. The artificial metabolism system mimics the three essential reaction domains of biological systems (**Fig.1-1-1(b))** [Xu et al. 2011]: (i) energy currency production domain where the reaction trigger (H_2O_2, "Z") is produced by using the ingredients (D-glucose, "Ra", and dissolved O_2, "Rb") with the help of enzymes (GOD, "X"), (ii) information polymer synthesis domain where the monomers (aniline, "S") are enzymatically activated (aniline radical cation, "S*", and HRPC, "Y") and then polymerized by using reaction trigger (Z) to form the artificial information polymer (PANI-ES, "Pn") on the surface of template vesicle, and (iii) membrane growth domain where the supplied membrane molecules (AOT, "Am") are selectively incorporated into vesicle membrane through the specific interaction with the vesicle surface-bound information polymer (Pn). This artificial metabolism system is similar to the Ganti's chemoton (**Fig.1-3-1**), however, the reaction network is not contained within the vesicle but confined on the outer surface of vesicle membrane in order to circumvent the transmembrane traffic of ingredients and wastes. Then, the artificial metabolism system is conceptually autocatalytic (or mutually catalytic) since the vesicle surface provide the reaction field for the synthesis of information polymer, at the same time, the surface-bound information polymer selectively promotes the incorporation of membrane molecules, resulting in vesicle membrane growth.

The biggest originality of my synthetic minimal cell lies in the design of the artificial information polymer, which is synthesized by the template polymerization mechanism [Połowiński 2002] using vesicle membranes as templates. In polymerization reaction of aniline, outcome of the reaction products depends on vesicles. In the absence of any vesicles or in the presence of vesicles that do not work as templates, the activated monomers (aniline radical cations, "S*") are polymerized to form extensively branched random sequence polymer with various side products since the interactions between monomers and vesicles are not enough strong to restrict the polymerization process. In contrast, in the presence of template vesicles composed of the negatively charged and sulfonated/sulfated polar head group such as AOT vesicles, there are electrostatic interaction and hydrogen bonds between vesicles and monomers which are strong enough to restrict the polymerization process. Then, the presence of specific template vesicles results in the relevant formation of regioselective regular sequence product, polyaniline in its emeraldine salt form (PANI-ES). The PANI-ES is known as electroconductive polymer [Ćirić-Marjanović et al. 2017], then the formation of regular sequence polyaniline is confirmed by the presence of unpaired electrons (*i.e.*, polaron structures). Furthermore, when membrane molecules are supplied to the vesicles coupled with the PANI-ES synthesis, the PANI-ES on vesicle surface selectively promote the incorporation

of membrane molecules that can form template vesicles, resulting in the vesicle membrane growth. This relationship between polymers and vesicles is one of the simplest forms of *Genotype-to-Phenotype* relationship, even if not so sophisticated as biological one (central dogma). In my synthetic minimal cell system, the artificial information polymer does not encode the sequence for intermediate molecules such as RNA and proteins, but directly associates with the composition of the vesicle membrane. The polymer reflects the property of specific vesicles as its regular sequence ("encode"), and the regular sequence-rich polymer encourages the incorporation of complementary types of membrane molecules, resulting in vesicle membrane growth ("decode"). Therefore, the vesicle membrane growth is not just an enlargement of reaction field. There is actually the catalytic relationship between vesicles and polymer.

One of the most challenging aspects for the construction of protocell and minimal cell is the realization of "reproduction pathway" of vesicles (**Fig.1-3-1**) (*i.e.,* growth of vesicle membrane → deformation → division → volume inflation). Through the pathway, an initial mother minimal cell must be reproduced to the two daughter minimal cells with the identical surface area and volume to their mother. Concerning to the deformation mechanisms in the contemporary biological systems, especially for bacteria, a protein called FtsZ forms a ring-shaped assembly (Z-ring) at the division site, and then the contraction of the ring causes the bacterial cell division [Weiss 2004; Rowlett and Margolin 2015]. To mimic this molecular mechanism with vesicle membrane is possible approach, however, such protein-based division involving complex macromolecules are unfavorable for my "minimal" cell design. To simply attain the reproduction of the synthetic minimal cell, I applied the knowledge of biomembrane physics. The membrane elasticity theory predicts that the spontaneous deformation to the neck formation (called "limiting shape") is possible by introducing the second membrane component with inverse cone shape lipid (with small polar head and bulky tails) [Seifert 1997]. In addition, spontaneous division of the neck is possible by the coupling between lipid shape and Gaussian curvature of the vesicle membrane [Chen et al. 1997; Sakuma & Imai 2011; Jimbo et al. 2016]. When the minimal cell system (**Fig.1-3-1**) is constructed with the 100% AOT vesicles, the minimal cell does not show reproduction cycles but shows membrane growth to the tubular shape. However, when the inverse cone shape lipid cholesterol is introduced to the vesicle membrane based on the above prediction, the minimal cell spontaneously shows recursive deformation and division coupled with the membrane growth, where the deformation is well reproduced by the simulation. In addition, I designed the vesicle inflation system which gives continuous osmotic pressure to the vesicles. Finally, integrating all the mechanisms into the single system, I

constructed synthetic minimal cell system which conceptually reproduces the three characteristics of biological systems in an artificial design.

The advantage of the above synthetic minimal cell design is that whole system for the reproduction process is clear. In addition to the experimental realization of my design, I also developed the mathematical model to describe the kinetics of artificial metabolism system, which reproduces well the kinetics on the artificial information polymer synthesis and membrane growth. Although my synthetic minimal cell system remains some issues to be discussed in order to be called “living”, the challenges to such simple model living systems which is accessible from physical sciences will have the great potential to the universal understanding of “What is Life?”.

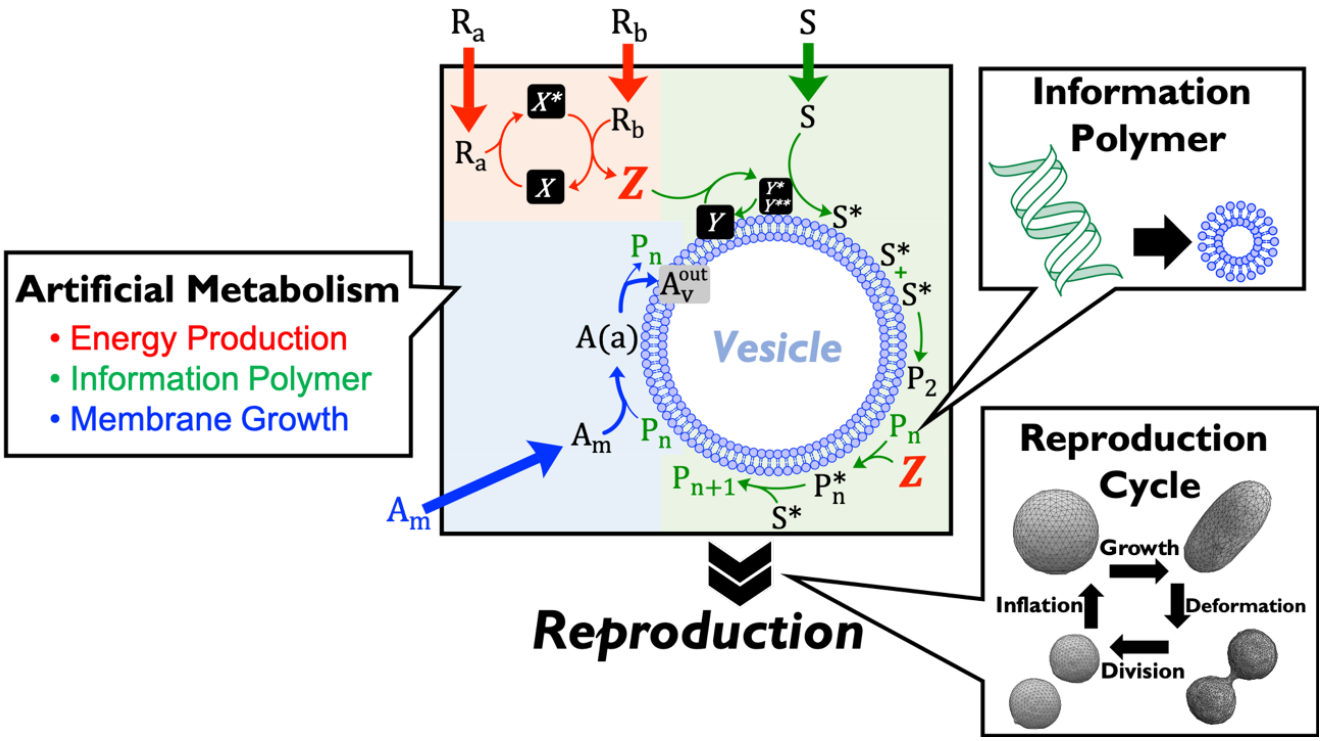

Figure 1-3-1. Design of my synthetic minimal cell system that conceptually reproduces three characteristics of biological systems (Information Polymer, Metabolism, and Reproduction) in an artificial way. Each symbol in the center scheme represents reaction component of the artificial metabolism system as follows: (energy currency production domain, Red) H_2O_2 (Z), D-glucose (Ra), dissolved O_2 (Rb), and enzyme GOD (X and X*); (information polymer synthesis domain, Green) aniline (S), aniline radical cation (S*), PANI-ES (Pn), PANI-ES with an activated site (Pn*), and enzyme HRPC (Y, Y*, and Y**); (membrane growth domain, Blue) free AOT molecule (Am), AOT molecule adsorbed to surface-localized PANI-ES (A(a)), and AOT molecule located in outer layer of AOT membrane (Av^{out}). The bold arrows indicating inward the rectangle represent supply of ingredients close to the vesicle. Please note that the reactions illustrated close to vesicle membrane are surface-confined reaction processes.

1.5 Outline of This Thesis

As an information polymer for protocell/minimal cell systems, most of the previous works have used biological information polymer, DNA. In chapter 2, I will first consider what is genetic information for living systems, and then explain my idea of simple and artificial information polymer. The artificial information polymer synthesized on vesicle surface roughly encodes the property of vesicles in its regular sequence, then selectively promote the incorporation of amphiphiles, resulting in vesicle membrane growth. In chapter 3, I will show my design of the artificial metabolism system which artificially mimics essential three reaction domains of biological systems, *i.e.*, energy production domain, information polymer synthesis domain, and membrane growth domain. The reaction network is constructed not inside but on the outer surface of vesicles to circumvent the difficulty in transmembrane molecular traffic. Chapter 4 focuses on the kinetic model of my artificial metabolism system, inspired by Ganti's chemoton. My synthetic minimal cell design has a concise and clear reaction network, therefore, whole the system is well-described. Through the kinetic model, I will confirm that the system is working well according to my design. In chapter 5, I will install the reproduction ability in the vesicle growth system based on the knowledge of membrane elasticity theory. The vesicle deformation pathway is controlled to show spontaneous neck formation and the neck destabilization, then I will demonstrate the recursive vesicle division. I also design the vesicle volume recovery system. Integrating all the processes into the single system, finally I will show my synthetic minimal cell, where the information polymer synthesis and membrane growth are linked via artificial metabolism system, and then the vesicle shows complete "reproduction cycle" (**Fig.1-3-1**). Chapter 6 concludes this thesis and discusses the insufficient points to be called "living" in my synthetic minimal cell system, and then I will emphasize the importance of constructive approach to the understanding of living systems.

Chapter 2

Artificial Information Polymer

2.1 Introduction

2.1.1 Central Dogma and Information Polymer

To extract the physical essence of information polymer, first we look into the biological information polymer, DNA. The genetic information of the living system is encoded as the regular sequence of the four bases, adenine (A), thymine (T), guanine (G) and cytosine (C) (**Fig.2-1-1(a)**). There are specific hydrogen bonds between each base pair, then only A and T or C and G can form base pairs. Therefore, when a new DNA chain is synthesized, the sequence of A, T, G, and C is determined according to the sequence of the template DNA chain. For example, in the case of **Fig.2-1-1(b)**, only T can be placed to the elongating chain out of four bases. To realize such a regular sequence precisely in a polymerization reaction, there should be a loss of thermodynamical entropy compared to random polymerization reaction. Here we consider Shannon entropy, the uncertainty of the sequence, at certain position (l) in the DNA sequence as follows:

$$H(l) = -\sum_{b} f_{b,l} \log_2 f_{b,l} \quad \text{(bits)} \tag{2.1}$$

where $f_{b,l}$ is the probability of four bases $b \in \{\mathrm{A}, \mathrm{T}, \mathrm{G}, \mathrm{C}\}$. Here the Shannon entropy becomes zero when the DNA sequence is completely selective, *e.g.*, $f_{A,l} = 1$ and $f_{T,l} = f_{G,l} = f_{C,l} = 0$. In the case of random sequence polymer chain, the Shannon entropy is given by:

$$H_r(l) = -\sum_{b} \frac{1}{4} \log_2 \frac{1}{4} = 2 \quad \text{(bits)} \tag{2.2}$$

where the possibility of four bases is $f_{b,l} = 1/4$. The information at the certain position (l) is the difference of the uncertainty between random and regular sequences as follows:

$$R(l) = H_r(l) - H(l) = 2 - H(l) \quad \text{(bits)} \tag{2.3}$$

When we sum up the entire position in the sequence length of *L*, the total information is given as follow:

$$R = \sum_{l=1}^{L} R(l) \quad \text{(bits)} \tag{2.4}$$

Here we assume that binding of individual bases with four possible states corresponds to the microstate of the system [Schneider 2010], then equate Shannon entropy (2.1) and thermodynamical entropy with:

$$S_{DNA} = k_B \, ln(2) \, H \tag{2.5}$$

Then, the changes in thermodynamical entropy of the regular sequence of DNA chain is given by:

$$\Delta S_{DNA} = -k_B \, ln(2) \, R \tag{2.6}$$

From the second law of thermodynamics expressed as the Clausius inequality, we obtain:

$$\Delta Q \leq T \Delta S \tag{2.7}$$

where T is temperature, and Q is heat. When the temperature and the pressure are constant, the heat transfer equals to the Gibbs free energy change in the binding process:

$$|\Delta Q| = |\Delta G| \geq |T \Delta S_{DNA}| \tag{2.8}$$

Here we have two important notices. First, synthesizing the regular sequence of information polymer results in the entropy loss. Second, when the temperature and the pressure is constant, such entropy loss should be covered by the further free energy gain. The required free energy is the cost of information, and in biological systems, such entropy loss for the information is covered by the enthalpy change from the binding energy of specific hydrogen bonds between the base pairs. For example, we can find such a relationship in the interaction between site-specific DNA binding protein (Fis protein) and its binding sites [Hengen et al. 1997]. We can estimate the thermodynamical entropy change as $\Delta S_{DNA} \sim -5.7 k_B$ from the uncertainty of the binding sites in the DNA sequence [Hengen et al. 1997]. In addition, the enthalpy change from binding energy is estimated as $\Delta H \sim -21 k_B T$ from the dissociation experiment [Tsai et al. 2016] or estimated as $\Delta H \sim -30 k_B T$ from the averaged binding energy [Stella et al. 2010] per one binding site involving 21 bases. The translational entropy change of the DNA binding protein is roughly estimated as $\Delta S_{trans} \sim -5 k_B$ from the binding site density compared to the genome size. Therefore, the thermodynamical entropy loss for the information ($|T \Delta S_{DNA}| = 5.7 k_B$) is confirmed to be covered by the further free energy gain in the binding process ($|\Delta G| = |\Delta H - T \Delta S_{trans}| = 16 k_B T$ or $25 k_B T$). Please note that we did not look into the rearrangement of water molecules here. This is the example of how biological systems treat information polymer obeying the second law of thermodynamics.

In biological systems, using specific hydrogen bonds, the genetic information is translated from the regular DNA sequence to another DNA sequence (using A, T, G, and C), from the DNA sequence to the RNA sequence (using A, C, G, and U (uracil) instead of T), and finally from the RNA sequence to the amino acid sequence of proteins (using twenty amino acids) (**Fig.2-1-2(a)**). This genetic information flow between the regular

sequence biopolymers is known as the central dogma of molecular biology. Afterwards proteins are folded into specific steric structures that can catalyze various chemical reactions in biological systems, and the reproduction of the compartment (cell membrane) is also catalyzed by proteins. Thus, genotype (genetic information) is translated into phenotype (function and structure), and the whole biological systems realize reproduction. Here, the biological information polymer (DNA) codes the structural information of proteins in the regular DNA sequence.

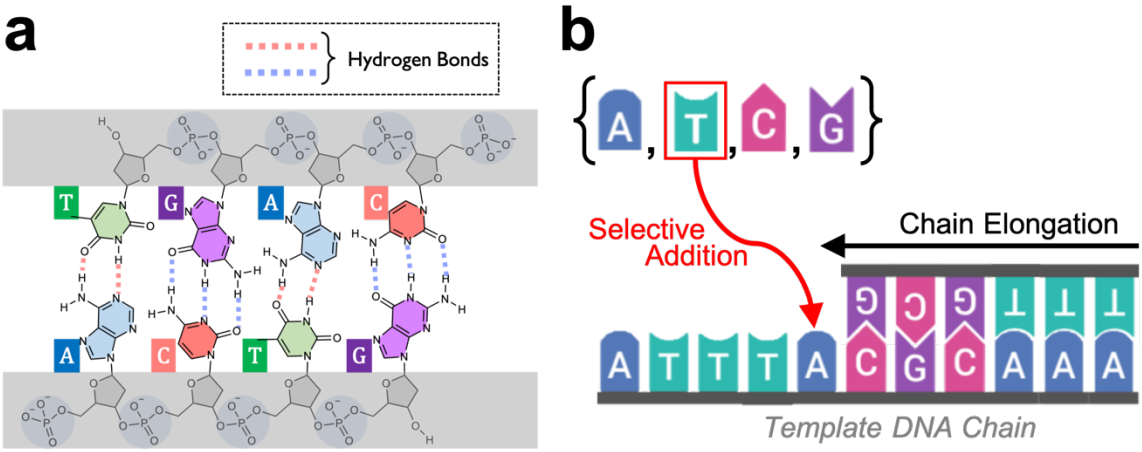

Figure 2-1-1. Chemical structure of DNA and its elongation mechanism [Alberts 2015].

(a) Chemical structure of DNA. Each base structure is colored as follows; blue: adenine (A), green: thymine (T), purple: guanine (G), and red: cytosine (C). The colored dotted lines represent specific hydrogen bonds between A and T (red) and G and C (blue). The structures colored in gray represent phosphate-deoxyribose backbones.

(b) Illustration on the elongation mechanism of a DNA chain. According to the regular sequence of the template DNA chain, the addition of bases to the elongating chain become selective.

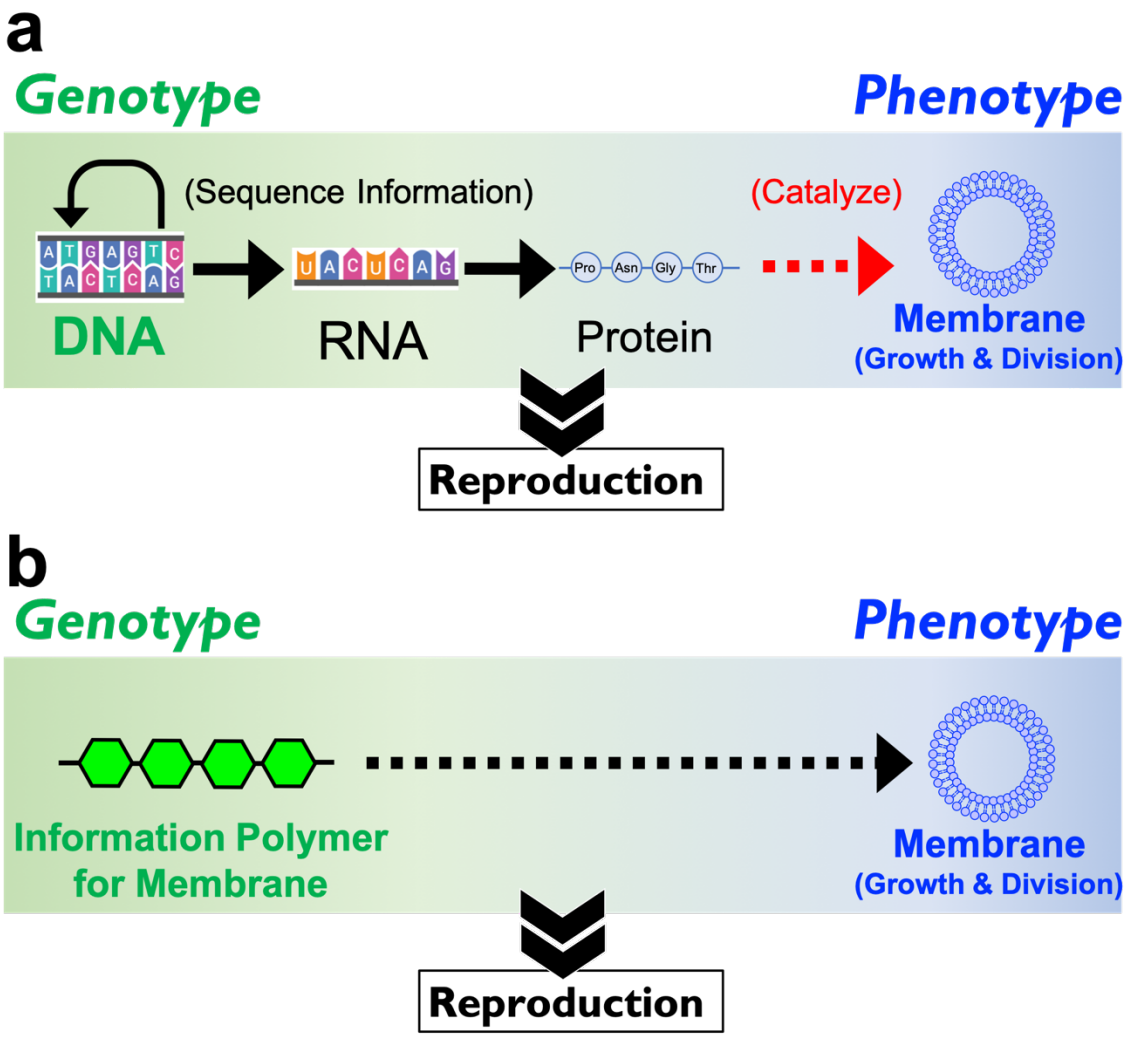

Figure 2-1-2. Genetic information flow from regular sequence of information polymer (Genotype) to the function and structures of the components in living systems (Phenotype).

(a) Central dogma of molecular biology. Biological information polymer, DNA, encodes the structures of proteins in its regular base sequence. Functional molecules in biological systems, proteins, catalyzes the reproduction of membranes.

(b) Design of artificial information polymer for synthetic minimal cell system. The information polymer encodes the properties of vesicle membrane and directly catalyzes membrane growth. For the simplification of the systems, the information polymer also plays the role of proteins (like ribozymes).

2.1.2 Concept of Artificial Information Polymer and Outline of This Chapter

When we consider to reconstruct a reproduction system in a minimal way, one of the promising approaches is to adopt the other artificial information polymer that directly realizes the reproduction of compartment (membrane growth). For the simplification of biological reproduction process, here the information polymer also plays the role of proteins like ribozymes. Thus, the artificial information polymer is not designed to code the sequences of functional molecules (proteins) but redesigned to directly code the structural information of its compartment (membrane) (**Fig.2-1-2(b)**). This is the concept of the artificial information polymer for my synthetic minimal cell system.

In this chapter, first, we will discuss which polymer can be the candidate for such an artificial information polymer for the vesicle membranes. Here we focus on the template polymerization reaction on vesicle surfaces. Second, we will experimentally confirm that the specific polymer can "encode" the property of vesicles as its regular sequence. Finally, we will construct the *genotype to phenotype* relationship between the polymer and vesicles. In other words, the specific polymer that encodes the property of vesicles (genotype) can selectively promote the membrane growth of corresponding vesicles (phenotype). Here, for the sake of simplification of the system, we do not synthesize membrane molecules, but selectively incorporate them from the environment. In the end, we will construct vesicle growth system coupled with the synthesis of information polymer of vesicles.

2.2 Artificial Information Polymer

2.2.1 Introduction to Template Polymerization

In my synthetic minimal system, the design of simple and artificial information polymer is one of the most original parts. Template polymerization is usually defined as a reaction process to synthesize a daughter polymer molecule in the presence of a mother "template" polymer (or macromolecule) which has a specific affinity to monomers [Połowiński 2002; Luginbühl et al. 2018; Akashi 2014]. Two ideal reaction mechanisms are generally accepted. The first one is called “zip” mechanism (**Fig.2-2-1(a)**), where the monomers are bound to the template by strong interactions, then polymerization reactions proceed. The second one is called “pick-up” mechanism (**Fig.2-2-1(b)**), where the polymerization reaction start in bulk solution at the beginning, and then the polymer chain is bound to the template structure after reaching the critical length. The reaction proceeds further along the template by adding monomers from bulk solution to the elongating chain. Two different reaction mechanism seems not very distinct and both reaches to the similar polymer duplex in the end, but the reaction kinetics is described differently [Połowiński 2002]. As observed in surface-confined reaction which we look into the kinetics in section 4.2.2, many template polymerizations are classified into “zip” mechanism due to the adsorption constant measurements of monomers. Here, the typical interactions between templates and monomers are electrostatic interaction, hydrogen bonding, covalent bonding, and difference of polarity from bulk solution. Therefore, the polymerization reaction is localized close to the templates, typically resulting in the increased reaction rate due to the concentrated monomers and guide of the obtained polymer length similar to the template polymer.

In biological systems, replications of DNA and synthesis of RNA and protein (*i.e.,* central dogma) are examples of highly sophisticated template polymerization. The discovery of the DNA double helix structure by Watson and Crick in 1953 and the elucidation of DNA replication mechanism led to an awareness of the importance of controlling the molecular structures in polymerization reactions [Ćirić-Marjanović et al. 2017; Luginbühl et al. 2018; Akashi 2005]. The four bases of DNA have complementary base pairs through specific hydrogen bonding, formed only in combinations of A and T or C and G. Therefore, when a DNA strand is replicated in vivo, the original single-strand works as a "template" that strongly restricts the chemical structure of the newly synthesized DNA strand by hydrogen bonding, as discussed in the former section. Thus, a newly synthesized DNA strand has the complementary base sequence to the original

DNA strand [Alberts et al. 2015]. Inspired by the DNA replication mechanism, although template polymerization system as sophisticated as such biological systems may not be achieved, various systems have been developed by using multiple structures as templates, *e.g.,* single-stranded polymers, vesicles membranes, nanoparticles, microtubes, micropores, and chemically modified interfaces [Połowiński 2002; Fergson & Shah1968; Liu et al. 1992; Samuelson et al. 1998; Liu et al. 1999; Wu et al. 2000; Nagarajan et al. 2001; Nabid & Entezami 2003 & 2004; Serizawa et al. 2004; Kim et al. 2006 & 2007; Guo et al. 2009 & 2011; Ikkala 2010; Junker et al. 2012; Matsuzaki et al. 2012; Wang et al. 2013].

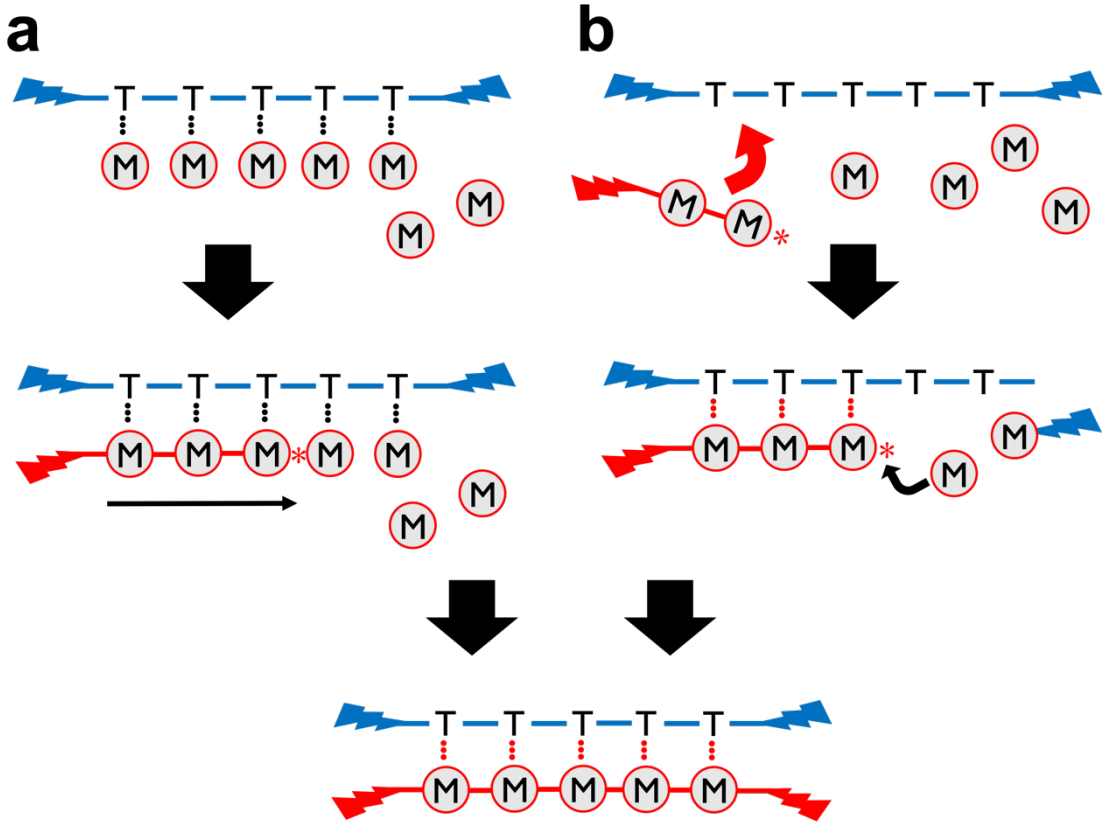

Figure 2-2-1. Two idealized reaction mechanisms in template polymerization [Połowiński 2002; Luginbühl et al. 2018]. The active site of polymer is represented as (*). In both cases, the reactions finally reach the similar polymer duplex.

(a) "zip" mechanism where monomers are pre-arranged to the template by strong interactions (hydrogen bonding or electrostatic interaction) before starting polymerization.

(b) "pick-up" mechanism where monomers are free before starting the reaction and one-by-one added to the active site of polymer.

2.2.2 Template Polymerization of Aniline on Vesicle Surface

As a promising system for the artificial information polymer which is directly related to vesicle membrane in the genotype to phenotype relationship, I focused on the template polymerization of aniline by using vesicles as templates. Template polymerization reaction of aniline itself was originally invented by using polymeric acid as template [Ćirić-Marjanović et al. 2017]. In the beginning works, polyaniline was synthesized in an acidic solution containing dispersed SPS (sulfonated polystyrene) as template polymer, which attempted to mimic DNA replication system [Liu et al. 1992; Sun et al. 1997; Samuelson et al. 1998]. Afterwards many chemical systems to obtain polyaniline by using templates were invented [Ćirić-Marjanović et al. 2017]. To the best of my knowledge, only two examples adopted vesicles as templates. The first one is the polymerization of aniline [Guo et al. 2009 & 2011; Junker et al. 2012], and the second one is the polymerization of pyrrole [Junker et al. 2015]. Since the details of the reaction mechanism have been intensely investigated, we focused on the former, the polymerization of aniline in the presence of template AOT vesicles.

In the template polymerization of aniline system, the vesicles composed of sodium bis-(2-ethylhexyl) sulfosuccinate (AOT) molecules are known to work as template to obtain specific form of polyaniline [Guo et al. 2011; Junker et al. 2012]. In the acidic aqueous solution containing NaH_2PO_4 (pH=4.3), aniline molecules are enzymatically oxidized with oxidant hydrogen peroxide (H_2O_2) and enzyme horseradish peroxidase isoenzyme C (HRPC) to produce aniline radical cations (**Fig.2-2-2**). Aniline radical cations are in equilibrium between four states, in which an unpaired electron locates at the nitrogen atom of amino group, at the *para* position, or at the two of the *ortho* positions. In the absence of any vesicle structures, the four states of aniline radical cations are randomly polymerized to form extensively branched structures with precipitations of the reaction products [Guo et al. 2011; Junker et al. 2012]. The obtained polymeric products are found to contain various side products based on the analytical studies by using aniline dimer (*p*-aminodiphenylamine, PADPA) as starting molecules to suppress the polymerization degree of the product, however, the precise product structures and distribution are still difficult to evaluate in this random polymerization system [Junker et al. 2014; Luginbühl et al. 2016 & 2017(a)(b)]. In contrast, in the presence of specific vesicles composed of AOT molecules, the polymerization reaction become sequence-regular due to the specific interaction between monomers and vesicle membranes. Here the cationic monomers are adsorbed and bound to the anionic AOT vesicle surface, then the polymerization reaction are localized on the vesicle membrane, resulting in the stable

vesicle-with-polymer suspension. In addition, the aniline radical cations join the reaction in the two of the four states (with an unpaired electron at the nitrogen atom or at *para* position), therefore, the linear N-C head-to-tail product is relevantly formed on the vesicle membrane [Guo et al. 2011; Junker et al. 2012]. This linear product is called the polyaniline emeraldine salt form (PANI-ES). **Figure 2-2-3** shows the chemical structure of the repeating unit of an ideal PANI-ES chain. It consists of four linearly connected anilines that are linked by the nitrogen atoms and the carbon atoms in *para*-position to the amino group. Furthermore, two aniline building blocks are oxidized and protonated, and the other two are reduced and not protonated. Such half-oxidized state of the repeating unit may result in the formation of the two polaron forms (polaron pair or separated polaron) and the bipolaron form of PANI-ES. In the two polaron forms, the repeating unit of PANI-ES has two unpaired electrons and all four benzene rings with fully delocalized π electrons (benzenoid structure). In the bipolaron form, unpaired electrons do not exist and the repeating unit contains benzenoid and quinoid structures. Three structures coexist, and the anionic counter ions (or "dopant") from the template vesicle forming molecules are bound to the ideal PANI-ES chains.

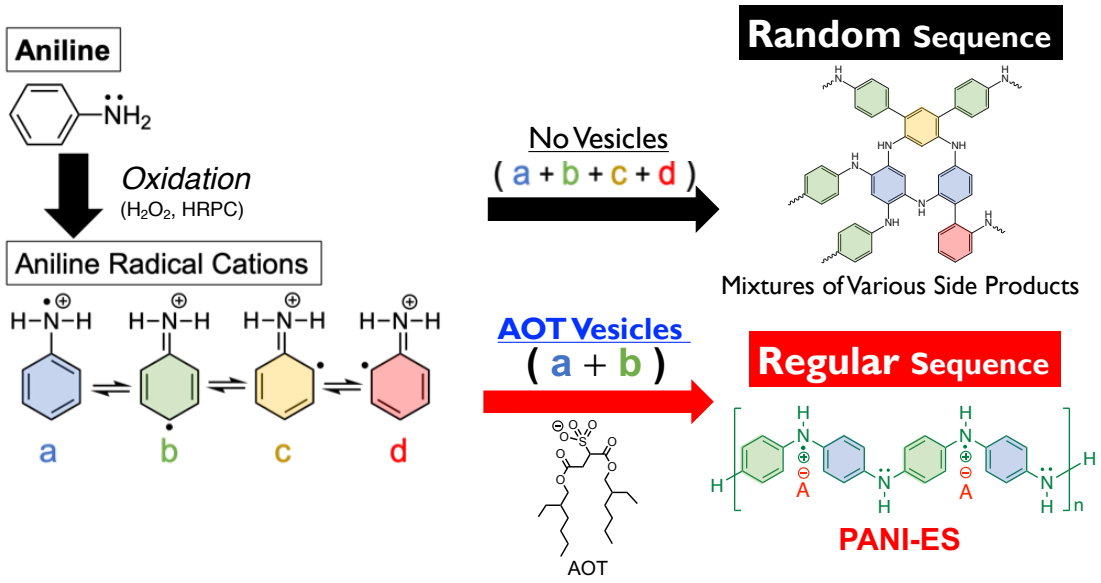

Figure 2-2-2. Scheme on polymerization of aniline with/without AOT vesicles.
In the acidic solution of NaH_2PO_4 (pH=4.3), aniline molecules are oxidized with H_2O_2 and HRPC to form four resonance states of aniline radical cations. The polymerization reaction is regulated in the presence of template AOT vesicles, resulting in the formation of regular sequence of polyaniline, called PANI-ES [Junker et al. 2012; Ćirić-Marjanović et al. 2017]. For the detailed polymerization process to form one repeating unit of PANI-ES, see the artificial metabolism design in section 3.2.3.

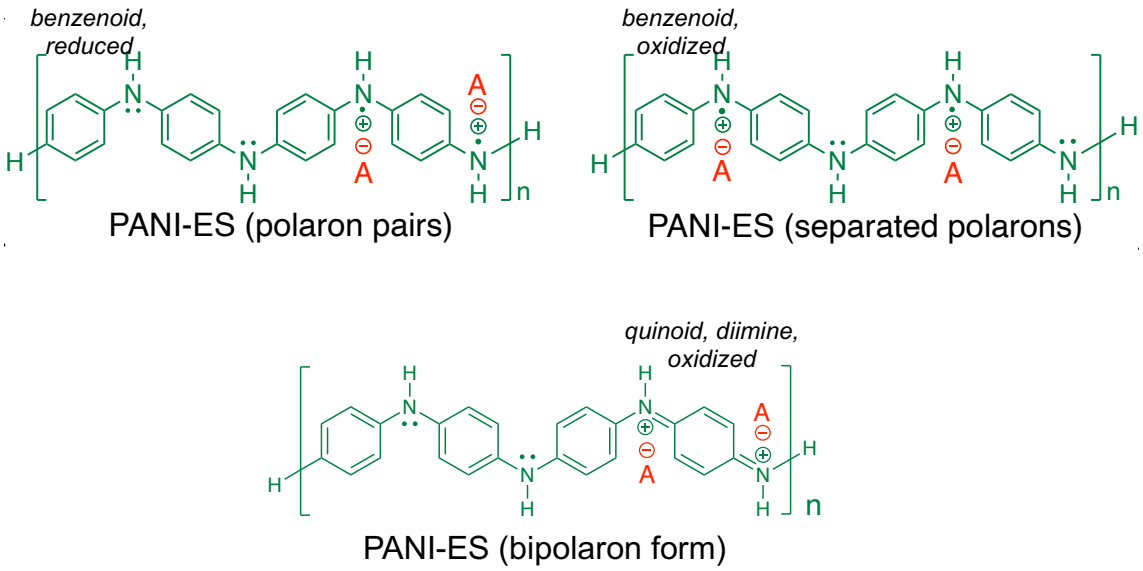

Figure 2-2-3. Chemical structures of the two polaron forms and the bipolaron form of the PANI-ES repeating unit. "A" in red represents the counter ion. [Chiang and MacDiarmid 1986; Wallace et al. 2009; Dmitrieva & Dunsch, 2011]

Concerning to the requirements of free energy cost for regular sequence polymer (information), we can compare the vesicle-assisted PANI-ES synthesis and the biological information polymer DNA. Compared to the random polymerization process in the absence of any template structures, the formation of regular sequence of PANI-ES in the presence of template vesicles is realized by the restriction of polymerization process mainly by the electrostatic interaction [Iwasaki et al. 2017] and the formation of hydrogen bonds [Iwasaki et al. 2017; Luginbühl et al. 2017(a)] between template vesicles and monomers. The molecular dynamics simulations also show that aniline molecules and the oligomer of anilines in the PANI-ES form are strongly bound or embedded to AOT vesicle membrane [Junker et al. 2014 & 2015; Luginbühl et al. 2016] by forming hydrogen bonds with vesicle forming molecules. Here we roughly estimate the quantitative relationship between the free energy cost and the thermodynamical entropy loss to produce one repeating unit of PANI-ES. Based on the ideal chemical structures of PANI-ES, we assume that four hydrogen bonds and two ion pairs are formed between N-H group of PANI-ES and sulfonated head group of AOT per one repeating unit of PANI-ES. Each binding energy is estimated as $16k_BT$ [Foreman & Monkman 2003] and $2k_BT$ [Schneider et al. 1992; Ngola et al. 1999], respectively, resulting in the enthalpy changes

from binding energy as $\Delta H \sim -60k_BT$. The translocation entropy change compared with the random polymerization system is roughly calculated as $\Delta S_{trans} \sim -34k_BT$ per one repeating unit of PANI-ES, where the free aniline molecules in bulk solution are assumed to be completely localized on vesicle surface. Thus, the free energy change by monomer binding is roughly estimated as $|\Delta G| = |\Delta H - T\Delta S_{trans}| = 26k_BT$. Please note that we do not consider the rearrangement of water molecules before and after the monomer binding. When we assume that the polymerization of aniline results in the formation of PANI-ES only in the ideal structures (**Fig.2-2-3**), the thermodynamical entropy loss per one repeating unit can be roughly estimated from Eq. (2.3), (2.4), and (2.6) as $\Delta S_{PANI} \leq -8k_BT$. Here we assumed the ideal system in which the preciseness of the polymer sequence was 100% (*i.e.,* $H(l) = 0$), and the four resonance states of aniline radical cations had equal possibility in the random polymerization (*i.e.,* $H_r(l) = 2\ (bits)$), whereas the theoretical work predicts that the unpaired electron at *para*-position is relevant in the resonance states [Karafiloglou & Launay 1998], resulting in $H_r(l) \leq 2\ (bits)$. All in all, based on above rough estimation, we can confirm that the thermodynamical entropy loss to obtain the regular sequence of polyaniline ($|T\Delta S_{PANI}| \leq 8k_BT$) is confirmed to be covered by the further free energy gain by the interaction with vesicle surface ($|\Delta G| = |\Delta H - T\Delta S_{trans}| = 26k_BT$).

PANI-ES has attracted interests from many researchers as a electroconductive polymer and organic semiconductor, therefore, its characterization method has been established. The formation of PANI-ES is characterized with UV/vis/NIR absorption measurements by the characteristic absorption with maximal absorbance at $\lambda_{max} \geq 800$ nm (assigned to the $\pi \rightarrow$ polaron transition), at $\lambda_{max} \sim 420$ nm (polaron $\rightarrow \pi^*$ transition), and at $\lambda_{max} \sim 300$ nm ($\pi \rightarrow \pi^*$ transition) [Huang & MacDiamid 1993; Nekrasov et al. 2001; do Nascimento and de Souza 2010; Bilal et al. 2015]. In addition, low absorbance at $\lambda_{low} \sim 500$ nm is indicative for a low content of chain branching [Liu et al. 1999(a)] or low content of byproduct phenazine formation [Luginbühl et al. 2017(a)]. The formation of PANI-ES is confirmed also by the electron paramagnetic resonance (EPR) measurements of the reaction mixtures. The presence of unpaired electrons in the polaron forms of PANI-ES is supported by the fact that the reaction products produce an EPR spectrum [Junker et al. 2012; Fujisaki et al. 2019]. Raman spectrum measurements also have been used to confirmed the formation of PANI-ES [Pasti et al. 2017; Fujisaki et al. 2019] based on the studies from the oligo-PADPA system. Out of the various characteristic bands for PANI-ES, the presence of delocalized polarons are again confirmed by the very strong band attributed to ν(C–N$^{\bullet+}$) vibrations, observed at ~ 1340 cm^{-1}. Thus, the formation of regular sequence polyaniline, PANI-ES, is confirmed

complementary with UV/vis/NIR, EPR, and Raman spectroscopy measurements.

Concluding this section, it is important to note that AOT vesicles restrict the polymerization process via specific interaction between vesicles and monomers, which prevents random polymerization and guides the reaction to form the regular sequence of polyaniline, PANI-ES. Although the system is not so sophisticated as the central dogma in biological system, the PANI-ES is the promising as an artificial information polymer of vesicles that can encodes the properties of vesicles as its specific regular sequence structure. Therefore, we will further investigate the relationships between obtained polyaniline sequences and the type of vesicles used as templates in the next experiment section.

2.3 (Experiment) Synthesis of Artificial Information Polymer

2.3.1 Materials

Amphiphiles used for vesicle preparation.

AOT (sodium bis-(2- ethylhexyl) sulfosuccinate, purity > 99%, Catalogue No. 86139) and SDBS (sodium dodecylbenzenesulfonate, hard type (mixture), >95%, No. D0990) were purchased from Sigma- Aldrich Japan (Tokyo, Japan) and Tokyo Chemical Industry (Tokyo, Japan), respectively. DOPC (1,2-dioleoyl-sn-glycero-3-phosphocholine, >99%, No. 850375), DOPA (1,2-dioleoyl-sn-glycero-3-phosphate sodium salt, >99%, No. 840875), DOPG (1,2-dioleoyl-sn-glycero-3-phospho-(1′-rac-glycerol) sodium salt, >99%, No. 840475), DOPS (1,2-dioleoyl-sn-glycero-3-phospho-L-serine, >99%, No. 840035), sulfatides (as ammonium salt, from porcine brain, >99%, No. 131305) and cholesterol (from ovine wool, >98%, No. 700000) were purchased from Avanti Polar Lipids, Inc. (AL, USA), and DA (decanoic acid, >99%, No. 041-23256) was from Wako Pure Chemical Industries (Osaka, Japan). The amphiphiles were used without further purification and dissolved in chloroform at 100 mM (AOT and SDBS) or at 10 mM (others) and stored at −20 °C as stock solutions.

Reagents for the polymerization of aniline.

Aniline (> 99%), hydrogen peroxide (H_2O_2) (30% in water, ~9.8 M), sodium dihydrogen phosphate (NaH_2PO_4) dihydrate (> 99%), and d(+)-glucose (> 99%), chloroform ($CHCl_3$, > 99%), acetonitrile (CH_3CN, > 98%) and perchloric acid ($HClO_4$, 60% in water), phosphoric acid (H_3PO_4, > 85%) were purchased from Wako Pure Chemical Industries (Osaka, Japan). 2,2′-azino-bis(3-ethylbenzothiazoline- 6-sulfonic acid) diammonium salt ($ABTS^{2-}(NH_4^+)_2$, > 98%) was purchased from Sigma-Aldrich. Oxo[5,10,15,20-tetra (4-pyridyl) porphyrinato] titanium (IV) (> 90.0%) was purchased from Tokyo Chemical Industry (Tokyo, Japan). Horseradish peroxidase isoenzyme C (HRPC, Grade I, PEO-131, 286 U/mg, RZ = 3.13, M ~ 40 kDa, Lot No. 74590) and glucose oxidase from *Aspergillus* sp. (GOD, Grade II, GLO-201, 166 U/mg, SA = 205, M ~ 153 kDa, Lot No. 74180) were purchased from Toyobo Enzymes (Osaka, Japan). The concentration of HRPC and GOD were determined spectrophotometrically using known molar absorptivity ε_{403}(HRPC) = 1.02×10^5 $M^{-1}cm^{-1}$ [Dunfold and Stillman 1976] and ε_{450}(GOD) = 2.82×10^4 $M^{-1}cm^{-1}$ [Swoboda and Massey 1965] as molar absorbance. Ultrapure water purified with a Direct-

Q 3 UV apparatus (Millipore, USA) was used to prepare all aqueous solutions and suspensions. All other chemicals used were of research grade. 20 mM or 100 mM dihydrogen phosphate solutions were prepared using NaH_2PO_4, water, and small amounts of H_3PO_4 to obtain pH = 4.3. These solutions are called "20 mM NaH_2PO_4 solution (pH = 4.3)" or "100 mM NaH_2PO_4 solution (pH = 4.3)", respectively.

2.3.2 Preparation of Template Vesicles

Preparation of LUVs.

AOT large unilamellar vesicles (LUVs) with an average diameter ~80-100 nm were prepared by using the freezing-thawing extrusion method [Junker, K. et al. 2012; Kurisu, M. et al. 2019 & 2021] to characterize the products obtained in the polymerization of aniline in the presence of vesicles from homogeneous reaction mixtures. Firstly, solid AOT (89.0 mg) was added to a 250 mL round bottom flask and dissolved in 5 mL chloroform. Then, a thin AOT film was prepared on the inner surface of the flask by using a rotary evaporator. The AOT film was put under a high vacuum overnight to remove chloroform completely. The AOT film was hydrated and dispersed by using 10 mL of a 20 mM NaH_2PO_4 solution (pH=4.3). The hydration temperature was $T \sim 25^{\circ}C$, and the hydration duration was $t \sim 2$ h. The obtained 20 mM AOT vesicle dispersions were rapidly frozen by placing the round bottom flask in liquid nitrogen and then thawed in a water bath heated to 60˚C. This procedure was repeated ten times. The repetitive freeze-thaw cycles are efficient to change the lamellarity of vesicles from multilamellar vesicles (MLVs) into unilamellar vesicles by removing interlamellar water and also efficient to cause fusion of small unilamellar vesicles (SUVs) into larger unilamellar vesicles [Traïkia et al. 2000; Kaasgaard et al. 2003]. Consequently, unilamellar vesicles become relevant and smaller vesicles (< 80 nm) are removed in the AOT vesicle dispersions. Then, the suspensions were extruded ten times through 200 nm pore size nucleopore polycarbonate membranes and another ten times through 100 nm pore size membranes by using LIPEX^{TM} Extruder (Northern Lipids Inc., Canada). The obtained AOT LUVs were characterized by dynamic light scattering (DLS), which showed that AOT LUVs prepared in 20 mM NaH_2PO_4 solution (pH=4.3) had an average hydrodynamic diameter of about 80 nm with a polydispersity of about 0.1 [Kurisu et al. 2019]. The AOT LUVs suspensions were stored at 25 ˚C and used within seven days.

20 mM SDBS/DA (1:1) LUVs, 5 mM phospholipids (DOPC, DOPA, DOPG, and

DOPS) LUVs, and 5 mM sulfatides LUVs were prepared by using 20 mM NaH_2PO_4 solution (pH=4.3) with the similar procedure described above. Firstly, 2 mL of each vesicle suspension (20 mM or 5 mM amphiphiles) were prepared in 5 mL glass vials using the gentle hydration method. Then, the obtained suspensions were frozen and thawed in liquid nitrogen and a water bath heated to 60˚C, respectively. After ten freeze-thaw cycles, the vesicle suspensions were extruded 21 times through a 100 nm pore-sized Nucleopore polycarbonate membrane using a Mini Extruder set (Avanti Polar Lipids, Inc., USA). The LUVs suspensions were stored at 25 ˚C and used within 7 days.

2.3.3 Protocols for Template Polymerization of Aniline

Enzymatic polymerization of aniline with HRPC and H_2O_2 in the presence of LUVs. The reaction condition to obtain PANI-ES by using AOT vesicles as templates was previously elaborated by others [Junker et al. 2012] and already used in various previous investigations [Junker et al. 2013; Pašti et al. 2017; Fujisaki et al. 2019]. Two differences from them is that the concentration of NaH_2PO_4 solution to adjust pH is not 100 mM (original condition) but 20 mM (my condition) while keeping the same pH value. This is for the easier preparation of nice giant vesicles, which will be used in the later section. In addition, I tested various vesicles as templates for polymerization reactions. Other reaction conditions were kept the same with the original ones.

The protocols to obtain PANI-ES is as follows. All components for the polymerization, except the H_2O_2 solution to trigger the polymerization reaction, were added to 349.9 μL of 20 mM NaH_2PO_4 solution (pH=4.3) in a 5 mL Eppendorf polypropylene tube: 75 μL AOT LUVs suspension (20 mM AOT in 20 mM NaH_2PO_4 solution), 50 μL aniline solution (40 mM in 20 mM NaH_2PO_4 solution, pH adjusted to 4.3 with H_3PO_4), 25 μL HRPC solution (18.4 μM in 20 mM NaH_2PO_4 solution, pH=4.3). After gentle mixing, the reaction was triggered by quick addition of 1.13 μL of freshly prepared H_2O_2 solution (2.0 M in water). The initial concentrations in the reaction mixture was as follows (**Table 2-3-1**): 3.0 mM AOT (LUVs), 4.0 mM aniline, 0.92 μM HRPC, 4.5 mM H_2O_2, 20 mM NaH_2PO_4 (pH=4.3), reaction volume of 0.50 mL, T ~ 25˚C (room temperature), reaction time t = 24 h. The reaction tubes were used with closed lid and kept standing during the reaction (**Fig.2-3-1**).

The polymerization of aniline was also performed by using various vesicles in addition to AOT LUVs. The reaction condition was the same as described above, except

that 300 µL of 5 mM LUVs suspensions and 124.9 µL of 20 mM NaH_2PO_4 solution (pH=4.3) were added to the microtube, instead of 75 µL of 20 mM AOT LUVs and 349.9 µL of NaH_2PO_4 solution described above.

Table 2-3-1. Reaction condition for the enzymatic polymerization of aniline with HRPC and H_2O_2 in the presence of AOT vesicles, which was previously elaborated for the synthesis of PANI-ES [Junker et al. 2012] and then I arranged NaH_2PO_4 concentration. The reactions take place at $T \sim 25$ ˚C (room temperature) for a reaction time of $t = 24$ h.

Component	Concentration
Amphiphile (as LUVs)	3.0 mM
Aniline	4.0 mM
HRPC	0.92 µM
H_2O_2	4.5 mM
$NaH_2PO_4 + H_3PO_4$	20 mM
H_3O^+	$10^{-4.3}$ M = 50 µM (pH = 4.3)

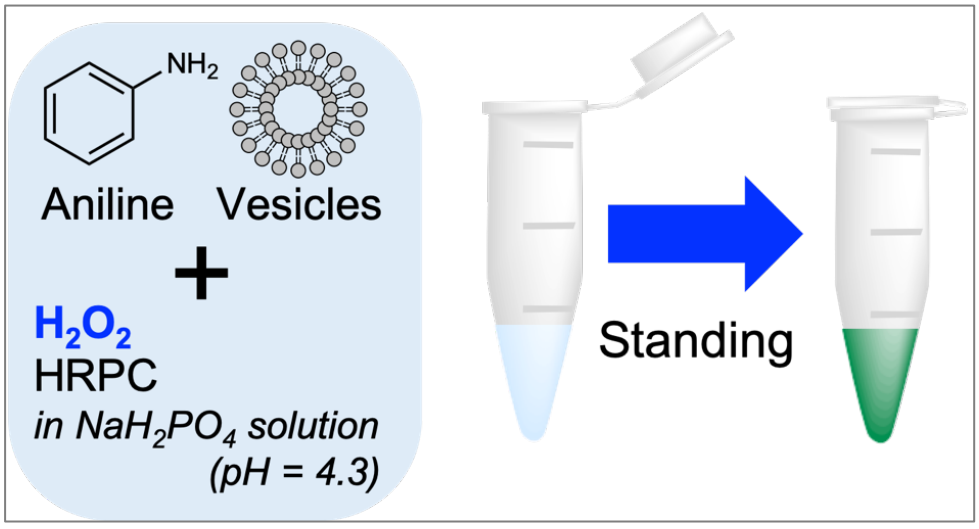

Figure 2-3-1. Scheme summarizing the protocol of polymerization of aniline. See also **Table 2-3-1**, for the concentrations of reaction components.

2.3.4 Characterization Methods of Reaction Products

UV/Vis/NIR absorption measurement.

Absorption measurements in the UV/Vis/NIR region of the spectrum were carried out with a V-730 spectrometer (JASCO, Japan) at 25 ˚C, using quartz cuvettes S15-UV-1 (GL Sciences Inc., Japan) with L=0.1 cm optical path length [Junker et al. 2012; Kurisu et al. 2019 & 2021].

EPR absorption measurement.

Electron paramagnetic resonance (EPR) measurements of the reaction mixtures were with a Bruker EMX X-band spectrometer equipped with a TM cavity. The spectra were measured at X-band microwave frequency with a modulation frequency of 100 kHz and modulation amplitudes of 1 G at room temperature [Junker et al. 2012; Kurisu et al. 2021].

Raman spectroscopy measurement.

Raman spectra were obtained by an inVia QONTOR Raman spectrometer (Renishaw, UK), equipped with a diode-pumped solid-state laser (532 nm, 50 mW), an optical microscope, and a CCD detector. The Raman spectra of the reaction mixtures obtained in the presence of LUVs were collected in non-confocal mode with an objective (N Plan L50x, NA=0.50 (Leica, Germany)). The reaction mixtures were placed in a holed silicone rubber sheet on a borosilicate glass slide. The hole had a diameter of 12 mm and a depth of 1 mm. The exposure time for one measurement run was 1.0 sec and accumulation of 30 runs with ~15 mW laser power on the sample stage.

Quantification of remaining aniline during the reaction.

The methods to determine the amounts of remaining aniline in the reaction mixture was developed by Junker et al. [Junker et al. 2012]. To quantify the remaining amounts of aniline, 30 μL of the reaction mixture was withdrawn and added to 1470 μL acetonitrile in a 2 mL polypropylene Eppendorf tube. After centrifugation to remove the reaction products, the UV/Vis/NIR absorption spectrum of the supernatant solution containing extracted aniline was measured. From the characteristic absorption intensity of aniline at λ = 238 nm (A_{238}), the concentration of aniline was calculated from the molar absorbance, ε_{238} (aniline) = 1.01 x 10^4 M^{-1} cm^{-1}, which was determined from a calibration curve prepared with known amounts of aniline (**Fig. 2-3-2**). This molar absorbance agreed well with the value determined previously, 0.955 x 10^4 M^{-1} cm^{-1} [Rajendiran & Swaminathan 1996].

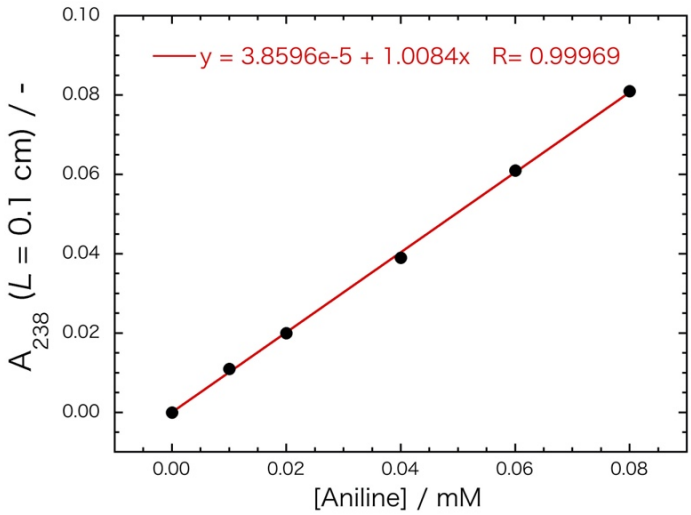

Figure 2-3-2. Calibration curve for the quantification of remaining aniline. Aniline present in samples withdrawn from the reaction mixtures is extracted into acetonitrile and then determined from the linear fit of A_{238} vs. known [aniline]. The concentrations given are the ones in the quartz cuvette used for the absorption measurements.

2.3.5 Results: Polyaniline Obtained with Various Vesicles

In the previous investigations on template polymerization by Junker et al., the optimal initial reaction condition for PANI-ES synthesis has turned out to be as follows [Junker et al. 2012]: 3.0 mM AOT (as LUVs), 4.0 mM aniline, 0.92 μM HRPC, 4.5 mM H_2O_2 in *100 mM* NaH_2PO_4 solution (pH=4.3), T = 25 °C, t = 24 h. The initial addition of H_2O_2 solution triggered the polymerization reaction. In this work, I changed two points from the previously established condition; (i) the concentration of NaH_2PO_4 solution (pH=4.3) was changed from 100 mM (by Junker et al.) to 20 mM (this work), (ii) various vesicles with three groups of head structures were used in addition to AOT (**Fig.2-3-3**), and otherwise the same reaction condition.

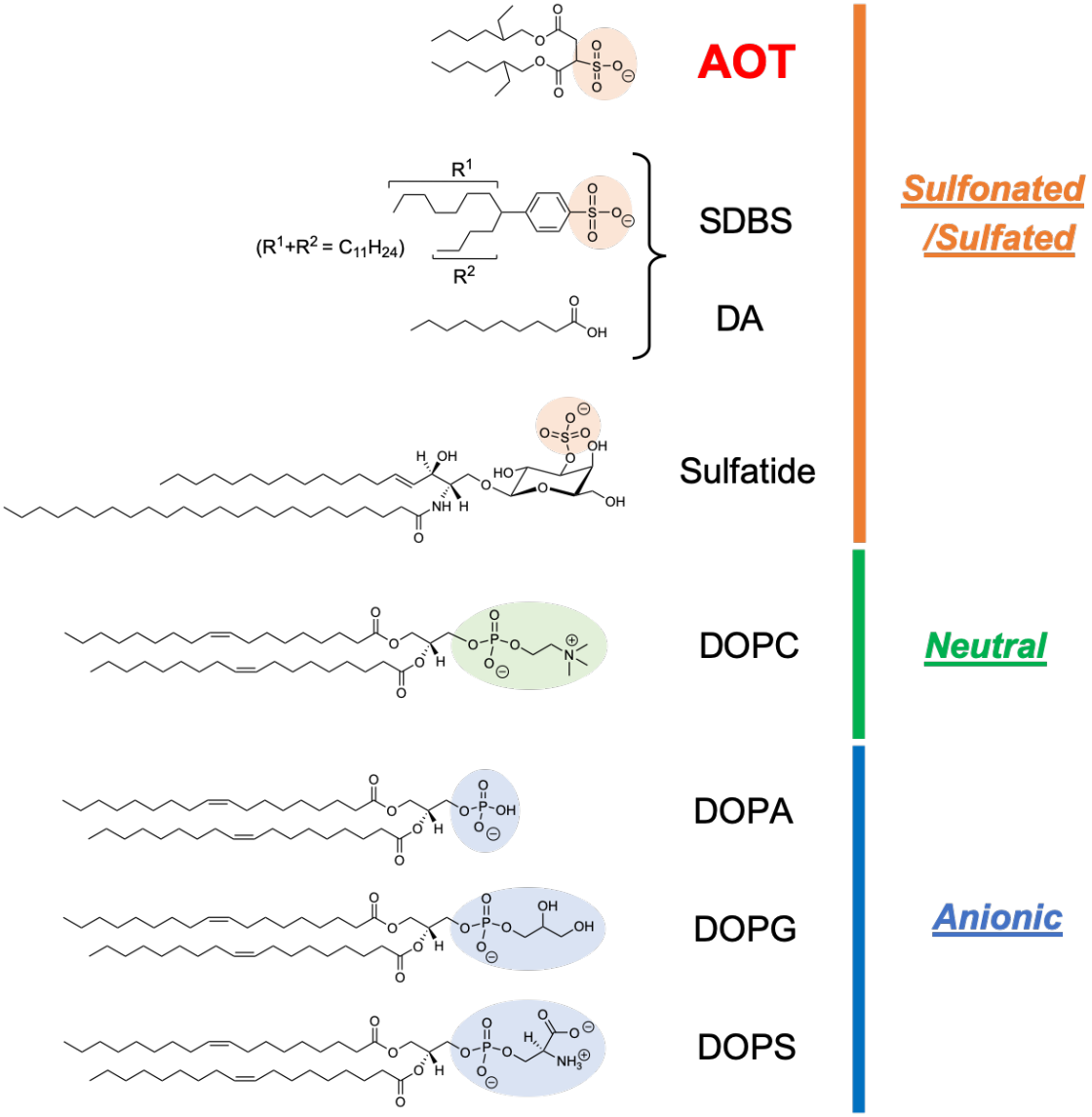

Figure 2-3-3. Vesicle membrane forming molecules used in the polymerization reaction of aniline. AOT vesicles, SDBS/DA (1/1) binary vesicles, and sulfatide vesicles have negatively charged and sulfonated or sulfate ($R\text{-}SO_3^-$, colored in orange) structures in their head groups of membrane molecules. DOPC vesicles has zwitterionic (totally neutral) head group (colored in green), and the polymerization reaction in the absence of any vesicles was also performed. DOPA vesicles, DOPG vesicles, and DOPS vesicles have again negatively charged head structures, but they do not contain sulfonated or sulfated structures (colored in blue).

Characterization of reaction product of polymerization of aniline obtained in the presence of AOT LUVs as templates.

The polymerization reaction was triggered by adding oxidant H_2O_2 to the AOT LUV suspensions in 20 mM NaH_2PO_4 solution (pH=4.3) containing aniline and HRPC. HRPC is the catalyst for initiating the reaction after being oxidized by H_2O_2. As a result, after the quick addition of H_2O_2 solution, the initially colorless reaction mixture soon became blue and then dark green with absorption maxima at $\lambda \approx 1000$, 420, and 300 nm and relatively low absorption at $\lambda \approx 500$ nm (**Fig.2-3-4(a)**), which is characteristic for the formation of the conductive form of polyaniline, PANI-ES, observed in previous works [Huang & MacDiamid 1993; Nekrasov et al. 2001; do Nascimento and de Souza 2010; Bilal et al. 2015]. The initial stage of the reaction progress was monitored by the time-dependent changes of the characteristic absorbance at λ=1000 (A_{1000}) for PANI-ES (**Fig.2-3-4(b)**) and the consumption of aniline (**Fig.2-3-4(c)**) in the reaction mixtures. These observations on reaction kinetics indicate that the polymerization reaction radically takes place at the initial ~ 60 sec after adding the reaction trigger H_2O_2, and then the reaction rate becomes slower in the closed microtubes.

The formation of products with rich PANI-ES repeating unit is further supported by the fact that reaction products produce an EPR spectrum which is indicative of the presence of unpaired electrons (expected for the polaron form of PANI-ES) (**Fig.2-3-5**) [Junker et al. 2012; Fujisaki et al. 2019]. The value of the G-factor was determined as 2.0064 for the product obtained with AOT LUVs (1), which is comparable with the values in the literature [Junker et al. 2012; Dimitrieva & Dunsch 2011; Dennany et al. 2011]. Therefore, the PANI-ES was confirmed to contain paramagnetic centers. Furthermore, the Raman spectrum measurement was performed for the obtained reaction mixture (**Fig.2-3-6**), and the assignment of the observed Raman bands are summarized in **Table 2-3-2**. The higher absorption in the NIR region and the presence of EPR signal correlate with a clear $\nu(C\sim N^{\bullet+})_p$ peak at ~ 1345 cm^{-1} due to the delocalized polarons of PANI-ES [Kashima et al. 2019; Fujisaki et al. 2019].

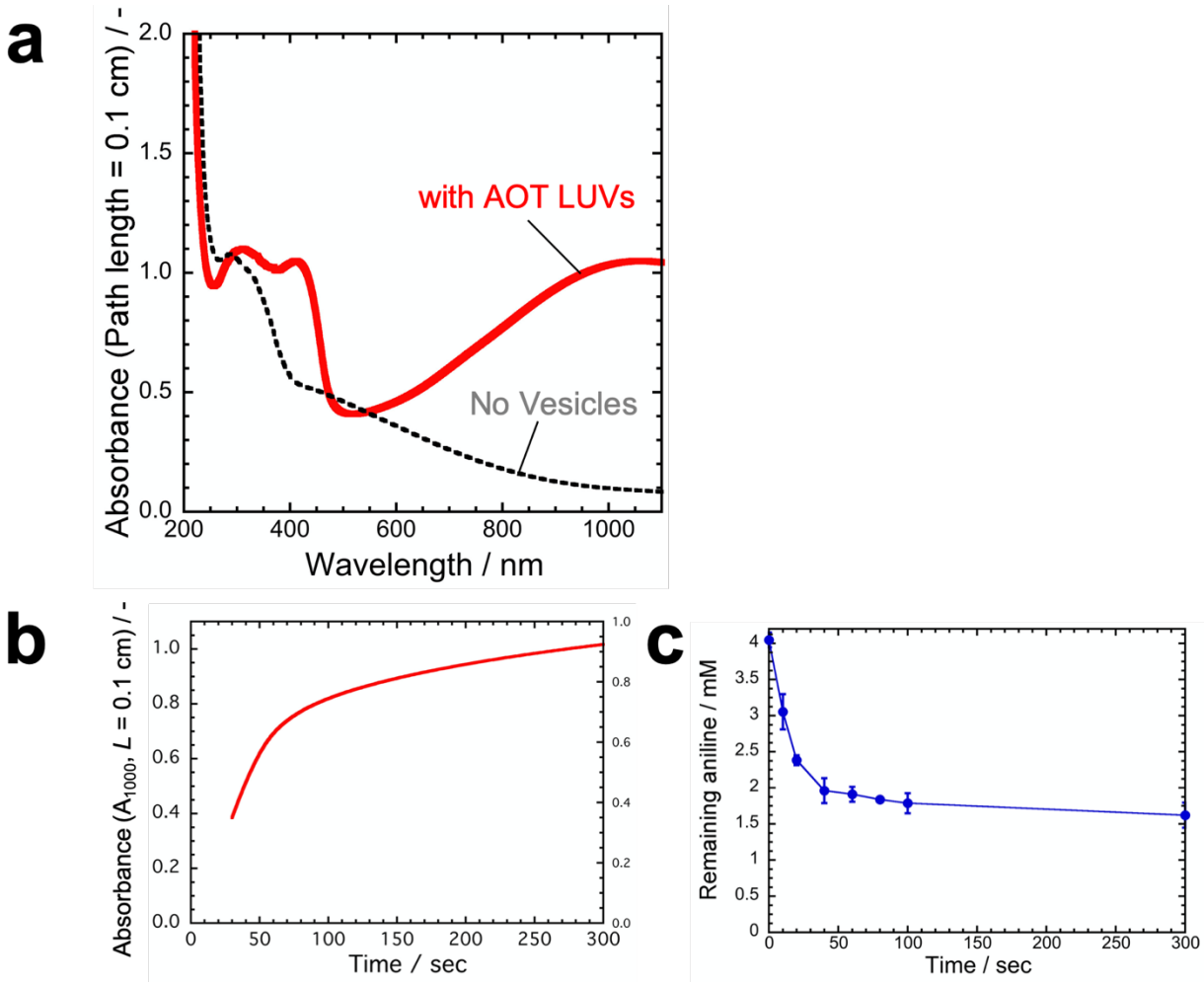

Figure 2-3-4. UV/Vis/NIR absorption spectrum and remaining aniline concentration of the reaction mixture prepared in the presence of AOT LUVs as templates, recorded at $T \sim 25$°C. The reaction conditions were as follows: [AOT]=3.0 mM or 0 mM, $[\text{aniline}]_0$=4.0 mM, [HRPC]=0.92 μM, $[H_2O_2]_0$=4.5 mM in 20 mM NaH_2PO_4 solution (pH=4.3).

a, Measured spectra, after t =24 h from the start of the reaction. Red solid line: product obtained in the presence of AOT LUVs, Black dotted line: without LUVs.

b, Time-dependent change of absorbance at λ=1000 nm (A_{1000}) of the reaction mixture in the presence of AOT LUVs. The absorbance was recorded after 30 sec from the start of the reaction due to the sample placement into the instrument.

c, Time-dependent change of remaining aniline in the reaction mixtures. Each plot was obtained by three independent experiments, and error bars represent standard deviation. The line between data points are drawn for guiding the eyes.

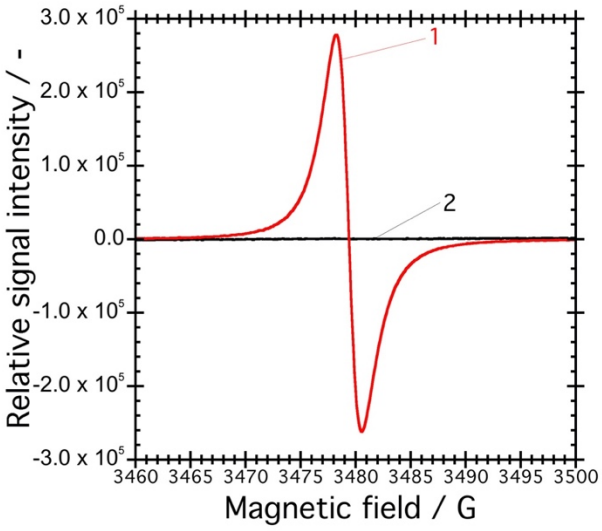

Figure 2-3-5. EPR spectra of **(1)** the reaction product obtained in the presence of AOT LUVs at $T \sim 25^{\circ}C$ and recorded after $t = 24$ h. $[AOT]=3.0$ mM, $[aniline]_0=4.0$ mM, $[HRPC]=0.92$ μM, $[H_2O_2]_0=4.5$ mM in 20 mM NaH_2PO_4 solution (pH=4.3). **(2)** Control measurement for (1), recorded from the reaction mixture before the start of the reaction (no addition of H_2O_2).

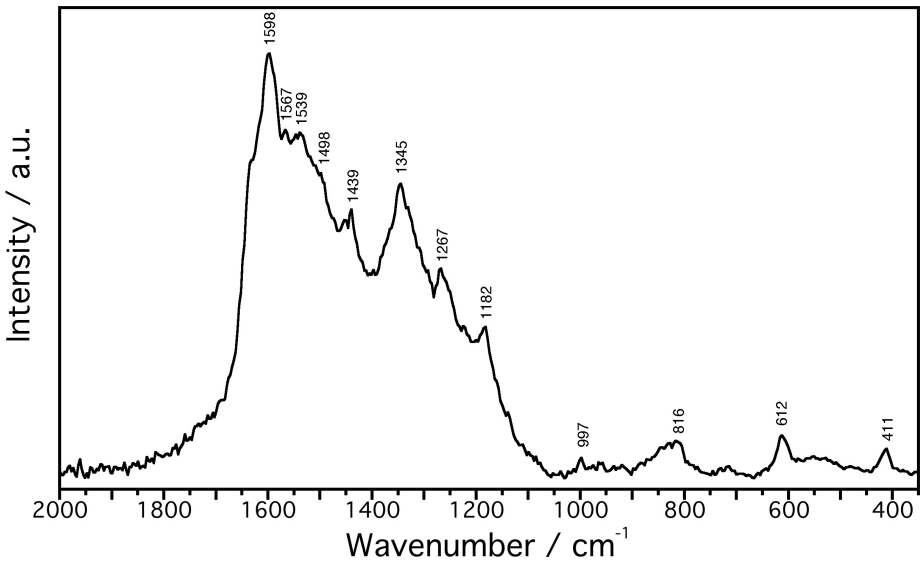

Figure 2-3-6. Raman spectrum measurements of the reaction mixtures obtained in the presence of AOT LUVs, recorded at $T \sim 25^{\circ}C$ after $t \sim 24$ h from the start of the reaction. $[AOT]=3.0$ mM, $[aniline]_0=4.0$ mM, $[HRPC]=0.92$ μM, $[H_2O_2]_0=4.5$ mM in 20 mM NaH_2PO_4 solution (pH=4.3).

Table 2-3-2. Overview of the Raman bands observed in the spectra for the polymerization of aniline in the presence of AOT LUVs, including their assignments to structural units and vibration types [Cochet et al. 2000; Edwards et al. 2000; Socrates 2001; Ćirić-Marjanović et al. 2008; Pasti et al. 2017; Luginbühl et al. 2017(a); Kashima et al. 2018; Fujisaki et al. 2019].

Band / cm^{-1}	**Structural unit[a]**	**Typical for PANI-ES[b]**	**Vibration type[c]**
612 - 616	B	Y	ν (C – S) / δ (SO_2) in-plane B ring def.
815 - 824	SQ, Q	Y	out-of-plane C-H wag. (SQ) / Q ring def.
~ 1176	SQ	Y	δ $(C-H)_{SQ}$
1181 - 1186	B	Y	δ $(C-H)_{B}$
1263 - 1267	B	Y	ν $(C-N)_{B}$
1341 - 1346	**delocalized polarons (SQ)**	**Y**	**ν $(C \sim N^{\bullet+})_{p}$**
1381 - 1383	*N*-phenylphenazine or localized polarons	N	ν (C – N^{+}) or ν (C ~ $N^{\bullet+}$)
1412 - 1427	Phenazine/*N*-phenylphenazine	N	ν (ring)
1438 - 1444	branching or intramolecular cyclization / substituted phenazine oligomers	N	ν (C = C)
~1498	QD	N	ν $(C=N)_{QD}$
1512 - 1519	SQ, B	Y	δ $(N-H)_{SQ,\,B}$
~ 1570	Phenazine, *N*-phenylphenazine, phenoxiazine	N	unclear
1594 - 1598	SQ	Y	ν $(C \sim C)_{SQ}$
	Q	Y	ν $(C=C)_{Q}$
1625	B	Y	ν $(C \sim C)_{B}$
1629 - 1632	Phenazine, *N*-phenylphenazine, phenoxiazine, convoluted with B	N	ν (C ~ C)

[a] B = benzenoid, Q = quinonoid, SQ = semiquinonoid, QD = quinonediimine.

[b] Y = Yes, N = No.

[c] Vibration type: ν = stretching vibration, δ = bending vibration.
The symbol "~" denotes a bond intermediate between single and double bond.

Characterization of reaction product of polymerization of aniline obtained in the presence of *various* LUVs as templates.

An important feature of the enzymatic polymerization of aniline in the presence of AOT vesicles is the interaction between the vesicle-forming amphiphile and monomers (*i.e.,* electrostatic interaction and hydrogen bonds) [Junker et al. 2014&2015; Iwasaki et al. 2017; Luginbühl et al. 2017(a); Foreman & Monkman 2003]. In this system, there is no doubt that regioselective regular sequence polyaniline structure, PANI-ES, is relevantly formed. Here, such a regular sequence will result in the thermodynamical entropy loss, but the further enthalpy gain from monomer binding energy will cover the "information cost". On the other hand, polymerization reactions in the absence of AOT vesicles result in the formation of extensively branched products with various side products, and no content or only very small content of PANI-ES structures were observed. Although the strict analysis on the composition and the distribution of such polymeric mixtures have been difficult, above description on random polymerization process has been supported by the analytical researches on the oligomeric reaction products obtained by starting from aniline dimer instead of monomers [Luginbühl et al. 2016&2017(b)] and the simple fact that the unpaired electron and polaron structures have not been detected from the product obtained without template vesicles [Guo et al. 2009; Luginbühl et al. 2017(b)].

To further develop the regular or random discussion on polyaniline, as the next step, various polar head group of membrane forming molecules were tested as the template vesicles for polymerization of aniline. The three types of LUVs were prepared in 20 mM NaH_2PO_4 solution (pH=4.3), which is the same conditions with the above AOT LUVs system (**Fig.2-3-3**). They were composed of either (i) negatively charged sulfated or sulfonated head group (sulfatides, AOT, or SDBS/DA (1/1) binary vesicles), (ii) a zwitterionic phospholipid (*i.e.,* neutral) (DOPC), or (iii) again negatively charged but *without* sulfated or sulfonated phospholipids (DOPA, DOPG, or DOPS). The polymerization reaction was triggered by adding oxidant H_2O_2 to the LUV suspensions in 20 mM NaH_2PO_4 solution (pH=4.3) containing aniline and HRPC. For all vesicle systems, the UV/Vis/NIR absorption spectra of the reaction mixtures were measured after 24 h from the start of the reaction.

The recorded spectra clearly depended on the type of LUVs used (**Fig.2-3-7**). With zwitterionic (overall neutral) DOPC LUVs (**Fig.2-3-7(b)**), the spectrum shows strong absorption in the range of 280-320 nm ($\pi \rightarrow \pi^*$ transition), a broad peak at 500 nm (indicative for extensive branching [Liu et al. 1999(a)] and phenazine unit formation [Luginbühl et al. 2017]), and low absorption at ~1000 nm (absence of $\pi \rightarrow$ polaron transition) as well as the absence of an absorption peak at ~ 400 nm (no polaron $\rightarrow \pi^*$

transition [do Nascimento & de Souza 2015]), *i.e.,* absence of characteristic transitions for PANI-ES in polaron state with its unpaired electrons [Junker et al. 2012; Guo et al. 2011; Huang & MacDiarmid 1993]. Therefore, the UV/Vis/NIR absorption measurements indicate that highly branched PANI, phenazine units-rich polymers, or both were obtained in the presence of DOPC vesicles. Thus, no significant "template" effect was observed for the polymerization in the presence of DOPC LUVs. In a control experiment, the enzymatic polymerization of aniline *without* vesicles was compared with the case of DOPC LUVs. The obtained products showed a very similar absorption spectrum to that of DOPC vesicles (**Fig.2-3-7(b)**) with product precipitation upon storage. For the reaction in the presence of anionic phospholipid LUVs (DOPG, DOPA, or DOPS), new weak bands appear at 440 nm and 1000 nm (**Fig.2-3-7(c)**). Thus, only a tiny amount of PANI-ES structural units in the polaron state is synthesized in the presence of anionic phospholipid vesicles. Compared to neutrally charged DOPC LUVs which almost did not show any template effect for PANI-ES, negatively charged LUVs supposed to mildly influence the polymerization process through the anion-cation interaction between vesicle surface and monomer, even though the interaction will be much weaker than the case of AOT vesicles. For LUVs prepared from anionic amphiphiles having a sulfonate or sulfate head group (AOT, SDBS/DA (1:1), or sulfatides), the spectra have high absorptions at 440 nm and 1000 nm and low absorption at 500 nm, indicating preferential synthesis of PANI-ES (**Fig.2-3-7(a)**).

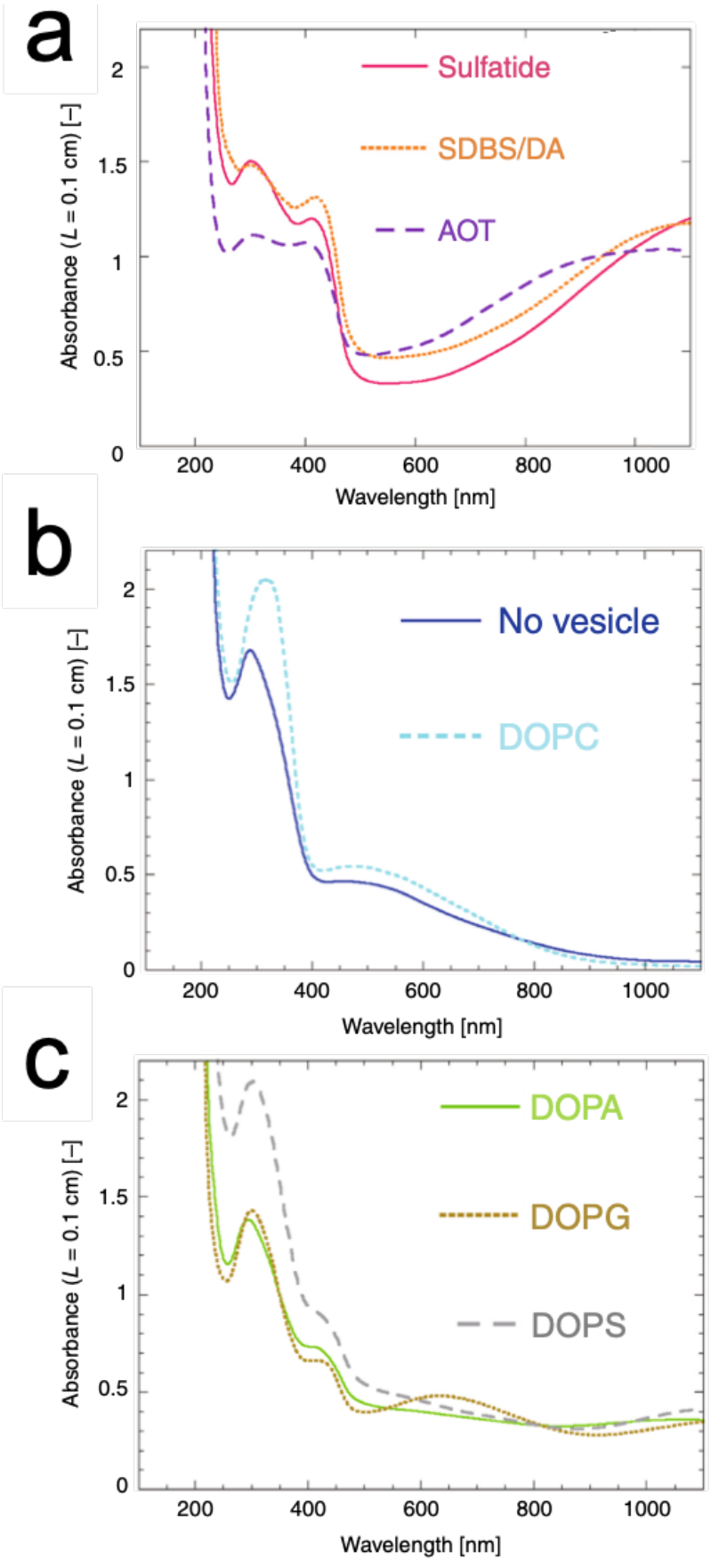
a
Sulfatide
SDBS/DA
AOT
Absorbance (L = 0.1 cm) [–]
Wavelength [nm]
b
No vesicle
DOPC
Absorbance (L = 0.1 cm) [–]
Wavelength [nm]
c
DOPA
DOPG
DOPS
Absorbance (L = 0.1 cm) [–]
Wavelength [nm]

Figure 2-3-7. UV/Vis/NIR absorption spectra of the polymerization products obtained with various template vesicles, recorded at $T \sim 25^{\circ}C$ after t =24 h from the start of the reaction. The reaction conditions were as follows: [Amphiphile]=3.0 mM (as LUVs), $[aniline]_0$ =4.0 mM, [HRPC]=0.92 μM, $[H_2O_2]_0$=4.5 mM in 20 mM NaH_2PO_4 solution (pH=4.3). The template vesicles used were either **a**, sulfatides, SDBS/DA (1/1), or AOT; **b**, DOPA, DOPG, or DOPS; **c**, DOPC or no vesicle

Discussions.

Depending on the chemical structure of the vesicle membrane-forming amphiphile's head group, the polymerization of aniline with H_2O_2 as an oxidant in the presence of vesicles result in the different results: the formation of regular sequence or random sequence polymer products. This agrees with the findings from similar experiments carried out with micelles or polyelectrolytes as templates [Liu et al. 1999(b)]. Significantly, we can say that the property of vesicle composition (the content of sulfonated/sulfated head group) is roughly "encoded" as the regular sequenced linear polyaniline, PANI-ES, through electrostatic, N-H···O-S hydrogen bonding, and steric interactions [Junker et al. 2012; Foreman & Monkman 2003; Luginbühl et al. 2017(b); Iwasaki et al. 2017].

Here, the vesicle membrane regulated the polymerization reaction on their surface through the interaction between polar head group and monomers. One promising approach to simply realize a *Genotype-to-Phenotype* relationship with vesicle and polymer is that the obtained regular sequence polymer gives positive and selective feedback to their template vesicles, such as selective membrane growth. Therefore, next, I investigated whether or not we could use such specific interaction to incorporate amphiphiles from the environment to the vesicle membrane.

2.4 Vesicle Membrane Growth

2.4.1 Introduction of Vesicle Membrane Growth

In the context of protocell/minimal cell research, membrane growth process has attracted significant interest from researchers. To make vesicles grow, two major types of vesicles are usually used: phospholipid vesicles and fatty acid vesicles (**Fig.2-4-1**). For the phospholipid vesicles, usually the ones with two long hydrocarbon chains are used. In aqueous solution, they have typical critical aggregation concentration (cac) values (see the next section) in nM regions due to their large hydrophobicity, and above such very low concentrations, they form molecular assembly such as vesicle structures [Israelachvili 2011]. On the other hand, fatty acid molecules with a single short hydrocarbon chain, such as decanoic acids, have relatively larger cac values in mM regions in vesicle phase, *i.e.*, relatively higher concentrations of fatty acids molecules can be present as monomers in equilibrium with vesicles in the solution [Morigaki et al. 2003]. Due to the presence of such a high concentration of monomers, short-chain fatty acid molecules in the external solutions can be relatively easily incorporated into vesicle membranes by generating chemical potential difference (see Eq. (2.24) below) such as by pH gradients near the vesicles, by supply of the small amount of micellar phase solution [Morigaki et al. 2003; Chen & Szostak 2004a; Zhu & Szostak 2009], and by the modification of vesicle surface state [Hanczyc 2003; Adamala & Szostak 2013]. However, in the case of phospholipid and long-tail fatty acid vesicles, we cannot generate enough molecular flux to make vesicles grow by the above methods since the monomer concentrations in the external solution (c in Eq. (2.24) below) is relatively low. Therefore, the synthetic approaches are adopted, where the membrane precursor molecules with relatively high solubility are chemically changed to the membrane molecules with very low cac values (higher chemical potential difference) near the vesicles (**Fig.1-2-4**) [Takakura & Sugawara 2004; Toyota et al. 2008; Walde et al. 1994].

In this section, since AOT has a relatively higher cvc value (~1.5 mM in 20 mM NaH_2PO_4 solution (pH=4.3)), I investigated whether the affinity between AOT molecules and PANI-ES is enough for the AOT vesicle growth by incorporation, the concept of which is closer to the fatty acid system.

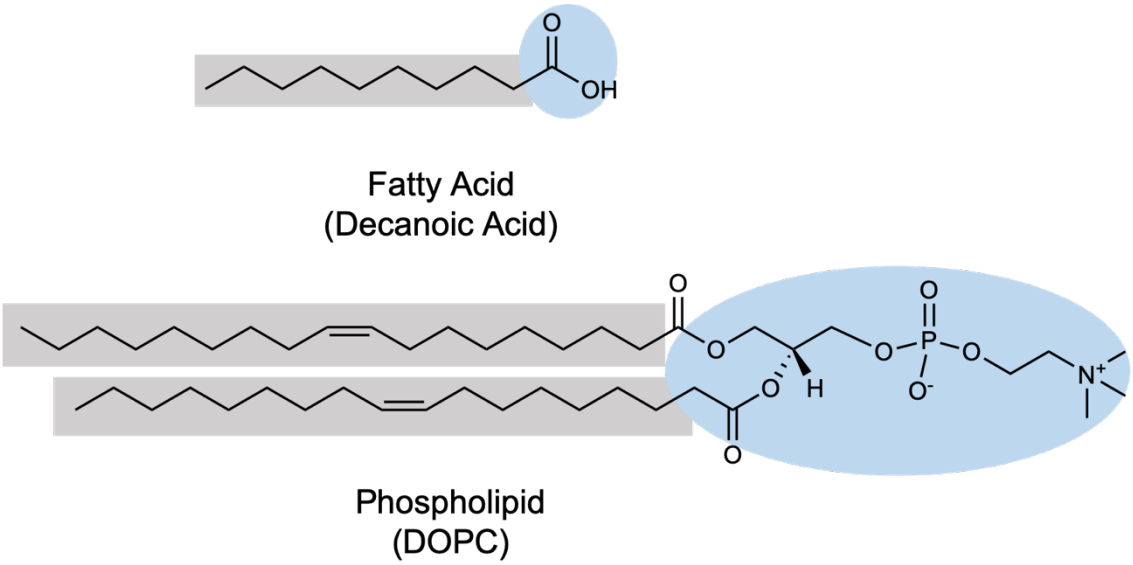

Figure 2-4-1. Fatty acid (decanoic acid) and phospholipid (DOPC). The area colored in grey represents hydrophobic hydrocarbon chains, and the area colored in blue represents the hydrophilic head group of amphiphiles. Generally, with longer hydrophobic chains, the amphiphile molecules feels more stress for exposing their chains to aqueous solution, and then forms aggregate structures like membrane in lower critical concentration values.

2.4.2 Incorporation of Membrane Molecules

Chemical potential of amphiphiles.

We consider a solution that contains amphiphiles present as both vesicles and monomers. The chemical potential of amphiphiles located in vesicle membrane (μ_v) and of monomers (μ_m) are given by:

$$\mu_v = \mu_{v,0} + \frac{k_B T}{n_v} \log\left(\frac{c_v}{c_{v,0}}\right) \tag{2.9}$$

$$\sim \mu_{v,0} \tag{2.10}$$

$$\mu_m = \mu_{m,0} + k_B T \log\left(\frac{c_m}{c_{m,0}}\right) \tag{2.11}$$

where c_v and c_m are the concentrations of vesicles and monomers, $\mu_{v,0}$ and $\mu_{m,0}$ are the reference chemical potentials of a single amphiphile located in the vesicle membrane or in the bulk solution at the reference concentration $c_{v,0}$ and $c_{m,0}$, respectively. n_v is the number of amphiphiles constituting single vesicles, k_B is the Boltzmann constant, and T is the temperature. Since $n_v \gg 1$, the chemical potential of amphiphiles located in vesicle membrane is assumed to be constant against concentration of vesicle structures, given as Eq. (2.10), whereas in the case of monomer, the chemical potential is dependent to monomer concentration. The chemical potential difference between a vesicle forming amphiphile and a monomer is given by:

$$\Delta\mu = \mu_{v,0} - \mu_{m,0} - k_B T \log\left(\frac{c_m}{c_{m,0}}\right) \tag{2.12}$$

Here we assume that the amphiphile solution reaches equilibrium between vesicles and monomers by increasing or decreasing the concentration of monomers from c_m to $c_{m,crit}$ to achieve $\Delta\mu = 0$. Then, from Eq. (2.12), we obtain:

$$c_{m,crit} = c_{m,0} exp\left[-\frac{\mu_{0,m} - \mu_{0,v}}{k_B T}\right] \tag{2.13}$$

By using $c_{m,crit}$ as the new reference concentration, we redefine the expression of chemical potentials Eq. (2.10) and (2.11) by using the monomer concentration in equilibrium state ($c_{m,crit}$) as a new reference concentration for chemical potential:

$$\mu_v \sim \mu_{v,0} \tag{2.14}$$

$$\mu_m = \mu_{v,0} + k_B T \log\left(\frac{c_m}{c_{m,crit}}\right) \tag{2.15}$$

Here, when we add further amphiphile monomers to increase the monomer concentration above $c_{m,crit}$, which results in the increase of μ_m and the generation of monomer flux, followed by the incorporation of monomers into vesicle bilayer or the formation of new

vesicles. Thus, while vesicles are formed in the amphiphile solution, the concentration of amphiphile monomers are kept constant in the solution, except the temperature or other solution conditions that influence $\mu_{0,m}$ and $\mu_{0,v}$ (such as by addition of ions and other amphiphiles) are changed. $c_{m,crit}$ is called as critical concentration for vesicle formation (cvc). The AOT cvc value in 100 mM NaH_2PO_4 solution (pH=4.3) is determined by the turbidity measurements in Appendix 3-A.

Fick's law for vesicle membrane growth.

The Fick's first law relates the diffusive flux to the gradient of concentrations as follows:

$$J_F = -D\frac{dn}{dx} \tag{2.16}$$

where J is the diffusion flux (number of particles per unit area and unit time), D is the diffusion coefficient (area per time), and n is the number density of particles. Eq. (2.16) can be rewritten by using molar density, c, instead of number density as follow:

$$J_F = -DL\frac{dc}{dx} \tag{2.17}$$

where L is the Avogadro constant.

On the other hand, the thermodynamic force to push the particles are described as follows:

$$f = -\left(\frac{\partial \mu}{\partial x}\right)_{T,p} \tag{2.18}$$

where μ is the chemical potential of the particles. Due to the expression of μ, Eq. (2.18) is further described as follows:

$$f = -k_B T\left(\frac{\partial \log c}{\partial x}\right)_{T,p} \tag{2.19}$$

$$= -\frac{k_B T}{c}\left(\frac{\partial c}{\partial x}\right)_{T,p} \tag{2.20}$$

where k_B is the Boltzmann constant and T is the temperature. When we assume that the flux of particles is a response to the thermodynamic force deriving from the concentration gradient, Eq. (2.17) is further described by using the relationship between Eq. (2.18) and Eq. (2.20) as follows:

$$J_F = -DL\frac{c}{k_B T}\left(\frac{\partial \mu}{\partial x}\right)_{T,p} \tag{2.21}$$

$$\sim \frac{LcD}{k_B T}\frac{\mu_1 - \mu_2}{l} \tag{2.22}$$

where μ_1 and μ_2 are the chemical potential at the specific points with the distance of l. l is the relevant length scale for the particle transport (or flux). In the case of vesicle membrane growth by incorporating membrane molecules located in the external solution, incorporation of each membrane molecule leads to the surface area increase by a (area per single molecule in the membrane). When we consider whole membrane surface, A, we obtain the following equations:

$$\frac{\partial A(t)}{\partial t} = J_F a A(t) \tag{2.23}$$

$$= \frac{LacD}{l\, k_B T} (\mu_{ext} - \mu_{mem})\, A(t) \tag{2.24}$$

Eq. (2.24) is the Fick's law on membrane growth. The relevant length scale of fatty acids is estimated to be ~2 μm when incorporated into the osmotically tensed phospholipid vesicles membrane [Dervaux et al. 2017].

2.5 (Experiment) Function of Information Polymer

2.5.1 Materials

Same materials with the experiments on artificial information polymer synthesis, see section 2.3.1.

2.5.2 Preparation of Vesicles

Preparation of GUVs.

Giant unilamellar vesicles (GUVs) composed of AOT were prepared by using the gentle hydration method [Reeves, J.P. & Dowben, R.M. 1969] by using the solution containing 20 mM NaH_2PO_4 (pH=4.3). Firstly, AOT (17.8 mg) was dissolved in 1 mL chloroform in a 5 mL glass vial, followed by the formation of a thin AOT film upon removal of chloroform with a rotary evaporator. Then, the AOT film was put under a high vacuum overnight to remove chloroform completely. The dried AOT film was hydrated and dispersed at 60 ˚C for 1-2 h with 2.0 mL of 20 mM NaH_2PO_4 solution (pH = 4.3) or 20 mM NaH_2PO_4 solution containing 100 mM sucrose (pH=4.3). This resulted in the formation of AOT GUVs with radii of 5-30 μm. The obtained 20 mM AOT GUV suspensions were stored at 25 ˚C and used within two days after preparation. Please note that this procedure is optimized to prepare 20 mM AOT GUVs suspension in the presence of 20 mM NaH_2PO_4 and that we could not prepare AOT GUVs in a similar way in the presence of 100 mM NaH_2PO_4, the different cvc condition for AOT.

Binary GUVs of AOT/Chol (9/1, molar ratio, 5.0 mM in total) in 20 mM NaH_2PO_4 solution (pH = 4.3) or in 20 mM NaH_2PO_4 / 100 mM sucrose solution (pH = 4.3) were prepared in the almost same way with AOT GUVs from the chloroform solutions containing the two amphiphiles in appropriate molar ratio. The differences are that the amphiphile concentration was not 20 mM but 5.0 mM and that AOT/Chol dried film was hydrated at 60 ˚C for 15-20 min. Please note that stable AOT/Chol GUVs could not be prepared when the concentration of Chol was above 10 mol%. Above 10 mol% Chol, white aggregates of Chol appeared in the solution during hydration at 60 ˚C.

Preparation of micellar solutions and SUV suspensions.

AOT, SDBS, and SDBS/Chol micellar solutions containing 2 M H_2O_2 or 100 mM D-glucose were prepared for the micro-injection experiments. 20 mM AOT micellar solutions were prepared by simply dissolving solid AOT (17.8 mg) in 2.0 mL of deionized water or in 2.0 mL of 100 mM D-glucose solution at room temperature (T ~ 25 ˚C) with a vortex mixer. 100 mM SDBS micelles were prepared in a similar way by simply dissolving solid SDBS (69.6 mg) in 2.0 mL of deionized water or in 2.0 mL of 100 mM D-glucose solution. 100 mM SDBS/0.5 mM Chol mixed micelles were prepared from the stock solutions in chloroform. Firstly, 500 μL of 100 mM SDBS solution in chloroform and 25 μL of 10 mM Chol solution in chloroform were mixed in a glass vial. The chloroform was removed using a nitrogen gas stream, and the vial wrapped with aluminium foil was put under a high vacuum overnight. Then, the dried SDBS/Chol mixture was hydrated with 0.5 mL of deionized water or 100 mM D-glucose solution using a vortex mixer, which resulted in the formation of SDBS/Chol (100 mM/0.5 mM) mixed micellar solution. The obtained micellar solutions were stored at 25 ˚C and used within two days after preparation. When we prepared micellar solutions containing 2 M H_2O_2, the AOT, SDBS, and SDBS/Chol micellar solutions prepared using deionized water were mixed with an H_2O_2 solution just before use. All micellar solutions were pressed through a 0.2 mm polypropylene filter (Puradisc 25 PP, from GE Healthcare UK Ltd., England) before being loaded into the micro-injection tip.

The small unilamellar vesicles (SUVs) suspensions of AOT, DOPC, and DOPA with a size range of ~20-100 nm in 20 mM NaH_2PO_4 solution (pH=4.3) containing 2 M H_2O_2 were also prepared for the micro-injection experiments. AOT, DOPC, and DOPA SUVs were obtained by sonicating the vesicle suspensions prepared in 20 mM NaH_2PO_4 solution (pH=4.3) (see section 2.3.2) for 5 min at room temperature (T ~ 25 ˚C) by using a Branson Sonifier model 150 (Emerson, USA). The SUV suspensions were mixed with an H_2O_2 solution before use and then pressed through a 0.2 mm polypropylene filter.

The prepared AOT SUV suspension and the micellar solution were characterized by DLS (dynamic light scattering). The obtained intermediate scattering function for 3.0 mM AOT SUV suspension was well described by a single exponential function. The cumulant analysis indicated that the AOT SUVs had an average hydrodynamic diameter of ~ 60 nm with a polydispersity of about 0.02. The scattering function for 20 mM AOT micelles in 2 M H_2O_2 solution was well described by two modes composed of a single exponential in shorter time region and a stretched exponential in the longer time region, which is frequently observed for wormlike micelle solutions [Moitzi et al. 2005]. The collective diffusion coefficient obtained from the single exponent mode was 5.2×10^{-10} m^2 s^{-1} and

the effective slow relaxation time from the stretched exponential mode was 2.1×10^{-3} s.

2.5.3 Double Micro-Injection Technique

Double micro-injection technique.

To observe the changes in the size and morphology of GUVs in response to the polymerization of aniline with the feeding of the amphiphiles, I developed double micro-injection technique (**Fig.2-5-1** and **Table 2-5-1**). The experiments were performed in a hole in a silicone rubber sheet placed onto a glass slide. The hole had a diameter of 12 mm and a depth of 1 mm. The GUV suspension mixed with the polymerization components, except H_2O_2 to trigger the reaction, was carefully transferred at room temperature (T~25˚C) from the glass vial into the sample chamber. The target GUVs in the sample chamber are located in the following reaction mixtures: 3.0 mM amphiphiles (GUVs), 4.0 mM aniline, and 0.92 μM HRPC in 20 mM NaH_2PO_4 solution (pH=4.3). The polymerization reaction was triggered by micro-injecting a 2 M H_2O_2 solution containing either SUVs (20 mM DOPC, DOPA, or AOT) or micelles (20 mM AOT, 100 mM SDBS, or 100 mM SDBS/0.5 mM Chol). Unless specifically mentioned otherwise, 20 mM NaH_2PO_4 solution (pH=4.3) was micro-injected from the second pipette as a counter flow. All solutions injected from the micro-pipettes were pressed through a 0.2 μm polypropylene filter Puradisc 25 PP (GE Healthcare, UK) before use.

The micro-injection experiments were performed using a phase-contrast light microscope (see below), equipped with a hydraulic micro-manipulator MMO-202ND (Narishige, Japan) to control the position of the micro-pipette, Femtojet system, and Femtotip II (Eppendorf, Germany) with a 0.5±0.2 μm diameter for the micro-injection. The distance between the tips of the two micro-pipettes was ~100 μm, and the distance from the tip to the bottom of the chamber was ~40 μm. The injection pressure of the pipettes was ~70 hPa, corresponding to ~0.10 nL/s (**Fig.2-5-1(b)**). The symmetrically configurated two injection flows trap the GUV at an almost fixed point of the bottom of the chamber during the observation, making it possible to measure changes in the size and morphology of the GUV quantitatively with high reproducibility.

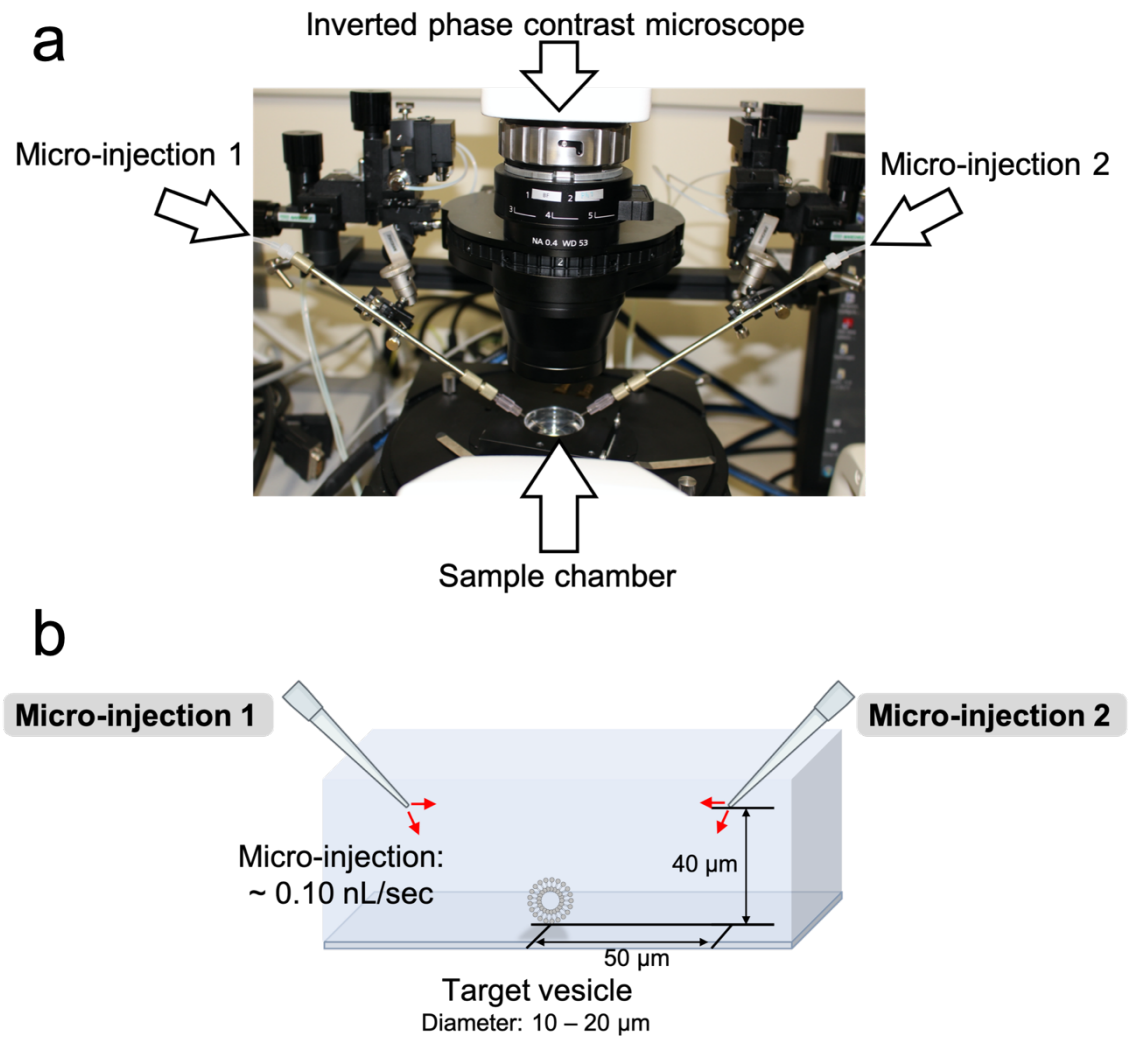

Figure 2-5-1. Double micro-injection setup coupled with microscopy observation.
(a) Appearance of equipment for the double micro-injection setup described above in section 2.5.3.
(b) Scheme of the double micro-injection setup described above in section 2.5.3. See **Table 2-5-1** below for the injected solution and the targeted bulk solution containing GUVs.

Table 2-5-1. Reaction components and their concentrations used in the double micro-injection experiment.

Micro-injection 1	**Concentration**
Amphiphiles (micelles or SUVs)	20 mM or 100 mM
H_2O_2	2 M
Micro-injection 2	
$NaH_2PO_4 + H_3PO_4$	20 mM (pH=4.3)
Bulk solution	
Amphiphiles (GUVs)	3.0 mM
Aniline	4.0 mM
HRPC	0.92 μM
$NaH_2PO_4 + H_3PO_4$	20 mM (pH=4.3)

Microscopic observation of GUVs.

The morphological changes of GUVs were followed by using an Axio Vert. A1 FL-LED inverted fluorescence microscope in phase contrast mode (Carl Zeiss, Germany) with a 40x objective (LD A-Plan 40x, NA=0.55) and a CCD camera Axiocam 506mono (Carl Zeiss, Germany) for recording the images. To estimate the morphological changes of GUVs, a 3D image of the GUV was reconstructed from the 2D microscope image by using the Surface Evolver software package [Jimbo et al. 2016; Brakke 1992]. The surface area and volume of the GUV were quantified by approximating the vesicle shape with an axisymmetric prolate shape.

2.5.4 Results: Vesicle Growth Coupled with Information Polymer Synthesis

Membrane growth of AOT GUVs coupled with the PANI-ES synthesis.

The first significant result in this section is the demonstration that AOT GUVs showed rapid growth coupled with the vesicle surface-confined template polymerization of aniline with the supply of AOT micelles. The PANI-ES formed on vesicle surface assisted the uptake of AOT molecules from the environment.

When AOT is dissolved in pure water, AOT molecules form micelles above the critical micellization concentration (cmc ~ 2.6 mM at room temperature [Nave et al. 2000]). In contrast, in 20 mM NaH_2PO_4 solution (pH=4.3), AOT forms vesicles above the critical concentration for vesicle formation (cvc ~ 1.5 mM [Kurisu et al. 2019]). As a consequence, when a small amount of AOT micelles (in water) is added to an AOT GUV suspension (in 20 mM NaH_2PO_4 pH = 4.3 solution) to exceed the cvc value, the AOT molecules originally constituting the micelles will either form new vesicles or incorporate into the preformed GUV membranes (see section 2.4.2). I then investigated whether AOT GUV growth is observed and whether the simultaneous PANI-ES synthesis on the vesicle surface significantly influences the growth process due to the specific interactions between AOT and PANI-ES, which may generate the chemical potential difference to incorporate AOT molecules into the vesicle membrane.

AOT GUVs were first prepared in 20 mM NaH_2PO_4 solution (pH=4.3), then mixed with reaction component for the PANI-ES synthesis to yield the mixture containing 3.0 mM AOT, 4.0 mM aniline, and 0.92 μM HRPC. Afterward, 2.0 M H_2O_2 solution containing 20 mM AOT micelles (prepared in pure water) was then micro-injected to a selected target GUV, and its size change was analyzed (entry #1 in **Table 2-5-2**). To estimate vesicle growth quantitatively, the distance between the target GUV and the tip of the micropipette was fixed by using a double micro-injection technique, where two simultaneous injection flows from opposite directions were applied to keep the target GUV in the fixed place (**Fig.2-5-2(a)**). After starting the micro-injection of AOT micelles/H_2O_2 solution, the target GUV maintained its spherical shape during the initial 15 sec (induction period) and then started to grow with deformation into a prolate shape (**Fig. 2-5-2(b)**). The prolate vesicle elongated with time from 15 to 45 sec by incorporating AOT molecules from the external solution. As seen in **Fig.2-5-2(b)**, the image of the vesicle suspension became dark with time, which is due to the formation of

dark green PANI-ES.

Time-dependent changes of the vesicle surface area, $A(t)$, were estimated by approximating the vesicle shape with an axisymmetric prolate shape using the Surface Evolver software package [Brakke 1992; Jimbo et al. 2016]. The obtained vesicle area is plotted as a function of time (**Fig. 2-5-3(a)**, entry #1) by normalizing the surface area with the initial spherical vesicle, $A(t = 0)$. For a better understanding of vesicle growth, several control experiments were performed.

Control experiments on AOT GUVs growth.

(i) Importance of "template" polymerization of aniline for vesicle membrane growth.
AOT micelles were micro-injected to AOT GUVs under conditions where no polymerization took place (**Table 2-5-2,** entry #2 - #5). First, when aniline and HRPC were not present in the external solution (entry #2), the growth of AOT GUVs induced by the micro-injection of AOT micelles and H_2O_2 was remarkably suppressed (**Fig.2-5-2(c)** and **Figs.2-5-3(a)** #2). The observed slight AOT GUV growth indicates that some of the AOT molecules supplied as AOT micelles are incorporated into the preformed GUV membrane since the injection of additional AOT micelles temporarily increases AOT concentration around the AOT GUV, although the extent of uptake was comparatively low.

Second, when the preformed GUV suspension did not contain aniline (entry #3) or HRPC (entry #4), micro-injection of AOT micelles/H_2O_2 solution did not result in a growth of the AOT GUV (**Fig.2-5-3(a)**). In addition, when only AOT micelles (without H_2O_2) were micro-injected to AOT GUVs in the presence of aniline and HRPC (entry #5), there was again no AOT GUV growth. Thus, the synthesis of PANI-ES on the AOT GUV surface remarkably accelerates the growth of AOT GUVs in these AOT micelle feeding experiments.

(ii) Membrane growth in the presence of different concentrations of aniline.
As confirmed above, the PANI-ES synthesis on the vesicle surface radically accelerates the growth of the vesicle membrane. To understand the kinetics of the system, we quantified AOT membrane growth in the presence of different concentrations of aniline while keeping all the other conditions the same: 4.0 mM (original, identical to **Fig.2-5-3(a)** entry #1), 2.0 mM, and 1.0 mM as shown in **Fig.2-5-3(b)**. The AOT GUVs tended to show exponential membrane growth coupled with the surface-confined formation of

PANI-ES, and their growth rates were increased by the more formation of PANI-ES on the vesicle surface. The experimentally observed membrane growth can be reproduced with the kinetic model, Eq. (IVa – IVf), as discussed later in section 4.3.4(iii). The simulation curves are overlaid with the experimental plots by each aniline concentration (red solid line: 4 mM, blue dashed line: 2 mM, and green dotted line: 1 mM).

Table 2-5-2. List of experimental conditions and the results for the AOT GUV observation coupled with the PANI-ES synthesis and the feeding of AOT micelles under the micro-injection system.

Condition	(Target GUV Suspension)		(Micro-Injection Solution)		PANI-ES Synthesis	Growth
	Aniline[a]	HRPC[b]	H_2O_2[c]	AOT micelles[d]		
# 1	✓	✓	✓	✓	Yes	Yes
# 2	–	–	✓	✓	No	Slight
# 3	–	✓	✓	✓	No	No
# 4	✓	–	✓	✓	No	No
# 5	✓	✓	–	✓	No	No

[a] [Aniline] = 4.0 mM, [b][HRPC] = 0.92 μM, [c][H_2O_2] = 2 M, [d][AOT] = 20 mM.

Note. "-" in the table represents that the reaction component is removed from the target solution or injection solution. "No" in the column "PANI-ES Synthesis" represents the PANI-ES is not synthesized with the micro-injection experiment due to the lack of some reaction components.

"**#1**" corresponds to the micro-injection setup shown in **Table 2-5-1**. "#2" represents the control system where H_2O_2 solution containing AOT micelles are micro-injected to a AOT GUV just in NaH_2PO_4 solution, without containing any other reaction components. "#3-5" also represent the control experiments where some of the reaction components and/or injected components are removed.

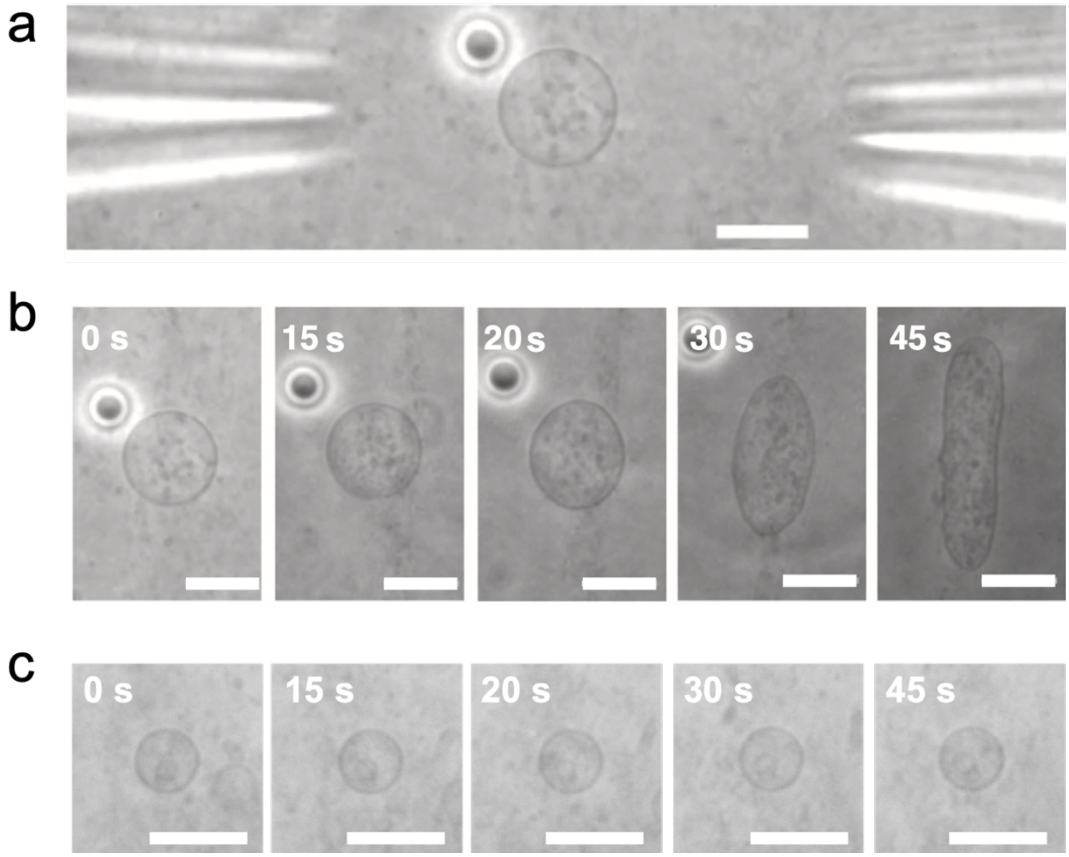

Figure 2-5-2. Phase-contrast light microscopy images of AOT GUVs under micro-injections.

(a) The image of the double micro-injection setup. A small amount of the reaction components is continuously supplied toward the target vesicle. With the two injection flows, the target GUV can be kept in almost the same place. The length of the scale bar: 20 μm.

(b) Condition "#1" of **Table 2-5-2**: A 3.0 mM AOT GUV suspension containing 4.0 mM aniline and 0.92 μM HRPC was first placed into the sample chamber, followed by micro-injection of two different solutions from opposite sites to a selected GUV. The dark particle with the white halo is an AOT aggregate that was not completely dispersed. An aqueous solution consisting of AOT micelles (20 mM AOT) and H_2O_2 (2.0 M) was micro-injected from the micropipette on the right-hand side. The 20 mM NaH_2PO_4 solution (pH=4.3) was injected from the micropipette on the left-hand side. The time-dependent changes are shown after starting the micro-injection for t = 0, 15, 20, 30, and 45 s. The length of the scale bar: 20 μm.

(c) Condition "#2" of **Table 2-5-2**: An AOT GUV in 20 mM NaH_2PO_4 (pH = 4.3) solution without aniline and HRPC under micro-injection of AOT micelles (20 mM AOT) and H_2O_2 (2.0 M). The images were taken at t = 0, 15, 20, 30, and 45 s. The length of the scale bar: 20 μm.

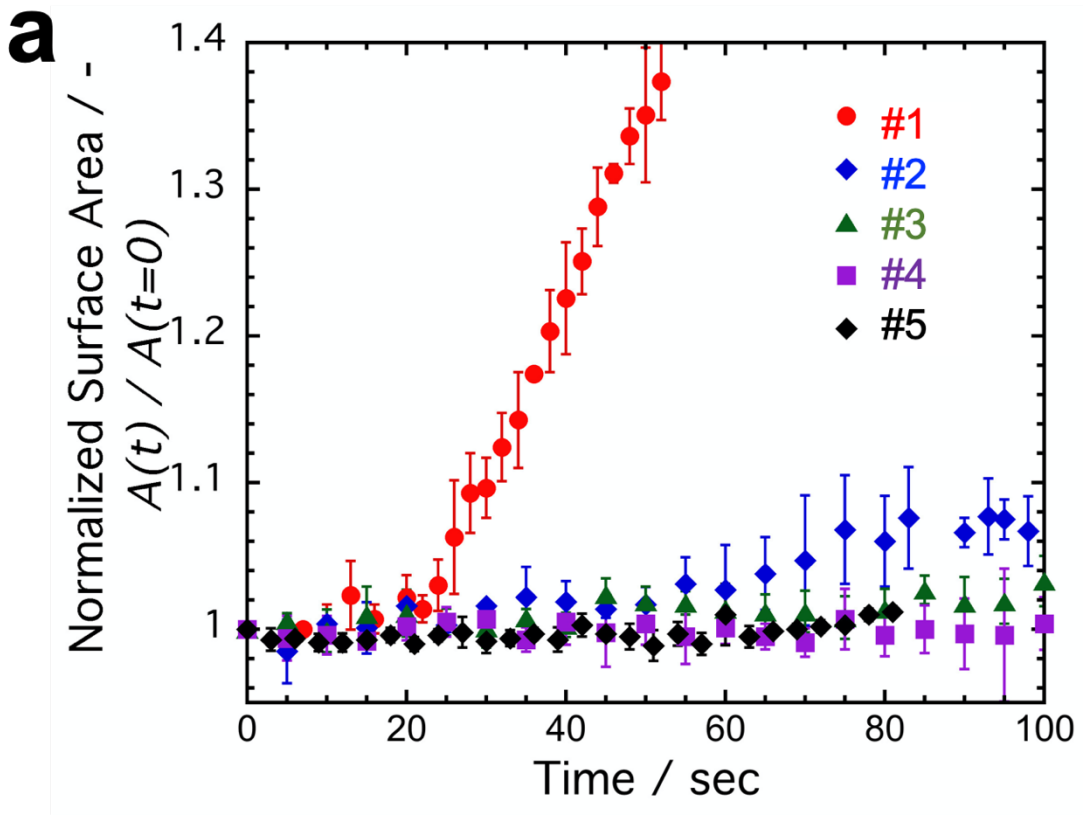
a
Normalized Surface Area / -
A(t) / A(t=0)
1.4
1.3
1.2
1.1
1
0
20
40
60
80
100
Time / sec
#1
#2
#3
#4
#5

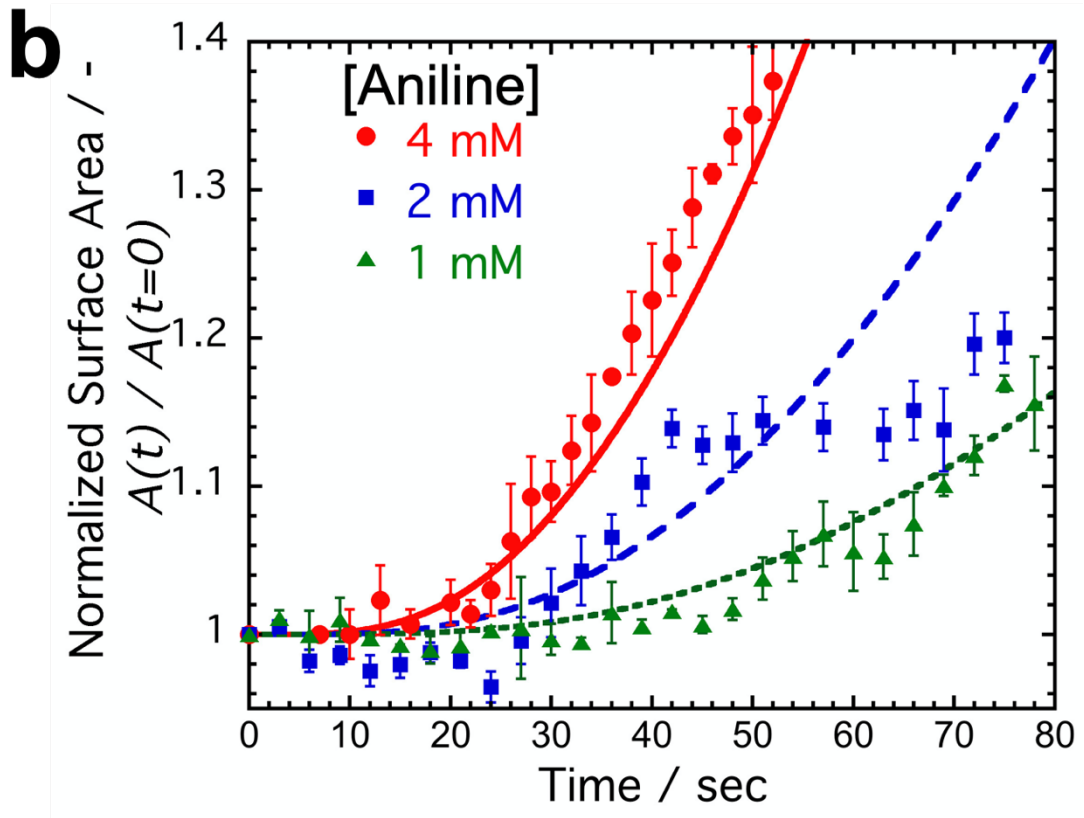
b
Normalized Surface Area / -
A(t) / A(t=0)
1.4
1.3
1.2
1.1
1
0
10
20
30
40
50
60
70
80
Time / sec
[Aniline]
4 mM
2 mM
1 mM

Figure 2-5-3. Growth of AOT GUVs in response to the micro-injection of AOT micelles under various conditions.

(a) Experiments with AOT GUVs for the different conditions listed in **Table 2-5-2**. Red circles (**#1**): Micro-injection of 2.0 M H_2O_2 and 20 mM AOT micelles in water to 3.0 mM AOT GUVs prepared in 20 mM NaH_2PO_4 (pH=4.3) solution with 4.0 mM aniline and 0.92 μM HRPC. Blue diamonds (**#2**): AOT GUV suspension without aniline and HRP. All other conditions are kept the same as entry #1. Green triangles (**#3**): AOT GUV suspension without aniline. All other conditions are kept the same as entry #1. Violet squares (**#4**): AOT GUV suspension without HRPC. All other conditions are kept the same as entry #1. Black diamonds (**#5**): The micro-injection solution did not contain H_2O_2. All other conditions are kept the same as entry #1. The error bars indicate standard deviations estimated from three to six different experiments.

(b) Further experiments with the condition (**#1**) in (**a)**, but the only difference is the concentration of aniline in the reaction system. Red circles: with 4.0 mM aniline, and these are the identical plots to the red circles in (**a)**. Blue squares: with 2.0 mM aniline. Green triangles: with 1.0 mM aniline. The experimentally observed membrane growth was reproduced with the kinetic model, Eq. (IVa – IVf), as discussed later in section 4.3.4(iii), overlaid with experimental plots: red solid line: 4.0 mM, blue dashed line: 2.0 mM, and green dotted line: 1.0 mM. Please note that the only difference between the three simulation curves is the concentration of aniline, and all other parameters are common between them. The error bars indicate standard deviations estimated from three to six different experiments.

Selectivity in types of amphiphile incorporation to vesicle membrane.

(iii) Selectivity of vesicle membrane growth coupled with the synthesis of PANI-ES.

As we have seen in **Fig.2-3-7**, the enzymatic polymerization of aniline in the presence of vesicles without sulfonated/sulfated head groups is considered to produce a mixture of various polymeric products which contain low PANI-ES repeating units, not linear but extensively branched products, and the products with different oxidation and protonation state from PANI-ES [Liu et al. 1999; Guo et al. 2009]. To examine the effect of the type of PANI product on the vesicle growth, four types of GUVs composed of either (i) DOPC, (ii) DOPA, (iii) AOT, or (iv) SDBS/DA (1/1), were prepared in 20 mM NaH_2PO_4 solution (pH=4.3) containing aniline and HRPC. The corresponding amphiphiles were supplied to each GUV suspension by micro-injection together with H_2O_2: either sonicated DOPC vesicles (DOPC SUVs), DOPA SUVs, AOT SUVs, or SDBS micelles (all prepared in 20 mM NaH_2PO_4 solution, pH = 4.3). The observed growth rates of the GUVs were roughly measured by linear fitting and then normalized by that of the growth observed for the AOT GUV/AOT SUV system, as summarized in **Table 2-5-3**. The green highlight represents the amphiphiles which work as template for PANI-ES synthesis. GUVs from neutral or anionic phospholipids did not show any significant growth.

On the other hand, GUVs composed of amphiphiles with a sulfonate head group showed growth (addition of AOT SUVs to AOT GUVs, or addition of SDBS micelles to SDBS/DA GUVs) (**Fig.2-5-4(a)** and (**b), A** and **B**). Thus, a coupling between template polymerization and vesicle growth is selectively observed only for those vesicle systems that yield PANI-ES rich products, and amphiphiles with a sulfonate head group are supplied. It is worth noting that growth of AOT GUVs was also induced by injection of SDBS micelles, and growth of SDBS/DA vesicles was also induced by the addition of AOT SUVs (**Fig.2-5-4(a)** and (**b), C** and **D**), although the supply of different membrane molecules from the target GUV composition did not induce the simple exponential growth.

Table 2-5-3. Observed relative growth of four types of GUVs.
GUVs were prepared from DOPC, DOPA, AOT or SDBS/DA (1/1), all at 3.0 mM total amphiphile concentration in 20 mM NaH_2PO_4 solution (pH = 4.3) upon micro-injection of 20 mM DOPC SUVs, DOPA SUVs, AOT SUVs, or 100 mM SDBS micelles. The observed growth rate of the GUV is roughly estimated with a linear fit and then normalized by that of the AOT GUV/AOT SUV system ($\Delta A(t) = 0.0086[s^{-1}]\ A(0)$). The growth rates were estimated from the growth stages in **Fig.2-5-4(b)**; *i.e.*, 10–40 s for AOT to AOT (A), 10–50 s for SDBS to SDBS/DA (B), 10–100 s for AOT to SDBS/DA (C), and 60–90 s for SDBS to AOT (D). "–" represents that no vesicle growth was observed in the condition. Green highlight represents the amphiphiles which work as template for PANI-ES synthesis.

Vesicle	***Supplied Molecule***			
	SUVs			Micelles
	DOPC	**DOPA**	**AOT**	**SDBS**
DOPC	–	–	–	–
DOPA	–	–	–	–
AOT	–	–	**1.0**	1.1
SDBS/DA	–	–	0.2	0.9

a

Condition	Micro-injected Amphiphile	Vesicle
A	AOT SUVs	AOT
B	SDBS micelles	SDBS/DA (1/1)
C	AOT SUVs	SDBS/DA (1/1)
D	SDBS micelles	AOT

b

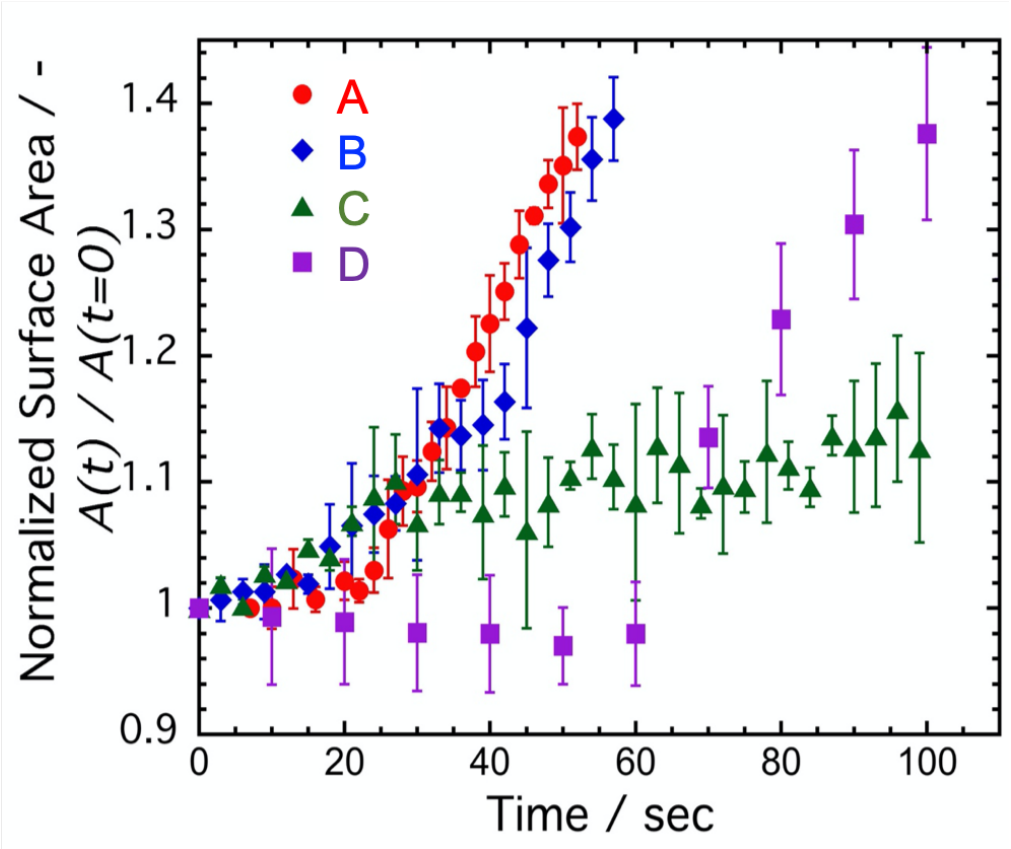

Figure 2-5-4. Growth of AOT or SDBS/DA (1/1) GUVs in response to the micro-injection of 20 mM AOT (SUVs) or 100 mM SDBS (micelles) under various conditions.

(a) For the understanding of the experimental condition. (**A**): AOT SUVs are supplied to AOT vesicles coupled with PANI-ES synthesis. (**B**): SDBS micelles are supplied to SDBS/DA (1/1) vesicles coupled with PANI-ES synthesis. (**C**): AOT SUVs are supplied to SDBS/DA (1/1) vesicles coupled with PANI-ES synthesis. (**D**): SDBS micelles are supplied to AOT vesicles coupled with PANI-ES synthesis.

(b) Experiments demonstrating the selectivity of the GUV growth, see also (**a**) and **Table 2-5-3**. Red circles (**A**): Micro-injection of 2.0 M H_2O_2 and 20 mM AOT SUVs in water to 3.0 mM AOT GUVs prepared in 20 mM NaH_2PO_4 (pH = 4.3) solution with 4.0 mM aniline and 0.92 µM HRPC (vesicle growth observed). Blue diamonds (**B**): Micro-injection of 2.0 M H_2O_2 and 100 mM SDBS prepared in 20 mM NaH_2PO_4 (pH = 4.3) solution to SDBS/DA (1/1) GUVs. All other conditions are kept the same as for (**A**) (vesicle growth observed). Green triangles (**C**): Micro-injection of 2.0 M H_2O_2 and 20 mM AOT SUVs prepared in 20 mM NaH_2PO_4 solution (pH = 4.3) to 3.0 mM SDBS/DA (1:1) GUVs prepared in 20 mM NaH_2PO_4 (pH = 4.3) solution with 4.0 mM aniline and 0.92 µM HRPC (slow vesicle growth observed). Violet squares (**D**): Micro-injection of 2.0 M H_2O_2 and 100 mM SDBS micelles prepared in 20 mM NaH_2PO_4 (pH = 4.3) solution to AOT GUVs. All other conditions are kept the same as (**A**) (vesicle growth observed with delay). The error bars indicate standard deviations estimated from three different experiments.

Discussions.

Based on the above control experiments, the sulfonate head group is responsible for the observed growth of the vesicle membrane induced by the surface-localized PANI-ES synthesis. This indicates that specific interactions between the polymer and the amphiphile play an essential role in the vesicle growth process. PANI-ES localized on vesicle surface recognizes externally added amphiphiles having a sulfonate head group, which results in selective incorporation into the vesicle membrane composed of the sulfonate amphiphiles, and then vesicles show membrane growth. Putting all experimental data presented in this section together, there is one key observation: concerning both sulfonated amphiphiles AOT and SDBS, AOT (or SDBS/DA) GUVs promote the synthesis of PANI-ES, and PANI-ES promotes the growth of the AOT (or SDBS/DA) GUVs. This *mutual catalytic relationship* is an essential feature of (our) minimal cells [Kauffman 1986; Kaneko 2002]. In this context, we call the PANI-ES, which is synthesized by the template polymerization in the presence of vesicle, as an "information polymer" of vesicles, *i.e.*, PANI-ES "encodes" the specific amphiphiles constituting vesicles as its own structures and "decodes" by the selective promotion of uptake of the amphiphiles.

For the detailed discussion on to what extent the incorporation rates increased by PANI-ES, see the discussion in section 4.5.

2.6 Conclusion

In this chapter, I focused on the template polymerization system using vesicle membrane as templates for the promising candidate for the simple and artificial information polymer of a minimal cell system. First, I confirmed that the regioselective structures of polyaniline, PANI-ES, is formed in the presence of AOT template vesicles as already reported in previous systems [Guo et al. 2011; Junker et al. 2012]. I tested various vesicles as templates for polymerization of aniline, then I found that regular sequence form of polyaniline (PANI-ES) was formed by using sulfonated/sulfated vesicles as templates, although the use of vesicles without such head structures results in the formation of random polymerization of aniline. The supposed mechanism is as follows. The enthalpy gain from the specific interactions (electrostatic and hydrogen bonds) between template vesicle surface and monomers cover the thermodynamical entropy loss, which prevents random polymerization and assists the formation of regular sequence form of polyaniline, PANI-ES. Second, I demonstrated that such specific interactions between PANI-ES and sulfonated/sulfate amphiphiles promoted the selective incorporations of the same type of amphiphile, resulting in the promotion of vesicle membrane growth. Therefore, there is a simple form of mutual catalytic or autocatalytic relationship [Bissette & Fletcher 2013; Vasas et al. 2012; Xavier et al. 2020] between vesicle membrane and regular sequence polyaniline (PANI-ES), *i.e.*, vesicle surface guides the polymerization reaction to specific way, and obtained polymer selectively promote the vesicle membrane growth.

Here, I adopt the regular sequence polyaniline (PANI-ES) as the artificial information polymer of my synthetic minimal cell system (**Fig.2-6-1**). In biological systems, the genetic information (genotype) is translated to functions and structures (phenotype) stepwise from DNA to RNA, from RNA to proteins, and proteins (enzymes) catalyze the synthesis of membrane molecules by using highly sophisticated (and at the same time, quite complex) molecular mechanism. On the other hand, in my vesicle growth system, I do not have to introduce such complex molecular mechanisms. The information on vesicle membrane (whether or not vesicles have sulfonated/sulfated head group) is encoded as regular sequence of information polymer (PANI-ES unit-rich structures), and then such “genotype” is translated into “phenotype” through the selective promotion of vesicle membrane growth. For the “minimal” cell system to consider the emergence of simplest forms of any possible living systems, this is enough for the information polymer. All in all, my artificial information polymer does not simplify the biological systems, but conceptually reproduces the essence in a minimal way.

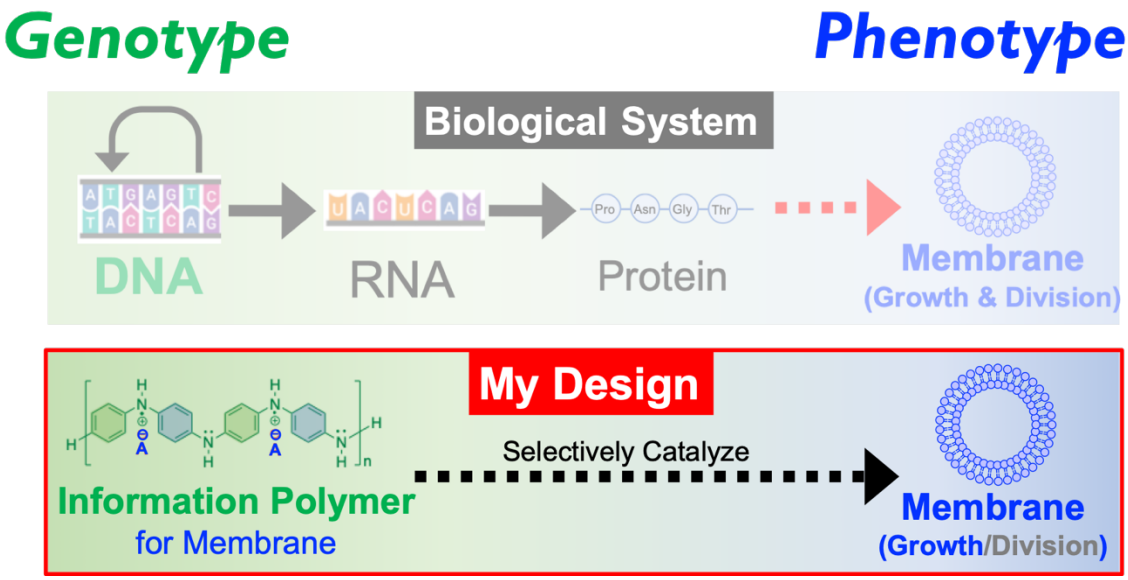

Figure 2-6-1. Graphical summary of this chapter, showing my artificial information polymer design. I focused on the template polymerization system using vesicle membranes as template. The artificial information polymer encodes the property of vesicles (sulfonated/sulfated polar head group) in its regular sequence structure (PANI-ES unit-rich structure). At the same time, the artificial information polymer selectively promote the incorporation of corresponding amphiphiles, resulting in the vesicle membrane growth.

The contents in this chapter is based on the following original paper:

Minoru Kurisu, Harutaka Aoki, Takehiro Jimbo, Yuka Sakuma, Masayuki Imai, Sandra Serrano-Luginbühl, and Peter Walde "Reproduction of vesicles coupled with a vesicle surface-confined enzymatic polymerization.", *Communications Chemistry*, **2**:117 (2019).

Chapter 3

Artificial Metabolism System

3.1 Introduction

Biological systems are composed of overwhelming number of chemical reaction networks, which is the biggest cause of the "gap of complexity" (**Fig.1-2-1**) hindering the understanding from physical sciences. At the same time, this complexity is one of the biggest motivations to work on the protocell / minimal cell research. Based on the recent molecular biology, the essence of such complex reaction networks is becoming clearer [Koonin 2000; Xu et al. 2011; Hutchison et al. 2016; Breuer et al. 2019]. Concerning to one of the simplest known bacteria, *Streptococcus sanguinis*, Xu et al. have identified its essential genes and associated with only three basic categories of biological functions (**Figs.1-1-1(a)**): energy production domain, processing of information domain, and maintenance of the cell membrane domain. Therefore, one of the promising approaches to design a metabolism system for synthetic minimal cell is to mimic the three reaction domains in a simple and artificial way. Related to this approach, "chemoton" proposed by Gánti (**Fig.1-2-2**), the pioneering model in this field, is also made up of similar reaction network: the metabolic cycle, the genetic cycle, and the membrane cycle [Gánti 1975 & 2003]. However, from the viewpoint of experimental realization, chemoton has a problem in transmembrane molecular traffic which incorporate and excrete molecules to sustain the encapsulated reaction networks.

Based on the above considerations, in this chapter, I design the artificial metabolism system not inside but outside of the vesicle membrane. My artificial metabolism system contains three reaction domains corresponding to the above two examples: energy currency production domain, information polymer synthesis domain, and membrane growth domain. As I already shown in the last chapter, my artificial information polymer is synthesized on the surface of vesicle membrane. Then, the reaction field of the synthetic minimal cell system is the outer surface of the vesicle, which prevents dissipation of the formed information polymer (due to the strong interaction with membrane) and enables the inflow and outflow of molecules much easier. In the next section, I will show the detailed chemical reaction networks.

3.2 Artificial Metabolism System

3.2.1 Overview of the Artificial Metabolism System

Fig. 3-2-1 represents the design of artificial metabolism system in my synthetic minimal cell, which shows the relevant reaction network (R1 – R9). The bold rectangle represents the reaction system close to the AOT vesicle, and colored bold arrows represent the inflow of ingredient molecules which are continuously supplied with micro-injection setup. The red region (R1) is the energy currency production domain, which produces energy currency molecules, oxidant H_2O_2, by enzymatic reaction with D-glucose, dissolved O_2, and enzyme glucose oxidase (GOD). The green region (R2 – R8) is the information polymer (PANI-ES) synthesis domain, which is the vesicle surface-confined template polymerization reaction of aniline, driven by energy currency molecules (H_2O_2) and assisted by enzyme horseradish peroxidase isoenzyme C (HRPC). The blue region (R9) is the membrane growth domain, which incorporate AOT molecules from the environment to the vesicle membrane through the interaction with the information polymer of vesicles, PANI-ES. Biological systems synthesize membrane molecules by themselves before incorporating them into cell membrane (**Fig.1-1-1(a)** and **(b)**), however, my artificial metabolism does not synthesize membrane molecules but only incorporate them from the environment, for the sake of simplification of the system. The whole detailed chemical reactions are described in the following sections.

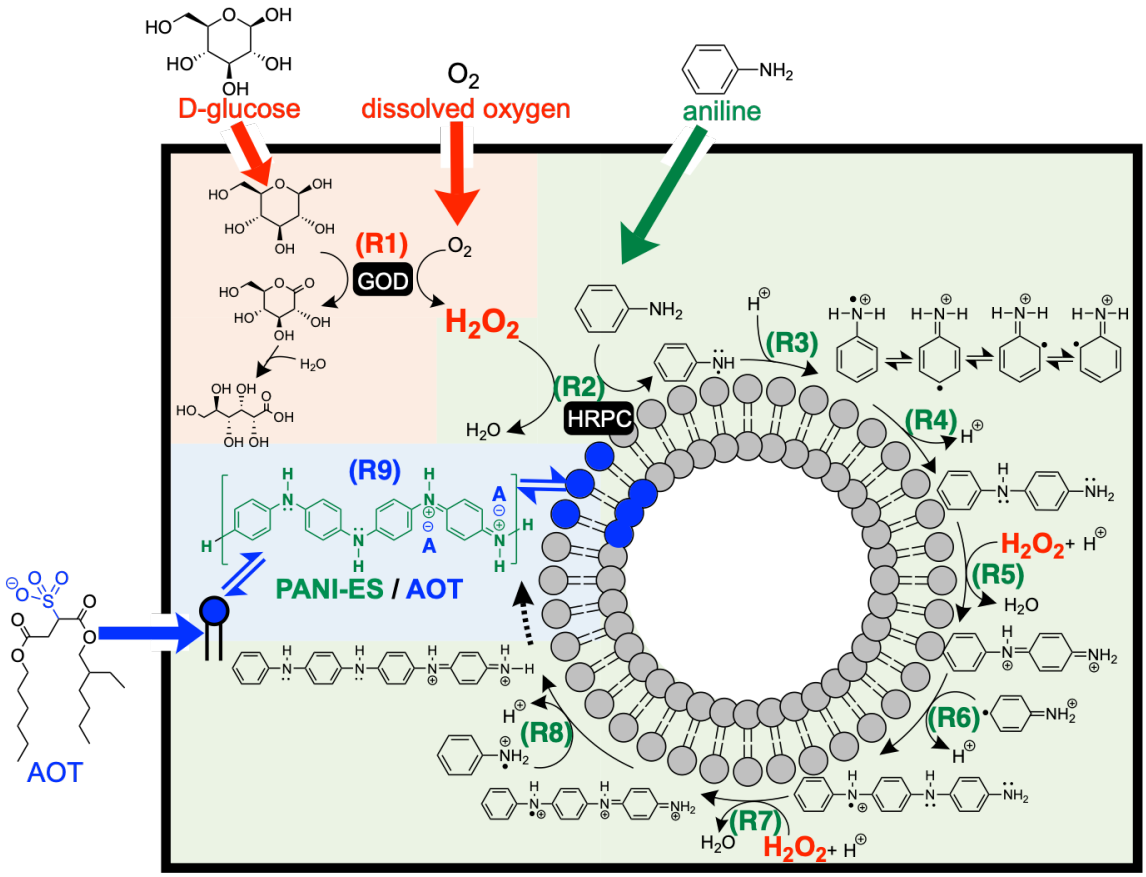

Figure 3-2-1. Scheme of artificial metabolism system, which shows the nine relevant reaction steps, (R1 – R9), in the essential three reaction domains; (red) energy currency production domain, (green) synthesis of information polymer domain, and (blue) membrane growth domain. The reactions in green and blue regions are vesicle-surface confined reactions. The bold rectangle represents the reaction system close to the vesicle surface, and bold arrows indicating inward represent that ingredients molecules are continuously supplied to the system by micro-injection technique. The PANI-ES structure is representatively shown as the bipolaron form, see also **Fig.2-2-3**. The detailed complete reaction sets consisting each reaction domain are shown in **Fig.3-2-2**, **Fig.3-2-3**, and **Fig.3-2-4** in the next section.

3.2.2 (R1) Energy Currency Production Domain

The detailed reaction process that produces H_2O_2, the "energy currency" in our synthetic minimal cell, is shown as (R1) and (R1a,b,c) in **Fig.3-2-2**. In 20 mM NaH_2PO_4 solution (pH=4.3), H_2O_2 is formed by oxidation of D-glucose with dissolved O_2 catalyzed by enzyme glucose oxidase (GOD) (R1). More specifically, the GOD-catalyzed formation of H_2O_2 is described as two elementary enzymatic processes and subsequent hydrolysis of byproduct as follows [Banker et al. 2009]: GOD in which its cofactor flavin adenine dinucleotide (FAD) is in the oxidized form (GOD-FAD) firstly reacts with one β-D-glucose molecule to yield one D-glucono-δ-lactone molecule and a glucose oxidase in which FAD is in the reduced form (GOD-$FADH_2$) (R1a). GOD-$FADH_2$ reacts with one dissolved O_2 molecule to yield one H_2O_2 molecule and GOD-FAD (R1b). The byproduct D-glucono-δ-lactone is hydrolyzed to D-gluconic acid (R9c). Overall, one dissolved O_2 molecule is reduced to one H_2O_2 molecule in a GOD cycle, while one β-D-glucose molecule is oxidized to form D-gluconic acid as a byproduct (R1).

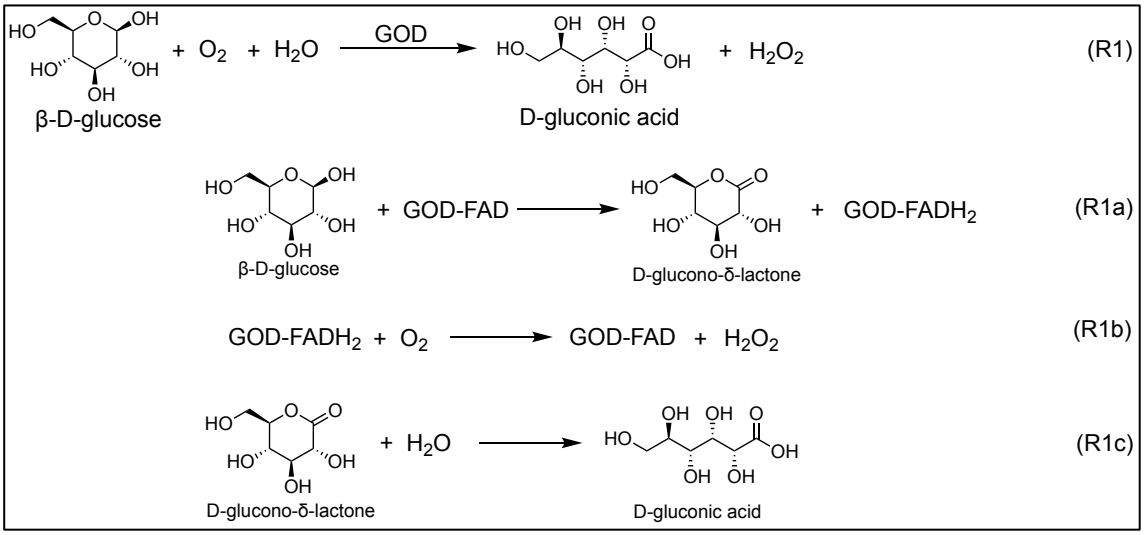

Figure 3-2-2. Reaction scheme of "energy production" domain, corresponding to (R1) in **Fig.3-2-1** red. The GOD-catalyzed formation of H_2O_2 (R1) is described as a GOD cycle to produce H_2O_2 (R1a,b) and subsequent hydrolysis of a byproduct (R1c). Typically, the initial reaction condition involves 100 mM D-glucose, 1.0 μM GOD, and dissolved O_2 in 20 mM NaH_2PO_4 solution (pH=4.3) with other reaction components for PANI-ES synthesis.

3.2.3 (R2 – R8) Information Polymer Synthesis Domain

Plausible reaction schemes for synthesizing polyaniline in its emeraldine salt form (PANI-ES) from aniline with HRPC and H_2O_2 are shown in **Fig.3-2-3** [Genies and Tsintavis 1985; Ding et al. 1999; Junker et al. 2012]. In the presence of AOT vesicle in NaH_2PO_4 solution (pH = 4.3), HRPC molecules and aniline molecules are extensively bound to the AOT vesicle surface via electrostatic interaction and hydrogen bonding [Guo et al. 2009 and 2011; Junker et al. 2015]. Therefore, the following reaction steps are considered to be localized on the AOT vesicle surface: The HRPC/H_2O_2-catalysed oxidation of aniline leads to the formation of the anilino radical (R2), which is represented as the peroxidase cycle of heme peroxidase involving native Fe(III) peroxidase, intermediate compound I with an Fe(IV) oxoferryl species with a cation radical, and compound II with an Fe(IV) oxoferryl species (R2a,b,c) [Dunfold 1999; Junker et al. 2013]. The anilino radical becomes protonated to the aniline radical cation (R3). While the unpaired electron of aniline radical cation can be localized either on the carbon atom in *para*-position (B), in one of the two *ortho*-position (C or D), or on the nitrogen atom (A), two aniline radical cations (A and B) react to form the NC-*para*-coupled aniline dimer (*p*-aminodiphenylamine, PADPA) in the presence of template vesicles (R4). Oxidation of PADPA with H_2O_2 yields the aniline dimer dication (N-phenyl-1,4-benzequinonediimine, PBQ (a)) (R5), which is in equilibrium with diradical dication form (PBQ (b)), then PBQ (b) and aniline radical cation (B) react to form aniline trimer radical cation (R6). After trimer radical cation is partially oxidized with H_2O_2 (R7), its another equilibrium form reacts with aniline radical cation (A) to form half-oxidized aniline tetramer dication that is a repeating unit of PANI-ES (R8). The overall stoichiometry of the reaction to obtain one repeating unit of PANI-ES is given at the bottom [Junker et al. 2012]. The distribution of the formed PANI-ES was confirmed to be localized almost homogeneously on the AOT GUV surface by the two-dimensional micro-Raman mapping technique (see **Fig.3-3-20**). The key feature in the reactions is the elongation of the PANI-ES chain realized by adding one aniline radical cation molecule to the oxidized radical cation of the growing PANI-ES chain.

HRPC: horseradish peroxidase isoenzyme C (enzyme)
$AOT_v^{\ominus}$: the surface of AOT vesicle membrane

Oxidation of aniline catalyed by HRPC:

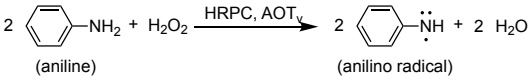

(R2)

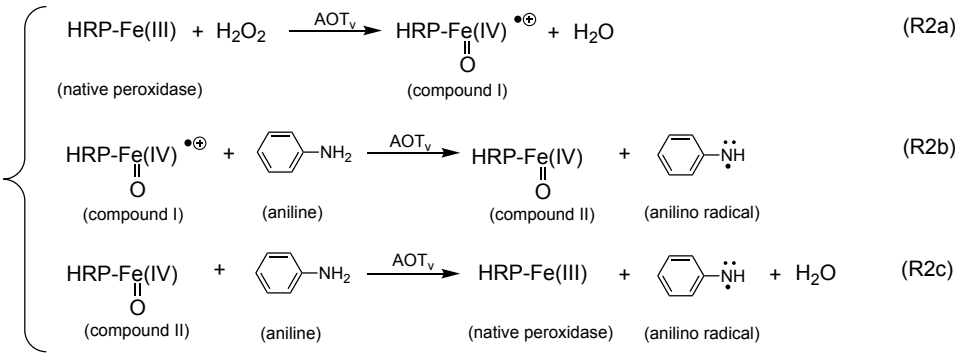

(R2a)

(R2b)

(R2c)

Protonation of anilne radical:

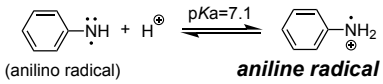

(R3)

aniline radical cation

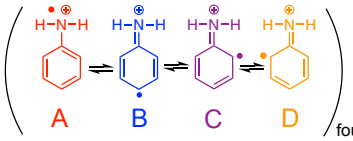

four resonance states

Formation of aniline dimer (PADPA):

(R4)

Oxidation of PADPA with H_2O_2:

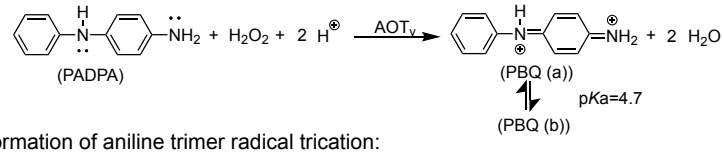

(R5)

Formation of aniline trimer radical trication:

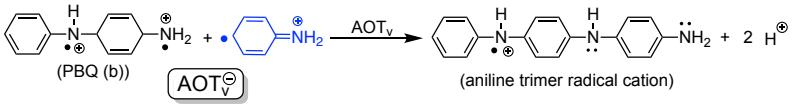

(R6)

Partial oxidation of aniline trimer radical cation:

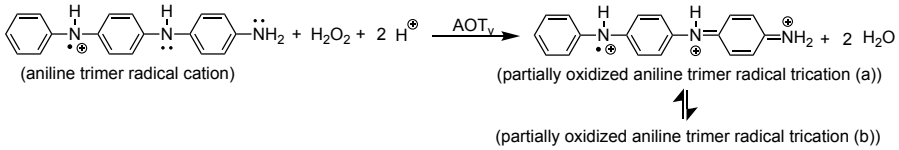

(R7)

Formation of half-oxidized aniline tetramer dication (repeating unit of PANI-ES):

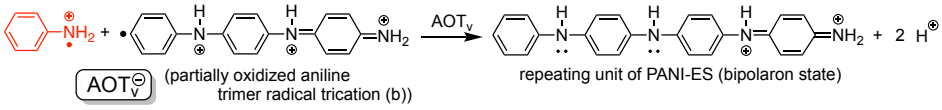

(R8)

Overall net reaction for the formation of PANI-ES repeating unit:

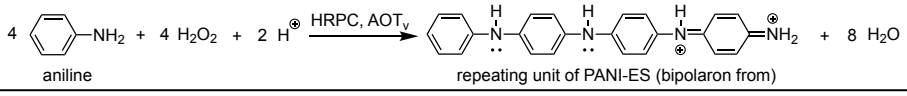

Figure 3-2-3. Plausible reaction schemes of "information molecule synthesis" domain, corresponding to (R2 -R8) in **Fig.3-2-1** green [Genies and Tsintavis 1985; Ding et al. 1999; Junker et al. 2012]. The HRPC-catalysed oxidation of aniline with H_2O_2 is described as the peroxidase cycle with native peroxidase and two intermediate compounds (R2a,b,c) [Dunfold 1999; Junker et al. 2013]. Typically, the initial reaction condition involves 3.0 mM AOT (vesicles), 4.0 mM aniline, 0.92 μM HRPC in 20 mM NaH_2PO_4 solution (pH=4.3) with other reaction components for GOD-catalysed H_2O_2 formation, such as 100 mM D-glucose and 1.0 μM GOD.

3.2.4 (R9) Membrane Growth Domain

Supposed molecular interactions between AOT molecules and PANI-ES formed on the surface of AOT vesicles are schematically shown in **Fig.3-2-4**. In 20 mM NaH_2PO_4 solution (pH=4.3) containing 3.0 mM AOT molecules, about 1.5 mM AOT molecules form vesicles, and another 1.5 mM AOT molecules are monodispersed in bulk solution (cvc~1.5 mM) [Kurisu et al. 2019]. When a small amount of 20 mM AOT micellar solution was externally supplied near AOT GUVs, the GUVs showed slight growth by uptake of supplied AOT molecules even without PANI-ES synthesis (**Fig.2-5-3(a)** #2 - #5). In addition, the growth of GUVs was extensively promoted when PANI-ES was formed on the surface of AOT GUVs (**Fig.2-5-3(a)** #1). However, when AOT micelles were not supplied or only a small amount of AOT micelles were supplied to the AOT GUVs during surface-confined PANI-ES synthesis, shrinkage or disappearance of AOT GUVs were observed in my previous work [Kurisu et al. 2019]. These results suggest the traffic of AOT molecules through the interaction with PANI-ES as follows:

$$A_m + P_n \rightleftarrows (A_m \bullet P_n) \rightleftarrows (P_n \bullet A_v^{out}) \rightleftarrows P_n + A_v^{out} \qquad \text{(R9)}$$

where A_m represents an AOT molecule monodispersed in bulk solution, A_v^{out} represents an AOT molecule located in the outer layer of the vesicle membrane, and P_n represents PANI-ES segments formed on AOT vesicle membranes. The second and third terms in (R9) represent supposed intermediate complex states composed of AOT molecules and PANI-ES through hydrogen bonding and electrostatic interactions [Junker et al. 2012; Foreman et al. 2003; Luginbühl et al. 2017]. When a small amount of AOT

micellar solution is externally supplied to AOT GUVs suspension without PANI-ES, the newly added AOT molecules closed to the GUVs (A_m) will be incorporated into preformed GUVs (A_v^{out}) (**Fig.3-2-4(a)**) or form new AOT vesicles. On the other hand, when PANI-ES is synthesized on the surface of AOT GUVs, PANI-ES is considered to play a role as a catalyst to promote the incorporation of AOT molecules (**Fig.3-2-4(b)**). The supposed mechanism is as follows: The adsorption of AOT molecules (A_m) to the surface of vesicles is promoted by the surface-confined PANI-ES (P_n) due to the formation of N-H•••O-S hydrogen bonding between PANI-ES and a hydrophilic head group of an AOT. Such a complex involving a hydrophilic head group of AOT ($A_m \bullet P_n$) will decrease the hydrophilicity of the adsorbed AOT molecules compared to the free AOT molecules (A_m), which is more advantageous for partitioning AOT molecules into the outer layers of vesicle membranes ($P_n \bullet A_v^{out}$) than the simple partitioning without PANI-ES (**Fig.3-2-4(a)**). The flip-flop rate of AOT molecules is considered to be much higher than that of phospholipids according to the outcome from MD simulations of AOT membrane [Junker et al. 2014 and 2015; Kashima et al. 2018] and experimentally observed higher fluidity [Iwasaki et al. 2017], which will result in the growth of vesicle membrane since the incorporated AOT molecules undergo flip-flop motions toward the inner monolayer. The shrinkage or disappearance of GUVs in control experiments, where PANI-ES (P_n) was formed on AOT membrane but AOT molecules (A_m) were not supplied enough, support this mechanism since the lack of free AOT molecules (A_m) in bulk solution under PANI-ES (P_n) formation will shift the equilibrium to the inverse direction of membrane growth.

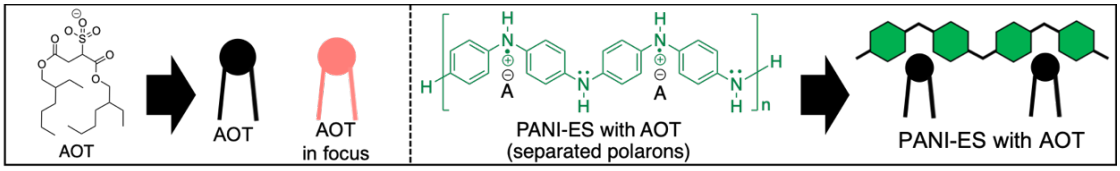

a: incorporation *without* PANI-ES

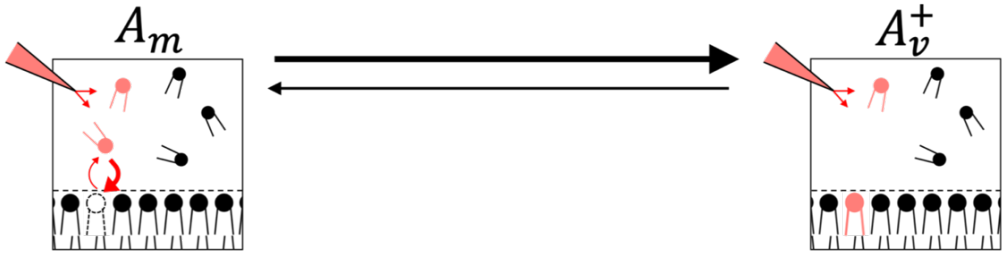

b: incorporation *with* PANI-ES

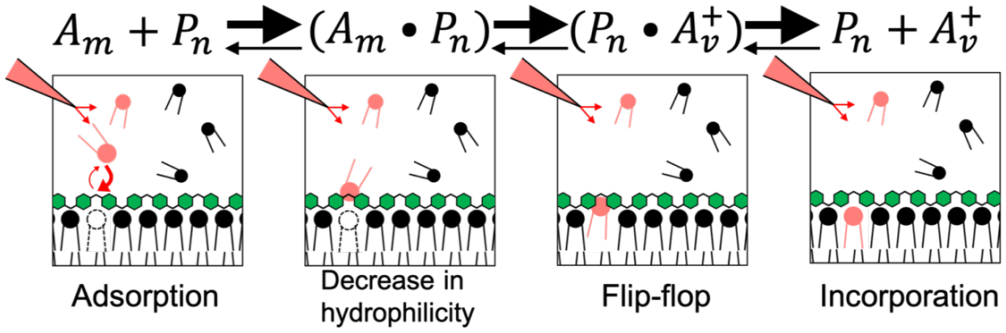

Figure 3-2-4. Supposed molecular mechanism of membrane growth of AOT GUVs coupled with surface-confined PANI-ES formation.

(a) Plausible molecular mechanism of AOT membrane growth observed in the control experiments in which PANI-ES is not formed on the surface of AOT GUVs. When a small amount of AOT micelles (in water) are supplied close to AOT GUVs (in 20 mM NaH_2PO_4 solution (pH=4.3), cvc~1.5 mM), the supplied AOT molecules will be incorporated into the preformed GUVs, or form new vesicles.

(b) Supposed molecular mechanism of AOT membrane growth coupled with the surface-confined formation of PANI-ES observed. The PANI-ES on the surface of AOT GUVs will promote adsorption of free AOT molecules in the external solution and decrease the hydrophilicity of AOT molecules due to the formation of hydrogen bonding between them. This will promote AOT molecules to partition into the outer layer of AOT GUVs.

3.3 (Experiment) Introduction of Energy Currency Production Domain

3.3.1 Materials

Amphiphiles used for vesicle preparation.

AOT (sodium bis-(2- ethylhexyl) sulfosuccinate, purity > 99%, Catalogue No. 86139) and SDBS (sodium dodecylbenzenesulfonate, hard type (mixture), >95%, No. D0990) were purchased from Sigma- Aldrich Japan (Tokyo, Japan) and Tokyo Chemical Industry (Tokyo, Japan), respectively. DOPC (1,2-dioleoyl-sn-glycero-3-phosphocholine, >99%, No. 850375) and cholesterol (from ovine wool, >98%, No. 700000) were purchased from Avanti Polar Lipids, Inc. (AL, USA). The amphiphiles were used without further purification and dissolved in chloroform at 100 mM (AOT) or at 10 mM (others) and stored at −20 °C as stock solutions.

Reagents for the polymerization of aniline.

Aniline (> 99%), hydrogen peroxide (H_2O_2) (30% in water, ~9.8 M), sodium dihydrogen phosphate (NaH_2PO_4) dihydrate (> 99%), and d(+)-glucose (> 99%), chloroform ($CHCl_3$, > 99%), acetonitrile (CH_3CN, > 98%) and perchloric acid ($HClO_4$, 60% in water), phosphoric acid (H_3PO_4, > 85%) were purchased from Wako Pure Chemical Industries (Osaka, Japan). 2,2′-azino-bis(3-ethylbenzothiazoline- 6-sulfonic acid) diammonium salt ($ABTS^{2-}(NH_4^+)_2$, > 98%) was purchased from Sigma-Aldrich. Oxo[5,10,15,20-tetra (4-pyridyl) porphyrinato] titanium (IV) (> 90.0%) was purchased from Tokyo Chemical Industry (Tokyo, Japan). Horseradish peroxidase isoenzyme C (HRPC, Grade I, PEO-131, 286 U/mg, RZ = 3.13, M ~ 40 kDa, Lot No. 74590) and glucose oxidase from *Aspergillus* sp. (GOD, Grade II, GLO-201, 166 U/mg, SA = 205, M ~ 153 kDa, Lot No. 74180) were purchased from Toyobo Enzymes (Osaka, Japan). The concentration of HRPC and GOD were determined spectrophotometrically using known molar absorptivity ε_{403}(HRPC) = 1.02×10^5 $M^{-1}cm^{-1}$ [Dunfold and Stillman 1976] and ε_{450}(GOD) = 2.82×10^4 $M^{-1}cm^{-1}$ [Swoboda and Massey 1965] as molar absorbance. Ultrapure water purified with a Direct-Q 3 UV apparatus (Millipore, USA) was used to prepare all aqueous solutions and suspensions. All other chemicals used were of research grade. 20 mM or 100 mM dihydrogen phosphate solutions were prepared using NaH_2PO_4, water, and small amounts of H_3PO_4 to obtain pH = 4.3.

3.3.2 Preparation of Template Vesicles

Preparation of LUVs.

AOT large unilamellar vesicles (LUVs) with an average diameter ~80-100 nm were prepared by using the freezing-thawing extrusion method [Junker, K. et al. (2012); Kurisu, M. et al. (2019) & (2021)] to characterize the products obtained in the polymerization of aniline in the presence of vesicles from homogeneous reaction mixtures. Firstly, solid AOT (89.0 mg) was added to a 250 mL round bottom flask and dissolved in 5 mL chloroform. Then, a thin AOT film was prepared on the inner surface of the flask by using a rotary evaporator. The AOT film was put under a high vacuum overnight to remove chloroform completely. The AOT film was hydrated and dispersed by using 10 mL of a 100 mM NaH_2PO_4 solution (pH=4.3), of a 100 mM NaH_2PO_4 containing 100 mM D-glucose solution (pH=4.3), of a 20 mM NaH_2PO_4 solution (pH=4.3), or of a 20 mM NaH_2PO_4 containing 100 mM D-glucose solution (pH=4.3). The hydration temperature was $T \sim 25^{\circ}C$, and the hydration duration was $t \sim 2$ h. The obtained 20 mM AOT vesicle dispersions were frozen by placing the round bottom flask in liquid nitrogen and then thawed in a water bath heated to 60˚C. This procedure was repeated ten times. The repetitive freeze-thaw cycles are efficient to change the lamellarity of vesicles from multilamellar vesicles (MLVs) into unilamellar vesicles by removing interlamellar water and also efficient to cause fusion of small unilamellar vesicles (SUVs) into larger unilamellar vesicles [Traïkia et al. 2000; Kaasgaard et al. 2003]. Consequently, unilamellar vesicles become relevant and smaller vesicles (< 80 nm) are removed in the AOT vesicle dispersions. Then, the suspensions were extruded ten times through 200 nm pore size nucleopore polycarbonate membranes and another ten times through 100 nm pore size membranes by using LIPEX^{TM} Extruder (Northern Lipids Inc., Canada). The obtained AOT LUVs were characterized by dynamic light scattering (DLS), which showed that AOT LUVs prepared in 20 mM NaH_2PO_4 solution (pH=4.3) had an average hydrodynamic diameter of about 80 nm with a polydispersity of about 0.1 [Kurisu et al. 2019]. The AOT LUVs suspensions were stored at 25 ˚C and used within seven days.

5 mM phospholipids DOPC LUVs was prepared by using 100 mM NaH_2PO_4 solution (pH=4.3), 100 mM NaH_2PO_4 containing 100 mM D-glucose solution (pH=4.3), 20 mM NaH_2PO_4 solution (pH=4.3), or 20 mM NaH_2PO_4 containing 100 mM D-glucose solution (pH=4.3) with the similar procedure described above. Firstly, 2 mL of vesicle suspension (5 mM amphiphiles) were prepared in 5 mL glass vials using the gentle hydration method. Then, the obtained suspensions were frozen and thawed in liquid nitrogen and a water bath heated to 60˚C, respectively. After ten freeze/thaw cycles, the vesicle suspensions

were extruded 21 times through a 100 nm pore-sized Nucleopore polycarbonate membrane using a Mini Extruder set (Avanti Polar Lipids, Inc., USA). The LUVs suspensions were stored at 25 ˚C and used within seven days.

Preparation of GUVs.

Giant unilamellar vesicles (GUVs) composed of AOT were prepared by using the gentle hydration method [Reeves, J.P. & Dowben, R.M. 1969] by using the solution containing 20 mM NaH_2PO_4 (pH=4.3). Firstly, AOT (17.8 mg) was dissolved in 1 mL chloroform in a 5 mL glass vial, followed by the formation of a thin AOT film upon removal of chloroform with a rotary evaporator. Then, the AOT film was put under a high vacuum overnight to remove chloroform completely. The dried AOT film was hydrated and dispersed at 60 ˚C for 1-2 h with 2.0 mL of 20 mM NaH_2PO_4 solution (pH = 4.3) or with a 2.0 mL of 20 mM NaH_2PO_4 solution containing 100 mM of D-glucose, or of sucrose (pH = 4.3). This resulted in the formation of AOT GUVs with radii of 5-30 μm. The obtained 20 mM AOT GUV suspensions were stored at 25 ˚C and used within two days after preparation. Please note that this procedure is optimized to prepare 20 mM AOT GUVs suspension in the presence of 20 mM NaH_2PO_4 and that we could not prepare AOT GUVs in a similar way in the presence of 100 mM NaH_2PO_4, the different cvc condition for AOT.

Binary GUVs of AOT/Chol (9/1, molar ratio, 5.0 mM in total) were prepared almost the same way as described above from the chloroform solutions containing the two amphiphiles in appropriate molar ratio. The differences are that the amphiphile concentration was not 20 mM but 5.0 mM and that AOT/Chol dried film was hydrated at 60 ˚C for 15-20 min. Please note that stable AOT/Chol GUVs could not be prepared when the concentration of Chol was above 10 mol%, according to my attempts.

Cvc determination of AOT.

The critical concentration for vesicle formation (cvc) of AOT in 100 mM NaH_2PO_4 solution (pH=4.3), and in 100 mM NaH_2PO_4 containing 100 mM D-glucose solution (pH=4.3) were estimated by turbidity measurement [Guo et al. 2011]. First, 20 mM AOT vesicle suspensions were prepared using the gentle hydration method [Reeves, J.P. & Dowben, R.M. 1969]. Solid AOT (89.0 mg) was added to a 250 mL round bottom flask

and then dissolved in 5 mL chloroform, followed by the formation of a thin AOT film upon removal of chloroform with a rotary evaporator. The AOT film was put under a high vacuum overnight to remove chloroform completely. The AOT film was then hydrated for ~2 h at $T \sim 60^{\circ}C$ by using 10 mL of a 100 mM NaH_2PO_4 solution (pH=4.3), or of 100 mM NaH_2PO_4 containing 100 mM D-glucose solution (pH=4.3). Then, the obtained 20 mM AOT vesicle suspensions were extruded five times through 200 nm pore size nucleopore polycarbonate membranes, followed by the dilution with each solution to different desired AOT concentrations. After incubation for 24 h at $T \sim 25^{\circ}C$, the turbidity of each solution with different AOT concentrations was determined. Absorbance at the arbitrarily chosen wavelength $\lambda = 400$ nm, A_{400}, was measured for each diluted sample by using a V-730 spectrophotometer (JASCO, Japan), and quartz cells with an optical path length of $L = 1$ mm. The A_{400} values were plotted against AOT concentrations. The cvc values of AOT in each solution were taken as the lowest AOT concentrations at which A_{400} clearly deviated from zero (~ 0.4 mM for 100 mM NaH_2PO_4 solution (pH=4.3) and 100 mM NaH_2PO_4 / 100 mM D-glucose solution (pH=4.3)), see Appendix 3-A. For more on the concept of cvc, see also section 2.4.2.

Preparation of micellar solutions.

AOT micellar solutions containing 100 mM D-glucose were prepared for the micro-injection experiments. 20 mM AOT micellar solutions were prepared by simply dissolving solid AOT (17.8 mg) in 2.0 mL of deionized water or in 2.0 mL of 100 mM D-glucose solution at room temperature ($T \sim 25\ ^{\circ}C$) with a vortex mixer. The obtained micellar solutions were stored at 25 ˚C and used within two days after preparation. All micellar solutions were pressed through a 0.2 mm polypropylene filter (Puradisc 25 PP, from GE Healthcare UK Ltd., England) before being loaded into the micro-injection tip.

3.3.3 Protocols for Template Polymerization of Aniline

Enzymatic cascade polymerization of aniline with D-glucose, GOD, dissolved O_2, and HRPC in the presence of LUVs (in *100 mM* NaH_2PO_4 solution)

I newly elaborated this reaction condition [Kurisu et al. 2021]. Before elaborating the reaction conditions in *20 mM* NaH_2PO_4 solution (pH=4.3), I first elaborated the optimal reaction condition in *100 mM* NaH_2PO_4 solution (pH=4.3), which is the widely used buffer concentration. The optimal concentrations of D-glucose and GOD for *in situ* formation of H_2O_2 that triggers the reaction were investigated by using the following protocols. All components of the reaction mixture, except the GOD solution, were added to 300 μL of 100 mM NaH_2PO_4 solution (pH=4.3) containing defined concentrations of D-glucose: 75 μL LUV suspension (20 mM in 100 mM NaH_2PO_4 solution containing a defined concentration of D-glucose), 50 μL aniline solution (40 mM in 100 mM NaH_2PO_4 solution, pH adjusted to 4.3 with H_3PO_4), 25 μL HRPC solution (18.4 μM in 100 mM NaH_2PO_4 solution, pH=4.3). After gentle mixing, the reaction was triggered by quick addition of 50 μL of a GOD solution of defined GOD concentration (prepared in 100 mM NaH_2PO_4 solution, pH=4.3), followed by gentle mixing and closure of the caps of the reaction tubes and sealing with Parafilm to avoid leakage of solution and air exchange. The tubes were then placed in a rotary mixer Magic Mixer TMM with an LH15x22 rack (KENIS, Japan) and continuously rotated at ~90 rpm during the reaction (**Fig.3-3-1**). The initial reaction condition was as follows: 3.0 mM AOT, 4.0 mM aniline, 0.92 μM HRPC and defined concentrations of GOD, and D-glucose in 100 mM NaH_2PO_4 solution (pH=4.3), reaction volume=0.50 mL, T~25˚C, t =24 h. The desired D-glucose concentration in the prelaid 300 μL D-glucose solution was obtained by mixing defined volumes of a D-glucose stock solution (prepared in 100 mM NaH_2PO_4, pH=4.3) of either 250 mM or 1 M and an appropriate volume of 100 mM NaH_2PO_4 solution (pH=4.3). The D-glucose stock solutions were prepared at least 24 h before use to allow D-glucose to reach equilibrium between the α- and β-forms.

Finally, the optimal reaction condition for the PANI-ES synthesis with enzymatic cascade reaction was found to be as follows (**Table 3-3-1**): 3.0 mM AOT, 4.0 mM aniline, 0.92 μM HRPC, 0.20 μM GOD, and 100 mM D-glucose in 100 mM NaH_2PO_4 solution (pH=4.3), reaction volume=0.50 mL, T=25˚C, t =24 h. See the Appendix 3-B, for the determination of the optimal reaction condition.

Table 3-3-1. Reaction condition for PANI-ES synthesis, which was first elaborated by using widely used NaH_2PO_4 concentration for the PANI-ES synthesis, 100 mM. PANI-ES is synthesized from aniline with HRPC, GOD, D-glucose, and dissolved oxygen in the presence of AOT LUVs as templates at $T \sim 25$ ˚C for a reaction time of $t = 24$ h.

Component	Concentration
AOT (LUVs)	3.0 mM
Aniline	4.0 mM
D-Glucose	100 mM
GOD	0.20 μM
HRPC	0.92 μM
$NaH_2PO_4 + H_3PO_4$	100 mM
H_3O^+	$10^{-4.3}$ M = 50 μM (pH = 4.3)

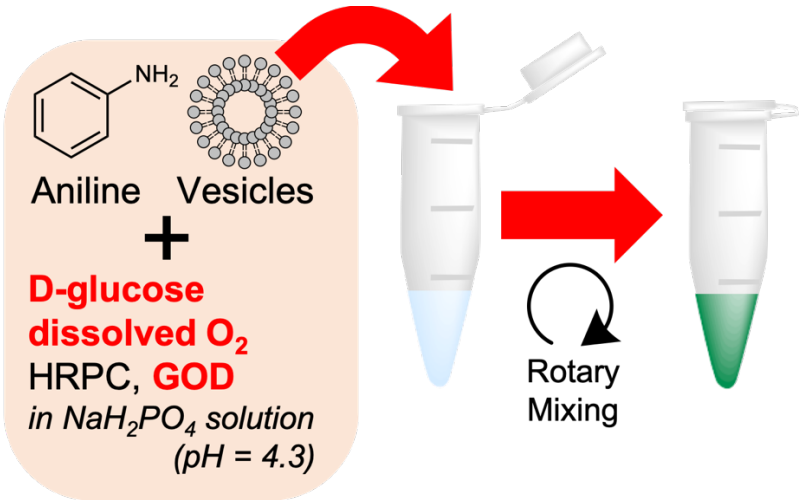

Figure 3-3-1. Scheme summarizing the protocol of the PANI-ES synthesis by introducing energy currency production domain (R1). See also **Table 3-3-1** and **3-3-2**, for the concentrations of reaction components.

Enzymatic cascade polymerization of aniline with D-glucose, GOD, dissolved O_2, and HRPC in the presence of LUVs (in *20 mM* NaH_2PO_4 solution, pH=4.3).

This reaction condition is just an extension of the just above reaction condition in *100 mM* NaH_2PO_4 (**Table.3-3-1**) to the appropriate condition for AOT GUV preparation in 20 mM NaH_2PO_4 (**Table.3-3-2**). To obtain a homogeneous reaction mixture, we still use AOT LUVs in 20 mM NaH_2PO_4 (pH=4.3). Another difference from (**Table.3-3-1**) is that the concentration of GOD is increased from 0.20 μM to 1.0 μM for the better yield of the PANI-ES products. All components of the reaction mixture, except the GOD solution, were added to 216.7 μL of 20 mM NaH_2PO_4 solution (pH=4.3) containing 100 mM D-glucose: 75 μL LUV suspension (20 mM in 20 mM NaH_2PO_4 solution containing 100 mM D-glucose), 50 μL aniline solution (40 mM in 20 mM NaH_2PO_4 solution, pH adjusted to 4.3 with H_3PO_4), 25 μL HRPC solution (18.4 μM in 20 mM NaH_2PO_4 solution, pH=4.3), and 83.3 μL D-glucose solution (250 mM in 20 mM NaH_2PO_4 solution, pH=4.3). After gentle mixing, the reaction was triggered by quick addition of 50 μL GOD solution (10 μM in 20 mM NaH_2PO_4 solution, pH=4.3), followed by gentle mixing and closure of the caps of the reaction tubes and sealing with Parafilm. The tubes were then placed in a rotary mixer Magic Mixer TMM with an LH15x22 rack (KENIS, Japan) and continuously rotated at ~90 rpm during the reaction (**Fig.3-3-1**). The initial reaction condition was as follows: 3.0 mM AOT, 4.0 mM aniline, 0.92 μM HRPC, 1.0 μM GOD, 100 mM D-glucose, and dissolved oxygen in 20 mM NaH_2PO_4 solution (pH=4.3), reaction volume=0.50 mL, T=25˚C.

Table 3-3-2. Reaction condition for the PANI-ES synthesis including energy production domain (R1), which is actually adopted for the artificial metabolism system. The concentration of NaH_2PO_4 solution (pH=4.3) is changed from 100 mM (**Table.3-3-1)** to 20 mM for the formation of AOT GUVs, and the concentration of GOD is changed from 0.20 μM to 1.0 μM for the better yields. PANI-ES is synthesized from aniline with HRPC, GOD, D-glucose, and dissolved oxygen in the presence of AOT LUVs as templates in 20 mM NaH_2PO_4 solution at $T \sim 25$ ˚C for a reaction time of $t = 24$ h.

Component	Concentration
AOT	3.0 mM
Aniline	4.0 mM
D-Glucose	100 mM
GOD	1.0 μM
HRPC	0.92 μM
$NaH_2PO_4 + H_3PO_4$	20 mM
H_3O^+	$10^{-4.3}$ M = 50 μM (pH = 4.3)

3.3.4 Characterization Methods of Reaction Product

UV/Vis/NIR absorption measurement.

Absorption measurements in the UV/Vis/NIR region of the spectrum were carried out with a V-730 spectrometer (JASCO, Japan) at 25 ˚C, using quartz cuvettes S15-UV-1 (GL Sciences Inc., Japan) with L=0.1 cm optical path length [Junker et al. 2012; Kurisu et al. 2019 and 2021].

EPR absorption measurement.

Electron paramagnetic resonance (EPR) measurements of the reaction mixtures were with a Bruker EMX X-band spectrometer equipped with a TM cavity. The spectra were measured at X-band microwave frequency with a modulation frequency of 100 kHz and modulation amplitudes of 1 G at room temperature [Junker et al. 2012; Kurisu et al. 2021].

Confocal micro-Raman spectroscopy.

Raman spectra were obtained by an inVia QONTOR Raman spectrometer (Renishaw, UK), equipped with a diode-pumped solid-state laser (532 nm, 50 mW), an optical microscope, and a CCD detector. The Raman spectra of the reaction mixtures obtained in the presence of AOT LUVs or DOPC LUVs were collected in non-confocal mode with an objective (N Plan L50x, NA=0.50 (Leica, Germany)). The reaction mixtures were placed in a holed silicone rubber sheet on a borosilicate glass slide (**Fig.3-3-2(a)**). The hole had a diameter of 12 mm and a depth of 1 mm. The exposure time for one measurement run was 1.0 sec and accumulation of 30 runs with ~15 mW laser power on the sample stage.

Two-dimensional micro-Raman mapping was performed to confirm PANI-ES distribution in the reaction mixture obtained in the presence of AOT GUVs, using the characteristic $\nu(C{\sim}N^{\bullet+})_p$ peak at ~1345 cm^{-1} due to the delocalized polarons of PANI-ES. The reaction mixtures prepared with AOT GUVs were loaded into a narrow borosilicate glass tube VitroTubes (#5001) (path length = 10 μm, width = 100 μm) (VitroCom, USA) (**Fig.3-3-2(b)**). The end of the glass tube was immersed into the reaction mixture containing AOT GUVs, and then the reaction mixture was fully taken up to the other end of the glass tube by the Laplace pressure. Both ends of the tubes were sealed with Capillary Wax (HR4-328) (Hampton Research, USA) heated to ~90 ˚C. Then, the glass tube was placed onto the bottom of a glass-bottom dish D11130H (Matsunami, Japan)

filled with ~3 mL water. Here the AOT GUVs covered with PANI-ES were confirmed to be loaded inside the glass tube by being stacked with slight deformation (**Fig.3-3-2(b)** center). Finally, Raman mapping of an AOT GUV with PANI-ES was performed in confocal mode with a water immersion objective (C-Apochromat 100x, NA=1.25 (Carl Zeiss, Germany)). The laser spot size was 520 nm in diameter and 680 nm in depth. The laser was focused on a GUV with a diameter of ~10 μm, immobilized in the tube. The target GUV was horizontally translated by a piezoelectric stage with a 0.5 μm step in both x and y directions, and ~680 points Raman spectra were collected in total. The exposure time was 30 sec per point with ~1.5 mW laser power on the sample stage, and it took ~ 6 h to complete the entire scanning of the target AOT GUV. All obtained spectra were baseline corrected. Please note that the exposure time, laser power, and mapping step must be carefully selected before measurement; otherwise, the laser will burn the target GUV while mapping. In addition, when the target GUV is not completely immobilized in the glass tube, the GUV might float during mapping since the focused laser attracts the membrane [Cherney et al. 2004].

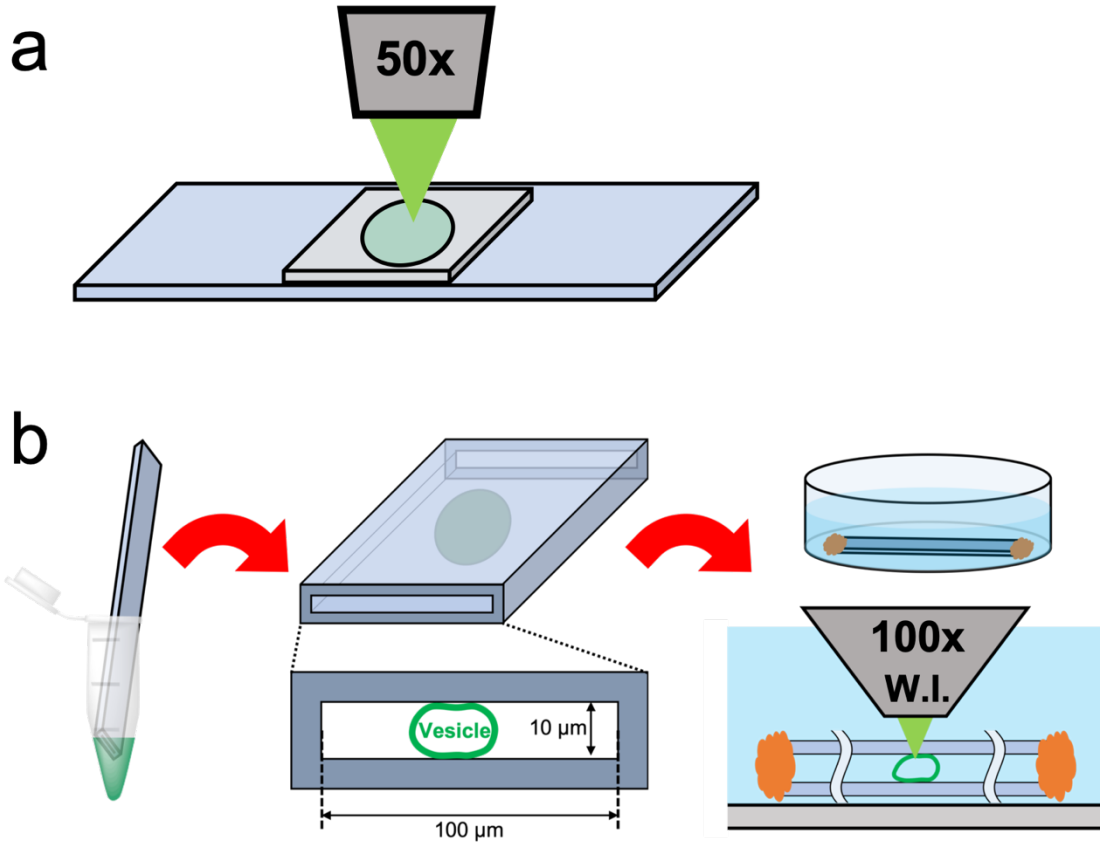

Figure 3-3-2. Scheme of sample preparation in the Raman spectrum measurements. **(a)** Scheme of Raman spectrum measurements of the reaction mixture obtained in the presence of LUVs. The reaction mixture was placed on the holed silicone sheet chamber with a diameter of 12 mm and a depth of 1.0 mm. **(b)** Scheme of micro-Raman mapping of AOT GUVs covered with PANI-ES. (Left): The reaction mixture containing AOT GUVs was loaded in a narrow glass tube by immersing the end of the tube into the reaction mixture. (Middle): The AOT GUVs were immobilized inside a glass tube with slight deformation. (Right): Both ends of the glass tube were sealed with wax, then the tube was placed at the bottom of a dish filled with water. The Raman spectra were collected with a water immersion objective.

3.3.5 Quantification of the Reaction Kinetics.

Quantification of aniline and H_2O_2 during the reaction.

The methods to determine the amounts of remaining aniline and H_2O_2 in the reaction mixture were developed by Junker et al. [Junker et al. 2012]. To quantify the remaining amounts of aniline, 30 µL of the reaction mixture was withdrawn and added to 1470 µL acetonitrile in a 2 mL polypropylene Eppendorf tube. After centrifugation to remove the reaction products, the UV/Vis/NIR absorption spectrum of the supernatant solution containing extracted aniline was measured. From the characteristic absorption intensity of aniline at λ = 238 nm (A_{238}), the concentration of aniline was calculated from the molar absorbance, ε_{238} (aniline) = 1.01 x 10^4 M^{-1} cm^{-1}, which was determined from a calibration curve prepared with known amounts of aniline (**Fig.2-3-2**). This molar absorbance agreed well with the value determined previously by Rajendiran and Swaminathan (0.955 x 10^4 M^{-1} cm^{-1}) [Rajendiran & Swaminathan 1996]. The reaction yield was defined based on the amount of remaining aniline against the amount before initiating the reaction.

To quantify the H_2O_2 concentration in the reaction mixture, the Ti-TPyP assay developed by Takamura et al. was used [Matsubara et al.1992; Takamura & Matsubara 2003; Takamura & Matsumoto 2009]. This is a spectrophotometric method based on the reaction between added oxo[5,10,15,20-tetra (4-pyridyl) porphyrinato] titanium(IV) (Ti-TPyP) and H_2O_2 present in the reaction mixture (**Fig.3-3-3**). The procedure was as follows: 125 µL of diluted or undiluted reaction mixture was added to 125 µL of a 4.8 M perchloric acid solution in a 2 mL polypropylene Eppendorf tube. Afterward, 125 µL of a Ti-TPyP solution (50 µM in 50 mM HCl) was quickly added. After gentle mixing and waiting for 5 min at T ~ 25 °C, 875 µL of water was added, followed by centrifugation. The absorption intensity at λ = 432 nm (A_{432}) of the supernatant solution was measured, then this value was compared to the value from a blank sample that did not contain H_2O_2. The concentration of H_2O_2 was calculated from a calibration curve (**Fig.3-3-4(a)** and **(b)**) which was obtained by plotting $\Delta A_{432} = A_{432}$ (blank) - A_{432} (sample) with known amounts of H_2O_2.

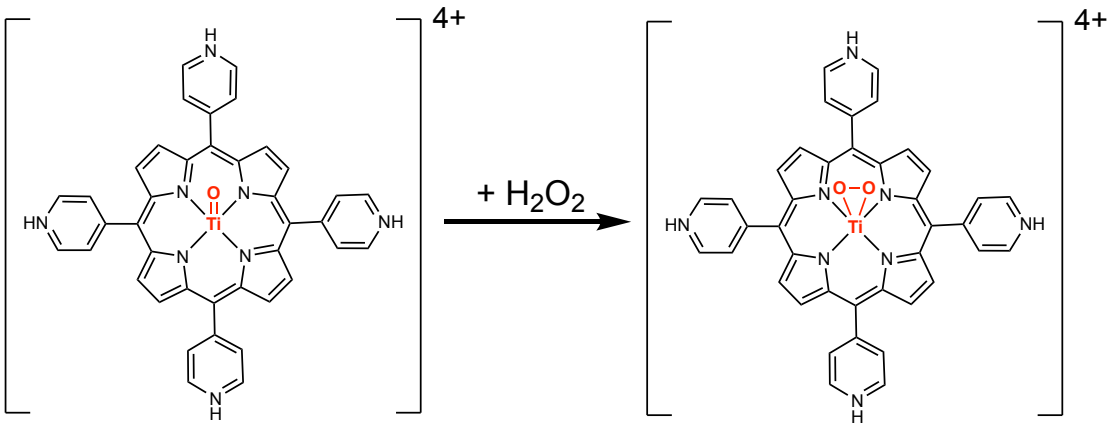

Figure 3-3-3. Reaction of the Ti-TPyP reagent with H_2O_2 to form the monoperoxo complex, $TiO_2(tpypH_4)^{4+}$, which shows the shift of characteristic absorbance, see also **Fig.3-3-4(a)**.

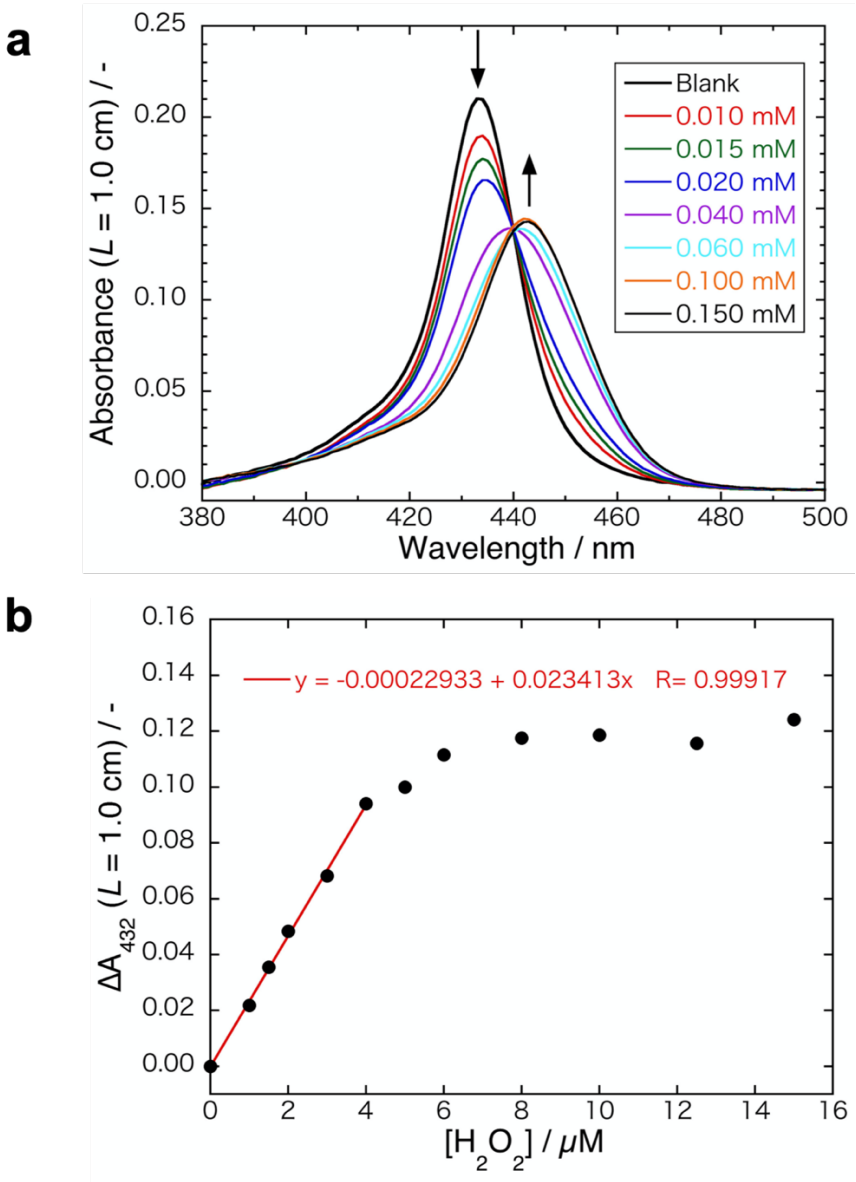

Figure 3-3-4. Calibration curve for the quantification of H_2O_2 with the Ti-TPyP assay. **(a)** Absorption spectrum of the assay solution was measured as a function of known H_2O_2 concentration in the sample solution (0 ("Blank") → 0.150 mM). The arrows indicate the changes in the spectrum with the increase in H_2O_2 concentration. **(b)** Measured values of $\Delta A_{432} = A_{432}$ (blank) - A_{432} (sample) based on the results of (a) are plotted as a function of H_2O_2 concentration in the cuvette. To obtain a calibration curve for the concentration of H_2O_2, a linear fit was made between $[H_2O_2] = 0$ and 4.0 μM.

Determination of the HRPC activity during the reaction.

The activity of HRPC in the reaction mixtures was determined spectrophotometrically by using $ABTS^{2-}$ as a reducing substrate and H_2O_2 as an oxidant in 10 mM MOPS buffer solution (pH = 7.0) according to the protocol developed by Ghéczy et al. [Ghéczy et al. 2016]. Oxidation of $ABTS^{2-}$ with HRPC and H_2O_2 yields a stable radical $ABTS^{\bullet-}$ with the transition of absorption maximum from at $\lambda = 340$ nm to at $\lambda = 414$ nm (**Fig.3-3-5**) [Childs & Bardsley 1975]. The following solutions were added in the sequence to a quartz cuvette (L = 1 mm) at $T \sim 25$ °C, followed by measuring the increase rate of absorption intensity at λ = 414 nm (A_{414}) during the first 60 s: 960 µL MOPS buffer solution (10 mM, pH = 7.0), 10 µL reaction mixture containing HRPC, 20 µL $ABTS^{2-}$ solution (50 mM in MOPS buffer solution, pH = 7.0), and finally 10 µL H_2O_2 solution (20 mM in water). After gentle mixing, the linear absorption increase rate $\Delta A_{414}/\Delta t$ was considered as a measure for the activity of HRPC withdrawn from the reaction mixture. The calibration curve was obtained using known amounts of HRPC (**Fig.3-3-6**). The initial substrate concentrations were $[ABTS^{2-}]_0$ = 1.0 mM and $[H_2O_2]_0$ = 0.2 mM, and the total assay volume was 1.0 mL.

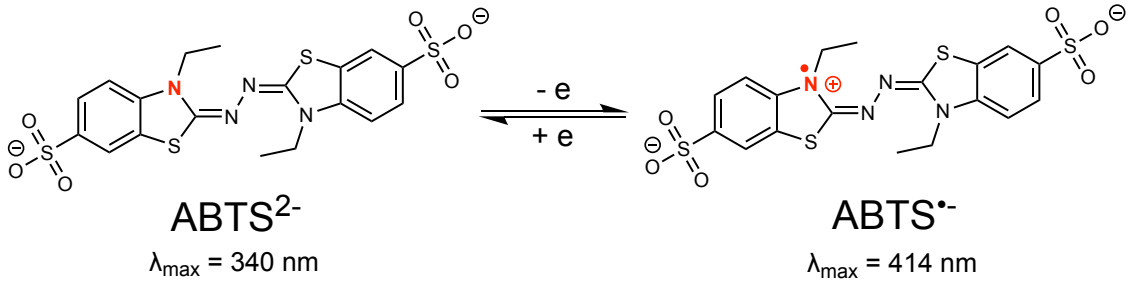

Figure 3-3-5. Reaction of the $ABTS^{2-}$ reagent with HRPC and H_2O_2, which shows the shift of characteristic absorbance and used for HRPC activity measurements.

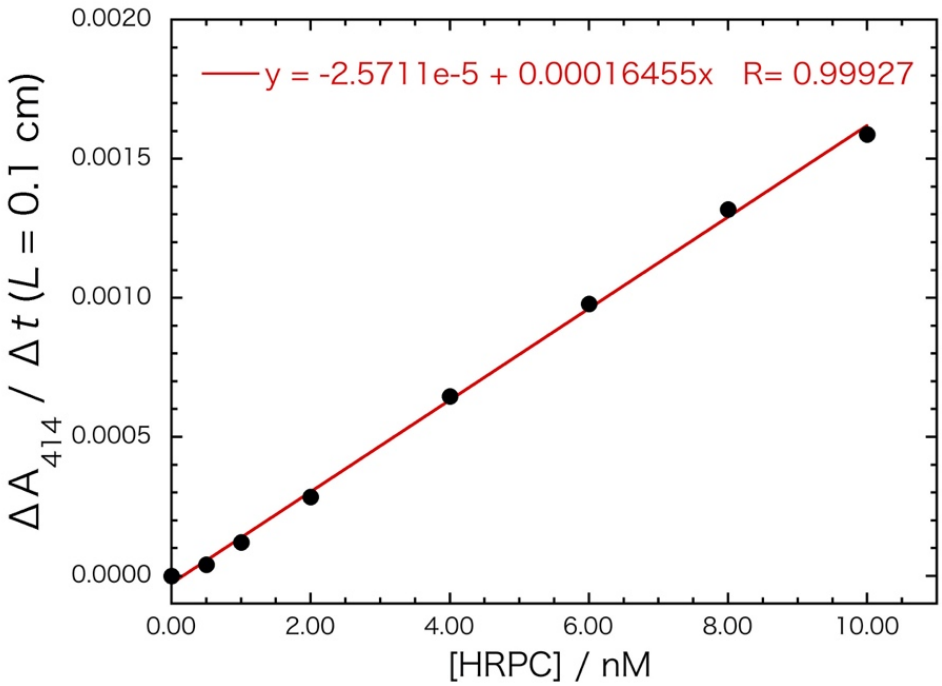

Figure 3-3-6. Calibration curve for the determination of HRPC activity.
The calibration curve was obtained by measuring the initial oxidation rate of $ABTS^{2-}$ with known amounts of HRPC in the presence of a fixed initial concentration of $ABTS^{2-}$ and H_2O_2. The HRPC activity was expressed as $\Delta A_{414} / \Delta t$ for the first 60 sec after starting the reaction. $[ABTS^{2-}]_0$ = 1.0 mM and $[H_2O_2]_0$ = 0.2 mM. The red line represents the linear fit.

Determination of the GOD activity during the reaction.

The activity of GOD in the reaction mixtures was determined spectrophotometrically with D-glucose and $ABTS^{2-}$ in 10 mM MOPS buffer (pH = 7.0) according to the protocol developed by Ghéczy et al. [Ghéczy et al. 2016] with slight modifications. The following solutions were added in the sequence to a quartz cuvette (L = 1 mm) at T ~ 25 °C, followed by measuring the increase rate of absorption intensity at λ = 414 nm (A_{414}) during the first 180 s: 865 µL MOPS buffer solution (10 mM, pH = 7.0), 10 µL reaction mixture

containing GOD, 5 μL HRPC solution (20 μM in MOPS buffer solution, pH = 7.0), 20 μL $ABTS^{2-}$ solution (50 mM in MOPS buffer solution, pH = 7.0), and finally 100 μL D-glucose solution (1.0 M in MOPS buffer solution, pH = 7.0). After gentle mixing, the linear absorption increase rate $\Delta A_{414}/\Delta t$ was considered as a measure for GOD activity withdrawn from the reaction mixture. The calibration curve was obtained by using known amounts of GOD (**Fig.3-3-7**). The initial concentrations of each component in the assay solution were as follows: [HRPC] = 0.1 μM, $[\text{D-glucose}]_0$ = 100 mM, $[ABTS^{2-}]_0$ = 1.0 mM, and the total assay volume was 1.0 mL.

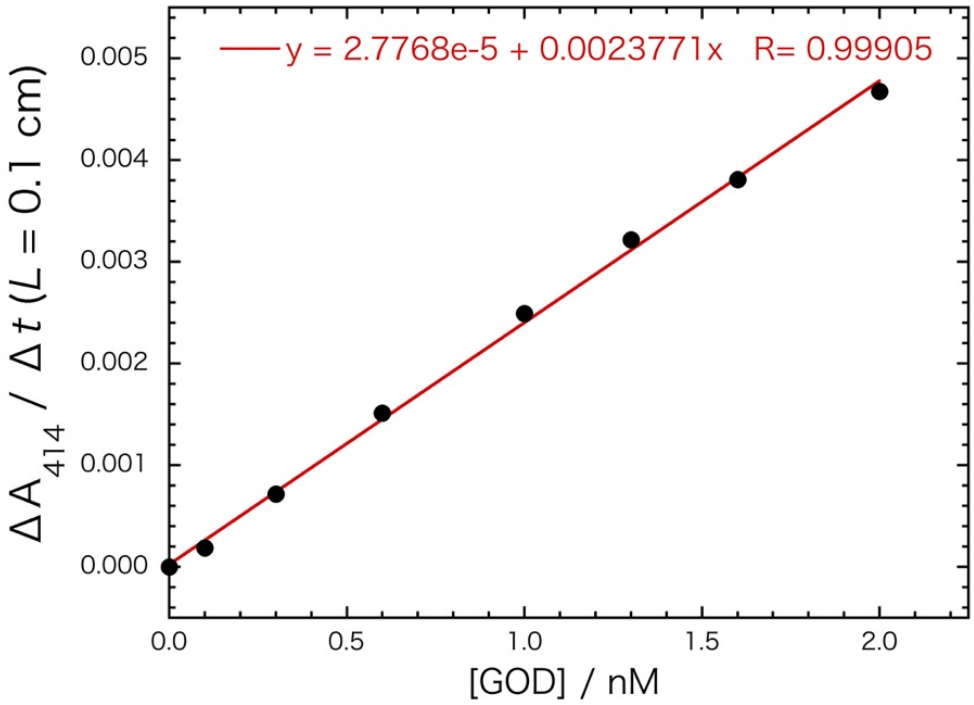

Figure 3-3-7. Calibration curve for the determination of GOD activity.
The calibration curve was obtained by measuring the initial oxidation rate of $ABTS^{2-}$ with known amounts of GOD in the presence of a fixed initial concentration of HRPC, D-glucose, and $ABTS^{2-}$. The GOD activity was expressed as ΔA_{414} / Δt for the first 180 sec after starting the reaction. $[\text{D-glucose}]_0$ = 100 mM, [HRPC] = 0.1 μM, and $[ABTS^{2-}]_0$ = 1.0 mM in presence of dissolved O_2. The red line represents the linear fit.

Quantification of D-glucose during the reaction.

The remaining D-glucose in the reaction mixtures was determined spectrophotometrically by withdrawing small volumes of reaction mixtures and then using the GOD/HRPC/$ABTS^{2-}$ assay, as described above. Since the initial concentrations of GOD (M ~ 153 kDa) and HRPC (M ~ 40 kDa) in the assay solution need to be fixed, the two enzymes were firstly separated from the reaction mixtures that contain D-glucose by ultrafiltration using Amicon® Ultra 0.5 mL centrifugal filters (regenerated cellulose, nominal molecular weight limit of 10 kDa) (Merck, Germany). Since this purification process takes some minutes, D-glucose cannot be quantified in the very beginning after starting the reaction compared with other reaction components. The purified enzyme-free reaction mixtures were then analyzed for D-glucose content by adding the following solutions in the sequence to a quartz cuvette (L = 1 mm) at T ~ 25 °C, followed by measuring the increase rate of absorption intensity at λ = 414 nm (A_{414}) during the first 180 s: 945 µL MOPS buffer solution (10 mM, pH = 7.0), 20 µL GOD solution (50 nM in 10 mM MOPS buffer solution, pH = 7.0), 5 µL HRPC solution (20 µM in MOPS buffer solution, pH = 7.0), 20 µL $ABTS^{2-}$ solution (50 mM in MOPS buffer solution, pH = 7.0), and finally 20 µL of the purified enzyme-free reaction mixture containing D-glucose. After gentle mixing, the linear absorption increase rate $\Delta A_{414}/\Delta t$ was considered to be a measure for the amount of D-glucose present in the assay mixture. The calibration curve was obtained by using known amounts of D-glucose (**Fig.3-3-8**). The initial concentrations of the assay solution were as follows: [GOD] = 1.0 nM, [HRPC] = 0.1 µM, $[ABTS^{2-}]_0$ = 1.0 mM, and the total assay volume was 1.0 mL.

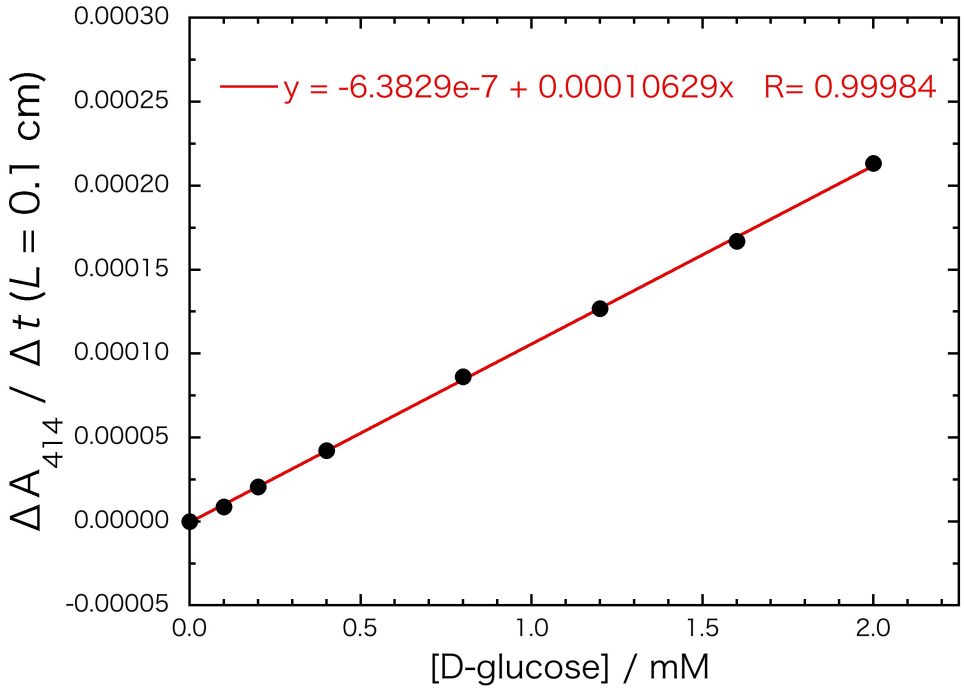

Figure 3-3-8. Calibration curve for the quantification of D-glucose.
The calibration curve was obtained by measuring the initial oxidation rate of $ABTS^{2-}$ with known amounts of D-glucose in the presence of a fixed initial concentration of GOD, HRPC, and $ABTS^{2-}$. The GOD activity was expressed as $\Delta A_{414} / \Delta t$ for the first 180 sec after starting the reaction. [GOD] = 1 nM, [HRPC] = 0.1 μM, and $[ABTS^{2-}]_0$ = 1.0 mM in the presence of dissolved O_2. The red line represents the linear fit.

3.3.6 Double Micro-Injection Technique

Double micro-injection technique.

To observe the changes in the size and morphology of AOT GUVs in response to the polymerization of aniline including energy currency production domain (condition in **Table 3-3-2**) with the feeding of the amphiphiles, we adopted the same double micro-injection setup, except the micro-injection solution components, with the ones described former (**Fig.2-5-1** and **Table 2-5-1**). The GUV suspension mixed with the polymerization components, except D-glucose to trigger the reaction, was carefully transferred from the glass vial into the sample chamber. The initial concentrations of the components of the reaction mixture were as follows: 3.0 mM AOT (GUVs), 4.0 mM aniline, 0.92 μM HRPC, 1.0 μM GOD, and dissolved oxygen in 20 mM NaH_2PO_4 solution (pH=4.3). The polymerization reaction was triggered by micro-injecting an 100 mM D-glucose solution containing 20 mM AOT micelles. Unless specifically mentioned otherwise, the same solution as bulk solution except GUVs was injected from the other pipette as a counter flow: 0 mM amphiphiles, 4.0 mM aniline, 0.92 μM HRPC, 1.0 μM GOD, and dissolved oxygen in 20 mM NaH_2PO_4 solution (pH=4.3). Please note that the counter flow solution contains reaction components such as enzymes by the same concentrations as in bulk solution, while the counter flow solution applied in the last chapter's condition contains only 20 mM NaH_2PO_4 (pH=4.3) (see **Table 2-5-1**). This is because the experimental setup was constructed after the rapid inactivation of enzymes was confirmed during the PANI-ES synthesis (**Fig.3-3-17**). For the consistent reaction condition during vesicle observation, the target vesicles are exposed to the constant concentrations of enzymes by using the counter flow (**Fig.3-3-3**). All solutions injected from the micro-pipettes were pressed through a 0.2 μm polypropylene filter Puradisc 25 PP (GE Healthcare, UK) before use.

Table 3-3-3. Reaction components and their concentrations used in the double micro-injection experiment.

Micro-injection 1	**Concentration**
Amphiphiles (micelles or SUVs)	20 mM or 100 mM
D-glucose	100 mM
Micro-injection 2	
Aniline	4.0 mM
HRPC	0.92 μM
GOD	1.0 μM
$NaH_2PO_4 + H_3PO_4$	20 mM (pH=4.3)
Bulk solution	
Amphiphiles (GUVs)	3.0 mM
Aniline	4.0 mM
HRPC	0.92 μM
GOD	1.0 μM
$NaH_2PO_4 + H_3PO_4$	20 mM (pH=4.3)

Microscopic observation of GUVs.

The morphological changes of GUVs were followed by using an Axio Vert. A1 FL-LED inverted fluorescence microscope in phase contrast mode (Carl Zeiss, Germany) with a 40x objective (LD A-Plan 40x, NA=0.55) and a CCD camera Axiocam 506mono (Carl Zeiss, Germany) for recording the images. To estimate the morphological changes of GUVs, a 3D image of the GUV was reconstructed from the 2D microscope image by using the Surface Evolver software package [Jimbo et al. 2016; Brakke 1992]. The surface area and volume of the GUV were quantified by approximating the vesicle shape with an axisymmetric prolate shape.

3.3.7 Result 1: Reaction Optimization

Introduction of energy currency production domain to the literature system.

Before elaborating the reaction condition for the artificial metabolism system, I introduced energy currency production domain (R1) to the slightly different system; the concentration of NaH_2PO_4 solution (pH=4.3) is not the artificial metabolism condition (20 mM) *but the standard condition widely used for PANI-ES synthesis research* (100 mM). *After confirming that energy currency production domain (R1) works well in this standard condition* (in 100 mM NaH_2PO_4)*, then in the next section 3.3.8, I will elaborate the condition appropriate for my artificial metabolism system* (in 20 mM NaH_2PO_4).

Concerning the reaction condition to obtain PANI-ES, the previously elaborated condition by Junker et al. with HRPC, aniline, and H_2O_2, were as follows [Junker et al. 2012]: 3.0 mM AOT (as LUVs), 4.0 mM aniline, 0.92 μM HRPC, 4.5 mM H_2O_2 in *100 mM* NaH_2PO_4 solution (pH=4.3), T = 25 °C, t = 24 h. The initial addition of H_2O_2 solution triggered the polymerization reaction. Under this condition, the initially colorless reaction mixture soon becomes blue and then dark green with absorption maxima at $\lambda \sim 1000$, 420, and 300 nm and relatively low absorption at $\lambda \sim 500$ nm (**Fig.3-3-9** "Reference reaction"), which is characteristic for the formation of PANI-ES. The formation of products with rich PANI-ES repeating unit is further supported by the fact that reaction products produce an EPR spectrum which is indicative of the presence of unpaired electrons (expected for the polaron form of PANI-ES) (**Fig.3-3-10 (3)**) [Junker et al. 2012; Fujisaki et al. 2019].

Instead of the initial addition of H_2O_2 that triggers the polymerization reaction, I newly introduced enzymatic reaction to form H_2O_2 from D-glucose and dissolved O_2 with GOD, the energy currency production domain (R1). All other conditions were kept the same, and polymerization of aniline was triggered by using *in situ* formed H_2O_2 in the reaction mixture. The optimal initial condition for the PANI-ES synthesis with the enzymatic cascade reaction was elaborated as follows (see Appendix 3-B for the determination of the optimal condition): 3.0 mM AOT, 4.0 mM aniline, 0.92 μM HRPC, 0.20 μM GOD, and 100 mM D-glucose in *100 mM* NaH_2PO_4 solution (pH=4.3), reaction volume = 0.50 mL, T=25˚C, t =24 h, with continuous rotary mixing (**Table 3-3-1**). Under this condition, the color of the reaction mixture turned from initially colorless to dark blue and finally dark green. UV/Vis/NIR spectrum of this cascade condition reaction mixture is shown with that of reference condition in **Fig.3-3-9** "Cascade reaction". Although both spectra are similar, they are clearly different. For the reference spectrum, the absorption

intensity at $\lambda \sim 1000$ nm is higher and at bout $\lambda \sim 700$ nm lower compared to the cascade system. The products obtained in the cascade system also showed an EPR spectrum (**Fig.3-3-10 (1)**) as observed in the reference system, which strongly supports the presence of PANI-ES products in the reaction mixture. Both spectra are very similar, with only slightly different G-factors (2.0063 for the "cascade reaction" and 2.0064 for the "reference system"). The EPR signal intensity for the PANI-ES products obtained with the reference system (**Fig.3-3-10 (3)**) was higher than in the case of the cascade system (**Fig.3-3-10 (1)**). This agrees well with the outcome of the UV/Vis/NIR absorption measurements for the reference system compared to cascade system, A_{1000} (reference, L =0.1 cm, t = 24 h) = 1.2 *vs* A_{1000} (cascade, L =0.1 cm, t = 24 h) = 0.8, since EPR signal intensities are known to correlate with the higher absorption in the NIR region.

According to the outcome from the UV/Vis/NIR absorption measurements and the EPR spectrum measurements, there is no doubt that PANI-ES is synthesized in an aqueous *100 mM* NaH_2PO_4 solution (pH=4.3) in the presence of AOT LUVs with a two-enzymatic cascade reaction including energy currency production domain (R1).

To observe the reaction kinetics, changes of the UV/Vis/NIR absorption spectrum of the reaction mixture were measured during the "cascade reaction" run in rotating tubes under the elaborated optimal conditions (**Table 3-3-1**). During the first phase of the reaction, there was a rapid increase in absorbance at $\lambda_{max} \sim 750$ nm (**Fig.3-3-11(a)** and **Fig.3-3-13(a)**), correlating with the observed appearance of blue color at the initial stage of the reaction. The intensity of this absorption band then slowly decreased with reaction time with a simultaneous increase in absorption in the NIR region, centered around $\lambda_{max} \sim 1000$ nm (**Fig.3-3-11(b)** and **Fig.3-3-13(b)**), correlating with the developing green color of the reaction mixture. Overall, these changes are very similar to the changes observed for the "reference reaction" previously [Junker et al. 2012]. However, there is a notable difference between the two systems. The initial increase in A_{750} is much faster for the “reference reaction” mixture with added H_2O_2 (4.5 mM, no D-glucose, no GOD) [Junker et al. 2012] than for the D-glucose/GOD system, “cascade reaction”. In this case, the formation of H_2O_2 from D-glucose and dissolved oxygen is considered to be a rate-limiting process for the PANI-ES synthesis, since there is almost no difference in an initial increase in A_{1000} between "reference condition" and "cascade condition" in *20 mM* NaH_2PO_4 solution (pH=4.3), where the concentration of GOD is increased from 0.20 µM to 1.0 µM.

The amount of remaining aniline, *in situ* formed and consumed H_2O_2, and remaining D-glucose in the "cascade reaction" mixture were measured, and the results are shown in

Fig.3-3-14, in **Fig.3-3-15**, and in **Fig.3-3-16**, respectively.

For the amount of remaining aniline, the time-dependent changes of the aniline consumption in the reaction mixture are shown in **Fig.3-3-14**. The kinetics of aniline consumption is similar to that observed in the "reference reaction" mixture [Junker et al. 2012], where the large fractions of aniline in the reaction mixture are rapidly consumed in about the first five minutes. After 24 h from the start of the reaction, about 10% of the initially added aniline remained. This value is also comparative to the "reference reaction" condition, which is known to stay at almost constant values of 5-10% after the rapid consumption in the initial reaction stage.

For D-glucose consumption, the changes of the initially present amount (100 mM) in the reaction mixture were determined by withdrawing small volumes from the reaction mixture during the reactions. Then, after eliminating the remained GOD and HRPC by ultrafiltration, the remained content is analyzed. As seen in **Fig.3-3-15**, after the initial consumption of about 5 mM D-glucose, the remained amount in the reaction mixture stayed almost constant at about 95 mM. This initial D-glucose consumption and the discontinuity of D-glucose oxidation agree well with the observed inactivation of GOD, as described below.

H_2O_2 is formed from D-glucose and dissolved oxygen with GOD and is simultaneously consumed for the HRPC-catalyzed oxidation of aniline. To determine the concentration in the reaction mixtures, a certain volume of the reaction mixtures was taken during the reaction. The quantification was carried out with the spectrophotometric Ti-TPyP assay [Junker et al. 2012]. Very different from the "reference reaction" where H_2O_2 is initially added to the reaction mixtures to be 4.5 mM, the determined concentration of H_2O_2 was consistently below 30 μM (**Fig.3-3-16**).

The activities of HRPC (both "reference reaction" as and "cascade reaction") and GOD (only in "cascade reaction") were measured by withdrawing small volumes from the reaction mixture and by analyzing them with either $ABTS^{2-}/H_2O_2$ (HRPC assay) or D-glucose/O_2/$ABTS^{2-}$/HRPC (GOD assay), see **Fig.3-3-17(a)** (HRP activity) and **Fig.3-3-17(b)** (GOD activity). For HRPC, the activity decreased rapidly during the formation of PANI-ES products in both reaction systems. The data obtained in "reference reaction" are in good agreement with what was observed in previous research [Junker et al. 2012]. The inactivation of HRPC is a consequence of the oxidation of aniline [Junker et al. 2012]. Without this reaction, HRPC is stable [Kurisu et al. 2021]. In the case of GOD, the activity also dropped rapidly during the formation of PANI-ES. After 10 min reaction time, no GOD activity could be detected with the method used. Like in the case of HRPC, GOD

inactivation is a consequence of the oxidation of aniline since GOD is stable without aniline [Kurisu et al. 2021].

I have reproduced previously elaborated HRPC-catalyzed enzymatic formation of PANI-ES in the presence of AOT LUVs in *100 mM* NaH_2PO_4 solution (pH=4.3) [Junker et al. 2012]. Then, I succeeded in elaborating the reaction condition for the GOD/HRPC-catalyzed enzymatic cascade system for the formation of PANI-ES in the presence of AOT LUVs in 100 mM NaH_2PO_4 solution (pH=4.3), by introducing the reaction process to form H_2O_2 from D-glucose and dissolved O_2 (R1) to "reference system". We also observe the reaction kinetics in this newly elaborated condition. The important notice for discussing the kinetics is that both enzymes HRPC and GOD are rapidly inactivated after starting the reaction. The inactivation of enzymes is considered in our simulation later in section 4.4.

Next, we shift from the AOT LUVs system (in 100 mM NaH_2PO_4) to the AOT GUVs system (in 20 mM NaH_2PO_4). I conducted further analysis on the "cascade system" for the PANI-ES synthesis by using AOT LUVs, however, they are out of interest for the purpose of constructing a synthetic minimal cell. See [Kurisu et al. 2021] for more details in this work.

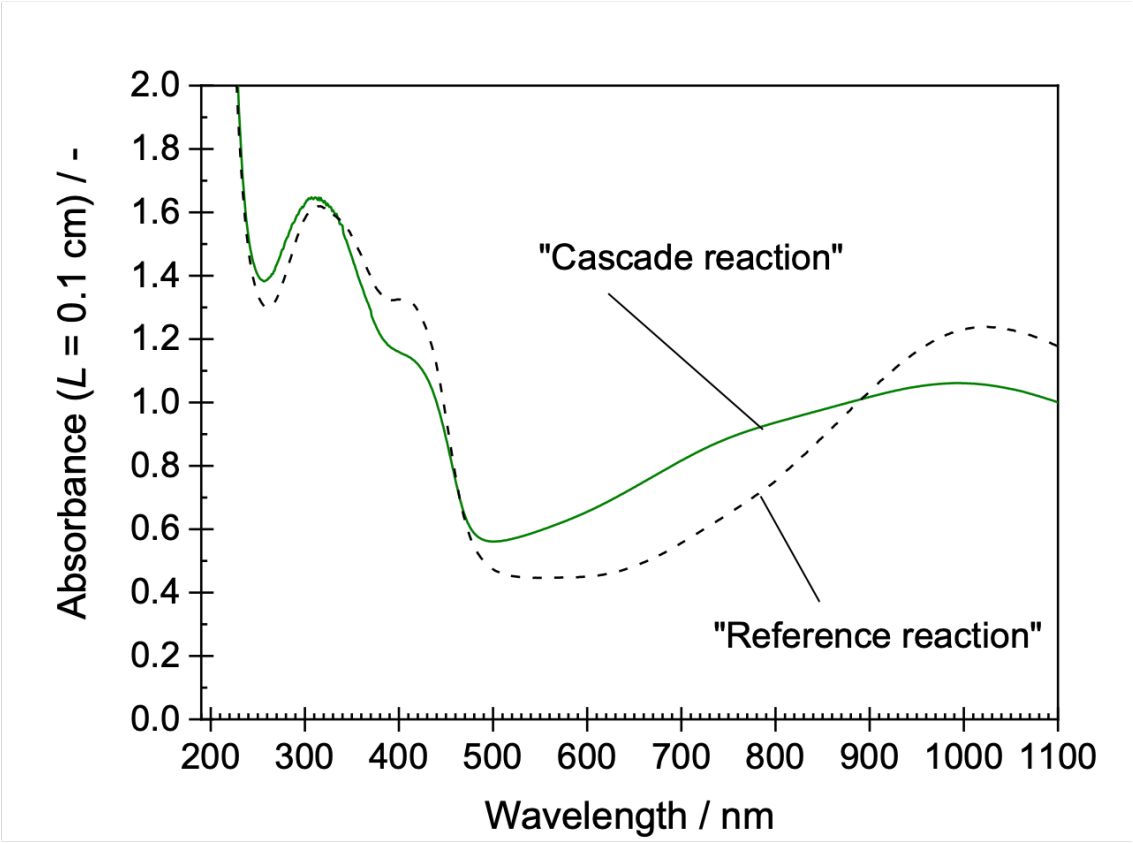

Figure 3-3-9. Comparison between the UV/Vis/NIR absorption spectrum recorded after t = 24 h for the optimal "cascade reaction" mixture (**Table 3-3-1**) with D-glucose and GOD at $[\text{D-glucose}]_0$ = 100 mM and [GOD] = 0.20 μM and the spectrum recorded for the "reference reaction" [Junker et al. 2012] with initially added H_2O_2 (4.5 mM); both with [AOT] = 3.0 mM; $[\text{aniline}]_0$ = 4.0 mM, and [HRPC] = 0.92 μM in *100 mM* NaH_2PO_4 solution (pH=4.3).

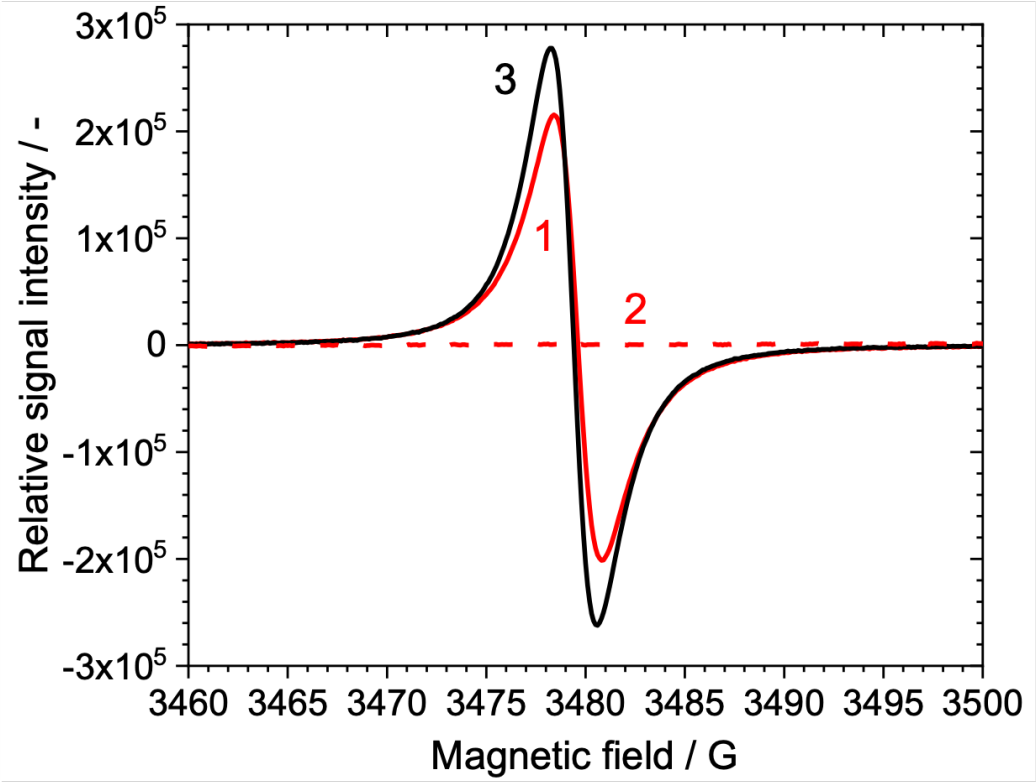

Figure 3-3-10. EPR spectra of **(1)** a "cascade reaction" run (**Table 3-3-1**) at T ~ 25 °C and recorded after t = 24 h. [AOT] = 3.0 mM, $[aniline]_0$ = 4.0 mM, $[D\text{-}glucose]_0$ = 100 mM, [GOD] = 0.15 μM, [HRPC] = 0.92 μM in 100 mM NaH_2PO_4 solution (pH=4.3). **(2) Control;** EPR spectrum of the reaction mixture used for the "cascade reaction" (1) before starting the reaction (no GOD added, control). **(3)** the "reference reaction" run at T ~ 25 °C and recorded after t = 24 h. [AOT] = 3.0 mM, $[aniline]_0$ = 4.0 mM, [HRPC] = 0.92 μM, $[H_2O_2]_0$ = 4.5 mM in 100 mM NaH_2PO_4 solution (pH=4.3).

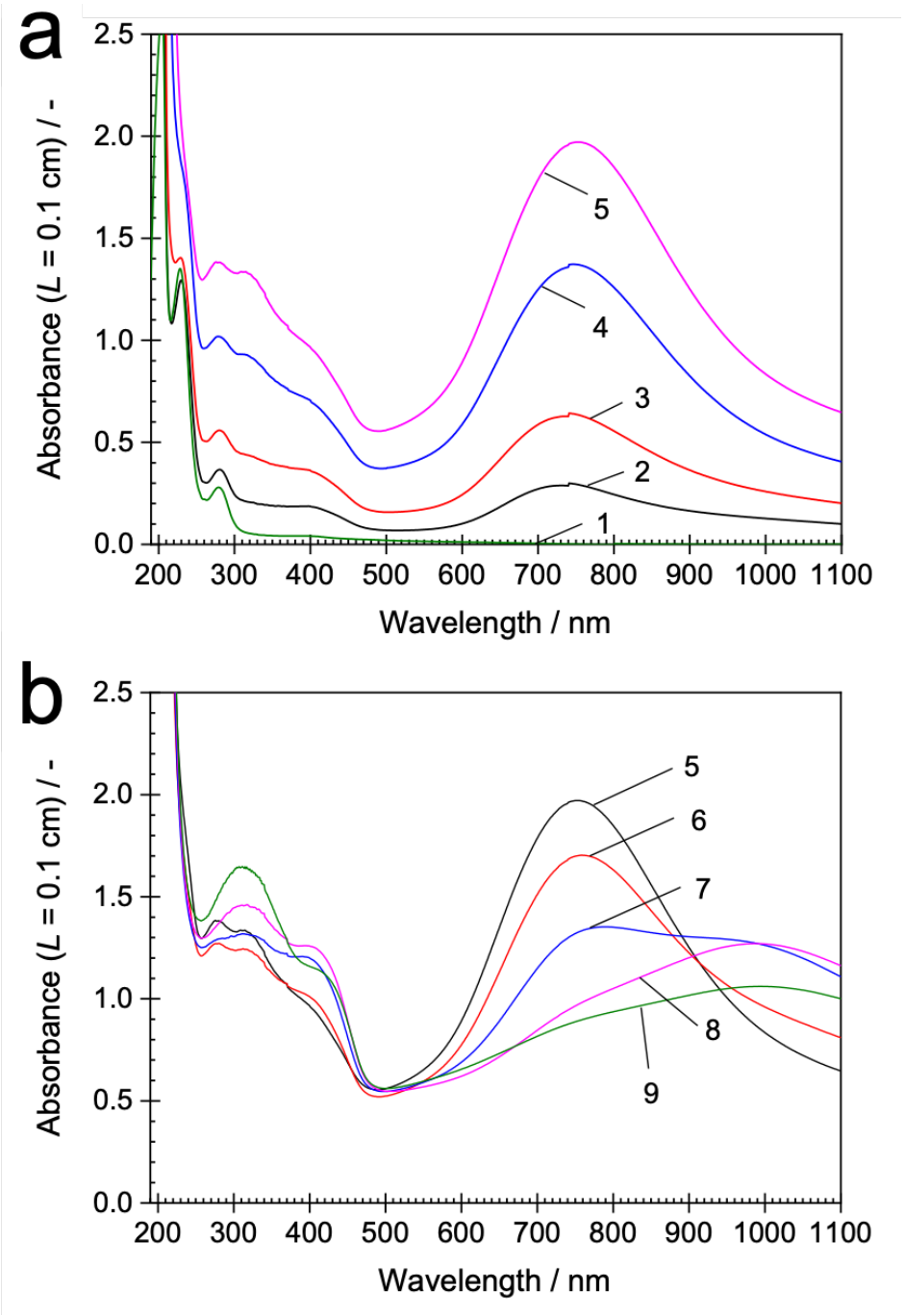

Figure 3-3-11. UV/Vis/NIR absorption spectra of "cascade reaction" (**Table 3-3-1**) samples which were withdrawn at predetermined times from the reaction. The reaction times were t = 0 s (1), 15 s (2), 30 s (3), 1 min (4), 3 min (5), 10 min (6), 60 min (7), 5 h (8) and 24 h (9). (**a)** Measured spectra for t = 0–10 min and (**b)** 10 min—24 h.

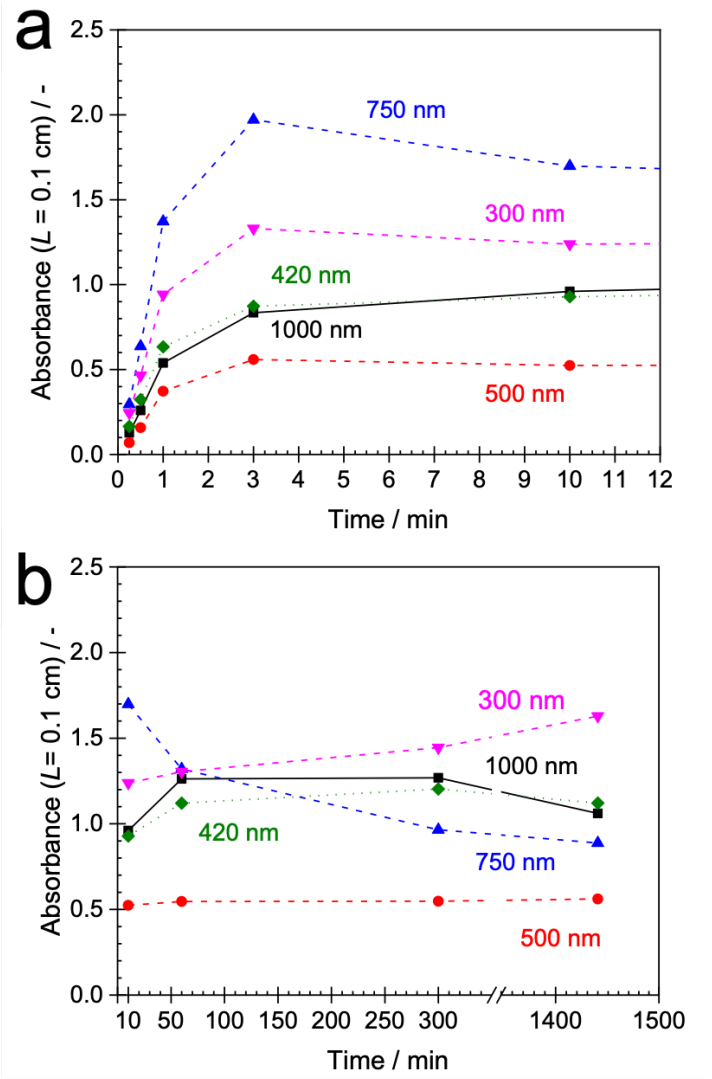

Figure 3-3-13. UV/Vis/NIR absorption spectra of "cascade reaction" (**Table 3-3-1**) samples which were withdrawn at predetermined times from the reaction mixtures. Time-dependent changes of A_{1000}, A_{750}, A_{500}, A_{420}, and A_{300} correspond to the absorption spectra changes shown in **Fig.3-3-12**.

(a) Absorption changes for t = 0–10 min and **(b)** 10 min—24 h. The lines between the data points are drawn for guiding the eyes. Please note that the spectra measured for t = 15 s and t = 30 s are only approximate spectra due to the rapid changes during the first phase of the reaction, also taking place during the recording of the spectra.

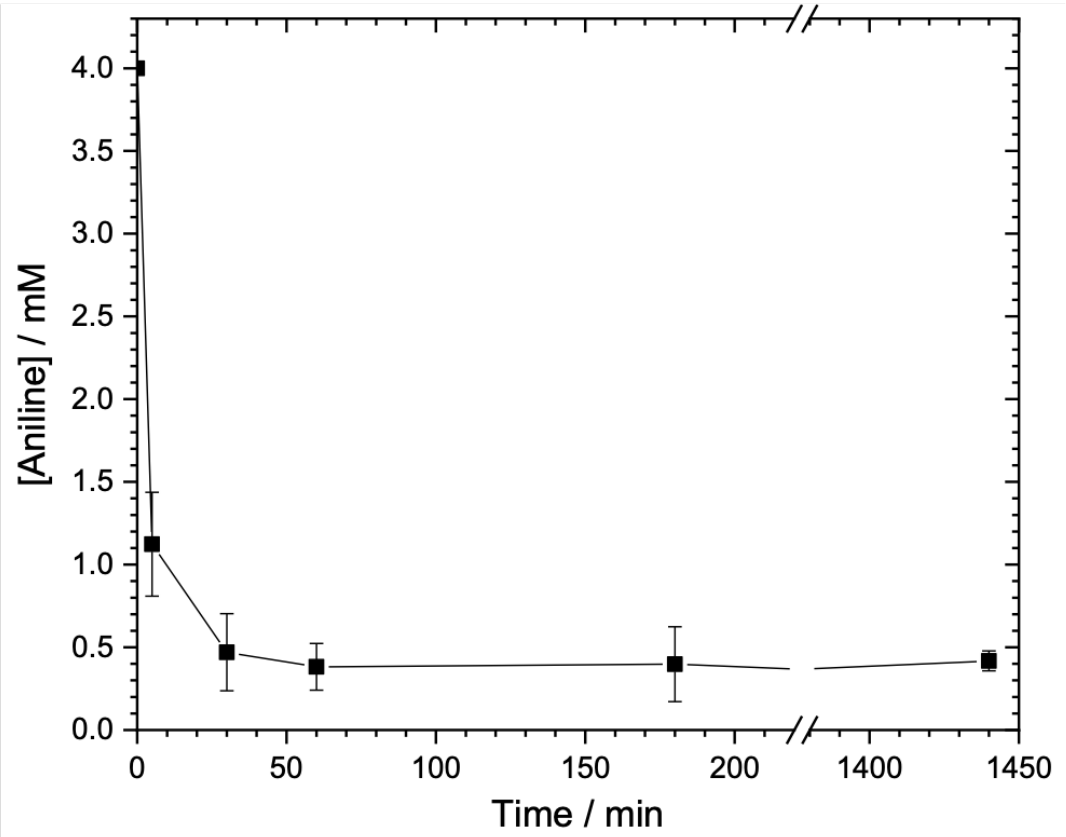

Figure 3-3-14. Time-dependent changes of the concentration of remaining aniline in the "cascade reaction" mixture (**Table 3-3-1**), as determined by analyzing samples withdrawn from the reaction mixture. The line between the data points is drawn for guiding the eyes. The error bars represent standard deviations from two to three measurements.

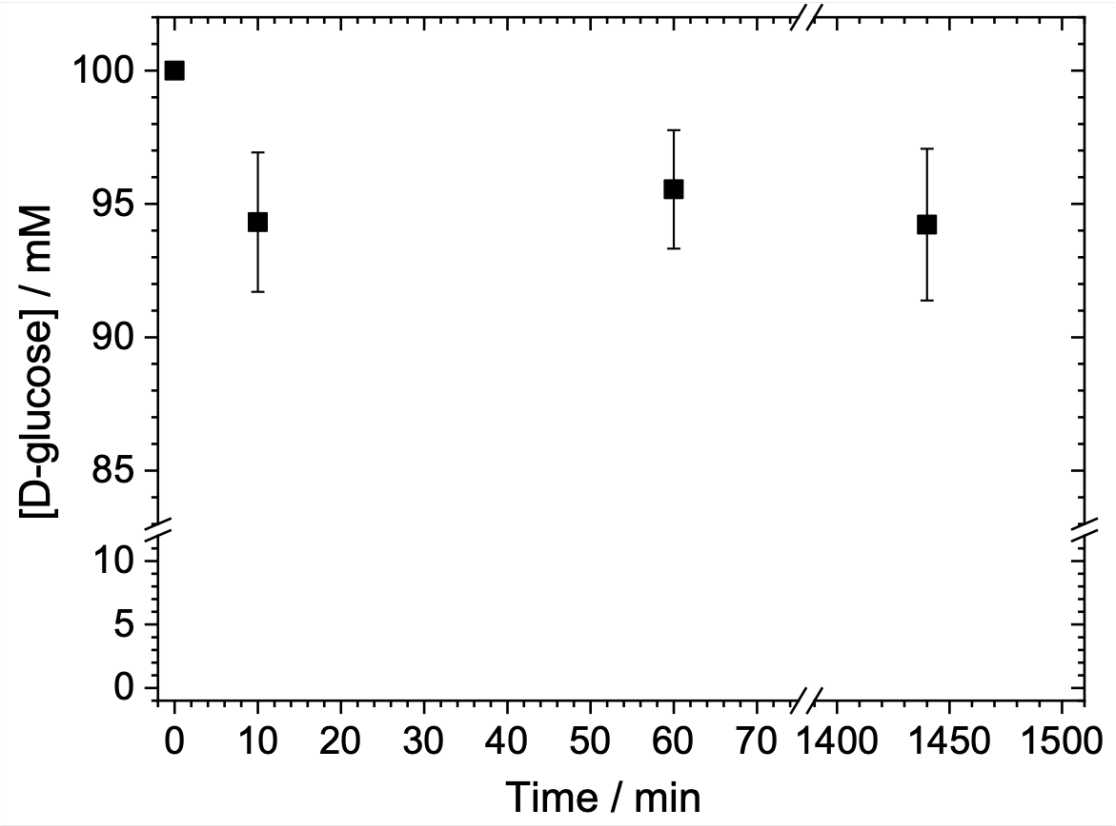

Figure 3-3-15. Quantification of the concentration of D-glucose in the "cascade reaction" mixture (**Table 3-3-1**), as determined by analyzing samples withdrawn from the reaction mixture. Error bars represent standard deviations from three measurements.

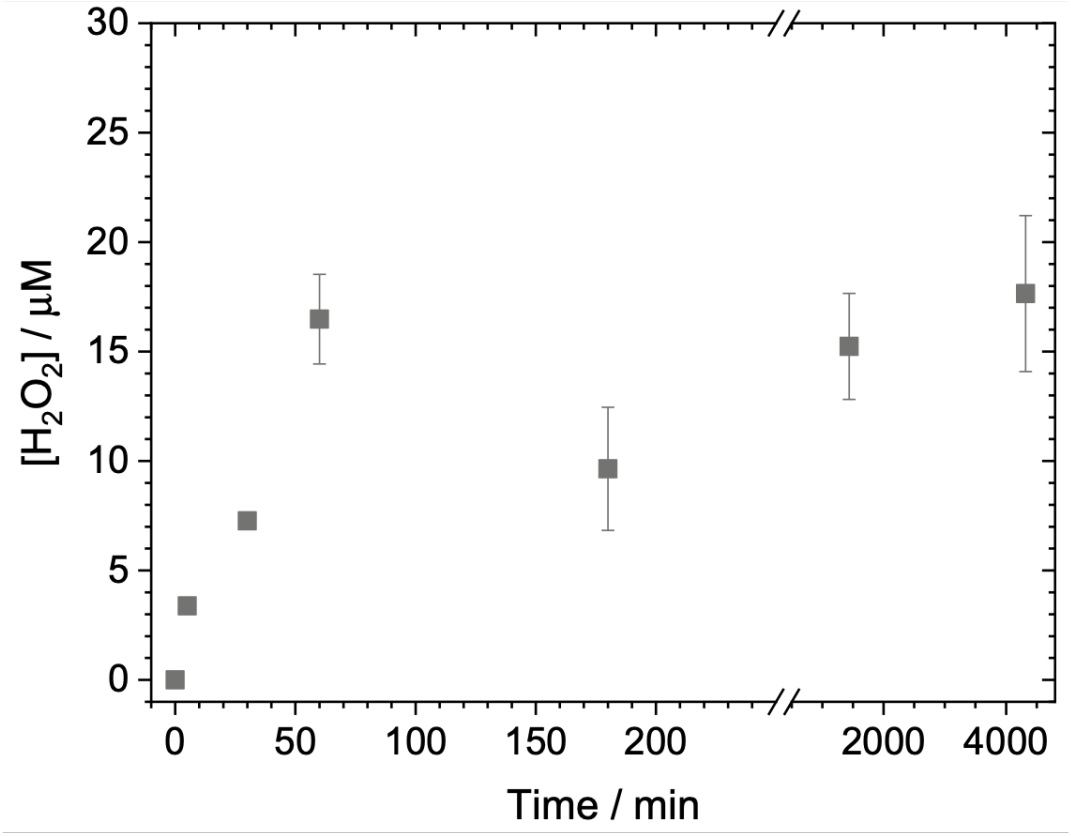

Figure 3-3-16. Quantification of the net concentration of in situ formed and consumed H_2O_2 in the "cascade reaction" mixture (**Table 3-3-1**), during the reaction, as determined by analyzing samples withdrawn from the reaction mixtures. The error bars represent standard deviations from three measurements.

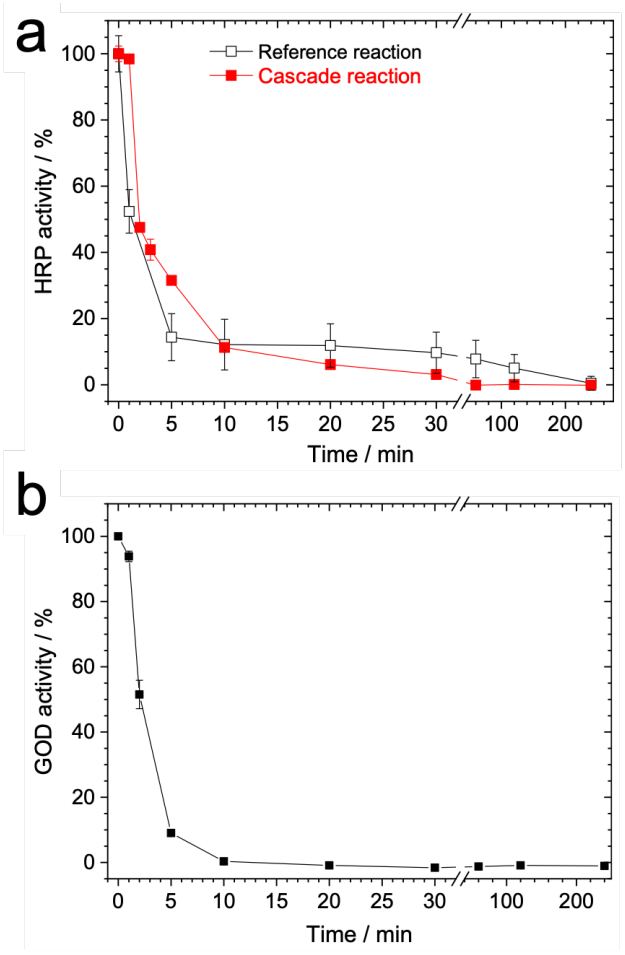

Figure 3-3-17. Time-dependent enzyme activity (**a**, HRPC and **b**, GOD) measurements during PANI-ES synthesis.

(a) Changes in the relative activity of HRPC during the reaction for the "cascade reaction" mixture (**Table 3-3-1**), (filled squares) and of the "reference reaction" mixture ($[H_2O_2]_0$=4.5 mM), (empty squares), as determined by analyzing samples withdrawn from the reaction mixtures. Hundred percent activity refers to the initial rate of reaction at time zero. The error bars represent standard deviations obtained from three measurements. The lines between the data points are drawn for guiding the eyes

(b) Changes in the relative activity of GOD during the reaction for the "cascade reaction" mixture (**Table 3-3-1**), as determined by analyzing samples withdrawn from the reaction mixture. Hundred percent activity refers to the initial rate of reaction at time zero. The error bars represent standard deviations obtained from three measurements. The line between the data points is drawn for guiding the eyes.

Introduction of energy currency production domain to the artificial metabolism system.

We finally demonstrate the PANI-ES synthesis, which involves energy production domain (R1) for the artificial metabolism system, the appropriate condition for the AOT GUVs preparation (*i.e.,* in *20 mM* NaH_2PO_4 solution (pH=4.3)). The reaction condition difference from the last section are (i) decrease in the concentration of NaH_2PO_4 solution (pH=4.3) from 100 mM to 20 mM for the GUV preparation, and (ii) increase in the concentration of GOD from 0.20 μM to 1.0 μM for the higher yield of the product. The obtained UV/Vis/NIR absorption spectra are shown in **Fig.3-3-18**, which shows the PANI-ES is undoubtedly synthesized and the reaction condition is well optimized for the artificial metabolism system, in 20 mM NaH_2PO_4. The initial reaction kinetics for the PANI-ES synthesis in this condition is also monitored (**Fig.3-3-19**), which indicates that the initial reaction progress is also not largely influenced by modification of the reaction condition.

The results of Raman spectrum measurements of polymerization products obtained by using AOT LUVs and DOPC LUVs are shown in **Fig.3-3-20**. The product obtained with AOT LUVs has a clear $\nu(C\sim N^{\bullet+})_p$ peak at ~ 1345 cm^{-1} due to the delocalized polarons of PANI-ES compared to the products obtained with DOPC vesicles (**Fig. 3-3-20(a)**), which agrees well with that of PANI-ES reported in the literature [Pasti et al. 2017]. Then, I synthesized PANI-ES not on homogeneous AOT LUVs (~80-100 nm) but on AOT GUVs (~15 μm). The formation of PANI-ES on AOT GUVs was directly confirmed by a micro-Raman mapping technique. Using the characteristic $\nu(C\sim N^{\bullet+})_p$ peak at around 1345 cm^{-1}, I constructed a two-dimensional map (0.5 μm resolution) that directly reflects the PANI-ES distribution. The obtained Raman image is shown in **Fig. 3-3-20 (b)** and (**c**). The agreement between the optical microscope image (**b**) and Raman image (**c**) indicate that PANI-ES is localized almost homogeneously on the AOT GUV surface. The two reference spectra of the mapping are shown in **Fig. 3-3-20(d)**, and the sampling points are indicated in the mapping image as "A" and "B".

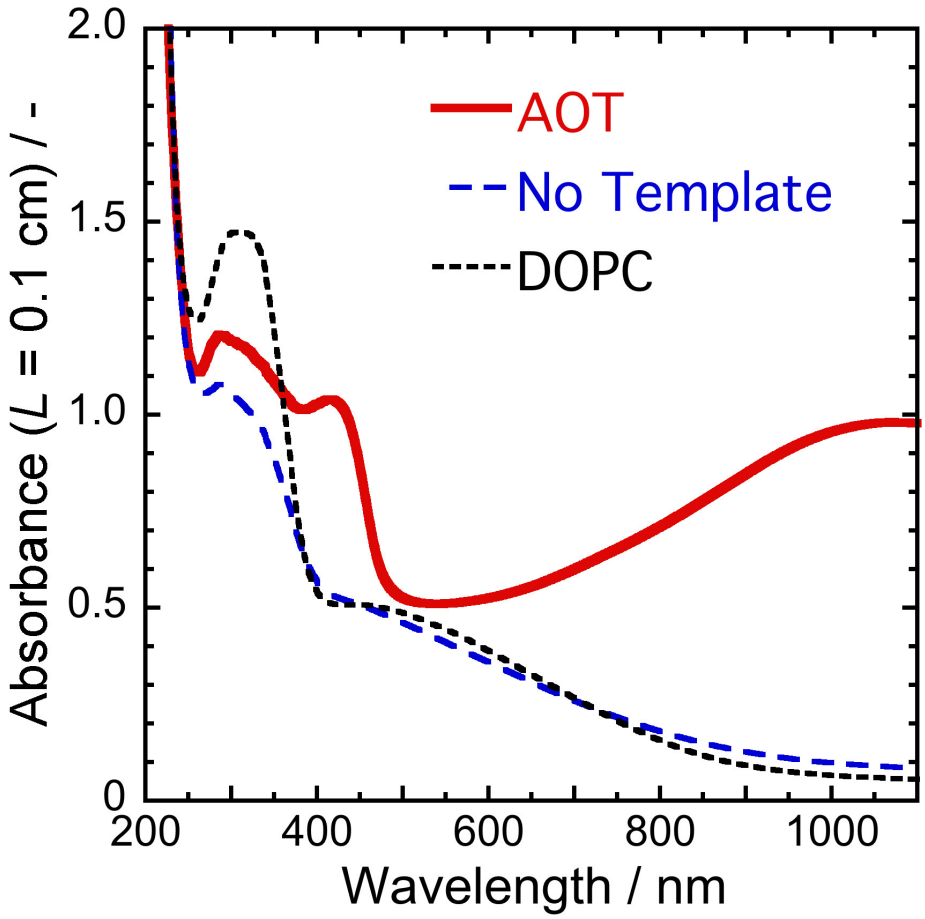

Figure 3-3-18. UV/Vis/NIR absorption spectra of the polymerization products. The products were obtained by polymerization of aniline (4.0 mM) with D-glucose (100 mM), dissolved oxygen, HRPC (0.92 μM), and GOD (1.0 μM) in 20 mM NaH_2PO_4 solution (pH=4.3), for 24 h at 25 ˚C, in the presence of LUVs formed from either AOT (red solid line), no template vesicles (blue dashed line), or DOPC (black dotted line). The amphiphiles concentration was 3.0 mM.

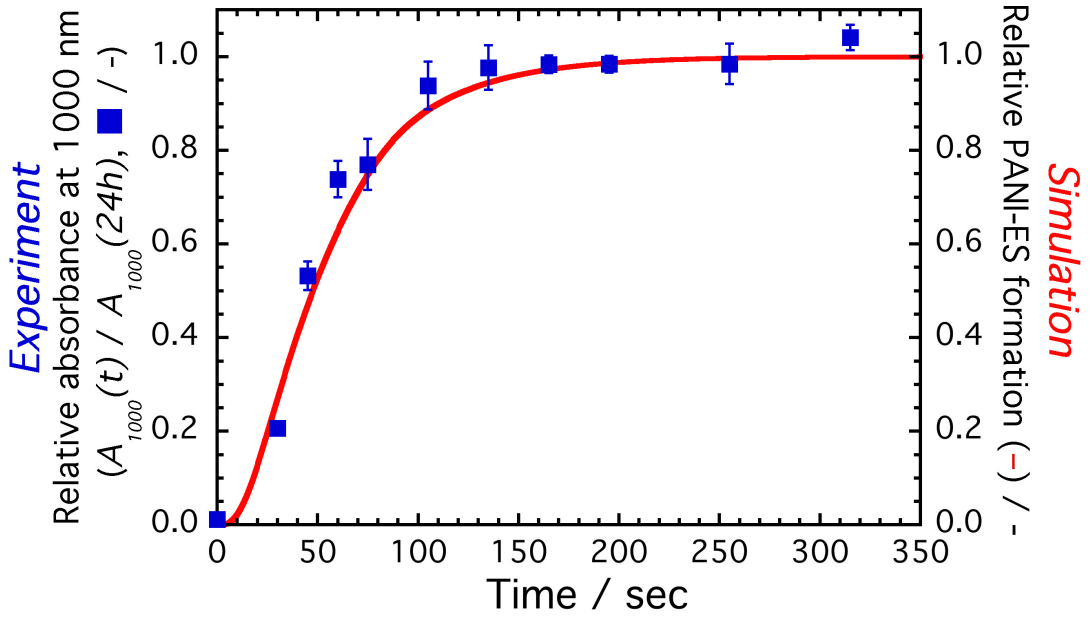

Figure 3-3-19. Time dependence of relative absorbance at λ=1000 nm of the reaction mixture (blue squares) obtained in the presence of AOT LUVs in 20 mM NaH_2PO_4 solution (pH=4.3). The polymerization was triggered by the *in situ* formation of H_2O_2 from D-glucose and dissolved oxygen with GOD. The changes in absorbance at λ=1000 nm ($A_{1000}(t)$) are normalized by the absorbance recorded after 24 h from the start of the reaction (A_{1000} of "AOT" in **Fig.3-3-18**). The red line is the theoretical prediction obtained by the kinetic model (fitted by Eq. (IIIa – IIIi) in section 4.3.4). The error bars indicate standard deviations estimated from three different experiments. Reaction conditions were as follows: [AOT]=3.0 mM (as LUVs), $[Aniline]_0$=3.0 mM, [HRPC]=0.92 μM, [GOD]=1.0 μM, $[D\text{-glucose}]_0$=100 mM and dissolved oxygen in 20 mM NaH_2PO_4 solution (pH=4.3), T~25˚C.

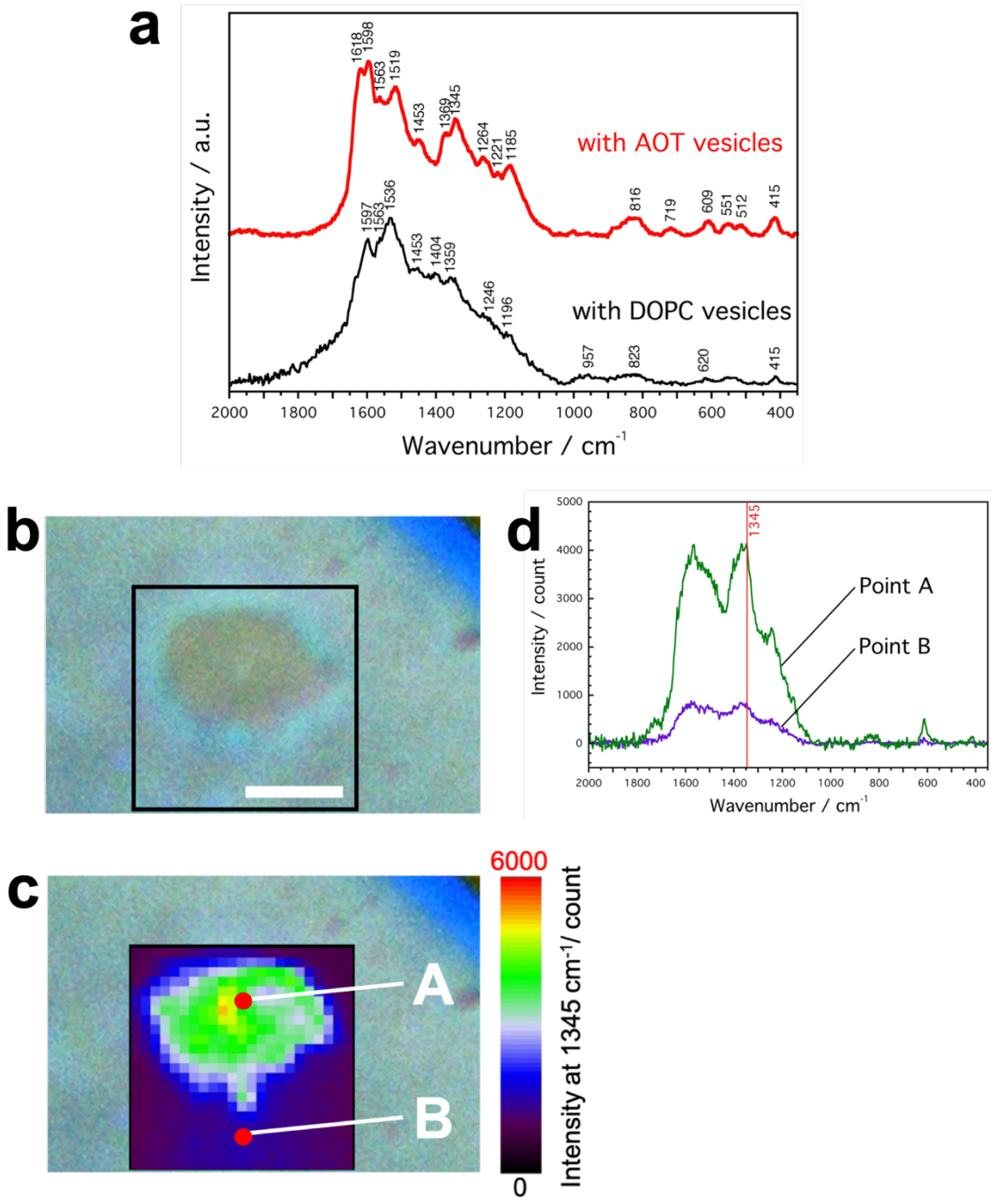
a
Intensity / a.u.
with AOT vesicles
with DOPC vesicles
Wavenumber / cm-1
b
c
A
B
6000
0
Intensity at 1345 cm-1/ count
d
Intensity / count
Point A
Point B
Wavenumber / cm-1

Figure 3-3-20. Raman spectrum measurements of the reaction products of polymerization of aniline obtained in the presence of LUVs. Reaction conditions were as follows: [Amphiphile]=3.0 mM (as LUVs), $[Aniline]_0$=3.0 mM, [HRPC]=0.92 μM, [GOD]=1.0 μM, $[D\text{-glucose}]_0$=100 mM and dissolved oxygen in 20 mM NaH_2PO_4 solution (pH=4.3), *T*~25˚C, *t*~24 h.

(a) Raman spectra of products obtained by polymerization of aniline in the presence of either AOT LUVs (red bold line) or DOPC LUVs (black plane line) with the cascade reaction scheme. The spectra were recorded after ~24 h from the start of the reaction.

(b) and **(c)** Spatial Raman mapping of an AOT/PANI-ES GUV using 1345 cm^{-1} peak, which is characteristic for the delocalized polarons of PANI-ES. Microscope bright field image (**b**) and Raman mapping image (**c**) of an AOT/PANI-ES GUV. The 532 nm line of a diode-pumped solid-state laser was focused on a position in a selected AOT GUV with a beam size of 520 nm in diameter. The Raman mapping image was obtained with an interval of 0.5 μm. The shadow in the upper right is the wall of the glass tube. Length of the scale bar: 5 μm.

(d) The raw representative point Raman spectrum, obtained from the point "A" and "B" indicated in the map (**c**).

Concluding the section.

In this chapter, I first determined the optimal reaction conditions (i) for the extension of the previous "reference condition" (R2 – R8), in which the direct addition of H_2O_2 triggers the polymerization reaction, to the "cascade condition" (R1 – R8), in which "energy currency molecule" H_2O_2 is *in situ* formed in the reaction mixture from D-glucose and dissolved oxygen with GOD in 100 mM NaH_2PO_4 solution (pH=4.3). For the construction of synthetic minimal cell, the microscopy observations of GUVs (~10 μm) is desirable, however, AOT molecules do not form GUVs in this condition. Then, we determined another optimal reaction conditions (ii) for the "cascade condition" valid in the AOT GUVs condition (*i.e.,* in 20 mM NaH_2PO_4) by modifying above "cascade condition" in 100 mM NaH_2PO_4 solution.

3.3.8 Result 2: Vesicle Membrane Growth Coupled with Artificial Metabolism

AOT GUVs membrane growth coupled with the energy currency production domain and information polymer synthesis.

The second significant result in this chapter is the demonstration of vesicle growth induced by coupling the synthesis of the information polymer with the energy production pathway (R1 – R9), the complete system of my artificial metabolism (**Fig.3-2-1**). Here, the reaction pathways for the synthesis of "information polymer" (PANI-ES) of vesicles are triggered by using *in situ* formed energy molecules (H_2O_2) formed from other ingredients in the reaction system. We observe the morphological changes of AOT GUVs using the double micro-injection setup.

We prepared AOT GUVs in the solution for the enzymatic cascade PANI-ES synthesis containing 1.0 μM GOD, 4.0 mM aniline, and 0.94 μM HRPC in 20 mM NaH_2PO_4 solution (pH = 4.3). It should be noted that the solution also contains dissolved oxygen. Then, 20 mM AOT micellar solution containing 100 mM D-glucose was micro-injected to the target AOT GUV by using a double micro-injection technique (entry **#1** in **Table 3-3-4**). The initially spherical AOT GUV began to grow with deformation into a prolate shape after ~ 60 sec from the start of injection (**Fig. 3-3-21(a)**), which roughly coincides with the kinetics of PANI-ES synthesis (**Fig.3-3-19**). The prolate vesicle elongated with time evolution by further uptake of AOT molecules from the environment. I quantified the vesicle surface area by approximating the shape with an axisymmetric prolate shape. Time evolution of the surface area, $A(t)$, coupled with the artificial metabolism system is plotted by red circles (**#1**) in **Fig. 3-3-22**, where the vesicle surface area is normalized by the surface area of the initial spherical vesicle, $A(0)$. The target vesicles clearly showed exponential growth. The experimentally observed membrane growth can be reproduced with the kinetic model, Eq. (Ia – Ig) in section 4.4.2. The simulation curves are overlaid with the experimental plots by a red solid line in **Fig.3-3-22**. As control experiments, we micro-injected AOT micelles to AOT GUVs under conditions where no polymerization took place (see **Table 3-3-4** and **Fig.3-3-22**), *i.e.*, without D-glucose (entry #2, blue squares), without aniline, HRPC, and GOD (entry #3, orange diamonds) or without D-glucose, aniline, HRPC, and GOD (entry #4c, black triangles). The microscopic images of vesicles of entry #4 are also shown in **Fig.3-3-21(b)**, for the

comparison to PANI-ES assisted membrane growth (entry **#1**). In these control conditions, the vesicle growth is suppressed, indicating that PANI-ES accelerates the growth of AOT vesicles. Thus, we have succeeded in achieving vesicle growth by coupling the synthesis of the information polymer pathway with the energy production pathway.

Table 3-3-4. List of reaction conditions for the vesicle growth experiments coupled with the artificial metabolism system.

Condition	(Target Vesicle)			(Micro-injection)		PANI-ES Synthesis
	Aniline[a]	HRPC[b]	GOD[c]	D-glucose[d]	AOT micelles[e]	
# 1	✓	✓	✓	✓	✓	✓
# 2	✓	✓	✓	–	✓	–
# 3	–	–	–	✓	✓	–
# 4	–	–	–	–	✓	–

[a] [Aniline] = 4.0 mM, [b][HRPC] = 0.92 μM, [c][GOD] = 1.0 μM, [d][D-glucose] = 100 mM,

[e][AOT] = 20 mM.

Note. "**#1**" represent that this condition corresponds to the artificial metabolism system. "#2 - #4" represent the control experiment where one or more reaction components lack to trigger the PANI-ES synthesis.

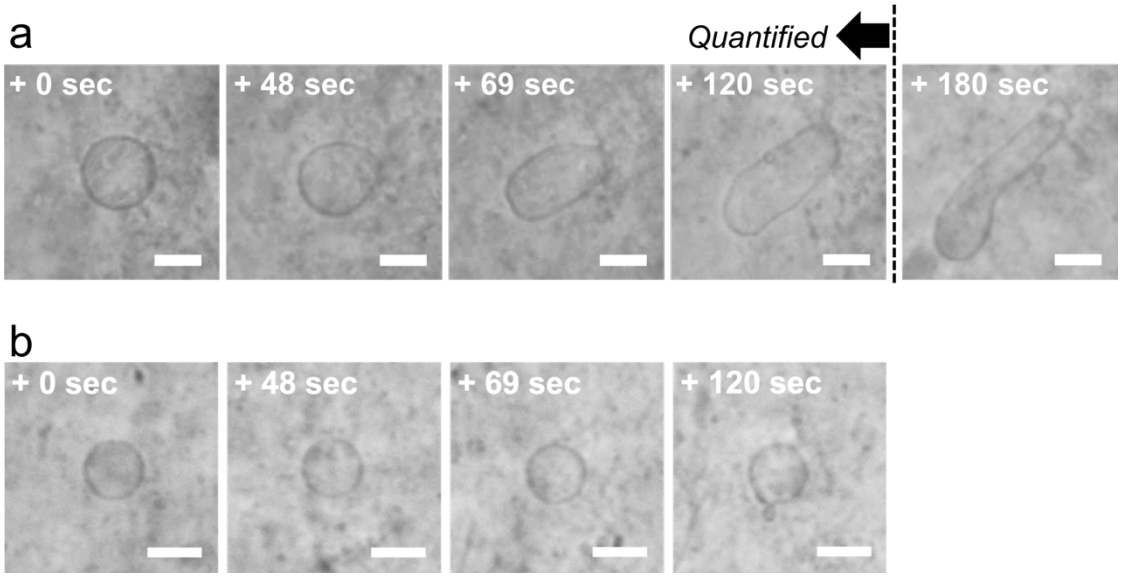

Figure 3-3-21. Phase-contrast light microscopy images of AOT GUVs under micro-injections.

(a) Condition "**#1**" of **Table 3-3-4**: Phase contrast light microscopy image of an AOT GUV during polymerization of aniline coupled with artificial metabolism system; 20 mM AOT micellar solution containing 100 mM D-glucose was micro-injected to the AOT GUV suspension containing 3.0 mM AOT, 4.0 mM aniline, 0.92 mM HRPC, 1.0 μM GOD, and dissolved oxygen in 20 mM NaH_2PO_4 solution (pH=4.3). From micro-pipette on the other side, 20 mM NaH2PO4 solution (pH=4.3) containing 4.0 mM aniline, 0.92 mM HRPC, 1.0 μM GOD, and dissolved oxygen is micro-injected to the same vesicle. The GUV showed further growth beyond $\sim 1.5A(0)$ (at *"+120 sec"*), while its shape was no longer approximated by axisymmetric shape. The elapsed time after starting the micro-injection is indicated in each image. Length of the scale bar: 10 μm.

(b) Condition "**#2**" of **Table 3-3-4**: An AOT GUV in 20 mM NaH_2PO_4 (pH = 4.3) solution without aniline and HRPC under micro-injection of AOT micelles (20 mM AOT) and D-glucose (100 mM). The elapsed time after starting the micro-injection is indicated in each image. Length of the scale bar: 10 μm.

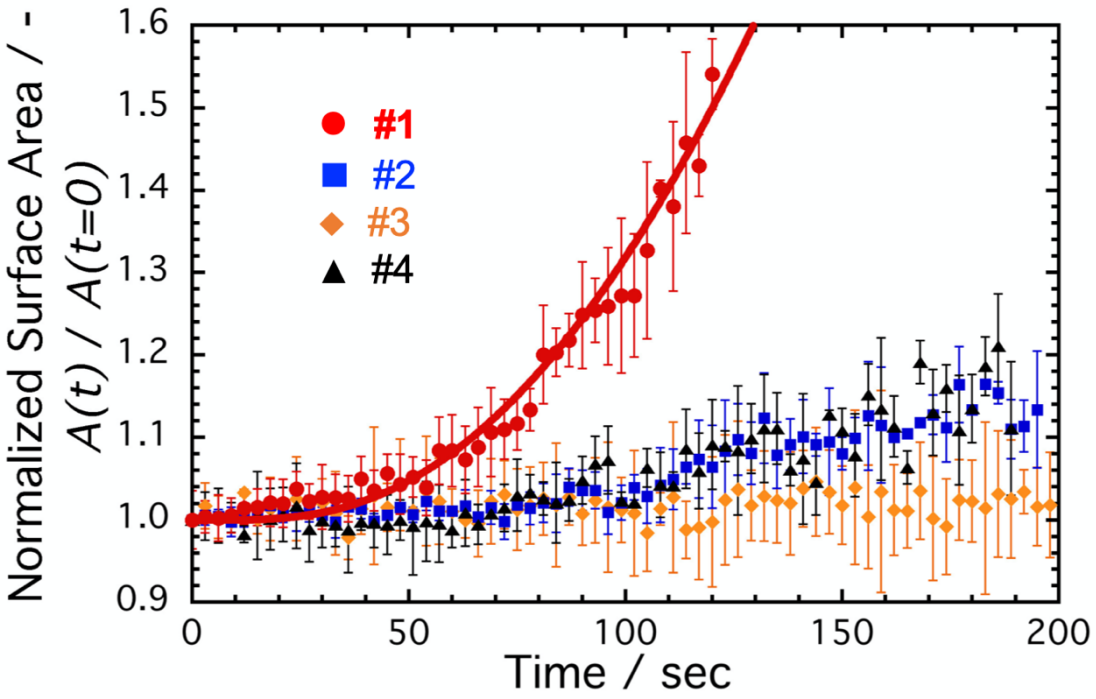

Figure 3-3-22. Growth of AOT GUVs in response to the micro-injection of AOT micelles under various conditions. Red circles (**#1**): Growth of AOT GUVs under the artificial metabolism system. Red solid line: Simulation curve given with the kinetic model Eq. (Ia – Ig) in section 4.4.2. Blue rectangles (#2): D-glucose is not contained in the micro-injection solution compared to #1. Orange diamonds (#3): Aniline, HRPC, and GOD are not contained compared to #1. Black triangles (#4): D-glucose is not contained in the micro-injection solution, and aniline, HRPC, and GOD is not contained compared to #1. The surface areas of GUVs are normalized by their initial values. The error bars indicate standard deviations estimated from four to six different experiments.

3.4 Conclusion

In the last chapter “Artificial Information Polymer”, I designed the artificial information polymer for vesicle membrane, where the polyaniline “encodes” the property of vesicle membrane (sulfonated/sulfated head structure) in its regioselective regular sequence structure (PANI-ES unit-rich structure) through the specific interaction between membrane and monomers, and the information polymer selectively promote the incorporation of amphiphiles from the environment to vesicle membrane (“decodes”). This system realizes information polymer synthesis and membrane growth. In this chapter, based on the recent molecular biology and Gánti’s chemoton model, I designed the artificial metabolism system for my synthetic minimal cell (**Fig.3-4-1**). The metabolism system conceptually reproduces three essential reaction domains for biological systems: energy currency production domain, information polymer synthesis domain, and membrane growth domain. The main focus in this chapter was introducing energy currency production domain to the PANI-ES synthesis system and vesicle membrane growth domain, which were already elaborated in the last chapter. By using *in situ* formed H_2O_2 from D-glucose and dissolved oxygen, the information polymer (PANI-ES) synthesis (**Fig.3-3-18**) and vesicle membrane growth (**Fig.3-3-22**) were successfully achieved.

Compared to biological metabolism network (**Fig.1-1-1(a)** and **(b)**), my artificial metabolism system is not encapsulated in membrane closure, but confined on the outer surface of vesicle membrane (**Fig.3-2-1**). This design circumvents the problem on transmembrane molecular traffic, which is serious for minimal cell design to sustain the reaction network.

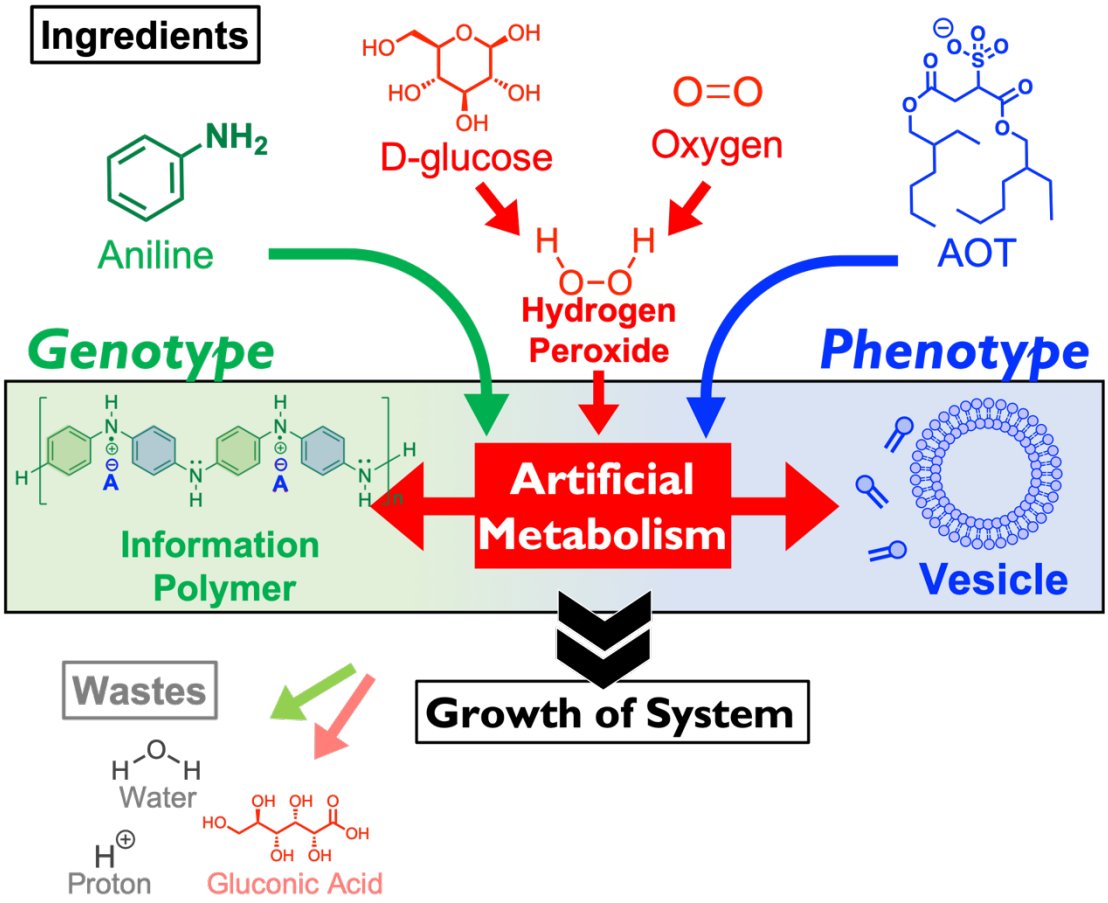

Figure 3-4-1. Graphical summary of the artificial metabolism design.
My synthetic minimal system shows the synthesis of information polymer (PANI-ES) and vesicle membrane growth, and they are linked by the simple and artificial reaction network composed of three domains: energy currency production domain, information polymer synthesis domain, and membrane growth domain. The system produces energy currency molecules (H_2O_2) from externally supplied D-glucose and dissolved oxygen. Energy currency molecules drive the polymerization of aniline on vesicle surface, resulting in the formation of regular sequence polyaniline (PANI-ES). The information polymer selectively promotes the incorporation of membrane molecules (AOT), resulting in membrane growth. Then, vesicle-polymer system realizes the growth. The micro-injection setup realizes continuous inflow and outflow, which keeps the reaction condition near the vesicle almost constant.

3.5 Appendix

Appendix 3-A: Cvc measurements of AOT.

The influence of D-glucose on the AOT cvc (critical concentration for vesicle formation) in 100 mM NaH_2PO_4 solution (pH=4.3) was investigated by the turbidity measurements of the solution containing certain concentrations of AOT (**Fig.3-5-1**). See section 3.3.2, for the detailed procedure. No gap was observed between the cvc values of AOT with/without the content of 100 mM D-glucose in 100 mM NaH_2PO_4 solution (pH=4.3).

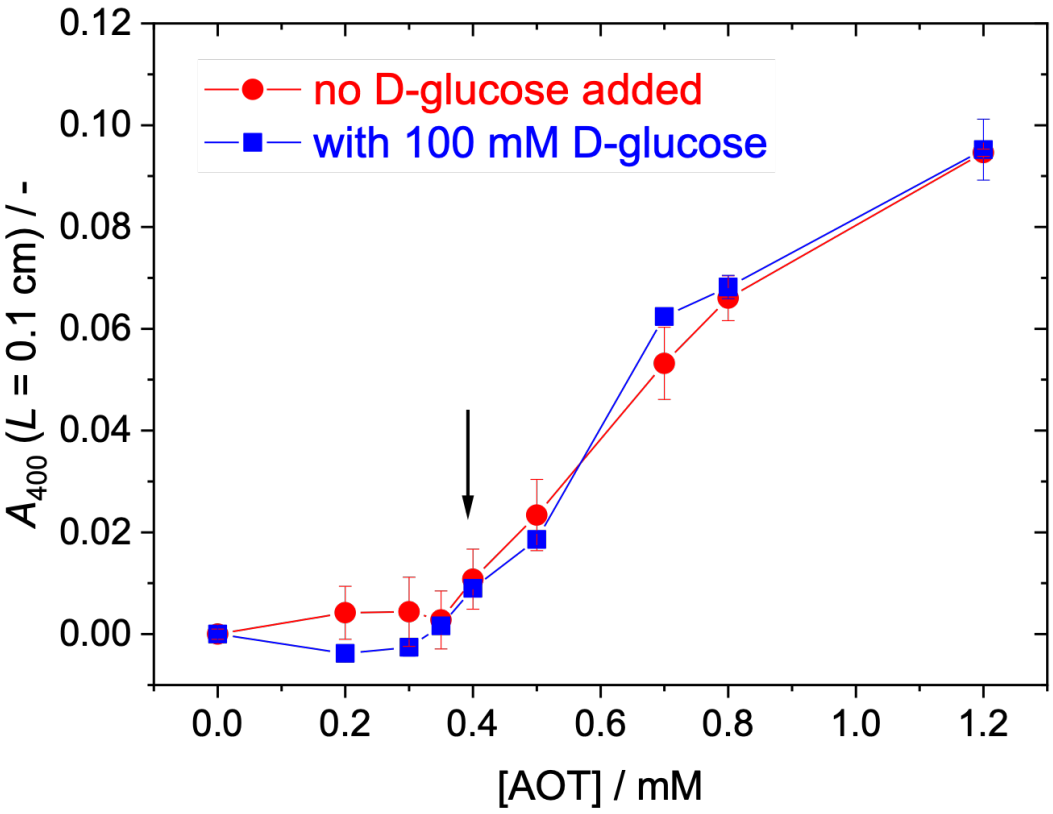

Figure 3-5-1. Estimation of the critical concentration for AOT vesicle formation (cvc) in 100 mM NaH_2PO_4 solution (pH = 4.3) at T ~ 25°C by turbidity measurements in the absence of D-glucose (red filled circles) or in the presence of 100 mM D-glucose (blue filled squares). In both cases, cvc ~ 0.4 mM (**arrow**), see section 2.3.2, for the experimental details. The error bars represent standard deviations from three measurements. The lines between the data points are drawn for guiding the eyes.

Appendix 3-B: Determination of optimal reaction condition for the enzymatic cascade polymerization of aniline

The optimal reaction condition for the PANI-ES synthesis in the "cascade system" (R1 – R8) in 100 mM NaH_2PO_4 solution (pH=4.3) was determined by replacing directly added amount of H_2O_2 in the "reference condition" (R2 – R8) with the particular amount of D-glucose and GOD in a systematic way. Briefly, we first concluded that the optimal concentration of D-glucose is 100 mM regardless of the concentration of GOD since the saturation in absorption spectra, such as shown in **Fig.3-5-2(a)** and **(b),** were observed in various GOD concentrations. Then, we concluded that the optimal concentration of GOD is 0.20 μM in 100 mM NaH_2PO_4 solution (pH=4.3) since the value was one of the most "economical" conditions concerning the behavior of absorption spectra (**Fig.3-5-3(a)** and **(b)**) and the amount of remaining aniline in the reaction mixture (**Fig.3-5-3(c)**) against the concentrations of GOD. For further details, see the reference [Kurisu et al. 2021]. The optimal concentration of GOD in *20 mM* NaH_2PO_4 solution (pH=4.3) was also determined as 1.0 μM, based on similar discussions.

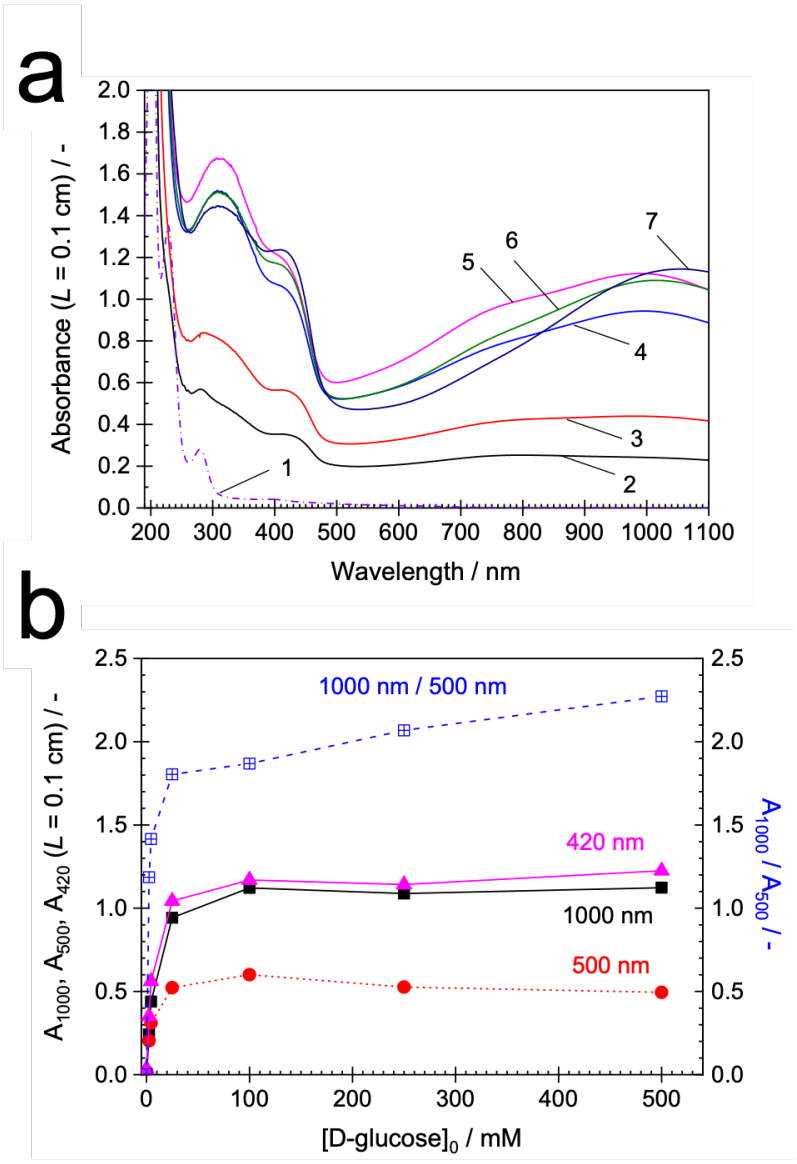

Table 3-5-2. For determination of the optimal initial concentration of D-glucose. UV/Vis/NIR absorption spectra of the reaction mixtures, recorded after t = 24 h from starting the reactions. See section 3.3.3, for the experimental details. [AOT]=3.0 mM; $[aniline]_0$=4.0 mM; $[D\text{-glucose}]_0$=0 mM (1), 2.5 mM (2), 4.5 mM (3), 25 mM (4), 100 mM (5), 250 mM (6), or 500 mM (7); [GOD]=0.30 μM; [HRPC]=0.92 μM; pH=4.3 (100 mM NaH_2PO_4).

(a) Measured spectra.

(b) A_{1000}, A_{500}, A_{420}, and A_{1000}/A_{500} vs $[D\text{-glucose}]_0$. The lines between the data points are drawn for guiding the eyes.

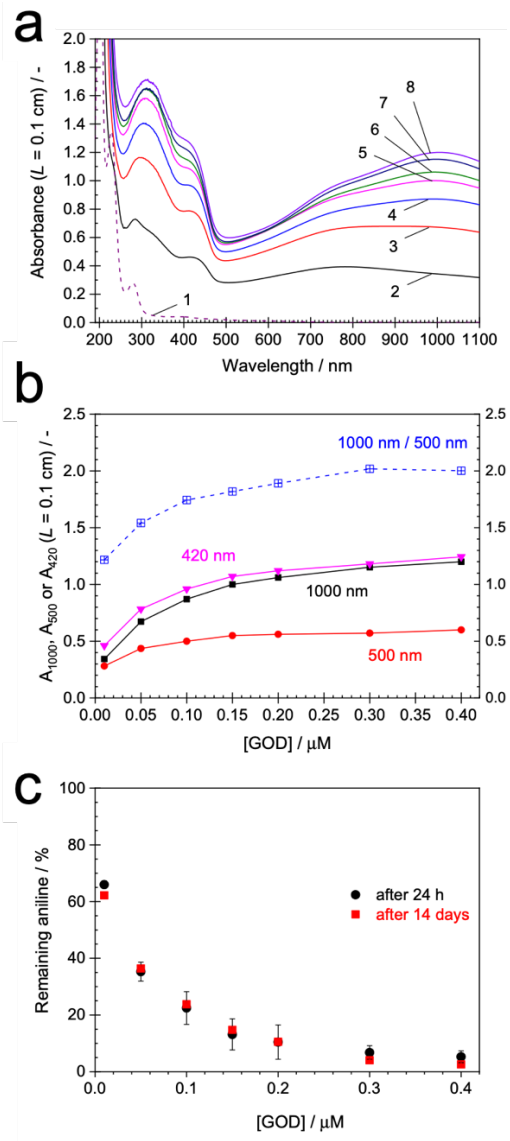

Table 3-5-3. For determination of the optimal concentration of GOD. UV/Vis/NIR absorption spectra of the reaction mixtures, recorded after t = 24 h from starting the reactions. See section 3.3.3, for the experimental details. [AOT]=3.0 mM; $[aniline]_0$=4.0 mM; $[D\text{-}glucose]_0$=100 mM; [GOD]= 0 μM (1), 0.01 μM (2), 0.05 μM (3), 0.10 μM (4), 0.15 μM (5), 0.20 μM (6), 0.30 μM (7), or 0.40 μM (8); [HRPC]=0.92 μM; pH=4.3 (100 mM NaH_2PO_4).

(a) Measured spectra.

(b) A_{1000}, A_{500}, A_{420}, and A_{1000}/A_{500} vs [GOD]. **c**, Dependence of the concentration of remaining aniline after t = 24 h and 14 days on [GOD]. The lines between the data points are drawn for guiding the eyes.

Chapter 4

Kinetic Model of Artificial Metabolism

4.1 Introduction

Up to this point, I have elaborated the experimental aspects of the artificial metabolism system. Under the continuous supply of ingredients molecules, the vesicle shows membrane growth coupled with the information polymer (PANI-ES) synthesis. However, for the minimal cell research, experimental construction of the system is only half way to the research goal. At least in my work, the minimal cell research is an approach to explore the universal essences underlying any possible living systems and to explore the mystery of their emergence from simple non-living molecular assemblies. For the purpose of them, I should extract physical essences from the experimental minimal cell system, and such a set of experimental realization and theoretical analysis to single minimal cell design will contribute to the future access from physical sciences to the essences of living systems. Fortunately, my synthetic minimal cell design has the simple and clear molecular mechanism. In this chapter, I will construct the reduced model system which extract the essences of my minimal cell design, and then I will construct the kinetic model based on the reduced system which reproduces well the experimental results. That is how I will demonstrate my artificial metabolism system is working well according to my design.

4.2 Enzymatic Reaction & Surface-Confined Reaction

4.2.1 Kinetic Model of Enzymatic Reactions

Michaelis-Menten equation.

An enzymatic reaction is usually modeled as an idealized two-step process as follows:

$$E + S \underset{k_{-1}}{\overset{k_1}{\rightleftarrows}} X \underset{k_{-2}}{\overset{k_2}{\rightleftarrows}} E + P \tag{4.1}$$

where a substrate S is bound with enzyme E to form an enzyme-substrate intermediate complex X, followed by a breakdown of the complex to form free enzyme E and reaction product P. $k_{i=1,2}$ is a rate constant, and $k_{i=-1,-2}$ is a rate constant of the reverse reaction. Normally, the concentration of enzymes and intermediate complexes are extremely lower than the concentration of substrates. Therefore, we apply the steady-state approximation assuming that the concentration of intermediate complex remains constant in time compared to the changes of concentration of substrates:

$$\frac{d[X]}{dT} = -(k_{-1} + k_2)[X] + k_1[E][S] + k_{-2}[E][P] = 0 \tag{4.2}$$

The initial concentration of enzymes and substrates are given by:

$$\begin{aligned} [E]_0 &= [E] + [X] \\ [S]_0 &= [S] + [P] \end{aligned} \tag{4.3}$$

In addition, the rate of substrate consumption is:

$$-\frac{d[S]}{dT} = \frac{d[P]}{dT} = k_1[E][S] - k_{-1}[X] \tag{4.4}$$

From Eq. (4.2) to (4.4), the rate of substrate consumption is described as follows:

$$-\frac{d[S]}{dT} = \frac{\frac{V_m}{K_m}[S] - \frac{V_p}{K_p}[P]}{1 + \frac{[S]}{K_m} + \frac{[P]}{K_p}} \tag{4.5}$$

where $V_m = k_2[E]_0$, $V_p = k_{-1}[E]_0$, $K_m = \frac{k_{-1}+k_2}{k_1}$, and $K_p = \frac{k_{-1}+k_2}{k_{-2}}$. Finally, the initial reaction rate of the enzymatic reaction (4.5), *i.e.,* reaction rate at $[P] \to 0$, is given by:

$$v_0 = \frac{V_m[S]}{K_m + [S]} \tag{4.6}$$

Eq. (4.6) is known as the Michaelis-Menten equation [Tominaga 2001; Marangoni 2003]. This equation is given without approximation when we ignore the reverse product release process (k_{-2}). The most significant feature of the enzymatic reaction described by Michaelis-Menten equation (4.6) is that the reaction rate is proportional to substrate concentration at lower substrate concentration. In comparison, the reaction rate remains approximately constant at higher substrate concentration (**Fig.4-2-1**).

In the actual enzymatic reactions, the substrate-enzyme intermediate complexes experience various elemental reaction processes before forming the reaction product. For example, the enzymatic reaction involving two intermediate complexes, X_1 and X_2, can be written as follows:

$$E + S \underset{k_{-1}}{\overset{k_1}{\rightleftarrows}} X_1 \underset{k_{-2}}{\overset{k_2}{\rightleftarrows}} X_2 \underset{k_{-3}}{\overset{k_3}{\rightleftarrows}} E + P \tag{4.7}$$

In this case, the rate of the reaction is given by the same form of Eq. (4.6), whereas the description of each constant changes, for example,

$$K'_m = \frac{k_2 k_3 + k_{-1} k_3 + k_{-1} k_{-2}}{k_1 (k_{-2} + k_2 + k_3)} \tag{4.8}$$

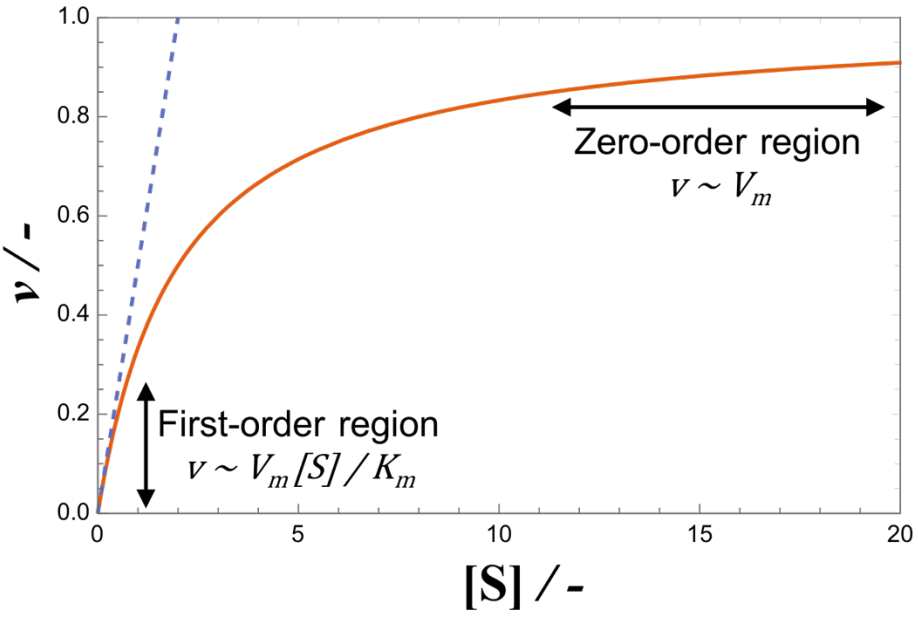

Figure 4-2-1. Plot of the Michaelis-Menten equation, Eq. (4.6). The solid curve is a Michaelis-Menten plot with the parameter values of $V_m = 1, K_m = 2$. The dashed line is the initial slope of the Michaelis-Menten plot, equivalent to $v = 0.5\,[S]$.

Two-substrate enzymatic reactions.

Michaelis-Menten equation, Eq. (4.6), describes the rate of the enzyme reactions with a single substrate. However, many enzymes catalyze reactions between two or more substrates. Two-substrate reactions are classified as the sequential or ping-pong mechanism by order of substrate addition and release of products within the reaction sequence [Cleland 1963]. In a sequential mechanism, all substrates add to the enzyme before any products are released. In the ping-pong mechanism, one or more products are released before all substrates add to the enzyme, and the enzyme exists in two or more stable forms during the reaction. These reactions can be further classified by the successive groups of substrate additions and product releases, such as by the use of uni (unimolecular), bi (bimolecular), and ter (termolecular). For example, ordered sequential bi bi (two substrates and two product) reaction and ping-pong bi bi reaction can be shown by using Cleland's diagram (**Fig.4-2-2**) [Cleland 1963; Marangoni 2003]. These two-substrate reactions are described by the respective rate equation, whereas they are the same in the type of reaction, $A + B \rightarrow P + Q$. Only under the condition where the concentration of one of the two substrates is kept constant while the other is variable, both reactions are described by the form of Michaelis-Menten equation, Eq. (4.6).

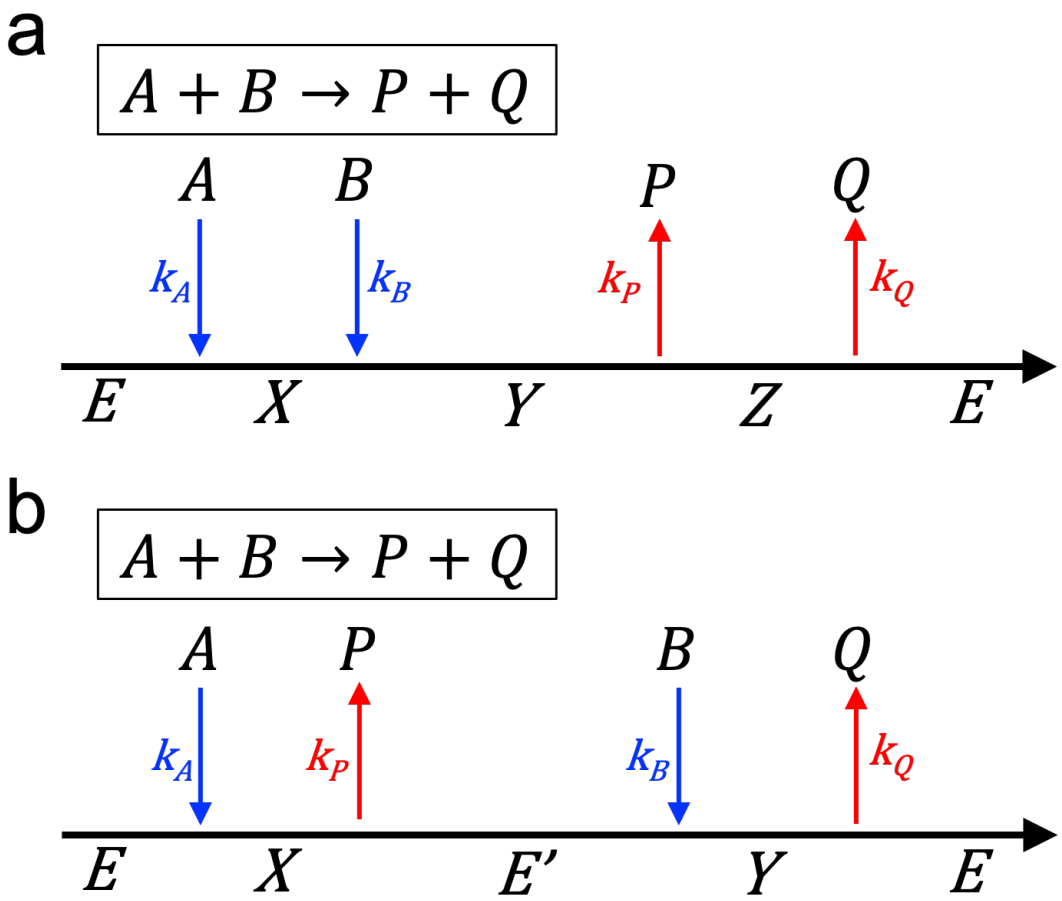

Figure 4-2-2. Cleland's diagram of two-substrate enzymatic reactions with (**a**) ordered sequential bi bi mechanism and (**b**) ping-pong bi bi mechanism. E is an enzyme, A and B are substrates, P and Q are products, X, Y, and Z are intermediate complexes, and E' is an intermediate state (not a complex) of E. Please note that each elemental reaction is reversible in general.

Reversible and irreversible ping pong bi bi mechanism.

There are numerous common reaction pathways through which two-substrate reactions can proceed. Here we focus on the two types of them.

(i) Ping pong bi bi mechanism.

In this mechanism, a free enzyme *E* must bind substrate *A* first, followed by the release of product *P* and the formation of an enzyme species *E'*. Then, the enzyme species *E'* must bind substrate *B*, followed by the release of product *Q* and free enzyme *E* (**Fig. 4-2-2(b)**). Please note that each elemental reaction is generally reversible, *i.e.,* each reaction has rate constant $k_{i=A,B,P,Q}$ and $k_{i=-A,-B,-P,-Q}$, respectively. The reaction rate is derived by applying the steady-state approximation where the concentrations of each enzyme intermediate remain constant and by considering mass conservation of enzymes and substrates, as we worked on the Michaelis-Menten equation. The initial reaction rate (*i.e.,* reaction rate at $[P] \to 0$) of the ping pong bi bi mechanism is given by:

$$v_0 = \frac{[E]_0}{\frac{1}{k_1} + \frac{1}{k_2[A]} + \frac{1}{k_3[B]}} \tag{4.9}$$

where $[E]_0$ is total concentrations of all enzyme intermediates and $k_{i=1,2,3}$ is the newly defined rate constant to avoid complicated expressions [Marangoni 2003; Dunford 1999]. The consequence of the reversibility is an upper limit in reaction rate. For lower substrate concentrations, the rate-limiting process is substrate binding. For the saturated condition with the substrate, the rate-limiting process is product release. Of the enzymes that appear in this thesis, glucose oxidase (GOD) strictly obeys this mechanism where *A* is D-glucose and *B* is oxygen.

(ii) Irreversible ping pong mechanism.

As seen in peroxidase kinetics, where enzyme-substrate complexes are very short-lived and almost undetectable, some enzyme kinetics are described by irreversible ping pong mechanism [Dunford 1999 and 1991]. Here we consider the three-substrate irreversible ping pong mechanism where the second and the third substrate are the same species (**Fig.4-2-3**). Please note that each elemental reaction is irreversible, *i.e.,* each reaction does not have rate constant for the reverse process, $k_{i=-A,-B,-C}$. In this case, we must define the rate clearly, either in terms of the rate of *A* disappearance or *B* disappearance. The rate of the reaction is derived by applying the steady-state approximation where the concentrations of enzyme intermediates *E*, *E**, and *E*** are remain constant, and by considering mass conservation of enzymes, $[E]_0 = [E] + [E^*] + [E^{**}]$. The reaction

rate defined in terms of disappearance of *A* is given by:

$$v = \frac{[E]_0}{\frac{1}{k_A[A]} + \frac{k_B + k_C}{k_B k_C[B]}} \tag{4.10}$$

Compared to Eq. (4.9), Eq. (4.10) is a simple steady-state rate equation that does not include newly defined rate constants. As a consequence of the irreversibility, there is no upper limit in reaction rate as observed in general non-enzymatic reaction, $A + B \rightarrow C$. See **Fig. 4-2-4** for comparing Eq. (4.9) and Eq. (4.10). Of the enzymes that appear in this thesis, hydrogen peroxidase isoenzyme C (HRPC) is considered to obey this mechanism where *A* is hydrogen peroxide, and *B* is aniline.

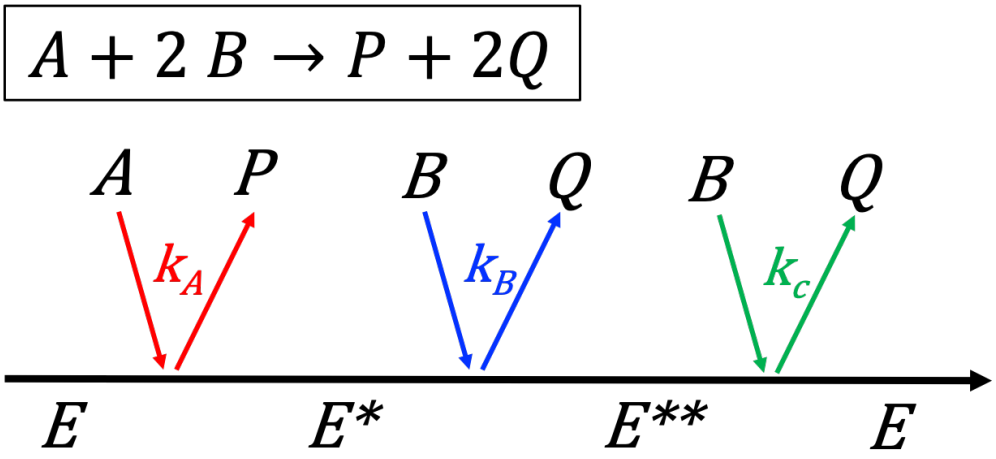

Figure 4-2-3. Cleland's diagram of three-substrate enzymatic reactions with irreversible ping pong mechanism. E is an enzyme, A and B are substrates, P and Q are products, and E* and E** are enzymes in their different oxidation states. Please note that the intermediate complexes between substrates and enzymes are very short-lived, and then products P and Q are shown to depart as soon as substrates contact the enzyme.

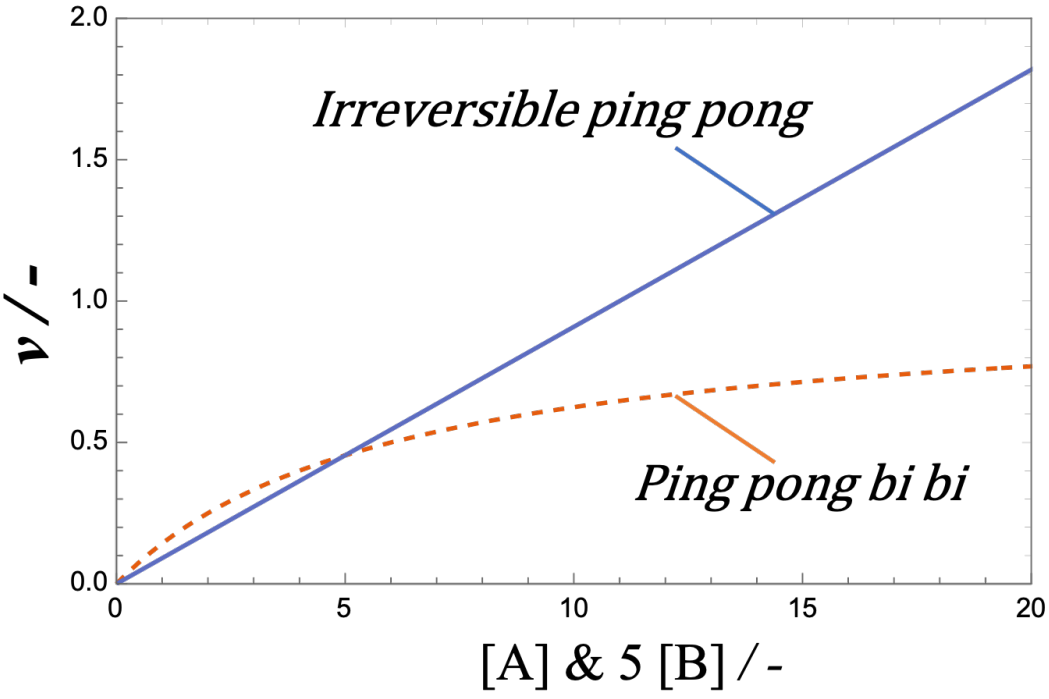

Figure 4-2-4. Plot of reaction rate given by the ping pong bi bi mechanism (dashed line), Eq. (4.9), or by the irreversible ping pong mechanism (solid line), Eq. (4.10). The values of parameters are $[E]_0 = k_{i=1,2,3,A,B,C} = 1$. The rate equations are plotted against simultaneous changes of two substrates, where the value of the concentration of substrate B is set to 1/5 of the one of substrate A.

4.2.2 Langmuir-Hinshelwood Mechanism

Herz-Knudsen equation.

For the system in equilibrium containing a large number of particles moving freely in idealized gases, the Maxwell-Boltzmann distribution is:

$$f(v)dv_x dv_y dv_z = (\frac{m}{2\pi k_B T})^{\frac{3}{2}} \exp\left[-\frac{m\left(v_x^2 + v_y^2 + v_z^2\right)}{2k_B T}\right] dv_x dv_y dv_z \qquad (4.11)$$

where $f(v)$ is a probability distribution function, dv_i is an infinitesimal element of velocity space, m is the particle mass, k_B is the Boltzmann's constant, and T thermodynamic temperature. Eq (4.11) is the probability distribution for velocity, and we get the distribution of the number of particles with a certain velocity by multiplying Eq (4.11) by the number of molecules per unit volume:

$$dN_v = \frac{N}{V}(\frac{m}{2\pi k_B T})^{\frac{3}{2}} \exp\left[-\frac{m(v_x^2 + v_y^2 + v_z^2)}{2k_B T}\right] dv_x dv_y dv_z \qquad (4.12)$$

The particles with velocity v_x which are located within the distance of $v_x \Delta t$ from a wall at x = 0 will strike the wall in Δt. Therefore, the number of particles that strike the wall per unit surface area and unit time is:

$$J_{HK} = \int_0^\infty \int_{-\infty}^\infty \int_{-\infty}^\infty \frac{N}{V}(\frac{m}{2\pi k_B T})^{\frac{3}{2}} \exp\left[-\frac{m\left(v_x^2 + v_y^2 + v_z^2\right)}{2k_B T}\right] v_x \, dv_x dv_y dv_z$$

$$= \frac{N}{V}\sqrt{\frac{m}{2\pi k_B T}} \int_0^\infty \exp\left[-\frac{m v_x^2}{2k_B T}\right] v_x \, dv_x \quad = \frac{N k_B T}{mV}\sqrt{\frac{m}{2\pi k_B T}}$$

$$= \frac{P}{\sqrt{2\pi m k_B T}} \qquad (4.13)$$

Eq. (4.13) is known as the Herz-Knudsen equation [Kolasinski 2012; Desjonquères & Spanjaard 2002], which relates the flux of molecules striking a surface to the pressure, P (or number density, equivalently).

Langmuir adsorption isotherm.

We consider adsorption of monatomic gas in equilibrium onto a homogeneous solid surface as follows:

$$A \quad + \quad * \quad \overset{K}{\leftrightarrow} \quad A(a) \tag{4.14}$$

where A is a gas molecule, $*$ is a free adsorption site on the surface, K is the adsorption-desorption equilibrium constant, and $A(a)$ represents the gas molecule in its adsorbed state occupying an adsorption site on the surface. Here we assume that each site can bind one molecule at most (monolayer coverage only). The fractional occupancy of the adsorption site is:

$$\theta_A = \frac{[A(a)]}{[A(a)]_0} \tag{4.15}$$

where $[A(a)]$ is the concentration of gas adsorbed on the surface and $[A(a)]_0$ is the maximal concentration of gas adsorbed on the completely occupied surface. When gas molecules strike the surface with free sites, $1-\theta_A$, the fraction α of the molecules is assumed to be actually adsorbed. Then, the rate of elementary adsorption process is given by using Eq. (4.13) as follows:

$$v_{ads} = \alpha J_{HK}(1-\theta_A) = \frac{\alpha P(1-\theta_A)}{\sqrt{2\pi m k_B T}} \tag{4.16}$$

In addition, the fraction β of the molecule covering the surface, θ_A, are assumed to desorb to the air. The rate of elementary desorption process is given by:

$$v_{des} = \beta\theta_A \tag{4.17}$$

Since adsorption and desorption are in equilibrium, $v_{ads} = v_{des}$, the fractional occupancy of the site is described as follows:

$$\frac{\theta_A}{1-\theta_A} = \frac{\alpha}{\beta\sqrt{2\pi m k_B T}} P \equiv KP \tag{4.18}$$

Therefore, the concentration of gas molecules in their adsorbed state is given by:

$$[A(a)] = [A(a)]_0\,\theta_A = [A(a)]_0 \frac{KP}{1+KP} \tag{4.19}$$

Eq. (4.19) is known as the Langmuir adsorption isotherm [Kolasinski 2012; Desjonquères & Spanjaard 1993; Tominaga 2001]. K is the adsorption-desorption equilibrium constant which only depends on temperature. When $P \to \infty$, $[A(a)]$ is approximated to $[A(a)]_0$, the maximal concentration of adsorbed molecules. In addition, when $P \to 0$, $[A(a)]$ is approximated to $[A(a)]_0 KP$, which shows a linear response to P (**Fig.4-2-5**). These behaviors of adsorption-desorption equilibrium are very similar to those of the idealized enzymatic reaction, the Michaelis-Menten equation, Eq. (4.6). If we further

look into K, it is given by using the site binding energy E as follows [Kolasinski 2012; Desjonquères & Spanjaard 1993]:

$$\frac{1}{K} = \left(\frac{2\pi\, m k_B T}{h^2}\right)^{3/2} k_B T\, exp\left(\frac{-E}{k_B T}\right) \tag{4.20}$$

In the competitive case where two species of gas molecules A and B can adsorb onto the site on the surface, Eq. (4.18) and (4.19) are described as follows:

$$\frac{\theta_A}{1-\theta_A-\theta_B} = K_A P_A, \quad \frac{\theta_B}{1-\theta_A-\theta_B} = K_B P_B \tag{4.21}$$

$$[A(a)] = N_s\theta_A = N_s \frac{K_A P_A}{1 + K_A P_A + K_B P_B},$$

$$[B(a)] = N_s\theta_B = N_s \frac{K_B P_B}{1 + K_A P_A + K_B P_B} \tag{4.22}$$

where N_s is the number of accessible sites per unit surface area, which is equivalent to $[A(a)]_0$ in Eq. (4.19).

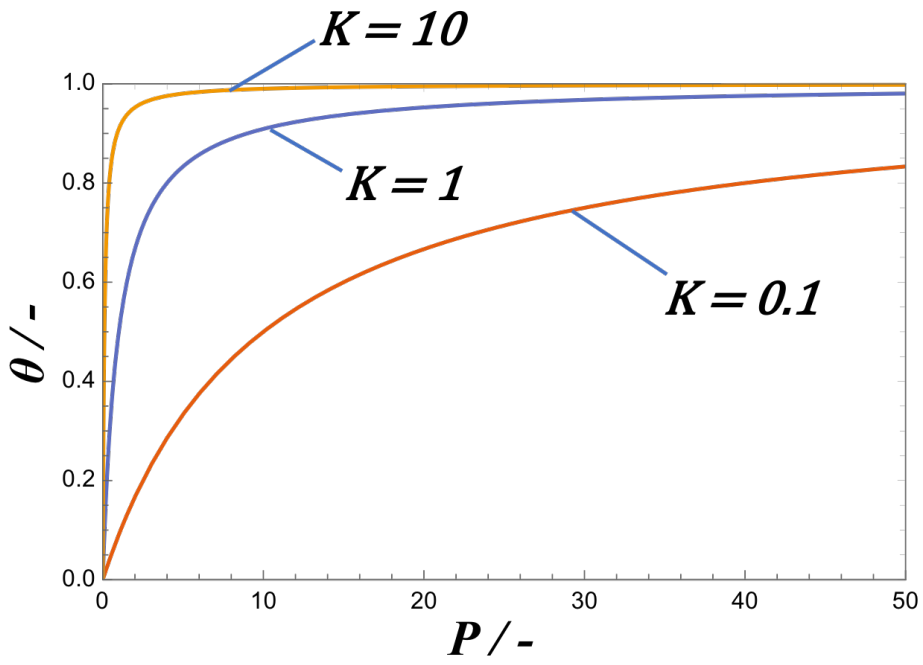

Figure 4-2-5. Plot of the fractional occupancy of the adsorption site of the Langmuir adsorption isotherm, $\theta = KP/(1+KP)$.

Langmuir-Hinshelwood mechanism.

There are two primary reaction mechanisms proposed for the surface-confined reaction, the Eley-Ridiel mechanism and the Langmuir-Hinshelwood mechanism. They are distinguished by the difference in elementary reaction processes considered as follows:

Eley-Ridiel: $A(a) + B \rightarrow AB$ (4.23)

Langmuir-Hinshelwood: $A(a) + B(a) \rightarrow AB$ (4.24)

where the Eley-Ridiel mechanism considers a reaction between adsorbed molecule $A(a)$ and free gas molecule B, and the Langmuir-Hinshelwood mechanism considers a reaction between the two adsorbed molecules on the surface (**Fig.4-2-6**). Conceptually they are both plausible mechanisms, however, many experimental works support that the Langmuir-Hinshelwood mechanism is preferred for the vast majority of surface reactions, while few reactions proceed via the Eley-Ridiel mechanism [Baxter & Hu 2002; Kuipers et al. 1991; Rettner 1992; Stampfl & Scheffler 1997]. In the Langmuir-Hinshelwood mechanism, if $A(a)$ and $B(a)$ do not react at attempt on the surface, they can wait for another opportunity since the reaction barrier is generally lower than the desorption energies of $A(a)$ and $B(a)$ (**Fig. 4-2-7**). The rate of the reaction per unit surface area in the Langmuir-Hinshelwood mechanism (4.24) is given by using (4.22) as follows:

$$\begin{aligned} r_s &= k_s N_s \theta_A \theta_B \\ &= k_s N_s \frac{K_A K_B P_A P_B}{(1 + K_A P_A + K_B P_B)^2} \end{aligned} \tag{4.25}$$

where k_s is a rate constant. When we assume that two species of molecules are adsorbed onto different species of sites on the same surface, and that molecules B are weakly adsorbed, *i.e.*, $K_B P_B \ll 1$, the rate of the reaction per unit surface area is given by:

$$\begin{aligned} r_s &= k_s' N_A N_B \frac{K_A K_B P_A P_B}{(1 + K_A P_A)(1 + K_B P_B)} \\ &\sim k_s' N_A N_B \frac{K_A K_B P_A P_B}{1 + K_A P_A} \\ &= k_s'' P_B \frac{K_A P_A}{1 + K_A P_A} \\ &= k_s'' P_B \theta_A \end{aligned} \tag{4.26}$$

where k_s' and k_s'' are the rate constants with different dimensions from k_s. Eq. (4.26) is known as the expression of reaction rate in the Eley-Ridiel mechanism.

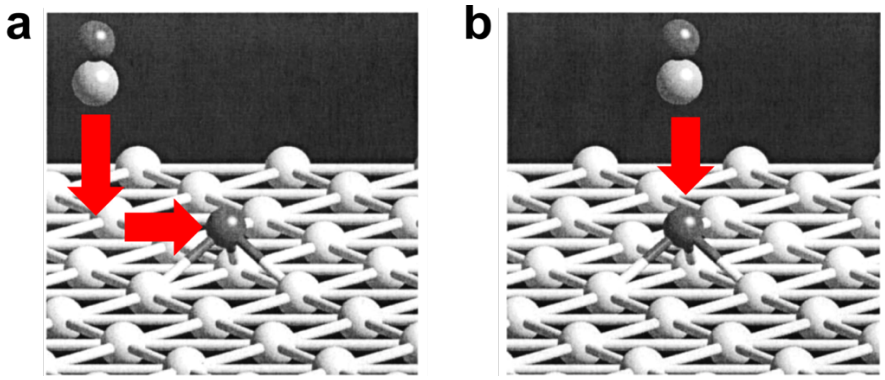

Fig. 4-2-6. Scheme of (**a**) Langmuir-Hinshelwood mechanism, where a free molecule is adsorbed onto the surface and then reacts with another molecule, and (**b**) Eley-Ridiel mechanism, where a free molecule directly reacts with a molecule adsorbed on the surface [Baxter & Hu 2002]. The illustrations represent the two supposed reaction mechanisms when a CO molecule reacts with O atom bound on metal surface.
Reprinted with permission from Baxter, R.J. & Hu, P., *J. Chemi. Phys.***116,** 4379-4381 (2002) © 2002 American Institute of Physics. Red arrows were added by M.K.

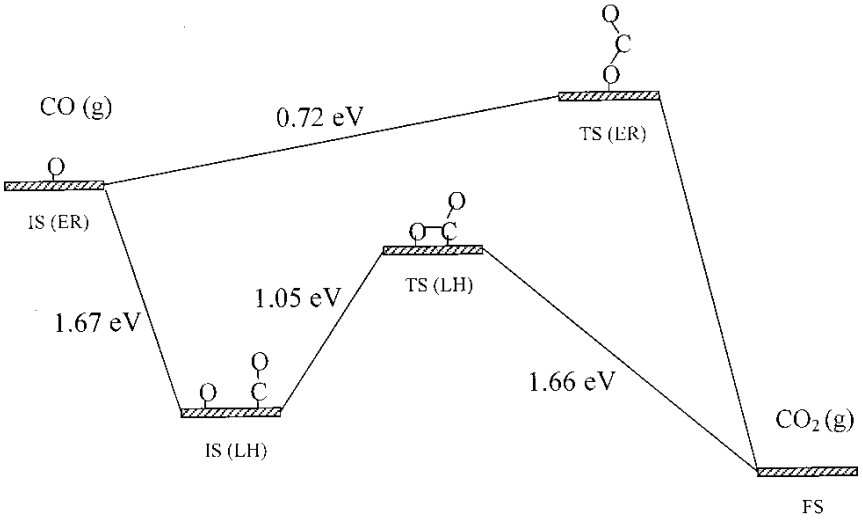

Fig. 5-2-7. Total energy diagram of both the Eley-Ridiel (ER) mechanism and the Langmuir-Hinshelwood (LH) mechanism for the formation of CO_2 with CO and O on Pt(111) surface. If CO and an O do not react at an attempt in LH mechanism, they can wait for another opportunity since the reaction barrier is lower than the desorption energies of both reactants.
Reprinted with permission from Baxter, R.J. & Hu, P., *J. Chemi. Phys.***116,** 4379-4381 (2002) © 2002 American Institute of Physics.

4.3 Kinetic model of our synthetic minimal cell

4.3.1 Reduced Model of Artificial Metabolism.

Overview of the model reactions.

Here I develop the idealized model reactions of my synthetic minimal cell to describe the kinetics of the system. I extract the essential processes of the system, then the original nine main reactions (R1 – R9) are reduced into the five model reactions (M1 – M5) as follows.

Model Reactions:

$$R_a + R_b + X \rightarrow Z + X \quad \text{(M1)}$$

$$2\,S + Y + Z \rightarrow 2\,S^* + Y \quad \text{(M2)}$$

$$2\,S^* + 2A_v^{out} \rightarrow P_2 + 2A_v^{out} \quad \text{(M3)}$$

$$S^* + Z + P_n + 2A_v^{out} \rightarrow P_{n+1} + 2A_v^{out} \quad \text{(M4)}$$

$$A_m + P_n \rightleftharpoons A(a) \rightleftharpoons A_v^{out} + P_n \quad \text{(M5)}$$

Each symbol represents an essential molecule of the system as follows: aniline (S), aniline radical cation (S^*), D-glucose (R_a), dissolved oxygen (R_b), enzyme GOD (X), enzyme HRPC (Y), H_2O_2 (Z), PANI-ES chain with the degree of polymerization n (P_n), AOT molecules located in the outer layer of the vesicle membrane (A_v^{out}), and supplied AOT molecules in external solution (A_m). Here the energy production domain (R1), the processing of information molecules domain (R2 - R8), and the membrane growth domain (R9) are contracted to (M1), (M2) – (M4) (activation of monomer, initiation reaction of PANI-ES synthesis by dimerization, and elongation reaction of PANI-ES synthesis), and (M5), respectively. The second and the third term in (M5) represents the transport of AOT molecules from the external solution (A_m) to vesicle membrane (A_v^{out}) through the intermediate complex (hydrogen-bonded PANI-ES and AOT) states on the surface of the membrane (see also **Fig.3-2-4**). The model reactions of our synthetic minimal cell are schematically shown in **Fig.4-3-1**, which should be compared with the equivalent scheme of the actual reaction (R1 – R9) (**Fig.3-2-1**).

The overall stoichiometry is preserved between actual chemical reactions (R1 - R8) and the model reactions (M1 - M4). For example, the overall net reaction to form one repeating unit of PANI-ES is given as follows:

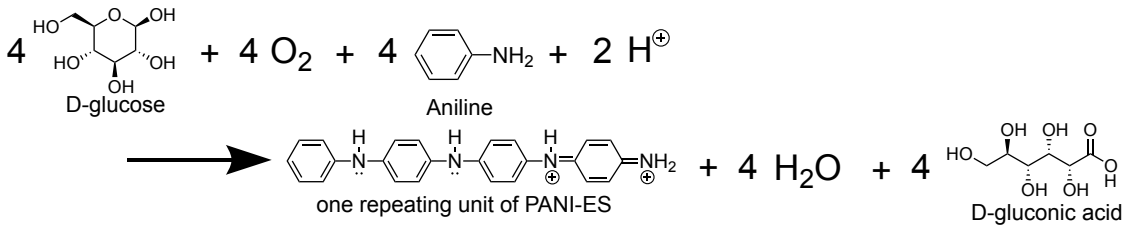

On the other hand, the overall net reaction to obtain one repeating unit of PANI-ES (P_4) in the model reactions are given by 4*(M1) + 2*(M2) + (M3) + 2*(M4) as follows:

$$4\,R_a + 4\,R_b + 4\,S \rightarrow P_4$$

Here the consumption of proton, formation of water, and gluconic acid molecules are ignored in the model system since we can apply the steady state approximation to protons and gluconic acids due to the continuous inflow and outflow around the vesicle (*i.e.,* Double Micro-Injection Technique), and since there are large excess water molecules. Besides these unimportant molecules, there is a stoichiometric agreement between the two expressions. There are no net production or destruction of the intermediate (S^* and Z) and enzymes (X and Y).

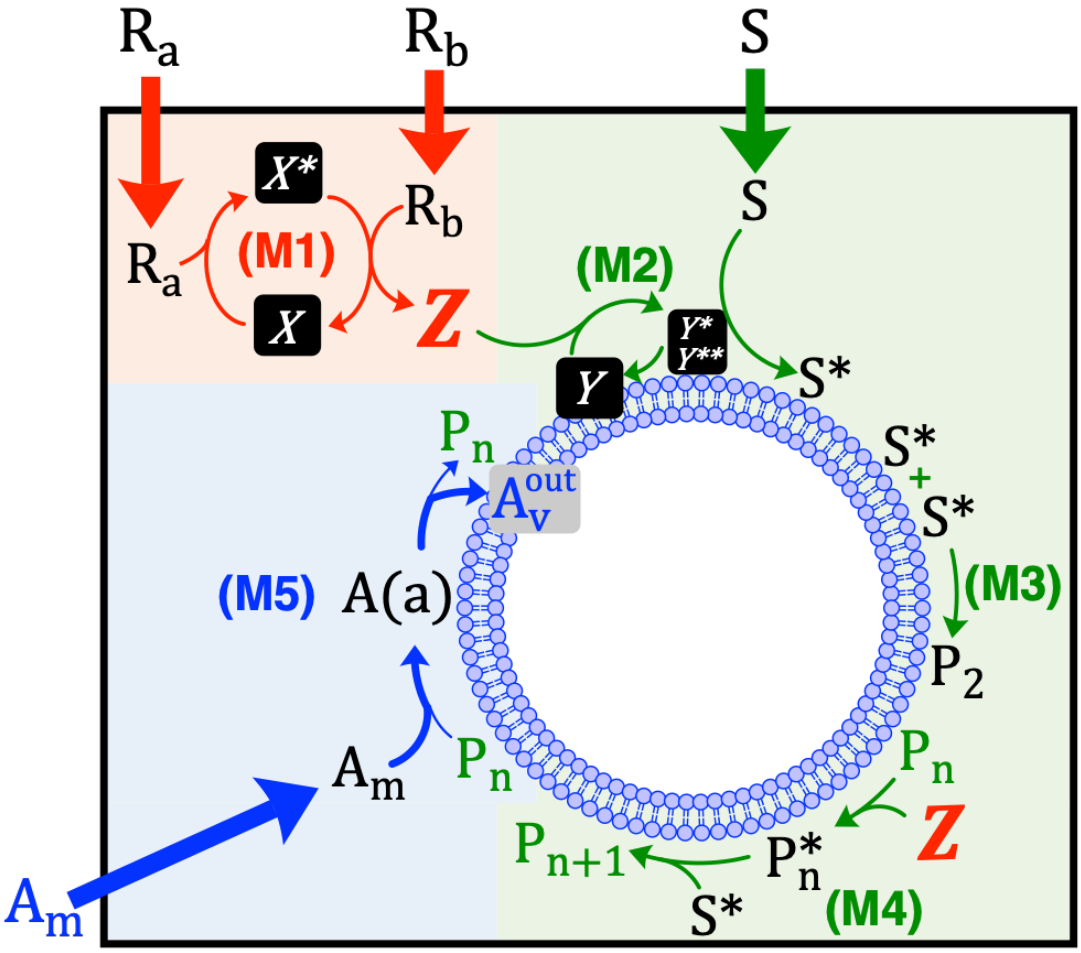

Figure 4-3-1. The reduced metabolic pathway of our synthetic minimal cell, which should be compared with the detailed metabolic pathway (**Fig.3-2-1**). The five reactions (M1 – R5) are assigned to three metabolic domains; energy production (orange), M1, synthesis of information polymer (green), M2 – M4, and membrane growth (blue), M5. The bold rectangle represents the reaction system close to the vesicle membrane, and bold arrows towards the inside of the rectangle represent that ingredients are continuously supplied close to the vesicles. Each symbol represents a relevant molecule of the system as follows: aniline (S), aniline radical cation (S^*), D-glucose (R_a), dissolved oxygen (R_b), enzyme GOD (X), enzyme HRPC (Y), H_2O_2 (Z), PANI-ES chain with the degree of polymerization n (P_n), AOT molecules located in the outer layer of vesicle membrane (A_v^{out}), supplied AOT molecules in external solution (A_m), and intermediate state of an AOT molecule adsorbed onto PANI-ES chain ($A(a)$). Please note that subsidiary reactions and molecules are omitted in the model reactions.

Derivation of model reactions and rate equations.

The five model reactions focus on the essence of our minimal cell system in which irrelevant reaction steps and molecules are omitted. Here we look into the details of each model reaction and then derive their rate equations. For values and units of the parameters described below, see the "Parameters List" (**Table 4-4-1**) in the next section.

(M1) Energy currency production:

The GOD (X)-catalyzed oxidation of D-glucose (R_a) by dissolved oxygen (R_b) to form H_2O_2 (Z), the "energy currency" of our minimal cell system, is described as reduced model reaction (M1) and **Fig.4-3-2** based on actual reaction (R1) (see **Fig.3-2-2** in section 3.2.2). This kinetics is known to strictly obey the ping pong bi bi mechanism [Bright & Porter 1975; Laskovac et al. 2005] (see 4.2.1). Here the native enzyme X is activated to X^* by using R_a and by forming D-glucono-δ-lactone that is a byproduct ignored in the model reaction system. The activated enzyme X^* produces energy currency Z from R_b, then returns to the native enzyme X.

The kinetics of GOD is known to strictly obey the ping pong bi bi mechanism, Eq. (4.9), [Bright & Porter 1975; Laskovac et al. 2005]. Therefore, the rate equation of (M1) is directly derived as follows:

$$v_1(t)[(mol\,L^{-1})\,s^{-1}] = \frac{[X]_0}{\frac{1}{k_{1,\,cat}} + \frac{1}{k_{1,\,red}[R_a(t)]} + \frac{1}{k_{1,\,ox}[R_b]}} \quad (4.27) \equiv (V1)$$

where $[X]_0$ is the total concentration of X, $[X]_0 = [X] + [X^*] + [X \bullet R_a] + [X^* \bullet R_b]$, and rate constants and equilibrium constants are newly defined for the sake of simplicity as follows: $k_{1,cat} = \frac{k_{1,b}k_{1,d}}{k_{1,b}+k_{1,d}}$, $k_{1,red} = \frac{k_{1,b}}{K_{1,A}}$, $k_{1,ox} = \frac{k_{1,d}}{K_{1,B}}$, $K_{1,A} = \frac{k_{1,-a}+k_{1,b}}{k_{1,a}} = \frac{[R_a][X]}{[X \bullet R_a]}$, and $K_{1,B} = \frac{k_{1,-c}+k_{1,d}}{k_{1,c}} = \frac{[R_b][X^*]}{[X^* \bullet R_b]}$. The values of rate constants are directly given by literature [Weibel & Bright 1971].

$$\text{(M1)} \quad R_a + R_b + X \rightarrow Z + X$$
$$\begin{pmatrix} R_a + X \rightarrow X^* \\ R_b + X^* \rightarrow X + Z \end{pmatrix}$$

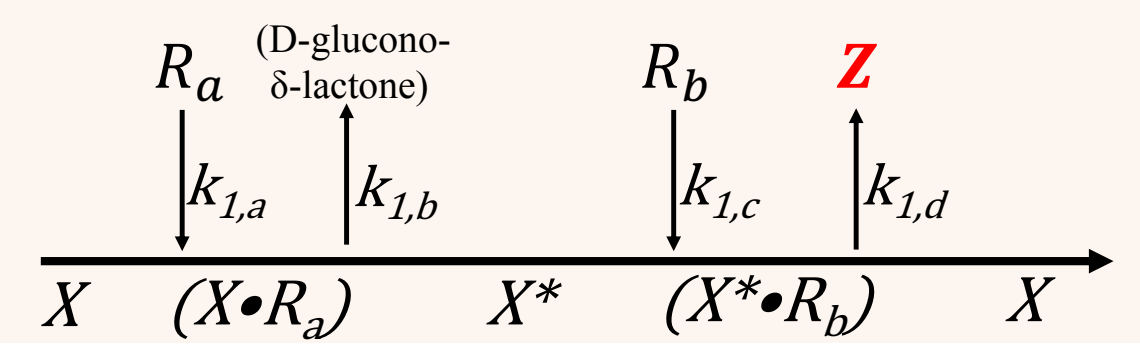

Figure 4-3-2. Cleland's diagram on the energy currency production domain (M1), driven by the ping pong bi bi mechanism.

(M2) Activation of monomer with energy currency:

The HRPC (Y) /H_2O_2 (Z)-catalyzed oxidation of aniline (S) to form anilino radical (*not shown*), which is followed by protonation to aniline radical cation (S^*), is described as reduced model reactions (M2) and **Fig.4-3-3** based on actual reactions (R2) and (R3) (see **Fig.3-2-3** in section 3.2.3). Since the intermediate anilino radical is assumed to be instantly protonated to aniline radical cation due to its p*K*a value (p*K*a=7.1, compared to pH=4.3 in the reaction solution) [Guo et al. 2009], the anilino radical is excluded from the discussion on model reactions. The formation of anilino radicals is known to obey the irreversible ping pong mechanism in which intermediate complexes between substrates and enzymes are very short-lived [Dunfold 1999]. Here the native enzyme Y receives energy currency molecule Z, then becomes one of the two activated states Y^*. The formation of a water molecule in this process is excluded from model reactions. Then, the activated enzyme Y^* activates two monomers S to S^* for the use in PANI-ES synthesis, while Y^* shifts its own states to another activation state Y^{**} and then to the native state Y. Consequently, one energy currency molecule is consumed to produce two

activated monomers within an enzyme cycle.

The formation of anilino radicals is considered to obey the irreversible ping pong mechanism, Eq. (4.9), in which intermediate complexes between substrates and enzymes are very short-lived [Dunfold 1999]. Therefore, the rate equation for the consumption of energy currency molecule is derived as follows:

$$v_2(t)\ [(mol\, m^{-2})\ s^{-1}] = \frac{[Y]_0}{\frac{1}{k_{2,a}[Z(t)]} + \frac{k_{2,b} + k_{2,c}}{k_{2,b}k_{2,c}[S(t)]}} \qquad (4.28) \equiv (V2)$$

where $[Y]_0$ is the total concentration of different oxidation states of Y, $[Y]_0 = [Y] + [Y^*] + [Y^{**}]$. The values of rate constants are given by literature [Dunford 1999; Dunford et al. 1978; Araiso & Dunford 1980; Job & Dunford 1976; Sakurada et al. 1990].

(M2) $2\,S + Y + Z \rightarrow 2\,S^* + Y$

$$\begin{pmatrix} Y + Z \rightarrow Y^* \\ Y^* + S \rightarrow Y^{**} + S^* \\ Y^{**} + S \rightarrow Y + S^* \end{pmatrix}$$

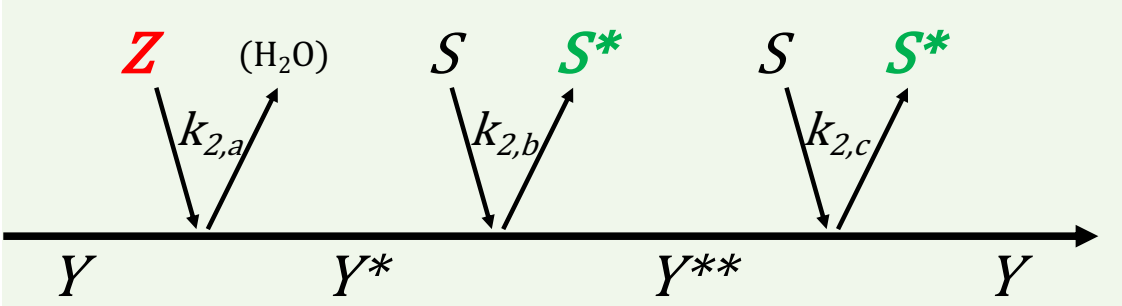

Figure 4-3-3. Cleland's diagram on the activation of monomer process (M2), driven by the irreversible ping pong mechanism.

(M3) Initiation reaction of information polymer:

Initiation reaction of information polymer PANI-ES is described based on actual reaction (R4) (see **Fig.3-2-3** in section 3.2.3) as the reduced model reaction (M3) and **Fig.4-3-4**, where the reaction between two aniline radical cations (S^*) to form aniline dimer (P_2) on the surface of AOT vesicle membrane [Junker et al. 2012; Genies & Tsintavis 1985; Ding

et al. 1999]. According to the previous studies on both experiment and simulation, aniline and anilinium cation molecules are expected to be bound to the surface of negatively charged AOT vesicle membrane due to the hydrogen bonding involving an amino group of aniline and sulfonate head group of AOT [Guo et al. 2009 and 2011; Junker et al. 2015; Iwasaki et al. 2017]. In addition, the outcome of MD simulation by Junker et al., which mimics the optimal situation for PANI-ES synthesis, indicates that anilinium cation molecules are concentrated near the membrane surface and forms hydrogen bonds to an average of 1.1 AOT molecules on AOT vesicle membrane [Junker et al. 2015]. Therefore, we assume that the dimerization process of aniline radical cations S^* is driven by the Langmuir-Hinshelwood mechanism (see 4.2.2). Here a free activated monomer close to a vesicle membrane S^* is adsorbed onto the outer layer of AOT vesicle membrane A_v^{out} with the adsorption-desorption equilibrium constant K_{S^*}. Then, the two adsorbed monomers $S^*(a)$ react to form a dimer P_2. This reaction produces a new chain of PANI-ES, followed by the next chain elongation process with the addition of monomers (M4).

The rate equation for the formation of a new chain of PANI-ES is derived based on the Langmuir-Hinshelwood mechanism, Eq. (4.25), as follows:

$$v_3(t)\ [(mol\, m^{-2})\ s^{-1}] = k_3 N_{AOT} \left(\frac{K_{S^*}[S^*(t)]}{1 + K_{S^*}[S^*(t)] + K_Z[Z(t)]} \right)^2 \quad (4.29) \equiv (V3)$$

where k_3 is a rate constant with undetermined value, K_{S^*} and K_Z are adsorption-desorption equilibrium constants of S^* and Z, respectively, and N_{AOT} is binding site density on vesicle surface, the value of which is given by the number of AOT molecules per unit surface area of AOT vesicle membrane. The K_{S^*} value is given by an adsorption-desorption equilibrium constant of anilinium cation, which is the accessible value through the outcome of MD simulations [Junker et al. 2015] (see Appendix 4-A). The value of the rate constant k_3 is determined by the experiment, see the later discussions (section 4.4.1). Please note that almost all aniline dimer P_2 is assumed to be localized to AOT bilayer according to the other MD simulations [Junker et al. 2014; Luginbühl et al. 2016], while some fractions of aniline radical cations (S^*) might be free from the membrane.

$$\textbf{(M3)}\quad 2\,S^* + 2A_v^{out} \rightarrow P_2 + 2A_v^{out}$$

$$\left(\begin{array}{c} S^* + A_v^{out} \rightarrow S^*(a) \\ 2\,S^*(a) \rightarrow P_2 + 2\,A_v^{out} \end{array}\right)$$

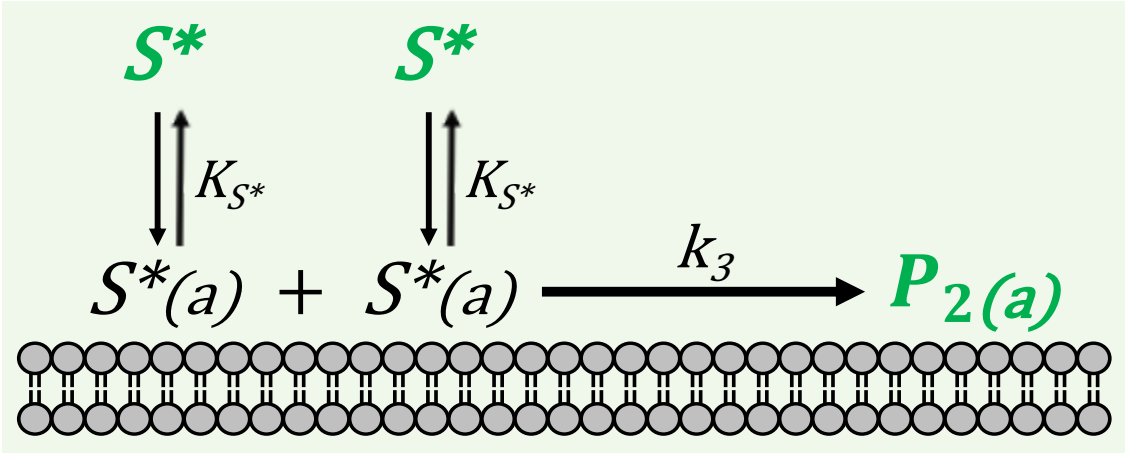

Figure 4-3-4. Reaction scheme on the initiation reaction of PANI-ES chain synthesis (M3), driven by the Langmuir-Hinshelwood mechanism.

(M4) Elongation reaction of information polymer:

Elongation reaction of information polymer PANI-ES is described by the combination of two reaction processes on the surface of AOT vesicles based on actual reactions (R5 - R8), where PANI-ES chain (P_n) is oxidized with H_2O_2 (Z), then aniline radical cation molecules (S^*) is added to the oxidized PANI-ES chain (P_n^*). We assume that the elongation process of PANI-ES synthesis is driven by the irreversible ping pong mechanism combined with the Langmuir-Hinshelwood mechanism (see 4.2.2) as described by reduced model reaction (M4) and **Fig.4-3-5**. Here the energy currency molecule Z close to the vesicle is adsorbed onto the outer layer of the vesicle membrane A_v^{out}, then the adsorbed energy currency $Z(a)$ activates the native PANI-ES P_n located on the surface of the vesicle. The activated monomer S^* close to vesicle membrane is also adsorbed onto the surface $S^*(a)$, then react with the active site of PANI-ES chain P_n^* to elongate the PANI-ES chain by one monomeric unit to P_{n+1}. The number of PANI-ES chains remains constant within an elongation cycle, and the concentration of native

P_n and activated P_n^* PANI-ES chain assume to be in equilibrium.

The rate equation of (M4) for the monomeric elongation of PANI-ES chain is described by the irreversible ping pong mechanism, Eq. (4.10), combined with the Langmuir-Hinshelwood mechanism, Eq. (4.25), as follows:

$$v_4'(t)[(mol\,m^{-2})\,s^{-1}] = \frac{\frac{[P(t)]_{chain}}{[A(t)]}}{\frac{1}{k_{4,a}N_{AOT}\left(\frac{K_Z[Z(t)]}{1+K_Z[Z(t)]+K_{S^*}[S^*(t)]}\right)}+\frac{1}{k_{4,b}N_{AOT}\left(\frac{K_{S^*}[S^*(t)]}{1+K_Z[Z(t)]+K_{S^*}[S^*(t)]}\right)}} \quad (4.30)$$

where $k_{4,a}$ and $k_{4,b}$ are rate constants with undetermined values, K_{S^*} and K_Z are adsorption-desorption equilibrium constants of $S^*$and Z, respectively, N_{AOT} is binding site density on vesicle surface, and $[P(t)]_{chain}/[A(t)]$ is the density of PANI-ES chains on vesicle surface since $[P(t)]_{chain}$ (mol/L) is the concentration of the total number of PANI-ES chains ($[P(t)]_{chain} = \sum_{n=1}^{\infty} N_n$, N_n:number of PANI-ES chains with the degree of polymerization of *n*), $[A(t)]$ (m^2/L) is the concentration of vesicle surface exposed to the external solution.

We made a few assumptions to obtain rate equation Eq. (4.30). Firstly, we assumed that the coverage of vesicle surface by PANI-ES chains does not interfere with initiation reaction (M3), adsorption and desorption of substrates ($S^*$and Z), *i.e.*, the coverage of PANI-ES is assumed to be dilute enough within the timescale of vesicle observation (~100 s), film-on-film growth mechanism is assumed, or both. Thus, the initiation reaction and elongation reaction of PANI-ES do not interfere with each other [Sapurina et al. 2001]. Secondly, we assume that all the PANI-ES chains are linear without branching structures, *i.e.*, all PANI-ES chains equally have the opportunity to react with Z and S^*, regardless of their degrees of polymerization n. This assumption is reasonable since the linear structure, PANI-ES, is relevant in the polyaniline products synthesized on the AOT vesicle surface. Finally, we apply an approximation to Eq. (4.30) to reduce the number of undetermined rate constants (fitting parameters for the experimental results) as follows:

$$v_4(t)[(mol\,m^{-2})\,s^{-1}] = k_4 N_{AOT}\frac{[P(t)]_{chain}}{[A(t)]}\frac{K_Z K_{S^*}[Z(t)][S^*(t)]}{(1+K_Z[Z(t)]+K_{S^*}[S^*(t)])(K_Z[Z(t)]+K_{S^*}[S^*(t)])} \equiv (V4) \quad (4.31)$$

where k_4 is a newly defined rate constant in (M4), assuming $k_4 = k_{4,a} = k_{4,b}$ for Eq. (4.30). As discussed later in section 4.4.1, the values of rate constants k_3 in (M3) and k_4 in (M4) are determined based on the experimentally observed kinetics of PANI-ES synthesis.

$$\textbf{(M4)}\quad S^* + Z + P_n + 2A_v^{out} \rightarrow P_{n+1} + 2A_v^{out}$$

$$\begin{pmatrix} S^* + A_v^{out} \rightarrow S^*(a) \\ Z + A_v^{out} \rightarrow Z(a) \\ Z(a) + P_n \rightarrow P_n^* + A_v^{out} \\ S^*(a) + P_n^* \rightarrow P_{n+1} + A_v^{out} \end{pmatrix}$$

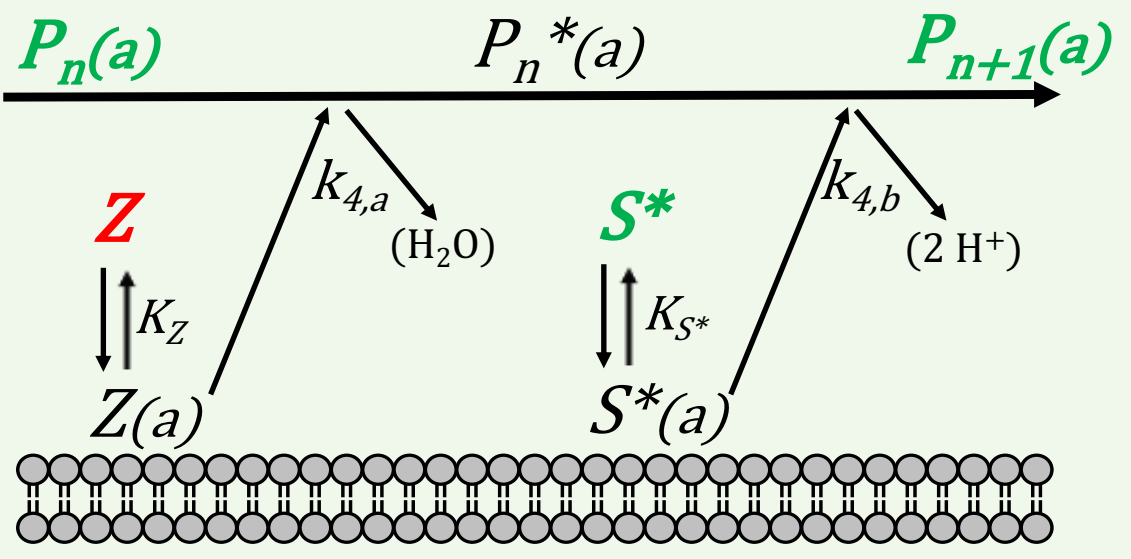

Figure 4-3-5. Cleland's diagram on the elongation reaction of PANI-ES chain synthesis (M4), driven by the irreversible ping pong mechanism combined with the Langmuir-Hinshelwood mechanism.

(M5) Vesicle membrane growth:

Initially, we suppose that the molecular mechanism of membrane growth involves two intermediate complex states between amphiphiles and PANI-ES (**Fig.3-2-4**), but here we suppose only one intermediate state for the sake of simplification (**Fig. 4-3-6**). This assumption does not change the form of rate equation, see Eq. (4.7) and (4.8). Here we assume that the two species of amphiphile (A_m and A_v^{out}) are competitive to adsorb onto the binding site, *i.e.,* PANI-ES segments (P_n), on the vesicle surface. For the incorporation of amphiphiles, free amphiphile close to vesicle A_m is adsorbed onto the surface-confined free PANI-ES segments P_n with the adsorption-desorption equilibrium constant K_m to form an amphiphile-PANI intermediate complex $A(a)$, followed by a breakdown of the complex to partition the amphiphiles into vesicle membrane A_v^{out} and to form a free binding site P. The rate equation for the incorporation of amphiphiles is given as Eq. (4.32) by applying the steady-state approximation to the surface density of adsorbed amphiphiles per unit surface area.

$$v_5(t)[(mol\,m^{-2})\,s^{-1}] = k_{5,m}\frac{K_m[A_m]}{1 + K_m[A_m] + K_v[A_v^{out}]}\frac{[P(t)]_{mono}}{[A(t)]} \quad (4.32)$$

$$\equiv k_5\frac{[P(t)]_{mono}}{[A(t)]} \quad (4.33) \equiv (V5)$$

where $k_{5,m}$ is a translocation rate constant, and $[P(t)]_{mono}/[A(t)]$ is the density of binding sites for amphiphiles on vesicle surface since $[P(t)]_{mono}$ (mol/L) is the concentration of the total number of the monomeric units of PANI-ES ($[P(t)]_{mono} = \sum_{n=1}^{\infty} n\,N_n$, N_n:number of PANI-ES chains with the degree of polymerization of *n*), $[A(t)]$ (m^2/L) is the concentration of vesicle surface exposed to the external solution. Here the values of $[A_m]$ and $[A_v^{out}]$ are assumed to be constant since the constant concentrations of amphiphiles are continuously supplied close to vesicles by micro-injection technique, and the density of amphiphiles located in vesicle membrane is almost constant. Therefore, we obtain Eq. (4.33) as the rate equation of (M5) by using the newly given rate constant k_5.

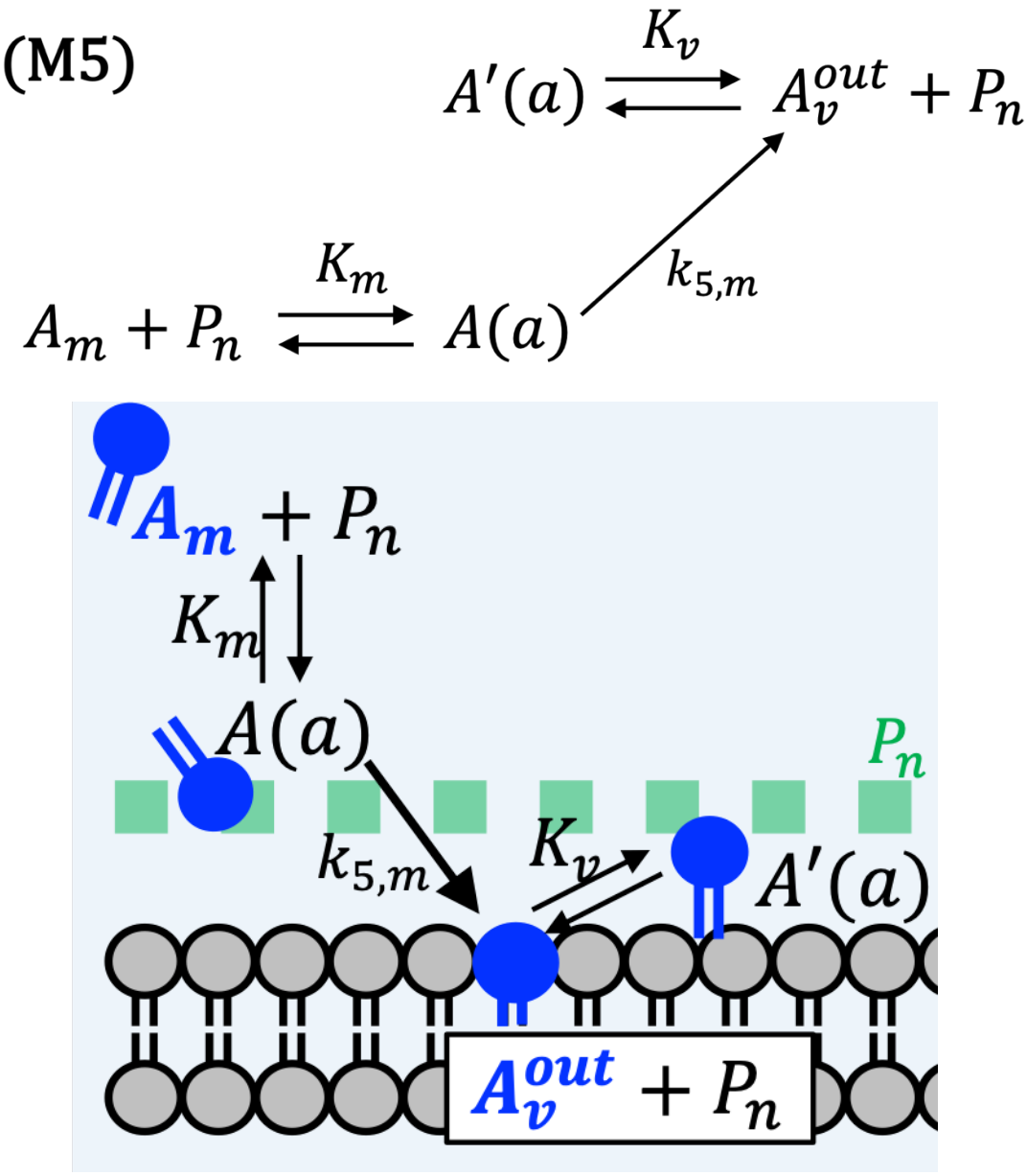

Figure 4-3-6. Diagram on the incorporation of membrane molecules (M5), driven via the competitive Langmuir adsorption.

4.3.2 Parameter List for Artificial Metabolism

Values and units of the rate equation parameters (V1 – V5) are shown in **Table 4-3-1**. The values of parameters k_3 in (V3), k_4 in (V4), and k_5 in (V5) are determined later based on the control experiments in section 4.4.1. Except these three parameters, all other values of the parameters in the list are given or estimated based on the literature.

Table 4-3-1. Parameters and their values used in the kinetic model of artificial metabolism.

	Parameter	Value [unit]	Comment	Reference
M1 *(V1)*	$v_1(t)$	$[(mol\ L^{-1})\ s^{-1}]$	Rate constant for the formation of energy currency molecule, Z, by using ingredients R_a and R_b. Please note that only $v_1(t)$ has a different dimension to other rate constants.	
	$[X]_0$	1.0 *10^{-6} [M]	The concentration of GOD. Initial concentration is given by experimental setup.	From experimental setup.
	$k_{1,cat}$	1.0 *10^3 [s^{-1}]	The redefined rate constant of ping pong bi bi mechanism. The value is given by literature, obtained at pH = 4.0, in potassium citrate buffer. $k_{1,cat} = \frac{k_{1,b}k_{1,d}}{k_{1,b}+k_{1,d}}$ (see **Fig. 4-3-2**)	[Weibel & Bright 1971]
	$k_{1,red}$	1.5 * 10^4 [M^{-1} s^{-1}]	The redefined rate constant of ping pong bi bi mechanism. The value is given by literature, obtained at pH = 4.0, in potassium citrate buffer. $k_{1,red} = \frac{k_{1,b}}{K_{1,A}}$ (see **Fig. 4-3-2**)	[Weibel & Bright 1971]
	$k_{1,ox}$	1.9 *10^6 [M^{-1} s^{-1}]	The redefined rate constant of ping pong bi bi mechanism. The value is given by literature, obtained at pH = 4.0, in	[Weibel & Bright 1971]

			potassium citrate buffer. $k_{1,ox} = \frac{k_{1,d}}{K_{1,B}}$ (see **Fig. 4-3-2**)	
	$[R_a(t)]$	*(initial value)* 0.100 [M]	The concentration of D-glucose. In the vesicle growth experiment, this is constant due to the continuous supply by micro-injection (see **Fig.2-5-1**). In the closed-microtube experiment, this value decreases due to consumption.	From experimental setup.
	$[R_b]$	*(saturated value)* 0.23 [mM]	The concentration of dissolved oxygen. O_2 is consumed for H_2O_2 production and simultaneously supplied externally during the reaction. The concentration of O_2 in the reaction mixture assumes to be in equilibrium at 10% (in rotary mixed closed microtube) or at 3% (in vesicle growth system (**Fig.2-5-1**)) of the *saturated value*.	[Reynafarje et al. 1985] [Millero et al. 2002]
M2 (V2)	$v_2(t)$	$[(mol\, m^{-2})\, s^{-1}]$	Rate constant for the activation of monomers, S, by using energy currency molecule, Z. The rate equation V2 is given for the consumption of Z.	
	$[Y]_0$	$3.04 * 10^{-9}$ [mol m^{-2}] ($0.92 * 10^{-6}$ [M])	The concentration of HRPC. The concentration in the reaction solution ($0.92 * 10^{-6}$ [M]) is converted to the concentration on the surface of the vesicle membrane ([mol m^{-2}]) by using the value of $[A]_0$, see below.	From experimental setup.
	$k_{2,a}$	$1.7 * 10^7$ [$M^{-1}\, s^{-1}$]	The rate constant of irreversible ping pong mechanism. The value is given by literature, obtained at pH = 7.0, in various solutions.	[Dunford 1999] [Dunford et al. 1978] [Araiso & Dunford 1980]

	$k_{2,b}$	2.4 *10^5 [M^{-1} s^{-1}]	The rate constant of irreversible ping pong mechanism. The value is given by literature, obtained at pH = 7.0, in phosphate buffer.	[Dunford 1999] [Job & Dunford 1976]
	$k_{2,c}$	8.6 *10^4 [M^{-1} s^{-1}]	The rate constant of irreversible ping pong mechanism. The value is given by literature, obtained at pH = 7.0, in sodium phosphate buffer.	[Dunford 1999] [Sakurada et al. 1990]
	$[S(t)]$	4.0*10^{-3} [M]	The initial concentration of aniline.	From experimental setup.
	$[Z(t)]$	*(initial value)* 0 [M], 2 [M], or 4.5*10^{-3} [M]	Concentration of H_2O_2. The initial concentration of H_2O_2 is 0 [M] (when H_2O_2 is *in situ* formed by M1), 2 [M] (when H_2O_2 is supplied by micro-injection (**Fig.2-5-1**)), or 4.5*10^{-3} [M] (when H_2O_2 is initially added to microtubes (**Fig.2-3-1**)).	From experimental setup.
	pH influence	Decrease to ~ 20%	At pH = 4.3, HRPC activity decreases to ~20% compared to the activity at pH = 7.	[Toyobo Enzymes]
M3 (V3)	$v_3(t)$	$[(mol\, m^{-2})\, s^{-1}]$	Rate constant for the initiation reaction of PANI-ES synthesis by dimerization of the activated monomers, S^*. The rate equation V3 is given for the formation of PANI-ES chain, $[P(t)]_{chain}$.	
	a_{AOT}	0.67 [nm^2]	Surface area per single AOT molecule in vesicle membrane.	[Grillo et al. 2000]
	N_{AOT}	2.48 *10^{-6} [mol m^{-2}]	Site density for S^* adsorption on vesicle membrane, given by the density of AOT molecules on vesicle surface, $1/a_{AOT}$.	[Grillo et al. 2000]
	k_3	1.0 * 10^4 [s^{-1}]	The rate constant of the initiation reaction for the PANI-ES synthesis. The value is determined based on experiments, see section 4.4.1.	Determined based on experiments.

	$[S^*(t)]$	*(initial value)* 0 [M]	The concentration of aniline radical cation.	From experimental setup.
	$[Z(t)]$	*(initial value)* 0 [M], 2 [M], or $4.5*10^{-3}$ [M]	Concentration of H_2O_2. The initial concentration of H_2O_2 is 0 [M] (when H_2O_2 is *in situ* formed by M1), 2 [M] (when H_2O_2 is supplied by micro-injection (**Fig.2-5-1**)), or $4.5*10^{-3}$ [M] (when H_2O_2 is initially added to microtubes (**Fig.2-3-1**)).	From experimental setup.
	K_{S^*}	2.29 [M^{-1}]	The equilibrium constant of Langmuir adsorption isotherm of aniline radical cation. The value is estimated from the outcome of MD simulation. The value of aniline cation assumes to be the same as that of aniline radical cation. See also Appendix 4-A.	[Junker et al. 2015] Appendix 4-A.
	K_Z	2.29 [M^{-1}]	The equilibrium constant of Langmuir adsorption isotherm of H_2O_2. We assume $K_Z = K_{S^*}$, since the value of K_Z does not affect the kinetic significantly.	
M4 (V4)	$v_4(t)$	$[(mol\, m^{-2})\, s^{-1}]$	The rate constant for the elongation reaction of PANI-ES synthesis by addition of the activated monomers, S^*, to a PANI-ES chain, $[P(t)]_{chain}$, by using an energy currency molecule, Z.	
	$[S^*(t)]$	*(initial value)* 0 [M]	The concentration of aniline radical cation.	
	$[Z(t)]$	*(initial value)* 0 [M], 2 [M], or $4.5*10^{-3}$ [M]	Concentration of H_2O_2. The initial concentration of H_2O_2 is 0 [M] (when H_2O_2 is *in situ* formed by M1), 2 [M] (when H_2O_2 is supplied by micro-injection (**Fig.2-5-1**)), or $4.5*10^{-3}$ [M] (when H_2O_2 is initially added to microtubes (**Fig.2-3-1**)).	From experimental setup.

	k_4	1.0 * $10^{7.5}$ [(mol m^{-2}) $^{-1}$ s^{-1}]	Rate constant on elongation reaction for the PANI-ES synthesis. The value is determined based on experiments, see section 4.4.1.	Determined based on experiments.
	L	6.02 * 10^{23} [mol^{-1}]	Avogadro constant.	
	cvc	1.5 [mM]	The concentration of AOT molecules present as the single-molecule state.	[Kurisu et al. 2019]
	$[A_v(t)]$	*(initial value)* 1.5 [mM]	The concentration of AOT molecules forming vesicles in the reaction mixture, 3.0 [mM] – cvc. We assume that the amphiphiles are equally partitioned into the inner and the outer layer of vesicles ($[A_v(t)]/2$), respectively.	[Kurisu et al. 2019]
	$[A(t)]$	*(initial value)* 3.03 *10^2 [m^2 L^{-1}]	Vesicle surface area per 10^{-3} m^3 dispersed in the reaction mixture. Given by: 1.5 [mM] * 1/2 * L [mol^{-1}] * a_{AOT}[nm^2]	From experimental setup.
	N_{AOT}	2.48 *10^{-6} [mol m^{-2}]	Site density for S^* adsorption on vesicle membrane, given by the density of AOT molecules on vesicle surface, $1/a_{AOT}$.	[Grillo et al. 2000]
	$[P(t)]_{chain}$	*(initial value)* 0 [M]	The concentration of PANI-ES chains formed via model reaction (M3). ($[P(t)]_{chain} = \sum_{n=1}^{\infty} N_n$, N_n: number of PANI-ES chains with the degree of polymerization of *n*)	
	K_{S^*}	2.29 [M^{-1}]	The equilibrium constant of Langmuir adsorption isotherm of aniline radical cation. The value is estimated from the outcome of MD simulation. The value of aniline cation assumes to be the same as that of aniline radical cation. See also Appendix 4-A.	[Junker et al. 2015] Appendix 4-A.

	K_Z	2.29 [M^{-1}]	The equilibrium constant of Langmuir adsorption isotherm of H_2O_2. We assume $K_Z = K_{S^*}$, since the value of K_Z does not affect the kinetic significantly.	
M5 (V5)	$v_5(t)$	$[(mol\ m^{-2})\ s^{-1}]$	Rate constant for the incorporation of free amphiphiles, A_m, through the adsorption onto PANI-ES structures, $[P(t)]_{mono}$.	
	$[A(t)]$	*(initial value)* 3.03 *10^2 [$m^2\ L^{-1}$]	Vesicle surface area per 10^{-3} m^3 dispersed in the reaction mixture. Given by: 1.5 [mM] * 1/2 * L [mol^{-1}] * a_{AOT}[nm^2]	From experimental setup.
	$[A_v(t)]$	*(initial value)* 1.5 [mM]	The concentration of AOT molecules forming vesicles in the reaction mixture, 3.0 [mM] – cvc. We assume that the amphiphiles are equally partitioned into the inner and the outer layer of vesicles ($[A_v(t)]/2$), respectively.	[Kurisu et al. 2019]
	k_5	6.0 * 10^{-3} [s^{-1}]	Rate constant on the incorporation of AOT molecules. The value is determined based on experiments, see section 4.4.1.	Determined based on experiments.
	$[P(t)]_{mono}$	*(initial value)* 0 [M]	The concentration of total PANI-ES monomeric units formed via model reactions (M3) and (M4). ($[P(t)]_{mono} = \sum_{n=1}^{\infty} n\ N_n$, N_n:number of PANI-ES chains with the degree of polymerization of *n*)	
	$[A_m]$	20 [mM]	The concentration of free AOT molecules supplied to the vesicles with micro-injection.	From experimental setup.

4.3.3 Kinetic Model: *Artificial Metabolism System*

Based on the above discussion (section 4.3.1) and parameters (section 4.3.2), the simultaneous differential equations describing the kinetics of the artificial metabolism system (**Fig. 4-3-1**) are given by:

$$\frac{d[P(t)]_{chain}}{dt} = v_3(t) * [A(t)] \tag{Ia}$$

$$\frac{d[P(t)]_{mono}}{dt} = \big(2 * v_3(t) + v_4(t)\big) * [A(t)] \tag{Ib}$$

$$\frac{d[S^*(t)]}{dt} = \big(2 * v_2(t) - 2 * v_3(t) - v_4(t)\big) * [A(t)] \tag{Ic}$$

$$\frac{d[Z(t)]}{dt} = v_1(t) - \big(v_3(t) + v_4(t)\big) * [A(t)] \tag{Id}$$

$$\frac{d[A_v(t)]}{dt} = v_5(t) * [A(t)] \tag{Ie}$$

$$[A(t)] = \frac{1}{2} * [A_v(t)] * L * \ a_{AOT} \tag{If}$$

$$\frac{d[A_m]}{dt} = \frac{d[S]}{dt} = \frac{d[R_a]}{dt} = \frac{d[R_b]}{dt} = 0 \tag{Ig}$$

where $[P(t)]_{chain}$ and $[P(t)]_{mono}$ are the concentration ([M]) of information polymer (PANI-ES) defined with the number of polymer chains and their consisting monomeric units, respectively, $[S^*(t)]$ ([M]) is the concentration of activated monomers, $[Z(t)]$ ([M]) is the concentration of energy currency molecules, $[A_v(t)]$ ([M]) is the concentration of amphiphiles which form vesicle membranes, $[A(t)]$ ($[m^2/L]$) is the concentration of vesicle surface area, $v_{i=1-5}(t)$ is the rate equation of each reduced model reaction (M1 – M5) derived in section 4.3.1, L is the Avogadro constant, and a_{AOT} is the surface area occupied by single amphiphile located in vesicle membrane. The concentrations of continuously supplied ingredients are kept constant, where $[A_m]$, $[S]$, $[R_a]$, and $[R_b]$ are the concentrations of supplied membrane molecules, monomer (aniline), and the ingredients for energy currency molecules (D-glucose and dissolved O_2), respectively.

The kinetic model is designed to enable the comparison between model and experiments. The kinetics of information polymer (PANI-ES) synthesis can be observed by the time-dependent change of characteristic absorbance for polaron structures of PANI-ES, which relates with the change of $[P(t)]_{mono}$. The kinetics of vesicle membrane growth can be directly observed by phase contrast optical microscopy, which

relates with the change of $[A(t)]$. The values of the three undetermined rate constants $k_{i=3,4,5}$ are determined based on the control experiments of artificial metabolism system and the corresponding kinetic models (shown just below). The time-dependent concentration changes of the intermediate components, $[Z(t)]$ (energy currency molecule), $[S]$ (aniline), and $[R_a]$ (D-glucose), are also observable with the analytical methods described in section 3.3.5.

4.3.4 Kinetic Model: *Control Systems*

To describe the kinetics of our synthetic minimal cell, we need to determine the values of parameters k_3 in (V3), k_4 in (V4), and k_5 in (V5) based on experiments. Therefore, in addition to the differential equations that describe synthetic minimal cell shown just above (section 4.3.3), we look into the three control sets of differential equations (i), (ii), and (iii) for the corresponding control experiments.

Control: Information polymer synthesis WITHOUT vesicle growth.

(i) PANI-ES synthesis *without* vesicle growth (M5), *without* energy production (M1).

Considering only the PANI-ES synthesis on vesicle surface by forgetting the concept of the minimal cell, energy production domain (M1) and vesicle growth domain (M5) are unnecessary (see **Fig.4-3-7**). In this case, the appropriate amount of energy currency molecule and aniline (Z_0 and $S^*{}_0$, respectively) are initially added to trigger the polymerization, and then the system reaches equilibrium after completely consuming the initially added one or both ingredients. The simultaneous differential equations describing time-dependence of PANI-ES synthesis in this system are given by:

$$\frac{d[P(t)]_{chain}}{dt} = v_3(t) * [A(t)] \qquad (IIa)$$

$$\frac{d[P(t)]_{mono}}{dt} = \big(2 * v_3(t) + v_4(t)\big) * [A(t)] \qquad (IIb)$$

$$\frac{d[S^*(t)]}{dt} = \big(2 * v_2(t) - 2 * v_3(t) - v_4(t)\big) * [A(t)] \qquad (IIc)$$

$$\frac{d[Z(t)]}{dt} = -\big(v_3(t) + v_4(t)\big) * [A(t)] \qquad (IId)$$

$$\frac{d[A_v(t)]}{dt} = 0 \qquad (IIe)$$

$$[A(t)] = \frac{1}{2} * [A_v(t)] * L * \ a_{AOT} \qquad (IIf)$$

$$\frac{d[S(t)]}{dt} = -2 * v_2(t) * [A(t)] \qquad (IIg)$$

where $[P(t)]_{chain}$ and $[P(t)]_{mono}$ are the concentration ([M]) of information polymer (PANI-ES) defined with the number of polymer chains and their consisting monomeric units, respectively, $[S^*(t)]$, $[Z(t)]$, $[A_v(t)]$ ([M]) are the concentrations of activated monomers, energy currency molecules, and vesicle forming molecules, respectively, $[A(t)]$ ($[m^2/L]$) is the concentration of vesicle surface area, $v_{i=2-4}(t)$ is the rate

equation of each model reaction (M2 – M4), L is the Avogadro constant, and a_{AOT} is the surface area per single vesicle forming molecule. The concentrations of aniline $[S(t)]$ and energy currency $[Z(t)]$ decreases monotonically from the initial values with the progress of information polymer synthesis. The corresponding experimental setup is **Fig. 2-3-1**. The values of rate constants k_3 in (V3) and k_4 in (V4) are determined by using (IIa – IIg), see the *Simulation* section below.

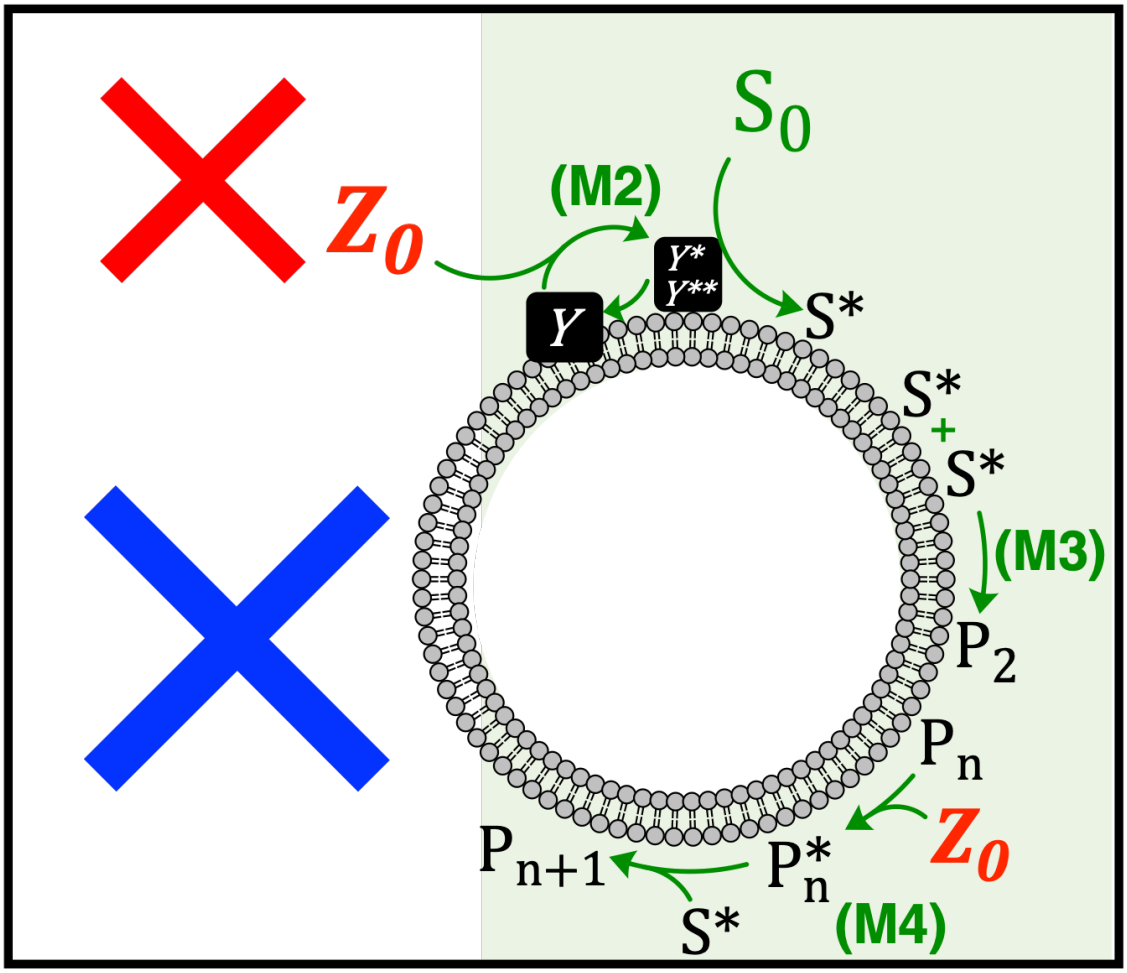

Figure 4-3-7. Scheme of the control system of the artificial metabolism where energy production domain and membrane growth domain are omitted, and initially added energy currency molecule Z_0 and aniline S_0 trigger the PANI-ES synthesis on the vesicle surface. When one or both ingredients are entirely consumed, the system reaches equilibrium.

(ii) PANI-ES synthesis *without* vesicle growth (M5).

Again, considering only the PANI-ES synthesis on vesicle surface by forgetting the concept of the minimal cell, here vesicle growth domain (M5) is omitted while energy production domain (M1) is introduced (see **Fig. 4-3-8**). In this case, the appropriate amount of ingredients ($R_{a,0}$ and $S^*{}_0$) are initially added to trigger the polymerization, and then the system reaches equilibrium after completely consuming the initially added one or two ingredients. The simultaneous differential equations describing this time-dependence of PANI-ES synthesis are given by:

$$\frac{d[P(t)]_{chain}}{dt} = v_3(t) * [A(t)] \qquad (IIIa)$$

$$\frac{d[P(t)]_{mono}}{dt} = \big(2 * v_3(t) + v_4(t)\big) * [A(t)] \qquad (IIIb)$$

$$\frac{d[S^*(t)]}{dt} = \big(2 * v_2(t) - 2 * v_3(t) - v_4(t)\big) * [A(t)] \qquad (IIIc)$$

$$\frac{d[Z(t)]}{dt} = v_1(t) - \big(v_3(t) + v_4(t)\big) * [A(t)] \qquad (IIId)$$

$$\frac{d[A_v(t)]}{dt} = 0 \qquad (IIIe)$$

$$[A(t)] = \frac{1}{2} * [A_v(t)] * L * a_{AOT} \qquad (IIIf)$$

$$\frac{d[S(t)]}{dt} = -2 * v_2(t) * [A(t)] \qquad (IIIg)$$

$$\frac{d[R_a]}{dt} = -v_1(t) \qquad (IIIh)$$

$$\frac{d[R_b]}{dt} = 0 \qquad (IIIi)$$

where $[P(t)]_{chain}$ and $[P(t)]_{mono}$ are the concentration ([M]) of information polymer (PANI-ES) defined with the number of polymer chains and their consisting monomeric units, respectively, $[S^*(t)]$, $[Z(t)]$, $[A_v(t)]$ ([M]) are the concentrations of activated monomers, energy currency molecules, and vesicle forming molecules, respectively, $[A(t)]$ ($[m^2/L]$) is the concentration of vesicle surface area, $v_{i=1-4}(t)$ is the rate equation of each model reaction (M1 – M4), L is the Avogadro constant, and a_{AOT} is the surface area per single vesicle forming molecule. The concentrations of aniline $[S(t)]$ and ingredient for energy currency (D-glucose) $[R_a]$ decreases monotonically from the initial values with the progress of information polymer synthesis. Another ingredient for energy currency (dissolved O_2) $[R_a]$ is kept constant due to the continuous supply. The

corresponding experimental setup is **Fig.3-3-1**. The validity of the values of rate constants k_3 in (V3), k_4 in (V4), which are determined by using (IIa – IIg), are examined by using (IIIa – IIIi), see the *Simulation* section below.

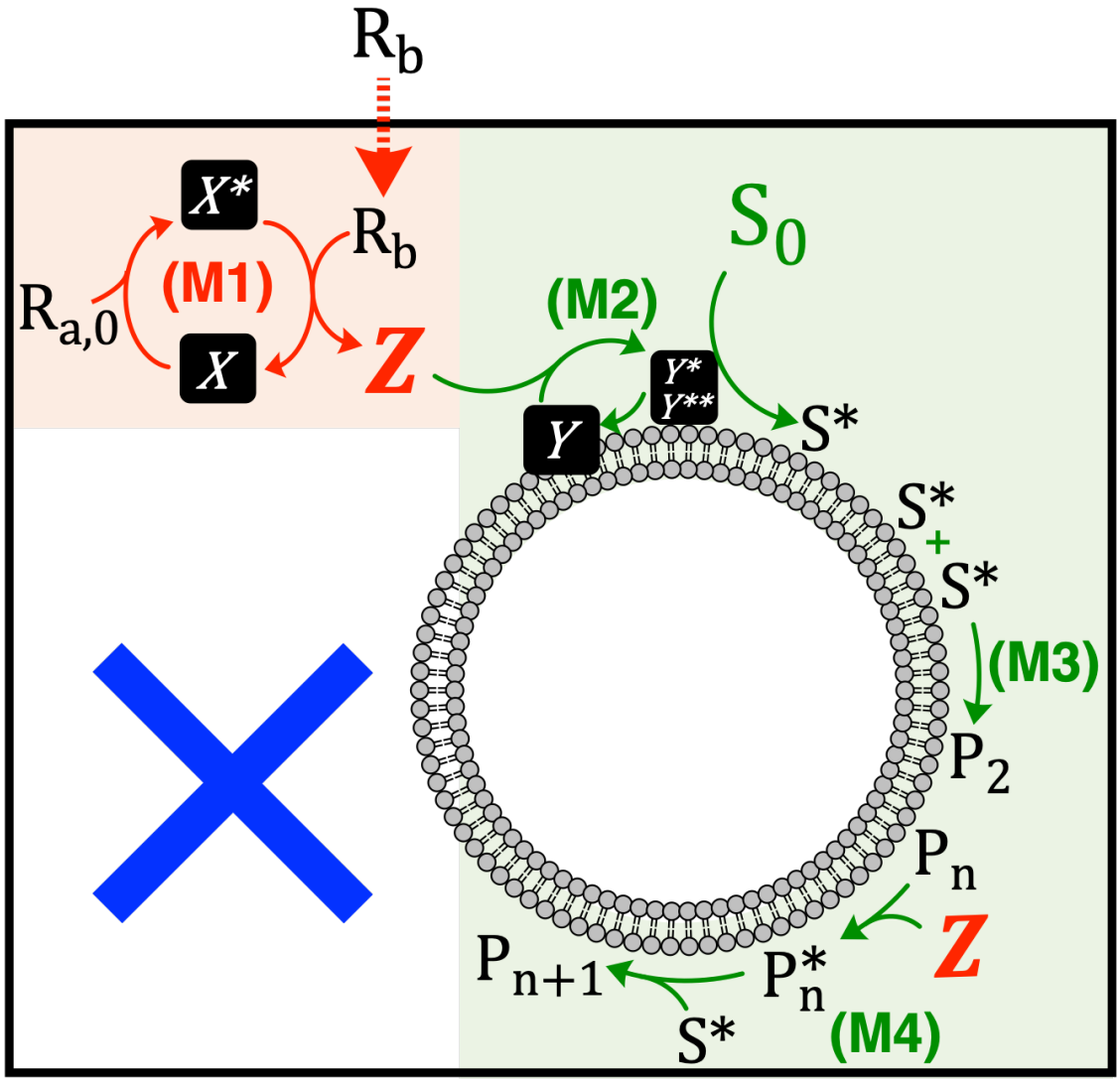

Figure 4-3-8. Scheme of the control system of the artificial metabolism where membrane growth domain is omitted, and initially added two ingredients ($R_{a,0}$ and S_0) trigger the PANI-ES synthesis on vesicle surface. When one or both ingredients are entirely consumed, the system reaches equilibrium.

Control: Artificial metabolism system with DIRECT SUPPLY of energy currency.

(iii) PANI-ES synthesis and vesicle growth *without* energy production (M1).

Even when omitting energy production domain (M1) from artificial metabolism and instead continuously supplying energy molecule, Z, the vesicle show growth coupled with PANI-ES synthesis (see **Fig. 4-3-9**). In this case, energy currency molecule, aniline, and amphiphiles (Z, S, and A_m, respectively) are continuously supplied to keep the reaction condition constant. The simultaneous differential equations describing this time-dependence of membrane growth coupled with PANI-ES synthesis are given by:

$$\frac{d[P(t)]_{chain}}{dt} = v_3(t) * [A(t)] \qquad (IVa)$$

$$\frac{d[P(t)]_{mono}}{dt} = \big(2 * v_3(t) + v_4(t)\big) * [A(t)] \qquad (IVb)$$

$$\frac{d[S^*(t)]}{dt} = \big(2 * v_2(t) - 2 * v_3(t) - v_4(t)\big) * [A(t)] \qquad (IVc)$$

$$\frac{d[Z(t)]}{dt} = \frac{d[S]}{dt} = \frac{d[A_m]}{dt} = 0 \qquad (IVd)$$

$$\frac{d[A_v(t)]}{dt} = v_5(t) * [A(t)] \qquad (IVe)$$

$$[A(t)] = \frac{1}{2} * [A_v(t)] * L * a_{AOT} \qquad (IVf)$$

where $[P(t)]_{chain}$ and $[P(t)]_{mono}$ are the concentration ([M]) of information polymer (PANI-ES) defined with the number of polymer chains and their consisting monomeric units, respectively, $[S^*(t)]$, $[Z(t)]$, $[A_v(t)]$ ([M]) are the concentrations of activated monomers, energy currency molecules, and vesicle forming molecules, respectively, $[A(t)]$ ($[m^2/L]$) is the concentration of vesicle surface area, $v_{i=2-5}(t)$ is the rate equation of each model reaction (M2 – M5), L is the Avogadro constant, and a_{AOT} is the surface area per single vesicle forming molecule. The concentrations of aniline $[S(t)]$, energy currency $[Z(t)]$, and amphiphile concentration are kept constant due to the continuous external supply. The corresponding experimental setup is **Fig. 2-5-1** with **Table 2-5-1**. The value of rate constants k_5 in (V5) is determined by using (IVa - IVf) and predetermined values of rate constants k_3 in (V3) and k_4 in (V4), see the *Simulation* section below.

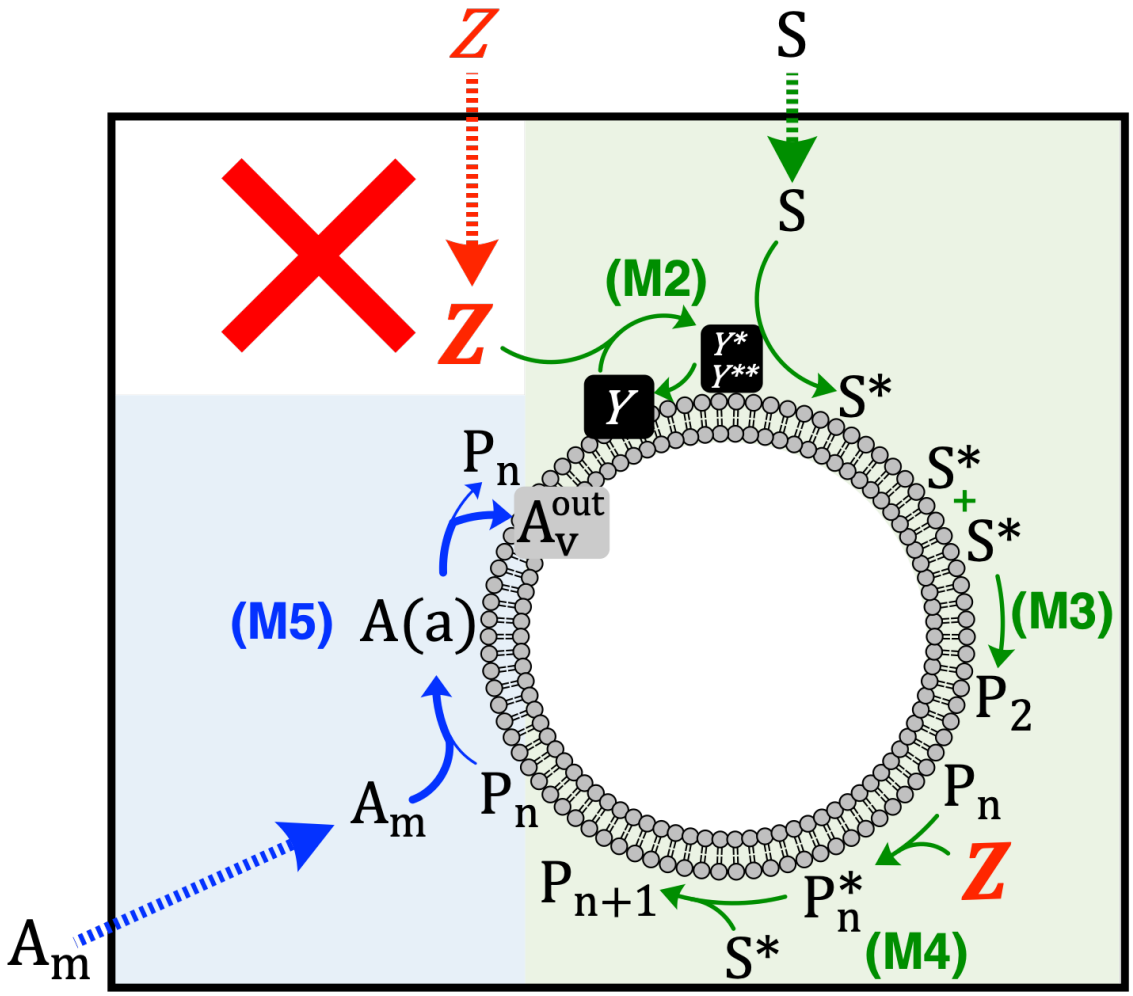

Figure 4-3-9. Scheme of the control system of the artificial metabolism where membrane growth domain is omitted, and continuously supplied ingredients (energy currency Z, monomer S, and amphiphile A_m) sustain the PANI-ES synthesis on vesicle surface and membrane growth.

4.4 Simulations

4.4.1 Determination of the Values of Rate Constants

Rate constants for the PANI-ES synthesis, k_3 and k_4.

We performed experiments to characterize the reaction kinetics. We measured the rate of PANI-ES synthesis in the HRPC-catalyzed reaction system triggered by initially added H_2O_2, (M2 - M4), as shown in the experimental setup **Fig.2-3-1**. The PANI-ES synthesis without the external supply of H_2O_2 (Z), aniline (S), and AOT molecules (A_m) takes place in the closed microtube. The PANI-ES synthesis uses aniline initially present in the reaction solution and initially added H_2O_2 (Z). Thus, aniline (S) and H_2O_2 (Z) decrease with the reaction progress, and the total surface area of vesicles in the system is constant. This situation can be simulated by the differential equations (IIa - IIg) (section 4.3.4(i)) as shown in **Fig.4-4-1**. The time-dependence of PANI-ES synthesis simulated by $[P(t)]_{mono}/[P(t=24h)]_{mono}$ in this model well reproduces the experimental data as shown in **Fig. 2-3-4(b)**, which gives the values of rate constants $k_3 = 1.0 * 10^4\ [s^{-1}]$ and $k_4 = 1.0 * 10^{7.5}\ [(mol\, m^{-2})\, s^{-1}]$.

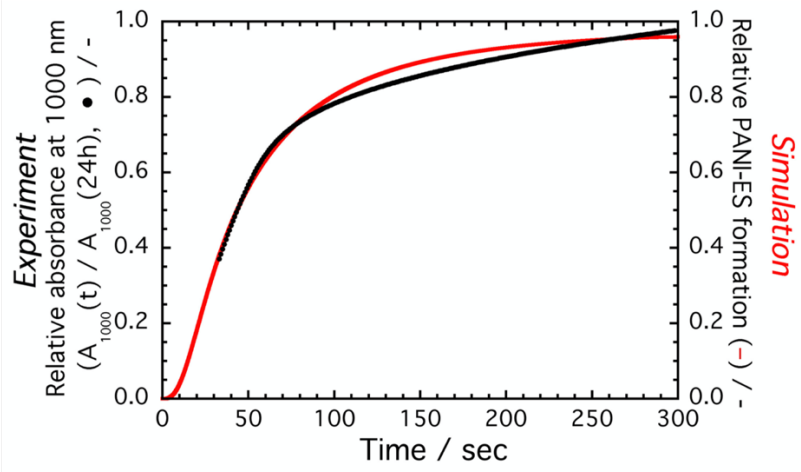

Figure 4-4-1. UV/Vis/NIR absorption spectrum which observed the kinetics of PANI-ES synthesis with its characteristic absorbance at λ=1000 nm (A_{1000}) of the reaction mixture. The black dots represent experimental data, which is identical plot to **Fig. 2-3-4(b)**. Red line is the simulation curve ($[P(t)]_{mono}/[P(t=24h)]_{mono}$) obtained with the equations (IIa - IIg) (section 4.3.4(i)) by using the values of rate constants on PANI-ES, $k_3 = 1.0 * 10^4\ [s^{-1}]$ and $k_4 = 1.0 * 10^{7.5}\ [(mol\, m^{-2})\, s^{-1}]$.

Rate constants for the vesicle growth, k_5.

We quantified growth of AOT membrane coupled with PANI-ES formation in the HRPC-catalyzed reaction system triggered by direct addition of H_2O_2, (M2 - M5), as shown in section 2.5.4. H_2O_2 (Z), aniline (S), and AOT molecules (A_m) are continuously supplied to vesicles by the double micro-injection technique, which keeps the reaction condition surrounding the vesicles almost constant. Then, the subsequent vesicle membrane growth coupled with the surface-confined PANI-ES synthesis is observed. This situation can be simulated by the differential equations (IVa - IVf) (section 4.3.4(iii)) by applying the values of k_3 and k_4 determined above. The time-dependence of vesicle surface area coupled with PANI-ES synthesis simulated by $[A(t)]/[A(t=0)]$ in this model reproduces the experiments well as shown in **Fig.3-4 b**, which gives the values of rate constants $k_5 = 6.0 * 10^{-3}\ [s^{-1}]$. As experimentally observed, our kinetic model reproduces the changes in membrane growth rate against the aniline concentrations $[S]$.

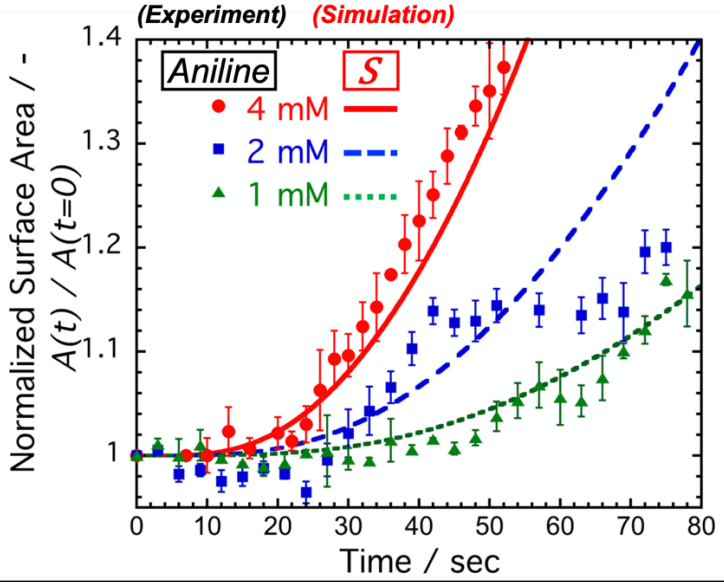

Figure 4-4-2. Growth of AOT GUVs in response to the micro-injection of AOT micelles and reaction trigger H_2O_2 in the presence of various concentrations of aniline. The data points represent the time-dependent changes of AOT vesicle membrane, which are identical plots to **Fig. 2-5-3(b)**. The red solid line, blue broken line, and green dotted line represent the simulation curves obtained with Eq. (IIIa – IIIi) (section 4.3.4(iii)) by using the predetermined values of rate constants on PANI-ES, $k_3 = 1.0 * 10^4\ [s^{-1}]$ and $k_4 = 1.0 * 10^{7.5}\ [(mol\, m^{-2})\, s^{-1}]$, and the value of rate constant on membrane uptake, $k_5 = 6.0 * 10^{-3}\ [s^{-1}]$. The only difference between the three simulation curves is the concentration of aniline ([S]), and all other parameters are common.

4.4.2 Simulation of Artificial Metabolism.

Information polymer synthesis coupled with artificial metabolism.

In the discussions just above, we determined the values of three rate constants (k_3, k_4, and k_5) based on the two control systems (section 4.3.4 (i) & (iii)), as a result, all the parameter values in our kinetic model are fixed. Then, we look into the validity of our kinetic model by using the last control system (section 4.3.4 (ii)), which synthesizes information polymer coupled with artificial metabolism system under the constant surface area of vesicle membrane.

First, we measured the rate of PANI-ES synthesis in the GOD/HRPC-catalyzed cascade reaction system triggered by initially added glucose (R_a), (M1 – M4), as shown in **Fig.3-3-1**. The PANI-ES synthesis without the external supply of glucose (R_a), aniline (S), and AOT molecules (A_m) takes place in the closed microtube. The PANI-ES synthesis is carried out by using aniline (S) initially present in the reaction solution and *in situ* formed H_2O_2 (Z) with initially added glucose (R_a) and continuously supplied oxygen (R_b) by rotary mixing the reaction tubes. Thus, aniline (S) and glucose (R_a) decrease with the reaction progress, and the total surface area of vesicles in the system is constant. This situation can be simulated by the differential equations (IIIa - IIIi) (see also **Fig.4-3-8**) by applying the values of k_3 and k_4 determined above. The time-dependence of PANI-ES synthesis ($[P(t)]_{mono}/[P(t=24h)]_{mono}$) in this model is overlaid with the experimental plots, which well reproduces the experimental data as shown in **Fig.4-4-3**. Please note that there are no adjustable parameters in this simulation, and all the parameter values are already fixed before this simulation.

Second, we measured the time evolution of the concentration of ingredients (glucose (R_a) and aniline (S)) and intermediates (H_2O_2 (Z)) in the part of the artificial metabolism system to produce information polymer (M1 – M4). These concentrations are defined with the unit of mol/L, then the simulation results and experimental results can be directly compared. The only notice is that the enzymes GOD (X) and HRPC (Y) are radically inactivated during polymerization reaction according to our investigations (see **Fig. 3-3-17 (a)** and **(b)**). In the case of closed microtube setup (**Fig.3-3-1** and **Fig.4-3-8**), the consideration of enzyme inactivation does not influence largely the simulation curve of the relative value $[P(t)]_{mono}/[P(t=24h)]_{mono}$ in **Fig. 4-4-3**, however, the time evolution of the concentration of intermediates is largely influenced depending on the enzyme decay rate. Then, I roughly assume the enzyme decay rates as $[X]_0 \rightarrow [X]_0 * 2^{-t/60[s]}$ and $[Y]_0 \rightarrow [Y]_0 * 2^{-t/60\,[s]}$. This assumption is applicable only for the discussion in the microtube setup where the amount of enzyme is limited to the initially

added one, in contrast to the micro-injection setup where the concentration of enzymes are supposed to be kept constant due to the continuous inflow and outflow around the vesicle. The simulation and experimental results on the time evolution of the concentrations of glucose (R_a), aniline (S), and H_2O_2 (Z) are compared as shown in **Fig. 4-4-4 (a), (b), and (c)**, respectively. For time-dependent changes of the concentrations of glucose (R_a) and aniline (S), our simulation roughly reproduces the actual chemical system. On the other hand, the concentration of intermediates H_2O_2 (Z) is about ten times higher than the experimental values. There are two supposed reasons of the lower experimental values: (i) the oxidant H_2O_2 (Z) is used also for the side reactions of PANI-ES synthesis which we ignored to consider the ideal setup, and (ii) the assumed mechanism for H_2O_2 (Z) to join the elongation reaction, M4, is not reasonable, *e.g.*, the value of adsorption equilibrium constant K_Z might cause a problem (see also Appendix 4-B). All in all, our kinetic model based on the model reactions (M1 – M5) reproduces well the actual chemical kinetics of both two outcomes of artificial metabolism (information polymer synthesis and vesicle growth) and the reaction components of the artificial metabolism (except one). If I designed the reduced model reactions and rate equations in more detailed, the whole parameters of the artificial metabolism system might be reproduced well by simulation, and the kinetic model instead would become more complicated. Considering the initial purpose to simply describe essences of the system, the present kinetic model seems to be enough.

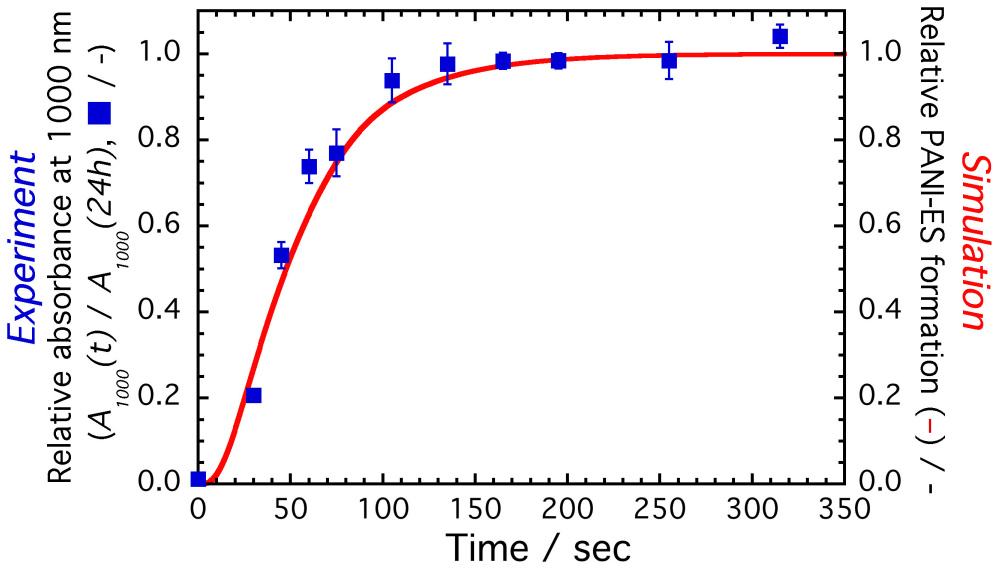

Figure 4-4-3. Time dependence of relative absorbance at λ=1000 nm of the reaction mixture (blue squares) obtained in the presence of AOT LUVs in 20 mM NaH_2PO_4 solution (pH=4.3). The polymerization was triggered by the *in situ* formation of H_2O_2 from D-glucose and dissolved oxygen with GOD. The growth profile indicates synthesis of PANI-ES in the artificial metabolism system. The changes in absorbance at λ=1000 nm ($A_{1000}(t)$) are normalized by the absorbance recorded after 24 h from the start of the reaction. The red line is the theoretical prediction obtained by the kinetic model (fitted by Eq. (IIIa – IIIi) in section 4.3.4). The error bars indicate standard deviations estimated from three different experiments.

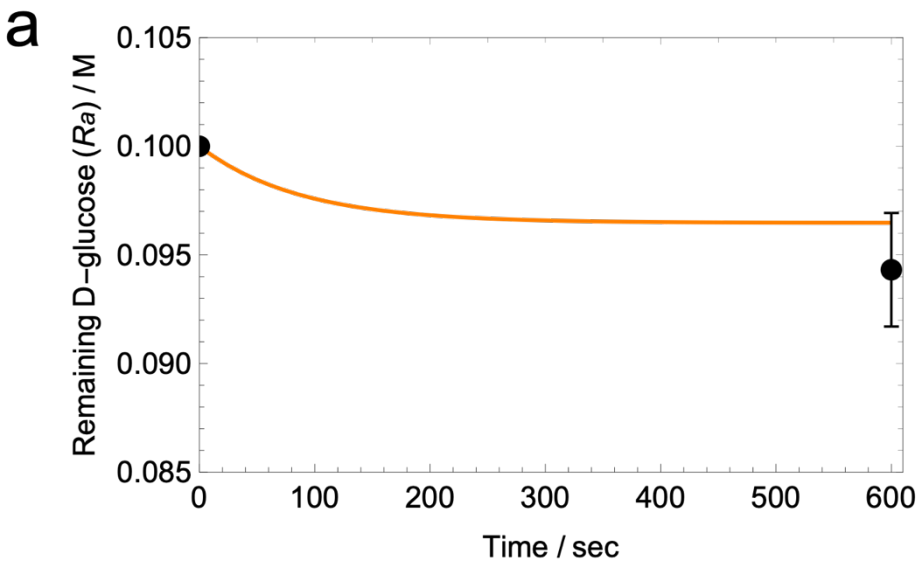
a
0.105
0.100
0.095
0.090
0.085
Remaining D−glucose (Ra) / M
0
100
200
300
400
500
600
Time / sec

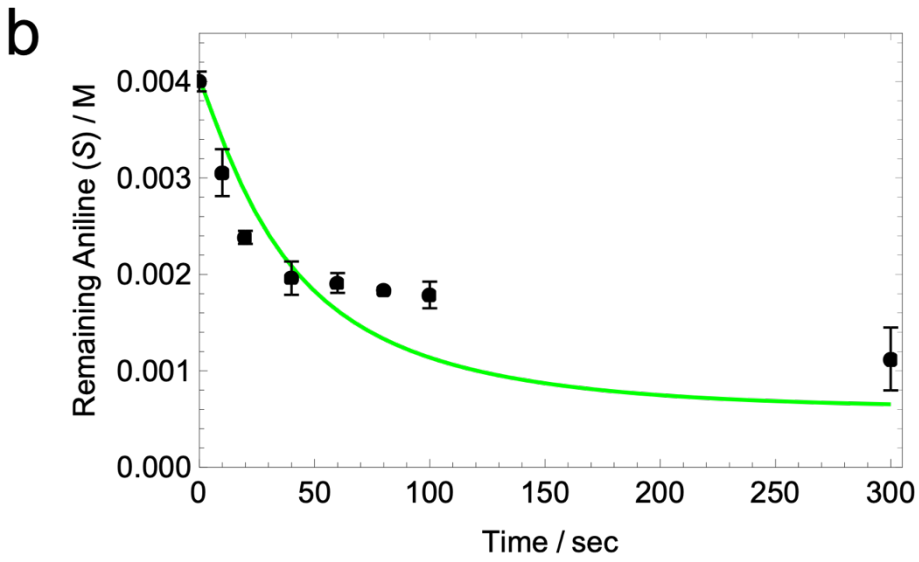
b
0.004
0.003
0.002
0.001
0.000
Remaining Aniline (S) / M
0
50
100
150
200
250
300
Time / sec

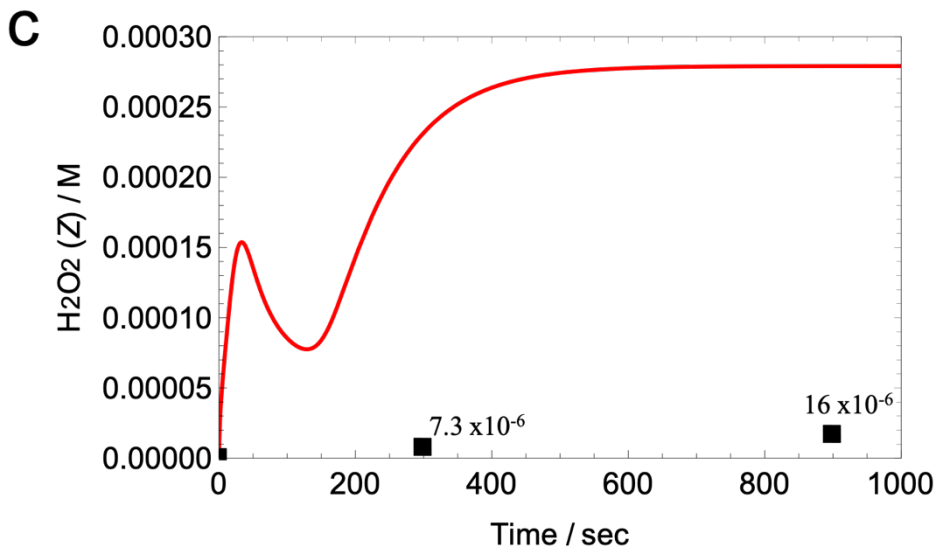
c
0.00030
0.00025
0.00020
0.00015
0.00010
0.00005
0.00000
H2O2 (Z) / M
7.3 x10-6
16 x10-6
0
200
400
600
800
1000
Time / sec

Figure 4-4-4. The time dependence of the concentrations of substrates (**a**: D-glucose (R_a) and **b**: aniline (S)) and intermediates (**c**: H_2O_2 (Z)) during the information polymer (PANI-ES) synthesis (M1 – M4) in the condition of no external supply of ingredients and no vesicle growth (experimental setup: **Fig.3-3-1** and model setup: **Fig.4-3-8**). The colored solid lines are simulation curve obtained by using differential equations (IIIa - IIIi) with the assumption of enzyme decays ($[X]_0 \rightarrow [X]_0 * 2^{-t/60[s]}$ and $[Y]_0 \rightarrow [Y]_0 * 2^{-t/60\,[s]}$). For the values of each parameter, see the parameters list. The black plots in each figure are obtained from experiments by the analytical methods described in section 3.3.5. The error bars represent standard deviations obtained from two or three measurements. Please note that the horizontal scale is different in each figure.

Vesicle membrane growth coupled with artificial metabolism.

The experimentally observed membrane growth (red circles in **Fig. 4-4-5**) coupled with PANI-ES formation in the optimized cascade reaction condition (M1 – M5) is well reproduced by $[A(t)]/[A(0)]$ (red solid line in **Fig.4-4-5**) with the kinetic model, Eq. (Ia – Ig). Here we assume that the ingredients (glucose (R_a), aniline (S), and AOT molecules (A_m)) are continuously supplied close to the vesicles by micro-injections, and their concentrations are kept constant. The important notice is that the three essential domains (energy production (M1), synthesis of information polymer (M2 – M4), and vesicle reproduction (M5)) are integrated into our synthetic minimal cell. In addition, the formation of information polymer (PANI-ES) and membrane growth of vesicles catalyze each other's pathway in a mutual catalytic or autocatalytic way, which are intrinsic to the many biological processes (such as *Central Dogma*) and are considered as a promising concept to bridge a gap between simple molecular assembly and biology [Bissette & Fletcher 2013; Vasas et al. 2012; Xavier et al. 2020].

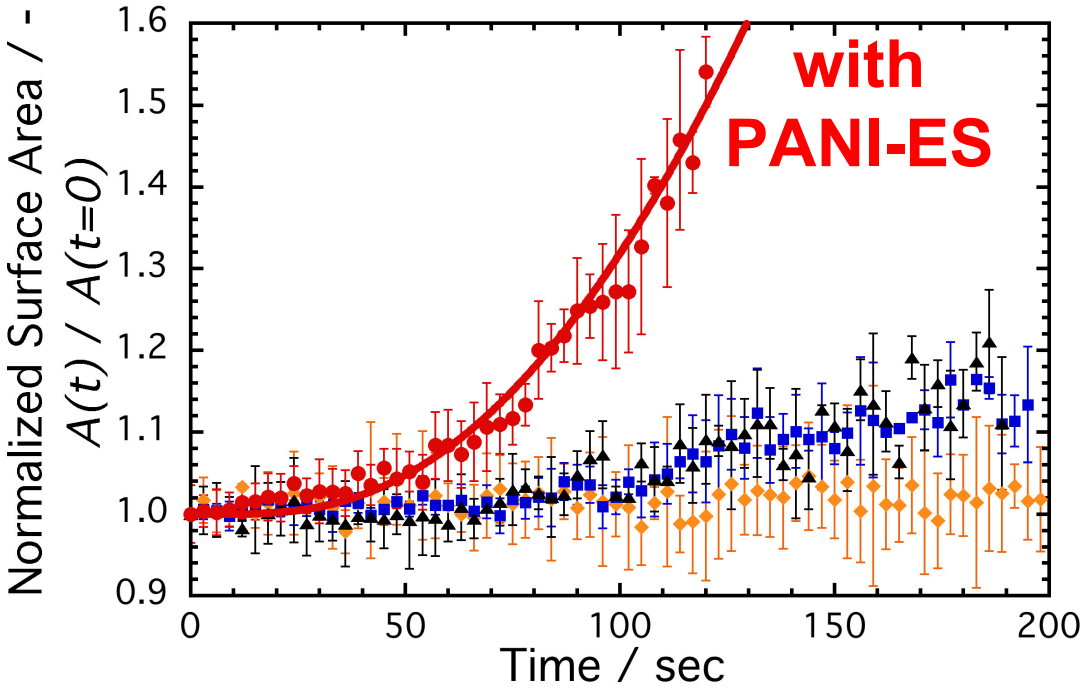

Figure 4-4-5. Time-dependent change of AOT vesicle surface area coupled with artificial metabolism system, which is identical experimental plots to **Fig. 3-3-22** overlaid with the simulation curve. (Red circles): coupled with information polymer synthesis; (black triangles, blue rectangles, orange diamonds): without polymer synthesis by lack of one or some reaction components. The surface areas of GUVs are normalized by their initial values. The simulation curve is given by $[A(t)]/[A(0)]$ obtained with the kinetic model Eq. (Ia – Ig) in section 4.3.3. The error bars indicate standard deviations estimated from four to six different experiments.

4.5 Discussions

To what extent advantageous for vesicle to use artificial metabolism.

As seen in **Fig.4-4-5** (black triangles, blue squares, and orange diamonds), AOT vesicles showed slight membrane growth in response to the supply of AOT micelles even without the information polymer synthesis. According to Fick's law (see section 2.4.2), the flux of membrane molecules from the external solution into the vesicle membrane (with surface area A) can be expressed by:

$$\frac{\partial A(t)}{\partial t} = \frac{LacD}{l\, k_B T} \Delta\mu\, A(t) \tag{4.34}$$

where L is the Avogadro constant, a is the surface area per single membrane molecule, c is the molar concentration of AOT molecules in the external solution, D is AOT diffusion coefficient, k_B is the Boltzmann constant, T is the temperature, and l is a relevant length scale of the flux. The driving force, $\Delta\mu = \mu_{ext} - \mu_{mem}$, is the chemical potential difference between AOT molecule in the external solution, $\mu_{ext} = \mu_0 + k_B T \log(c/c_0)$, and in the vesicle membrane, μ_{mem}. Here μ_0 is the reference chemical potential at the reference concentration c_0. At the equilibrium state when the amphiphile concentration is above cvc, both chemical potentials have the same value, *i.e.*, $\Delta\mu = 0$ and then no flux. The injection of additional AOT micelles temporarily increases AOT concentration around AOT GUV, which increases μ_{ext} resulting in the flux of AOT molecule to the membrane. Here we assume that the membrane growth observed in the absence of information polymer was triggered only by the presence of excess free AOT molecules in the external solution above the cvc value (~ 1.5 mM). We fit the membrane growth with Eq. (4.34) as shown in green solid line in **Fig. 4-5-1**, then we obtained the following vesicle growth rate in the control system:

$$r_{cont.} \equiv \frac{LacD}{l\, k_B T} \Delta\mu = 6.0 * 10^{-6}[s^{-1}] \tag{4.35}$$

Using $a_{AOT} = 0.67 * 10^{-18}[m^2]$ [Grillo et al. 2003], $c = 1.5 * 10^{-3}[M]$ (cvc), and typical values $D = 10^{-10}[m^2 s^{-1}]$ and $l = 10^{-5}[m]$, Eq.(4.35) yields the chemical potential difference to generate the flux, $\Delta\mu_{cont.} \sim 0.10\, k_B T$. From the expression of chemical potential of amphiphiles, the concentration gradient of AOT in this length scale is estimated as $\Delta c \sim 0.11\, c_0$, which is about 0.16 mM, corresponding to 11% increase from the cvc value. We supplied 20 mM AOT micelles at the point of ~ 65 μm from the target vesicle, therefore, the estimated concentration gradient (0.16 mM) is reasonable.

On the other hand, as we discussed through this thesis, experimental results and our simulations show that the synthesis of information polymer (PANI-ES) on the surface of

AOT GUVs significantly enhanced the growth of GUVs by incorporating amphiphiles. In model reaction (M5), we have considered the rate equation on the incorporation of AOT molecules:

$$v_5(t) = k_5 \frac{[P(t)]_{mono}}{[A(t)]} \ (= V5) \tag{4.36}$$

where rate constant k_5 is determined based on experiments as $6.0 * 10^{-3}$ $[s^{-1}]$ (see section 4.4.1). Using typical concentration of vesicle surface area $[A(t)] = [A]_0 = 3.03 * 10^2 [m^2 L^{-1}]$ and typical concentration of information polymer $[P(t)]_{mono} = 4.0 * 10^{-3} [mol\, L^{-1}]$, Eq. (4.36) yields $v_{5,typ.} = 7.9 * 10^{-8}$ $[mol\, m^{-2}\, s^{-1}]$. There are following relationship between the surface area growth rate r_{PANI} and the amphiphile incorporation rate $v_5(t)$:

$$\frac{\partial A(t)}{\partial t} = r_{PANI}(t)\, A(t) \tag{4.37}$$

$$r_{PANI}(t) \equiv \frac{1}{2} v_5(t) La_{AOT} \tag{4.38}$$

Applying the typical rate constant $v_{5,typ.}$, Eq. (4.38) yields $r_{PANI} = 1.6 * 10^{-2} [s^{-1}]$. Therefore, since $r_{PANI}/r_{cont.} \sim 27$, the typical vesicle membrane growth rate is estimated to become about 27 times higher in the case with information polymer (PANI-ES) synthesis on vesicle surface. Since the same concentration of AOT micelles is supplied with the same distance from target vesicles, here we assume that there are no differences between two experimental conditions, except the presence of PANI-ES. Then, we can estimate the chemical potential difference generating the flux of AOT molecules as $\Delta\mu_{PANI} = \mu_{ext} - \mu'_{mem} \sim 2.7\ k_B T$. This value is reasonable since the free energy for the stabilization of an organic ion pair in aqueous media is $\sim 2.0\ k_B T$ [Schneider et al. 1992; Ngola et al. 1999]. These results suggest that the transport of AOT molecules in the external solution into the vesicle membrane is actually catalyzed by the interaction with PANI-ES (see **Fig.4-3-6**).

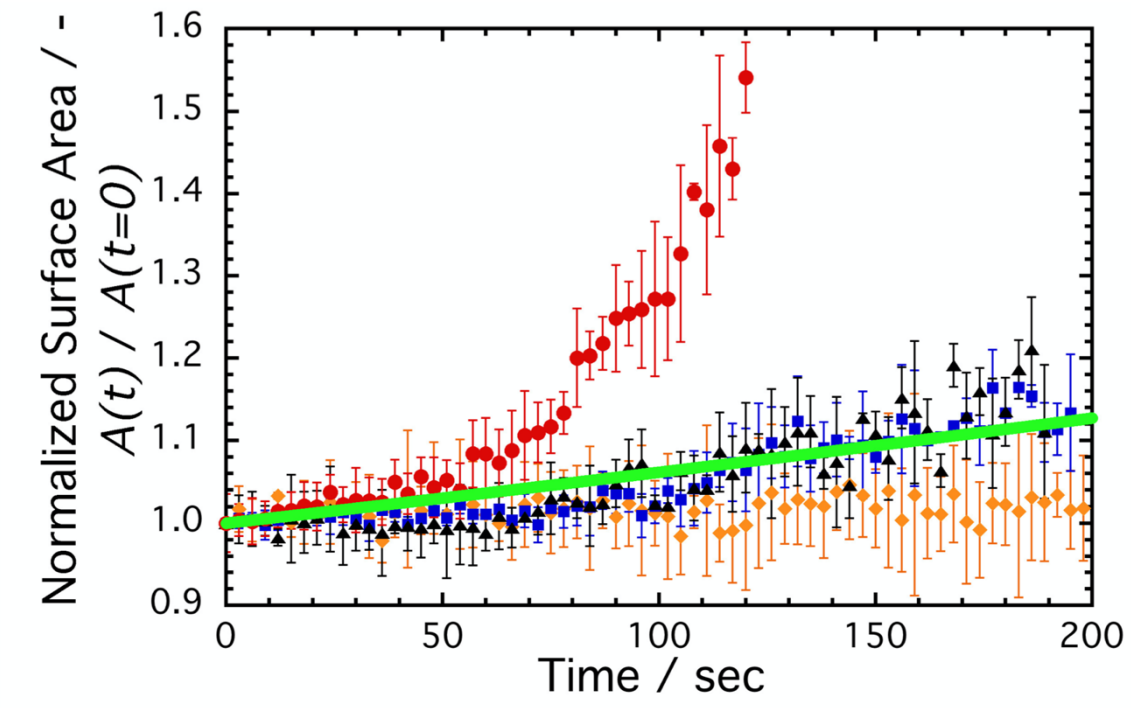

Figure 4-5-1. Fitting curve from Eq. (4.34) (green solid line) overlaid with the plots of AOT GUV growth. The colored plots are obtained from various experimental conditions. Red circles represent the growth of AOT GUV coupled with PANI-ES synthesis in the synthetic metabolism system (M1 – M5), and other colored plots are control conditions where PANI-ES is not synthesized. See the caption of **Fig.3-3-22**, for more details. The fitting curve is given by $A(t)/A_0 = \exp(6.0 * 10^{-6}[s^{-1}]\, t[s])$.

4.6 Conclusion.

In this chapter, first I introduced the reaction kinetics of enzymatic reactions and surface confined reactions. Based on them, I constructed reduced model reaction system of the artificial metabolism system (**Fig.4-3-1**) in the expression way of Gánti's chemoton (**Fig.1-2-2**). The reduced model preserves the stoichiometry between the original actual reaction system (R1 – R9) and reduced model system (M1 – M5). Then, I derived rate equations on each model reaction. The values of all parameters are given from literature or determined based on the control experiment system, therefore, I can describe the kinetics of outcome of the artificial metabolism (information polymer synthesis (**Fig.4-4-3**) and membrane growth (**Fig.4-4-5**)), of ingredients (D-glucose and aniline), and of energy currency molecule (H_2O_2) without any arbitrary parameters.

For the minimal cell system as the approach to explore the simplest form of any possible living systems, the system should be well-described to enable the access from physical science. The coupling between experimental realization of the artificial metabolism design and the development of clear kinetic model of the system is one of the biggest advantages of my synthetic minimal cell system.

4.7 Appendix

Appendix 4-A: Adsorption-Desorption Equilibrium Constant, K_{S^*}.

As a course of fundamental research on enzymatic polymerization of aniline using vesicle membrane as a template, Junker et al. worked on MD simulations of an AOT membrane fragment with aniline molecules in the system imitating the similar conditions for polymerization [Junker et al. 2015]. The simulation setup was briefly as follows: 27 aniline molecules (9 as neutral and 18 as protonated), 512 AOT, 134 $H_2PO_4^-$, 1 H_3PO_4, 628 Na^+, and 62552 water molecules. This setup corresponds to 20 mM aniline, which is five times higher than our experimental setup, and contains higher concentrations of AOT molecules. The outcome of the simulations shows that 84% of protonated anilines are close to AOT, compared to 59% of neutral aniline. A simulation snapshot is shown in **Fig.4-7-1**. By using these results, we estimate the values of adsorption-desorption equilibrium constants.

For protonated aniline (S_+) and neutral aniline (S_0), the fractional occupancies of the adsorption sites are respectively given by:

$$\theta_+ = \frac{[S_+]}{[S_+]_0} = \frac{K_+S_+}{1 + K_+S_+ + K_0S_0} \tag{4.39}$$

$$\theta_0 = \frac{[S_0]}{[S_0]_0} = \frac{K_0S_0}{1 + K_+S_+ + K_0S_0} \tag{4.40}$$

Here we assume that the value of adsorption site density equals the number of AOT molecules constituting a bilayer fragment, $[S_+]_0 = [S_0]_0 = 512$. Then, following simultaneous equations (5.39)' and (5.40)' on K_+S_+ and K_0S_0 gives the estimated values of equilibrium constants.

$$\theta_+ = \frac{18 * 0.84}{512} = \frac{K_+S_+}{1 + K_+S_+ + K_0S_0} \tag{4.39}'$$

$$\theta_0 = \frac{9 * 0.59}{512} = \frac{K_0S_0}{1 + K_+S_+ + K_0S_0} \tag{4.40}'$$

$$\xrightarrow{yields} \begin{cases} K_+S_+ = 0.0305 \\ K_0S_0 = 0.0108 \end{cases} \xrightarrow{yields} \begin{cases} S_+ = 20 * 10^{-3} * \frac{2}{3}\ (M) \\ K_+ = 2.29\ (M^{-1}) \end{cases} \ \& \ \begin{cases} S_0 = 20 * 10^{-3} * \frac{1}{3}\ (M) \\ K_0 = 1.62\ (M^{-1}) \end{cases}$$

Therefore, we apply the value of $2.29\ (M^{-1})$ as the adsorption-desorption equilibrium constant of aniline radical cation (K_{S^*}).

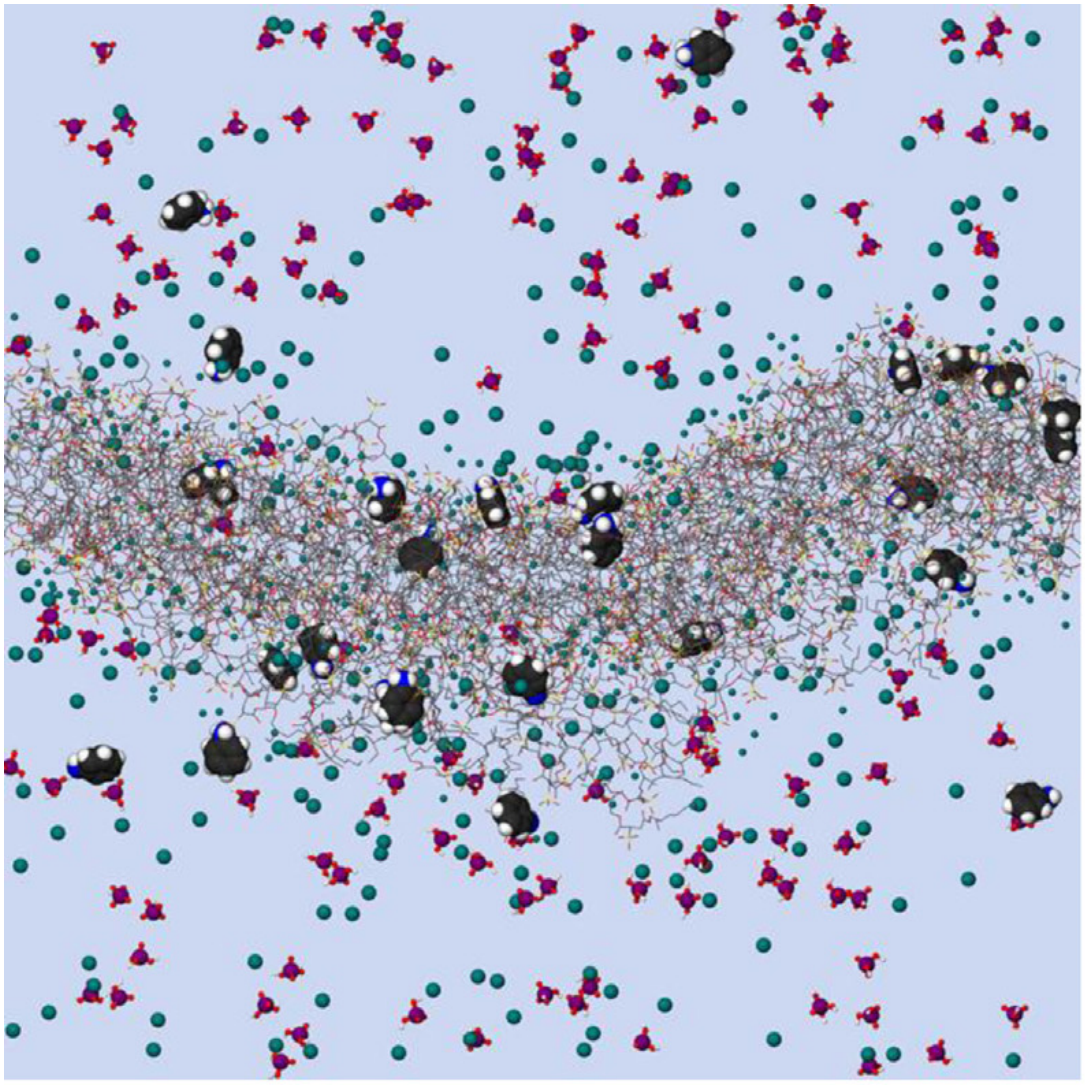

Figure 4-7-1. MD simulation of the interaction of aniline and AOT bilayer fragment at pH=4.3 (100 mM NaH_2PO_4) [Junker et al. 2015]. Snapshot of a side-view showing the AOT bilayer fragment with localized aniline molecules, either as neutral aniline or as cationic anilinium. Aniline is shown as a space-filling model. AOT is displayed as a thin-wire drawing. Reprinted with permission from Junker, K. et al. *Synth. Met.* **200**, 123 – 134 (2015) © 2015 Elsevier B.V.

Appendix 4-B: Averaged Degree of Polymerization, Experiments vs Simulations.

For the description of our synthetic minimal cell with the kinetic model, we focused on the time evolution of the concentration of PANI-ES monomeric structures ($[P(t)]_{mono}/[P(t=24h)]_{mono}$), which is the experimentally observable value by using a spectrophotometer. The values of rate constants on PANI-ES synthesis, k_3 and k_4, are both determined based on this parameter. Our kinetic model and the given parameters' value generally reproduce well the time-dependence of the membrane growth, the formation of PANI-ES monomeric units, and the concentration of substrates. However, the outcome of our simulations does not reproduce well some other characteristic parameters of PANI-ES, for example, the length of PANI-ES chains. Previously, Guo et al. worked on the mass spectrometric analysis of the reaction products obtained in the early stage of the reaction with HRPC-enzymatic polymerization of aniline in the presence of SDBS/decanoic acid (1/1) vesicles [Guo et al. 2009]. While the species of template vesicles and the initial concentrations of reaction components are different from our experimental system, here we discuss the degree of polymerization of the reaction products, comparing their measurements with our simulation results.

Guo et al. previously reported that the mass center of the reaction products obtained in the closed microtube system after 30 sec (**Fig.4-7-2(a)**) and after 60 sec (**Fig.4-7-2(b)**) from the start of the reaction was about m/z = 1087 in both cases, which corresponds to about 12-mer of aniline since one monomeric unit is estimated to m/z ~ 90 – 92. On the other hand, our kinetic model with a similar setup, where PANI-ES is synthesized by using H_2O_2 (Z) and aniline (S) initially present in the mixture (Eq. (IIa – IIg) and **Fig. 4-3-7**), show that the averaged degree of polymerization of PANI-ES ($\equiv [P(t)]_{mono}/[P(t)]_{chain}$) approach asymptotically to ~5.95 (**Fig.4-7-3**). Please note that Guo's polymeric products was obtained by using SDBS/DA (1/1) binary vesicles, which is different from my experiment using AOT vesicles. In addition, the reaction condition such as the initial concentration of aniline, oxidant and enzymes is different (relatively dilute condition). Although my estimation based on the kinetic model cannot be directly compared with the Guo's mass spectrometric analysis results, we can suppose that the average length of PANI-ES chains is simulated considerably lower in my kinetic model than in the actual experimental system. A few disagreements with the experiment and simulation might originate from the balance between rate constants on the chain initiation reaction, k_3 in (V3), and on the chain elongation reaction, k_4 in (V4).

a

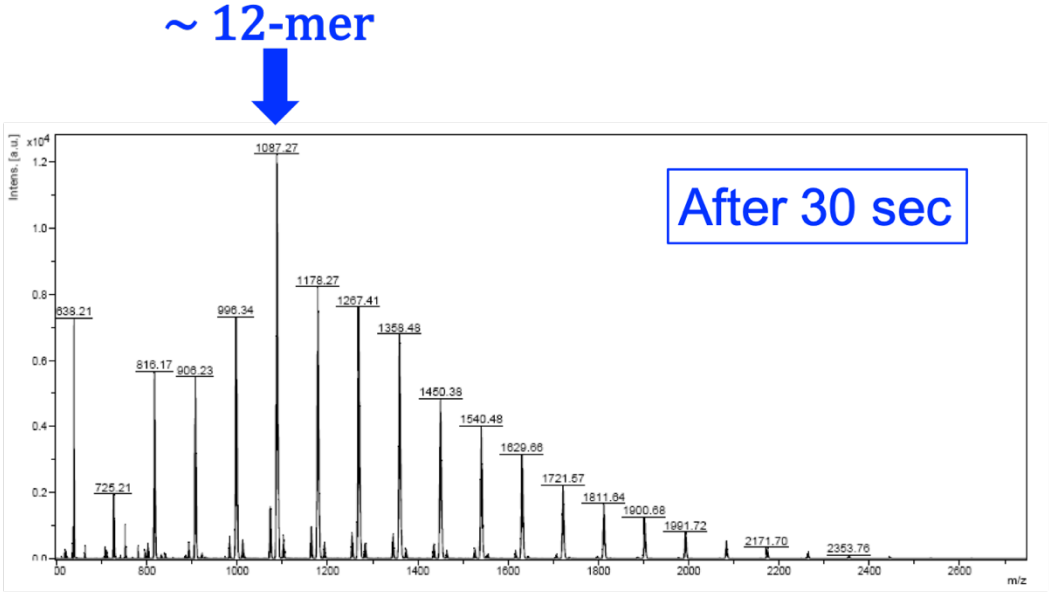
~ 12-mer
After 30 sec
Intens. [a.u.]
x10^4
1087.27
1178.27
1267.41
1358.48
996.34
838.21
816.17
906.23
1450.38
1540.48
1629.66
1721.57
1811.84
1900.68
1991.72
2171.70
2353.76
725.21
m/z

b

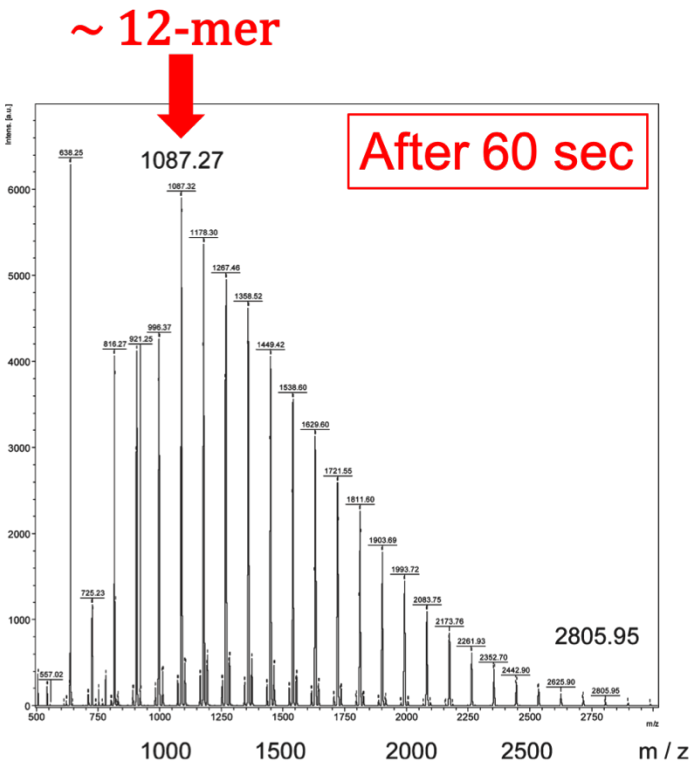
~ 12-mer
After 60 sec
1087.27
2805.95
m / z

Figure 4-7-2. Mass spectrometric analysis of the polymerization of aniline during the early stage of the reaction [Guo et al. 2009]. MALDI-TOF analysis of PANI-ES isolated from the reaction mixture after (**a**) 30 sec and (**b**) 60 sec from initiating the reaction. One aniline unit corresponds to m/z ~ 90 – 92. Please note that SDBS/DA (1/1) binary vesicles are used as templates for this measurement, and that the initial concentrations of reaction components were [aniline] = 1.3 mM, [HRPC] = 25μg/mL, [H_2O_2] = 1 mM, in 0.1 M NaH_2PO_4 (pH=4.3). Reprinted with permission from Guo, Z. et al., *Langmuir*, **25**, 11390-11405 (2009) © 2009 American Chemical Society.

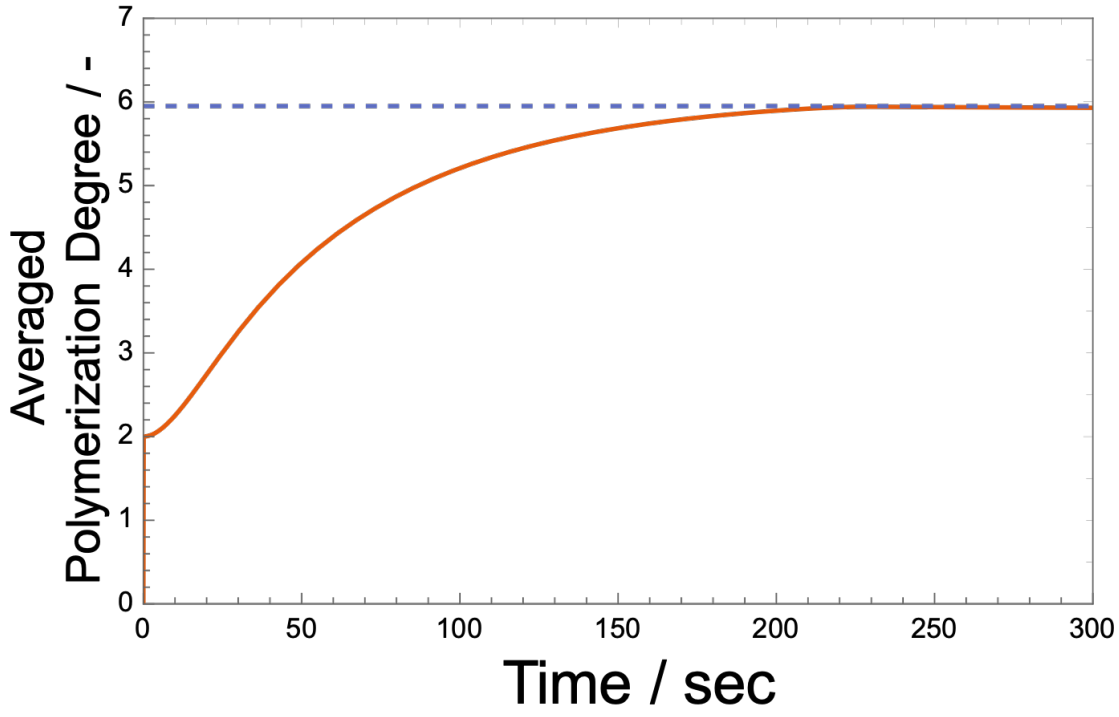

Figure 4-7-3. Averaged degree of polymerization of PANI-ES ($[P(t)]_{mono}/[P(t)]_{chain}$), simulated by using our kinetic model for the PANI-ES synthesis in the closed-tube condition with reference condition, Eq. (IIa – IIg). The averaged polymerization degree asymptotically approaches ~5.95.

Appendix 4-C: Mathematica Source Code

In the simulation study, we used "Wolfram Mathematica 12" for Mac OS X. The Mathematica source code for the simulation of artificial metabolism system (vesicle membrane growth coupled with information polymer synthesis, M1 – M5) by using differential equations Eq. (Ia – Ig) is shown below. The simulation will be finished in a few seconds using an ordinary laptop computer.

```
ClearAll;
```
すべてをクリア

In[•]:=
```
(*Initial Values*)
diff0 = {
   (*concentration of total number of PANI chains [M]*)
   PaniN[0] == 0,
   (*concentration of total PANI monomeric units [M]*)
   PaniE[0] == 0,
   (*concentration of aniline radical cation [M]*)
   Ss[0] == 0,
   (*concentration of aniline [M]*)
   S[0] == 4.0*10^(-3),
   (*concentration of H2O2 [M]*)
   Z[0] == 0,
   (*concentration of D-glucose [M]*)
   Ra[0] == 100*10^(-3),
   (*molar concentration of AOT forming vesicle membrane [M]*)
   Amol[0] == 1.5*10^(-3)
  };

(*Parameters*)
params = {
   (*v1 [M s-1]: Formation of Z(H2O2)*)
   (*concentration of oxygen [M]*)
   Rb → 0.23*10^(-3)*0.03,
   (*concentration of GOD [M]*)
   X0 → 1.0*10^(-6),
   (*rate constant on ping pong bi bi mechanism [s-1]*)
   k1cat → 1.0*10^3,
   (*rate constants on ping pong bi bi mechanism [M-1 s-1]*)
   k1red → 1.5*10^4,
   k1ox → 1.9*10^6,

   (*v2[(mol m-2) s-1]: Formation of Ss(aniline radical cation)*)
   (*concentration of HRPC [mol m-2]*)
   Y0 → 3.04*10^(-9)*0.2,
   (*rate constants on irreversible ping pong mechanism [M-1 s-1]*)
   k2a → 1.7*10^7,
   k2b → 2.4*10^5,
   k2c → 8.6*10^4,
```

(Next page)

```
  (*v3[(mol m-2) s-1]: Initiation reaction of PANI chain *)
  (*rate constant on dimerization of Ss [s-1]*)
  k3 → 1.0*10^(4),
  (*adsorption-desorption equilibrium constant of Ss [M-1]*)
  KSs → 2.3,
  (*site density (density of AOT in monolayer) [mol m-2]*)
  Naot → 2.48*10^(-6),

  (*v4[(mol m-2) s-1]: Elongation reaction of PANI chain*)
  (* rate constant [(mol m-2)-1 s-1]*)
  k4 → 1.0 * 10^(4) * (1.0*10^3.5),
  (*adsorption-desorption equilibrium constant of Z [M-1]*)
  KZ → 2.3,

  (*v5[(mol m-2) s-1]: Incorporation of amphiphile*)
  (*rate constant on incorporation [s-1]*)
  k5 → 6.0*10^(-3)
 };
```

(*Rate Equations*)

```
rateeq = {
  (*fractional occupancy of the adsorption site*)
  ThetaSs[t] == (KSs*Ss[t] / (1 + KSs*Ss[t] + KZ*Z[t])),
  ThetaZ[t] == (KZ*Z[t] / (1 + KSs*Ss[t] + KZ*Z[t])),
  (*surface concentration of AOT forming vesicle membrane [m^2 L-1]*)
  Aarea[t] == Amol[t]*0.5*(6.02*10^23)*(0.67*10^(-18)),

  (*[(mol L-1) s-1]*)
  v1[t] == X0 / (1/k1cat + 1/(k1red*Ra[t]) + 1/(k1ox*Rb)),
  (*[(mol m-2) s-1]*)
  v2[t] == Y0 / ((1/(k2a*Z[t])) + (k2b + k2c)/(k2b*k2c*S[t])),
  v3[t] == k3 *Naot*ThetaSs[t]^2,
  v4[t] == k4*Naot*(PaniN[t]/Aarea[t])/(1/ThetaZ[t] + 1/ThetaSs[t]),
  v5[t] == k5*(PaniE[t]/Aarea[t])
 };
```

(Next page)

```
(*Simultaneous Differential Equations*)
(*[M s-1]*)
diffeq = {
    PaniN'[t] == v3[t] * Aarea[t],
    PaniE'[t] == (2 * v3[t] + v4[t]) * Aarea[t],
    Ss'[t] == (2 * v2[t] - 2 * v3[t] - v4[t]) * Aarea[t],
    S'[t] == 0,
    Z'[t] == v1[t] - (v2[t] + v4[t]) * Aarea[t],
    Ra'[t] == 0,
    Amol'[t] == v5[t] * Aarea[t]
   };
```

```
(*Simulation*)
Sol1 =
  NDSolve[{diffeq, rateeq, diff0} /. params,
  |微分方程式の数値解
    {PaniN, PaniE, Z, Ss, S, Ra, Amol}, {t, 0, 600}, MaxSteps → Infinity];
                                                    |最大ステ…   |無限大

{PaniE1[t_], PaniN1[t_], Z1[t_], Ss1[t_], S1[t_], Ra1[t_], Amol1[t_]} =
  {PaniE[t], PaniN[t], Z[t], Ss[t], S[t], Ra[t], Amol[t] / Amol[0]} /.
   Sol1[[1]];
```

```
(*Import of experimental plots file*)
 (*The Excel file has 3 columns with Time, Plot Data, and Error Bars.*)
dataA = Import["Desktop/4mMCascGrowth.xlsx", "Data"];
        |インポート
dataB = Join[dataA];
        |繋ぐ
dataC = dataB[[1]];
lengthC = Length[dataC];
          |長さ
plotData =
  Table[{dataC[[i]][[1]], Around[dataC[[i]][[2]], dataC[[i]][[3]]]},
  |リストを作成                  |不確かな数
    {i, 1, lengthC}];
```

(Next page)

```
(*Plot the simulation curve with
the experimental data.*)
Show[
示す
 (*Plot of the simulation curve*)
 Plot[
 プロット
  {Amol1[t]}, {t, 0, 140}, PlotRange → {{0, 140}, {0.95, 1.7}},
                                  プロット範囲
  PlotStyle → {Red, Thickness [0.01]},
  プロットスタイル 赤    太さ
  PlotTheme → "Scientific",
  プロットテーマ
  FrameLabel → {{"Normalized Surface Area / -", ""},
  枠ラベル
    {"Time / sec", ""}}, LabelStyle → {Black , 15}
                                  ラベルスタイル    黒
 ],

 (*Plot of the experimental data*)
 ListPlot[
 リストプロット
  {plotData}, PlotMarkers → {Automatic, 6},
              プロットマーカー    自動
  PlotStyle → {Blue},
  プロットスタイル 青
  IntervalMarkersStyle → {"Fences", Blue, Thickness → 0.002}
  区間マーカーのスタイル                    青      太さ
 ]
 , AspectRatio → 1 / 1.5
   縦横比
]
(*Example*)
```

Out[ ]=

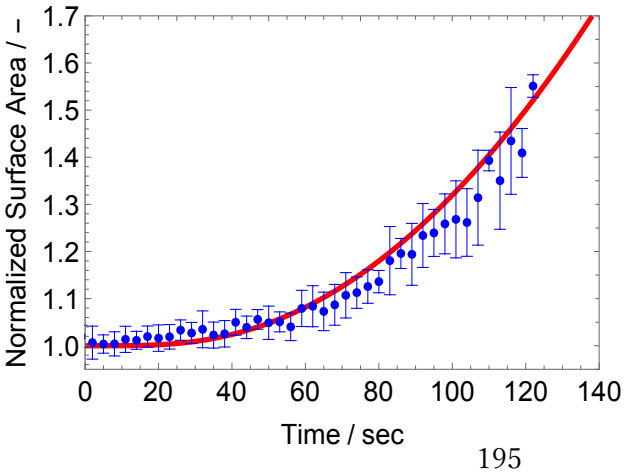

(END)

Chapter 5

Reproduction of Synthetic Minimal Cell

5.1 Introduction

To realize "reproduction" of a vesicle, not only "growth" to increase the amount of its own components, but also "division" of the vesicle is required. In the cell division of bacteria, the circular DNAs are first replicated and separated into two polar regions within the cell, and then protein called FtsZ appears at the division site to form a ring-shaped structure, the Z-ring. The contraction of this Z-ring causes cell division [Weiss 2004; Rowlett & Margolin 2015]. However, this protein-based division system is too complicated to apply to our minimal cell concepts. To realize a "minimal" reproduction system, how can we simply realize the vesicle division? This chapter explains the membrane elasticity model governing the vesicle deformation and division, then demonstrates the recursive growth and division cycles of vesicles coupled with the artificial metabolism system. However, if we focus only on the recursive membrane growth and division, which results in the decrease in the vesicle size by generations since there is no volume recovery mechanism. Then, I will also design the osmotic inflation mechanism for the vesicle volume recovery after the division, and I finally integrate all the processes for the complete reproduction cycle, *i.e.*, membrane growth → deformation → division → inflation, as shown in **Fig.1-3-1**.

5.2 Introduction to Membrane Elasticity Theory

5.2.1 Membrane Elasticity Model for Vesicle.

When we consider a cell-size giant unilamellar vesicle (GUV), their sizes are ~10 μm, whereas the membrane thickness is about a few nm. Then, the shapes of vesicles can be considered as two-dimensional surfaces. Here the basic elastic energy model for vesicles is the spontaneous curvature model (SC model) derived by Helfrich [Helfrich 1973 & 2000], where the shape of a vesicle is determined to minimize the total elastic energy under constraints on vesicle area A and vesicle volume V:

$$W_{SC} = \frac{\kappa}{2}\oint dA\,(C_1 + C_2 - C_0)^2 + \kappa_G \oint dA\,C_1 C_2 \tag{5.1}$$

where $C_{i=1,2}$ is the principal curvature of the membrane, C_0 is the spontaneous curvature originating from the asymmetry in the bilayer. κ and κ_G are the bending rigidity and the Gaussian bending rigidity, respectively. The first term expresses bending energy caused by vesicle deformation, and the second term expresses Gaussian bending energy that depends only on the topology and does not depend on the vesicle shape. In this model, the second term can be neglected for the vesicle deformation, except in the case of division. Due to the Gauss-Bonnet theorem [Do Carmo 2016], the second term is expressed by:

$$\kappa_G \oint dA\,C_1 C_2 = 4\pi\kappa_G(1-g) \tag{5.2}$$

where g is the genus given by the number of handles (holes) of the vesicle surface (a spherical vesicle has genus 0, and a torus vesicle has genus 1). Thus, this term has a constant value for the vesicle deformation to the limiting shape, but it plays an essential role for the vesicle division (fission of the neck of limiting shape).

Two geometric parameters describe the vesicle deformation process. The first one is the "reduced volume" defined as:

$$v = \frac{V}{\frac{4\pi}{3}R_0^3} \tag{5.3}$$

where $R_0 = \sqrt{A/4\pi}$ is the sphere radius with the same surface A as the deformed vesicle. In addition, the second geometric parameter is the "reduced spontaneous curvature," defined as:

$$c_0 = C_0 R_0 \tag{5.4}$$

The reduced volume is a measure of the volume/area ratio. The phase diagram of the SC model using v and c_0 and typical vesicle shapes that appeared in the phase diagram are

shown in **Fig. 5-2-1** [Seifert et al. 1991]. In this phase diagram, the limiting shape (L^{pear}) is located on the line L^{pear}, where the vesicle membrane must have a non-zero reduced spontaneous curvature. At the left end of the line L^{pear}, the vesicle has a symmetric limiting shape, and as it moves to the right on the line L^{pear}, the limiting shape becomes asymmetric.

In unilamellar vesicles, the vesicle membrane is composed of an inner leaflet and an outer leaflet, which gives another intrinsic parameter, the "preferred area difference," expressed by:

$$\Delta A_0 = \left(N^{out} - N^{in}\right) a_0 \tag{5.5}$$

where N^{out} and N^{in} are numbers of membrane molecules in the outer and inner leaflet, respectively, and a_0 is the equilibrium cross-section area of a membrane molecule. On the other hand, the vesicle has a geometrical area difference given by:

$$\Delta A = A^{out} - A^{in} = 2d \oint dA\, H \tag{5.6}$$

where $A^{out}$and A^{in} are the surface areas of the membrane in the outer and inner leaflet, respectively, d is the distance between the neutral surfaces of the two leaflets [Marsh 2007] (roughly, half of the bilayer thickness), and $H = (C_1 + C_2)/2$ is the mean curvature. In the case of phospholipid vesicles, the time scale of flip-flop motion (~ several hours) [Nakano et al. 2007] is much slower than the vesicle deformation timescale (~several seconds). Then, since N^{out} and N^{in} can be regarded as constant, the difference between ΔA_0 and ΔA will be compensated by expanding or compressing the cross-section area of membrane molecules. This elastic energy associated with the deformation of molecules is called the area difference elastic energy and is expressed by:

$$W_{ADE} = \left(\frac{\kappa_r}{2Ad^2}\right)(\Delta A - \Delta A_0)^2 \tag{5.7}$$

where κ_r is the nonlocal bending rigidity [Waugh et al. 1992]. The elastic energy model expressed by a sum of the bending energy and the area difference elastic energy is called the "area difference elasticity model" (ADE model) [Bozic et al. 1992; Wiese et al. 1992; Seifert et al. 1992], which quantitatively describes the deformation of double-chain phospholipid vesicles [Döbereiner et al. 1997; Sakashita et al. 2012]. On the other hand, for single-chain fatty acid vesicles, the difference between ΔA_0 and ΔA is quickly relaxed [Chen & Szostak 2004b; Bruckner et al. 2009; Urakami et al. 2021] due to the fast flip-flop motion (~ milliseconds) [Hamilton 2003; Mansy 2009]. Thus, the SC model describes the deformation of fatty acid vesicles ($\Delta A_0 = \Delta A$).

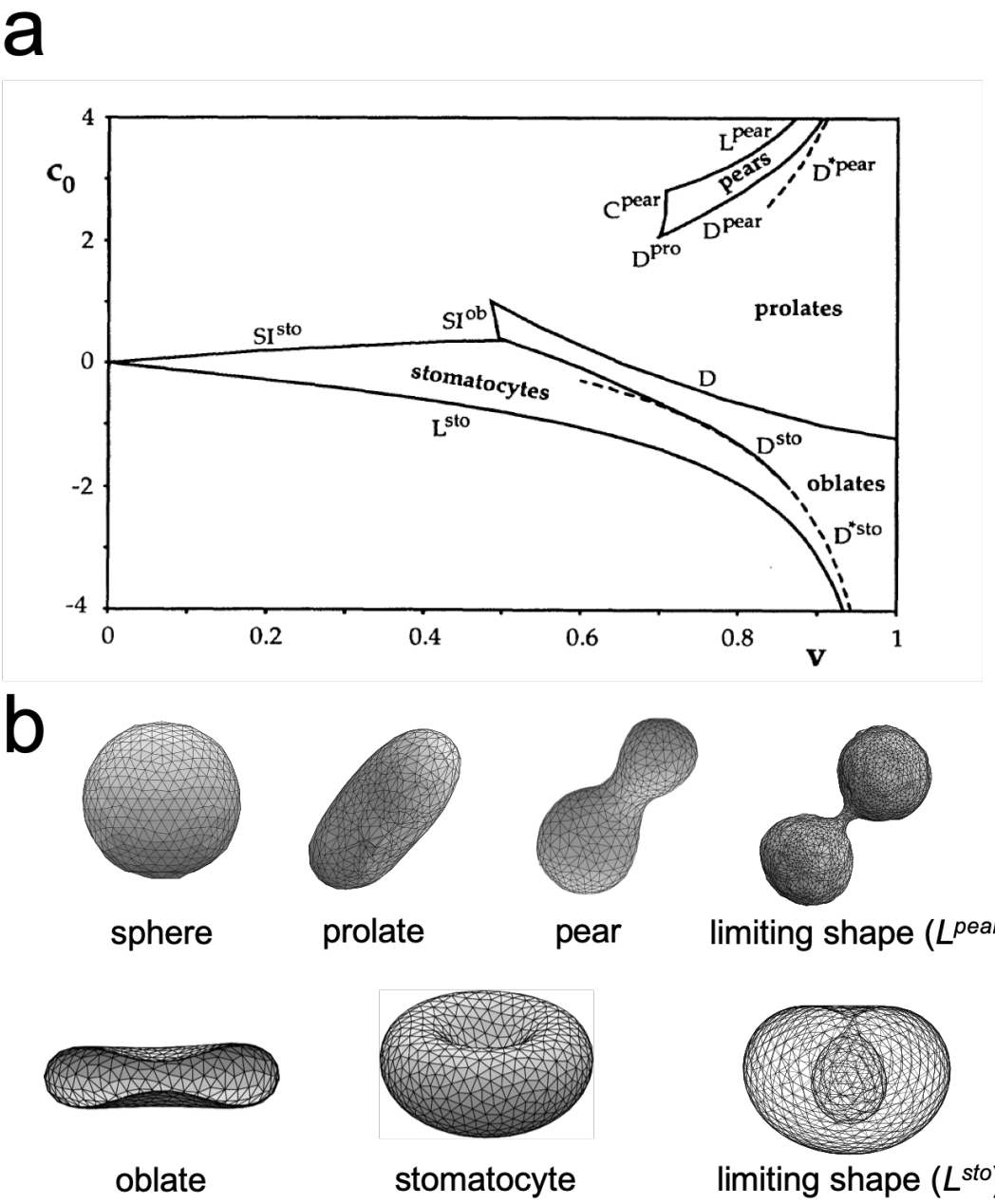

Figure 5-2-1. Phase diagram of SC model and typical vesicle shapes.
(a) Phase diagram of SC model of vesicle shapes, using reduced volume, v, and reduced spontaneous curvature, c_0, as parameters [Seifert et al. 1991]. Reprinted with permission from Seifert, U. et al., *Physical Review A*, **44**, 1182-1202.
(b) Vesicle shapes appeared in the phase diagram (**a**).

5.2.2 Division of Vesicles.

The neck of the limiting shape vesicle (*i.e.*, the narrow lipidic connection between two spherical vesicles) needs to be destabilized for the vesicle division. According to the SC model, the dependence of the bending energy of a pear vesicle on the neck radius a_{ne} is given by:

$$W_{SC}(a_{ne}) - W_{SC}(0) \sim 4\pi a_{ne}\kappa\left(C_0 - \frac{1}{R_1} - \frac{1}{R_2}\right) - 2\pi\kappa\left(\frac{1}{R_1^2} + \frac{1}{R_2^2}\right)a_{ne}^2 \ln a_{ne} \qquad (5.8)$$

where the pear vesicle is expressed by two spheres with radii R_1 and R_2 ($R_1 \neq R_2$) connected by a narrow neck with radius a_{ne}, and $a_{ne} = 0$ for the limiting shape vesicle [Lipowski 2020; Fourcade et al. 1994; Steinkühler et al. 2020]. For $(1/R_1 + 1/R_2) > C_0$, the neck with a finite size becomes stable, whereas for $(1/R_1 + 1/R_2) < C_0$, the lowest energy state is the one with neck size $a_{ne} = 0$, *i.e.*, the destabilization of the neck. In other words, if the spontaneous curvature is larger than $(1/R_1 + 1/R_2)$, breaking of the neck is expected to occur. To compare the elastic energy between the one-vesicle state (before division) and a two-vesicle state (after division), the Gaussian bending energy term plays an important role. Although the estimation of the Gaussian bending rigidity, κ_G, is still controversial [Landau et al. 1986; Helfrich & Harbich 1987; Siegel & Kozlov 2004; Hu et al. 2012; Nakagawa & Noguchi 2016; de Lange et al. 2021], it is sufficient to use the rough estimation $\kappa_G \sim -\kappa$. When a mother spherical vesicle divides into one large spherical vesicle with radius R_1 and one small spherical vesicle with radius R_2, (*i.e.*,$R_2 \ll R_1$), the free energy difference between the resulting two-vesicle state, $W_{sp,2}$, and the initial one-vesicle state, $W_{sp,1}$, (both states having the same membrane area) is given by:

$$W_{sph,2} - W_{sph,1} \sim 8\pi\kappa(1 - R_2C_0) + 4\pi\kappa_G = 4\pi\kappa_G \sim -4\pi\kappa < 0 \qquad (5.9)$$

where the vesicle membrane is assumed to have a large spontaneous curvature $C_0 = 1/R_2$. Thus, vesicle division is encouraged if the membrane has a large spontaneous curvature [Lipowski 2020], although the vesicle has to overcome the energy barrier between the one-vesicle state and the two-vesicle state.

Based on the membrane elasticity model, the spontaneous curvature (asymmetry of the bilayer) is a crucial parameter both for the vesicle deformation into limiting shape (L^{pear}) and the division to occur, as we discussed above. The one promising way to impose the necessary spontaneous curvature to the bilayer is the addition of "asymmetrically shaped" membrane molecules, *i.e.*, membrane molecules that do not have a cylindrical shape for optimal packing into a flat bilayer. Generally, membrane molecules that form vesicles have an almost cylindrical (symmetrical) shape [Israelachvili 2011]. When cone-

shaped molecules (molecules with a large head group and small hydrophobic tails: positive molecular spontaneous curvature) are added to the bilayer of a spherical vesicle, they prefer to stay in the outer leaflet due to the molecular shape preference [Sakuma & Imai 2011], whereas when inverse-cone-shaped molecules (molecules with a small head group and large (or bulky) hydrophobic tails: negative molecular spontaneous curvature) are added to the bilayer of a vesicle, they prefer to stay in the inner leaflet. The coupling between molecular shape and membrane mean curvature generates the spontaneous curvature and plays an important role in the biological functions of cell membranes [Mayor et al. 1993; Sakuma et al. 2008 & 2010]. When asymmetrically shaped lipids are added to a vesicle bilayer composed of cylinder-shaped lipids, the spontaneous curvature of the binary membrane is expressed by:

$$C_0 = \frac{1}{2} C_a \left(\phi_a^{out} - \phi_a^{in} \right) = \frac{1}{2} C_a \Delta\phi_a \tag{5.10}$$

where C_a is the molecular spontaneous curvature of an asymmetric lipid and ϕ_a^{out} and ϕ_a^{in} are the area fraction of the asymmetric lipids in the outer and inner leaflets, respectively [Jimbo et al. 2016]. The equilibrium distribution of asymmetrically shaped lipids in the inner leaflet and outer leaflet, $\Delta\phi_a$, is determined by the balance between the elastic energy and the mixing free energy [Derganc 2007; Tian & Baumgart 2009]. Therefore, inverse-cone-shaped lipids should be present in the vesicle bilayer to induce the deformation to a limiting shape (L^{pear}) and finally achieve the vesicle division. For example, Phosphatidylethanolamines (PE) lipids with $C_a \sim -0.3\, nm^{-1}$[Kamal et al. 2009] induce the vesicle division [Sakuma et al. 2011]. Calculations show that such a molecular spontaneous curvature is much larger than the curvature of spherical GUV with the radius R ~10 mm, then spherical binary GUV composed of DPPC (cylinder-shaped lipids) and DLPE (asymmetric lipid) with $\Delta\phi_a \sim -0.002$, *i.e.*, $c_0 = C_0 R \sim 3$ (R = 10 μm and area fraction of DLPE is $\phi_a = 0.2$) is known to cause the deformation to the limiting shape [Jimbo et al. 2016].

For the spontaneous vesicle division, in addition to the deformation to the limiting shape, the destabilization of the neck structure of the limiting shape is another important process. For the further detailed mechanism on destabilization of the neck, see the following references [Chen et al. 1997; Sakuma & Imai 2011; Jimbo et al. 2016; Urakami et al. 2018].

5.3 (Experiment) Reproduction of Vesicles

5.3.1 Micro-Injection Technique.

Double micro-injection setup that directly supplies energy currency molecules ("reference system").

To observe the morphological changes and membrane growth of GUVs in response to supply of membrane molecules and information polymer (PANI-ES) synthesis triggered by direct feeding of H_2O_2 (energy currency molecules), we adopted the double micro-injection setup named "reference system" (**Fig.5-3-1** and **Table 5-3-1**(#1-#3)). The experiments were performed in a holed silicone rubber sheet chamber. The AOT GUV or AOT/Chol (9/1) binary GUV suspension mixed with the reaction components for polymerization, except H_2O_2 to trigger the reaction, was carefully transferred from the glass vial into the sample chamber. The initial concentrations of the components for the reaction mixture were as follows: 3.0 mM amphiphiles (GUVs), 4.0 mM aniline, and 0.92 μM HRPC in 20 mM NaH_2PO_4 solution (pH=4.3). The polymerization reaction was triggered by micro-injecting a 2 M H_2O_2 solution containing 20 mM AOT micelles, 100 mM SDBS micelles, or 100 mM SDBS/0.5 mM Chol micelles. Except the condition #3, the same solution as bulk solution except GUVs was injected from the other pipette as a counter-flow: 0 mM amphiphiles, 4.0 mM aniline, 0.92 μM HRPC in 20 mM NaH_2PO_4 solution (pH=4.3).

Double micro-injection setup that realizes artificial metabolism system ("cascade system").

To observe the morphological changes and membrane growth of GUVs in response to information polymer (PANI-ES) synthesis triggered by feeding of D-glucose, dissolved O_2 and amphiphiles (artificial metabolism system), we adopted the double micro-injection setup named "cascade system" (**Fig.5-3-1** and **Table 5-3-1**(#4)). The experiments were performed in a holed silicone rubber sheet chamber. The AOT GUV or AOT/Chol (9/1) binary GUV suspension mixed with the polymerization components, except D-glucose to trigger the reaction, was carefully transferred from the glass vial into the sample chamber. The initial concentrations of the components for the reaction mixture were as follows: 3.0 mM amphiphiles (GUVs), 4.0 mM aniline, and 0.92 μM HRPC, 1.0 μM GOD, 100 mM sucrose in 20 mM NaH_2PO_4 solution (pH=4.3). Please note that 100 mM sucrose is contained in the reaction mixture to prevent volume decrease of the target

vesicles due to the osmotic imbalance while micro-injections. The polymerization reaction was triggered by micro-injecting a 100 mM D-glucose solution containing 20 mM AOT micelles from one side and a 100 mM D-glucose solution containing 100 mM SDBS/0.5 mM Chol micelles from the other side.

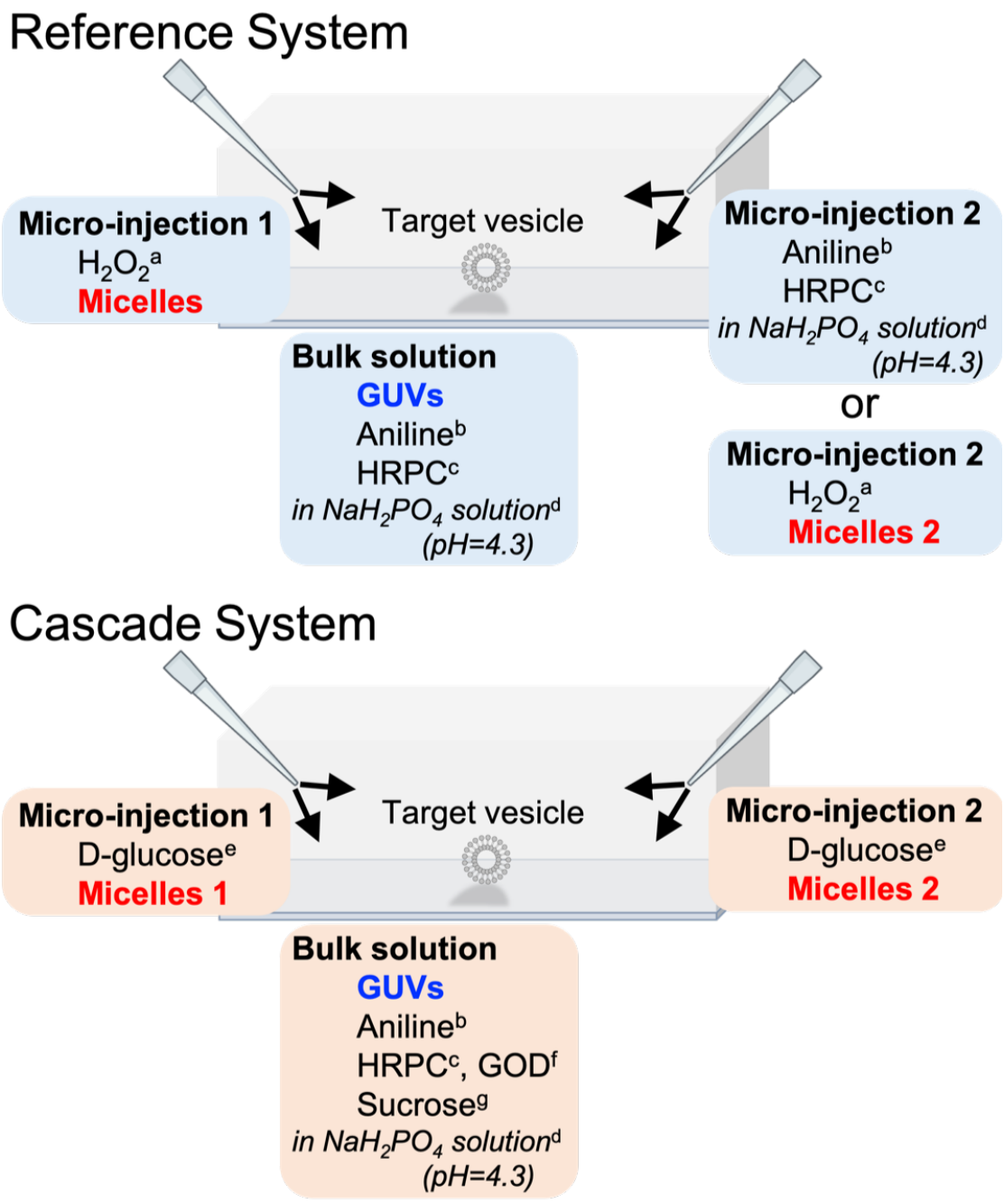

Figure 5-3-1. Scheme of double micro-injection setup used in 5.3.1 (reference system) and in 5.3.1 (cascade system). For the composition of GUVs and micro-injected micelles, see **Table 5-3-1** below. For the detailed configuration of the micro-injection system, see **Fig.2-5-1**.

[a][H_2O_2] = 2 M, [b][aniline] = 4.0 M, [c][HRPC] = 0.92 μM, [d][NaH_2PO_4 + H_3PO_4] = 20 mM, [e][D-glucose] = 100 mM, [f][GOD] = 1.0 μM, [g][sucrose] = 100 mM.

Table 5-3-1. Reaction components and their concentrations used in double micro-injection setup, especially on the combination of the target GUV composition and micro-injected micelles. See also **Fig.5-3-1**. The micro-injected amphiphiles are also shown below.

Condition	Target GUVs	Micro-injected Micelles	Reference or Cascade
# 1	AOT	100 mM SDBS	Ref
# 2	AOT/Chol (9/1)	20 mM AOT	Ref
# 3	AOT	100 mM SDBS /0.5 mM Chol + 20 mM AOT	Ref
# 4	AOT/Chol (9/1)	100 mM SDBS /0.5 mM Chol + 20 mM AOT	Cas

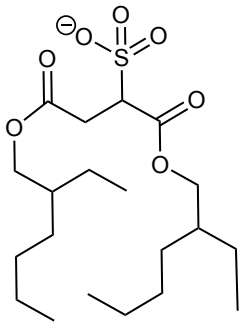

AOT

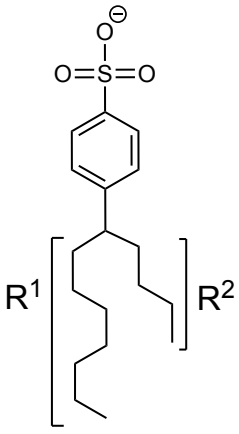

SDBS

(R^1+R^2 = $C_{11}H_{24}$)

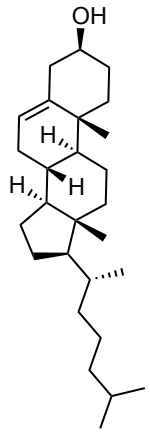

Cholesterol

5.3.2 Osmotic Inflation System.

Osmotic inflation of vesicles by transfer.

An osmotic pressure difference is applied between the inside and outside of the GUV membrane to make vesicle volume grow by using the water inflow across the membrane. In this context, a certain concentration of osmolyte is usually encapsulated inside a GUV, then the GUV is transferred into the solution that contains a lower concentration of osmolyte. However, such a system leads to the cessation of the osmotic swelling immediately due to the dilution of the GUV encapsulating solution. Therefore, for the sustainable volume increase of GUVs, it is necessary to keep the total concentration of osmolytes in the GUVs constant to the volume increase. In addition, the external solution of GUVs needs to contain sufficient free membrane molecules to be incorporated into the membrane. Otherwise, the membrane tension caused by the volume increase will cause the membrane fracture [Mally et al. 2013].

Here we show the mechanism of osmotic inflation in our minimal cell. AOT GUVs encapsulating sucrose solution (orange) were brought into the solution containing fructose and AOT (green) (**Fig.5-3-2(a)**). The AOT membrane is permeable to fructose but almost impermeable to sucrose (**Fig.5-3-2(b)**). This asymmetrical permeation maintains the osmotic pressure difference over time, resulting in the long-term inflation of the AOT GUVs. In addition, the external solution of AOT GUVs contains sufficient free AOT molecules to be incorporated into the vesicle membrane since AOT has high cvc (~1.5 mM) in 20 mM NaH_2PO_4 solution (pH=4.3). The experimental setup is as follows: AOT GUV suspension (20 mM AOT) was prepared in 20 mM NaH_2PO_4 solution containing 100 mM sucrose (pH=4.3) by the gentle hydration method. The 20 mM AOT GUV suspension was diluted to 3.0 mM AOT with the same NaH_2PO_4 sucrose solution and then transferred into the first microscope sample chamber, a hole in silicone rubber sheet placed on a glass slide. The hole had a diameter of 12 mm and a depth of 1 mm. The GUVs with the diameter of ~15 μm in the first chamber were trapped in a micro-pipette VacuTip II (inner diameter of 60 μm) using a CellTram Vario (Eppendorf, Germany) and then carefully transferred into the second microscope sample chamber filled with 2.0 mL of 20 mM NaH_2PO_4 solution (pH=4.3) containing 100 mM D-fructose and 3.0 mM AOT (cvc~1.5 mM). The second sample chamber was a glass-bottom dish D11130H (Matsunami, Japan), and the original NaH_2PO_4 solution containing 3.0 mM AOT in the second chamber was sonicated for 5 min at room temperature using a Branson Sonifier model 150 (Emerson, USA) and pressed through a 0.2 μm polypropylene filter Puradisc 25 PP (GE Healthcare, UK) before use. After the transfer, the second chamber

was quickly covered by a plastic slip to prevent water turbulence induced by airflow. The transferred GUVs containing 100 mM sucrose were located at the bottom of the chamber due to the difference in the specific gravity and then started swelling. The osmotic inflations of GUVs were recorded at room temperature ($T \sim 25^{\circ}$C) with phase-contrast light microscopy.

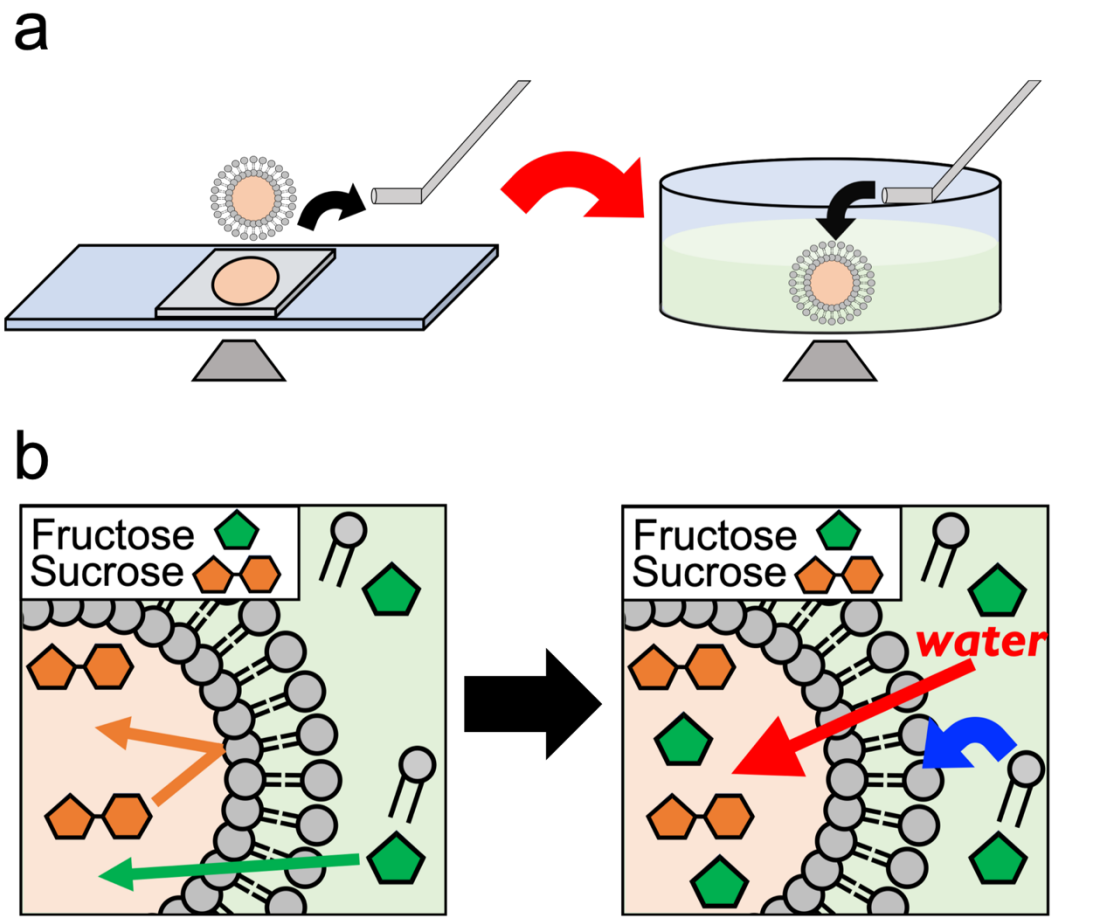
a
b
Fructose
Sucrose
Fructose
Sucrose
water
c
Cascade System
Target vesicle:
AOT/Chol (9/1)
Micro-injection 1
D-glucose[e]
20 mM AOT
Micro-injection 2
D-glucose[e]
100 mM SDBS
/0.5 mM Chol
Bulk solution
AOT[h]
Aniline[b]
HRPC[c], GOD[f]
Fructose[g]
in NaH2PO4 solution[d]
(pH=4.3)
Inner solution
AOT[h]
Sucrose[g]
in NaH2PO4 solution[d]
(pH=4.3)

Figure 5-3-2. Experimental setup for the osmotic inflation of vesicles and for the reproduction cycles of vesicles coupled with volume recovery.

a, Schematic of the experimental setup for osmotic swelling of AOT GUVs. The sample chamber for microscope observation was filled with the AOT GUV suspension prepared in 20 mM NaH_2PO_4 solution (pH=4.3) containing 100 mM sucrose and 3.0 mM AOT. AOT GUVs with a diameter of ~15 μm were trapped in a micro-pipette (inner diameter ~60 μm) and then carefully transferred into the second sample chamber filled with 2.0 mL of 20 mM NaH_2PO_4 solution (pH=4.3) containing 100 mM D-fructose and 3.0 mM AOT.

b, Schematic of osmotic inflation of vesicles using two types of osmolytes (fructose in green and sucrose in orange) with asymmetric membrane permeability. The AOT membrane is permeable to fructose but almost impermeable to sucrose. The osmotic drag couples the inflow of fructose with the inflow of water, while sucrose is encapsulated in the GUV. This asymmetrical permeation maintains the osmotic pressure difference over time, resulting in the long-term inflations of the AOT GUVs. In addition, the external solution contains sufficient free AOT molecules (cvc~1.5 mM) to be incorporated into the vesicle membrane to relax the membrane tension caused by the volume increase.

c, Scheme of double micro-injection setup used for the "reproduction cycle" of AOT/Chol binary GUVs (*i.e.,* growth, deformation, division, and inflation) coupled with enzymatic cascade synthesis of PANI-ES. The experimental setup is almost identical with entry #1 in **Table 3-3-4**, and the only difference is that the AOT/Chol binary GUV encapsulates 100 mM sucrose solution, whereas the bulk solution contains 100 mM D-fructose instead of sucrose.

[b][aniline] = 4.0 M, [c][HRPC] = 0.92 μM, [d][NaH_2PO_4 + H_3PO_4] = 20 mM, [e][D-glucose] = 100 mM, [f][GOD] = 1.0 μM, [g][sucrose] = [g][fructose]=100 mM, [h][AOT]=3.0 mM (cvc~1.5 mM).

5.3.3 Reproduction of Synthetic Minimal Cell

Reproduction of AOT/Chol (9/1) binary GUVs coupled with information polymer synthesis under osmotic inflation system.

To realize recursive vesicle reproduction, the enzymatic cascade polymerization of aniline on the GUVs using the micro-injection system (growth → deformation → division) was performed under the osmotic swelling condition (inflation). First, AOT/Chol (9/1, 5 mM amphiphiles) binary GUVs were prepared in 20 mM NaH_2PO_4 solution (pH=4.3) containing 100 mM sucrose (osmolyte) by using the gentle hydration method. Then, the polymerization components (75 μL of 267 mM sucrose solution, 50 μL of 40 mM aniline solution, 25 μL of 18.4 μM HRPC solution, and 50 μL of 10 μM GOD solution; all these solutions were prepared in 20 mM NaH_2PO_4 solution (pH=4.3)) were added to 300 μL of the AOT/Chol GUV suspension. After gentle mixing, the GUV suspension was dropped into the hole in the silicone sheet chamber for microscope observation, and then a selected GUV was carefully transferred into the 2.0 mL of 20 mM NaH_2PO_4 solution (pH=4.3) containing 3.0 mM AOT, 4.0 mM aniline, 0.92 μM HRPC, 1.0 μM GOD, dissolved oxygen, and 100 mM D-fructose in the glass bottom chamber. The bulk solution in the glass chamber was passed through a 0.2 μm polypropylene filter Puradisc 25 PP (GE Healthcare, UK) before use. The main difference in components between inside and outside the AOT/Chol (9/1) GUV was the osmolytes (100 mM sucrose inside the GUV and 100 mM D-fructose outside the GUV). It should be noted that D-fructose easily penetrates from the external solution through the membrane inside the vesicle, whereas sucrose is hard to pass through the membrane (see **Fig.5-3-2(b)**). Then, the osmotic drag couples the inflow of D-fructose with the inflow of water, causing the vesicle to swell, while AOT molecules in the external solution increase the membrane surface area by incorporating into the membrane. After transferring the AOT/Chol (9/1) GUV, the polymerization was triggered by the micro-injection of 100 mM D-glucose solution containing micelles (20 mM AOT and 100 mM SDBS/0.5 mM Chol) (**Fig.5-3-2(c)**). The configuration and injection pressure were the same as described above.

5.3.4 Result 1: Growth and Division of Vesicles

Growth and deformation to limiting shape of AOT GUVs supplied with SDBS micelles, entry #1 in Table 5-3-1.

By feeding spherical AOT GUVs with AOT molecules from the external solution coupled with the surface-localized synthesis of PANI-ES, the AOT GUVs grow to a prolate shape. However, they never show any vesicle reproduction (**Fig.2-5-2(b)**), *i.e.*, they never show a deformation to the limiting shape (a pair of spherical vesicles connected by a narrow neck, see **Fig.5-2-1(b)**) and fission of the neck. Thus, the shape and topology of the growing vesicles have to be controlled by other means. The deformation and division of vesicles are well described by the elastic theory of membranes [Seifert 1997; Sakashita et al. 2012]. Most importantly, the membrane elasticity model shows that vesicle division is hard to observe in one-component vesicles [Seifert 1991; Fourcade et al. 1994], which agrees well with experimental observations [Döbereiner et al. 1993]. Then, first of all, we simply extend our previous one-component AOT GUV growth system with direct addition of H_2O_2 (energy currency molecules) in chapter 2 to the two-component system by feeding AOT GUVs with other sulfonated amphiphiles, such as SDBS (see **Table 5-3-1**). SDBS works as a template for the PANI-ES synthesis (see **Fig.2-3-7(a)**), and by supplying SDBS micelles to AOT GUVs coupled with the synthesis of PANI-ES, I confirmed that the incorporation of SDBS molecules from the external solution is promoted, then the AOT GUVs show growth (see **Table 2-5-3** and **Fig.2-5-4**). The chapter 2 focused only on the time-dependent changes in vesicle surface area. Here we focus on the time-dependent changes in the morphology of AOT GUVs with the feeding of SDBS micelles, and the results are shown in **Fig.5-3-3** below. As already observed in the quantitative membrane growth experiment (plot D in **Fig.2-5-4**), the AOT GUV started showing membrane growth after the induction period (~ 38 sec). The difference in morphology from the AOT one-component system is that the GUV grows not to the prolate shape but grows and deforms to the limiting shape (at "64 sec"). The AOT molecules are almost cylindrical (symmetric) shape in vesicle membrane [Pan et al. 2015]. In contrast, SDBS molecules are cone-shaped surfactants with a large hydrophilic head and small hydrophobic tails (*i.e.,* positive molecular spontaneous curvature), which are considered to prefer to stay in outer layer, resulting in the generation of membrane spontaneous curvature and the deformation to the limiting shape with the progress of incorporation of SDBS molecules. However, the observed neck structures were very stable (see *"101 sec"* and *"113 sec"* in **Fig.5-3-3** and Appendix 5-A), and no fission of the neck was observed in more than twenty times experiments.

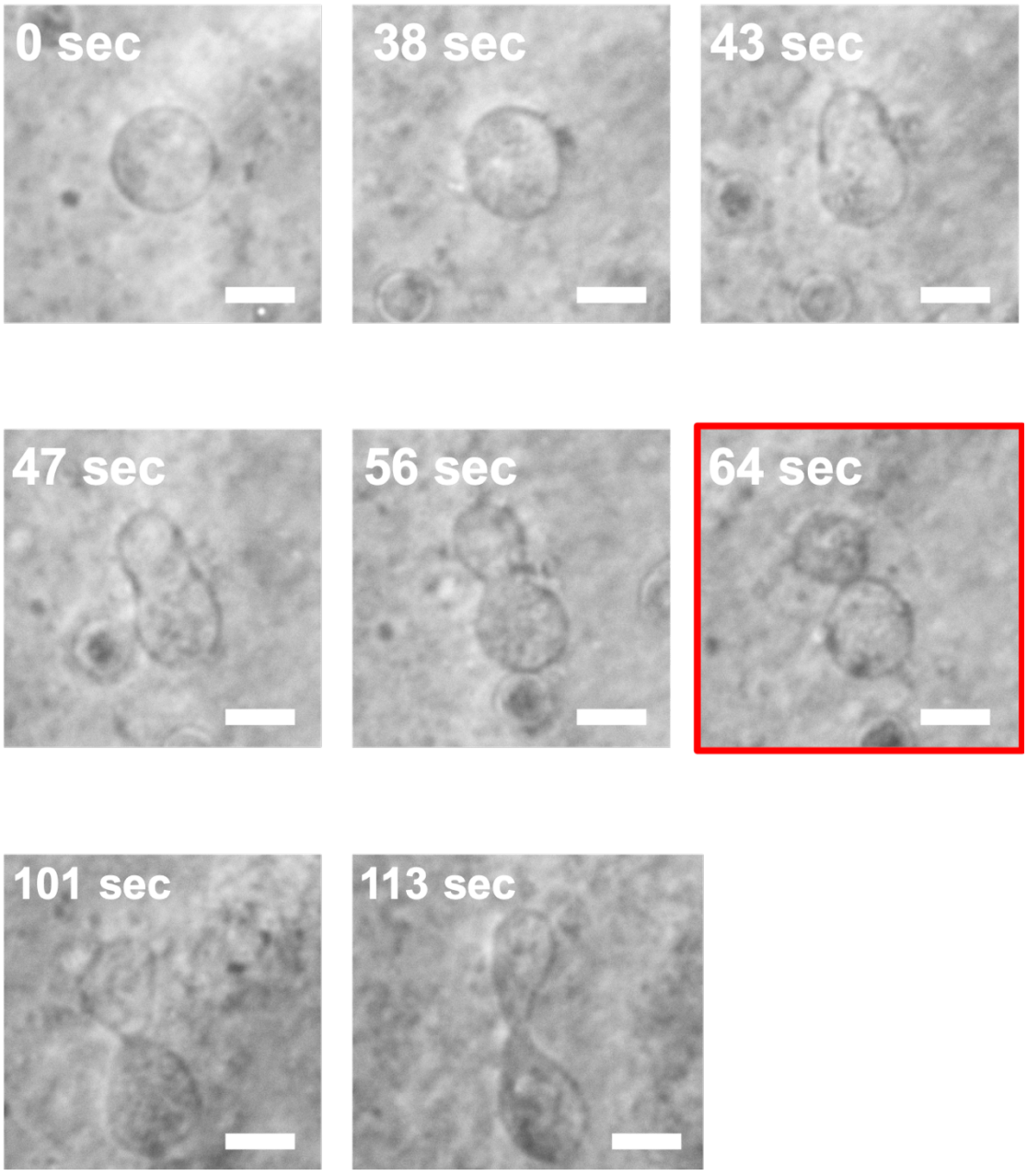
0 sec
38 sec
43 sec
47 sec
56 sec
64 sec
101 sec
113 sec

Figure 5-3-3. Phase-contrast light microscopy images AOT GUVs, taken in the "reference condition" with the supply of 100 mM SDBS micelles (entry #1 in **Table 5-3-1**), coupled with PANI-ES synthesis. The initially spherical GUV showed growth and deformation to a limiting shape (at *"64 sec"*), but the neck is stable and not divided. The time-dependent changes are shown after starting the micro-injection for t = 0, 38, 43, 47, 56, and 64 sec to show the deformation to limiting shape, and for t = 64, 101, and 113 sec to show the neck is not divided. The length of the scale bar: 10 μm.

Reproduction of AOT/Chol binary GUVs supplied with AOT micelles, entry #2 in Table 5-3-1.

Next, the shape and topology for the growing vesicles should be controlled by other means. The promising way is to introduce a second amphiphile having a negative molecular spontaneous curvature (*i.e.,* with a small polar head group and bulky hydrocarbon part) [Sakuma & Imai 2011; Jimbo et al. 2016]; whereby the coupling between the membrane curvatures and the local amphiphile composition is responsible for the deformation and division of the vesicle [Jimbo et al. 2016; Urakami et al. 2018; Chen et al. 1997]. Cholesterol with its small polar head group (–OH) and bulky hydrocarbon part (*i.e.*, negative spontaneous curvature property) maybe suited as the second amphiphile. To test this, we prepared binary GUVs composed of AOT and cholesterol (at a molar ratio of 9:1, 2.7 mM AOT, 0.3 mM cholesterol) in 20mM NaH_2PO_4 solution (pH = 4.3) containing 4.0 mM aniline and 0.92 μM HRPC, and micro-injected to individual binary GUVs a micellar solution consisting of 20mM AOT and 2.0 M H_2O_2 (see entry #2 in **Table 5-3-1.**). Immediately after injection, the targeted GUVs started to deform to the limiting shape (at *"11 s"*) and then spontaneously divided into two daughters GUVs in about 20 s (**Fig.5-3-4**). The vesicle reproduction was confirmed by more than 20 identical experiments where the binary AOT/Chol GUVs almost always showed the first division and rarely showed the second division of daughter vesicles when the micro-injections continued. The vesicles showed no more division with further micro-injection, and the morphologies were not obvious. For example, sometimes the vesicle deformed to tube-like shapes after the first or second division, and sometimes multiple tubes are formed from the daughter vesicles, which are considered to be caused by the depletion of

cholesterol in the target vesicle membrane. We analyzed the vesicle division processes (n = 4) induced by the simultaneous micro-injection of AOT micelles and H_2O_2. When the mother GUV with initial surface area $A(0)$ and volume $V(0)$ showed growth and division, the surface area and volume of the GUV increased to $(1.25 \pm 0.05)A(0)$ and $(1.05 \pm 0.05)V(0)$, respectively.

A suggested molecular interpretation consistent with the microscopic observations is the following: AOT molecules present in the external solution bind to the formed PANI-ES through electrostatic interactions or hydrogen bonding. This binding decreases the hydrophilicity of the AOT molecules, which promotes the incorporation of the bound AOT molecules into the outer monolayer of the AOT/Chol GUVs. The incorporated AOT molecules increase the area of the outer monolayer. Flip-flop motions of the AOT molecules coupled with the negative molecular spontaneous curvature of cholesterol relax the initially spherical vesicle shape to a prolate shape and then to the limiting shape [Jimbo et al. 2016]. In the limiting shape, cholesterol molecules are excluded from the neck due to the coupling between the molecular shape and the membrane Gaussian curvature, which destabilizes the neck and causes vesicle division [Urakami et al. 2018]. For further detailed discussions, see below.

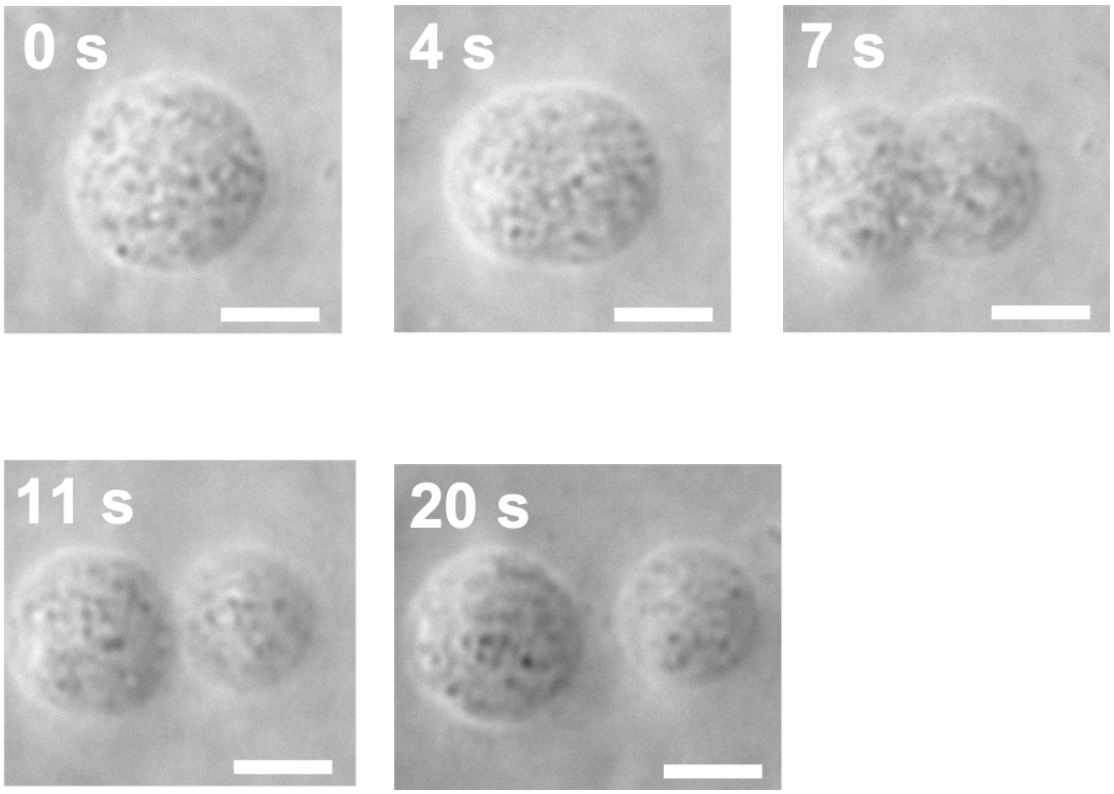

Figure 5-3-4. Phase-contrast light microscopy images AOT/Chol (9/1) binary GUVs, taken in the "reference condition" with the supply of 20 mM AOT micelles (entry #2 in **Table 4-1**), coupled with PANI-ES synthesis. The time-dependent changes are shown after starting the micro-injection for t = 0, 4, 7, 11, and 20 sec. The initially spherical GUV showed growth, deformation to limiting shape (at *"11 sec"*), and then the neck is spontaneously divided (at *"20 sec"*). The length of the scale bar: 10 μm.

Discussion 1: Growth and division of AOT/Chol binary GUVs based on the ADE model.

As we briefly mentioned in section 5.2.1, vesicle shapes are obtained by minimizing the membrane elastic energy with the ADE model [Heinrich et al. 1993; Miao et al. 1994; Jimbo et al. 2016], given by:

$$W_{ADE} = \kappa \left[\frac{1}{2} \oint dA\,(2H)^2 + \frac{1}{2Ad^2} \frac{\kappa_r}{\kappa} (\Delta A - \Delta A_0)^2 \right] \tag{5.11}$$

where κ and κ_r are local bending constant and the nonlocal bending modulus, respectively, $H = (C_1 + C_2)/2$ is the mean curvature, d is the distance between the neutral surfaces of the two leaflets, and ΔA_0 and ΔA are a preferred area difference and a geometrical area difference, given by Eq. (5.5) and Eq. (5.6), respectively. Typically, $\kappa_r/\kappa = 3$ is used to describe phospholipid vesicle shape [Sakashita et al. 2012]. The first term expresses the bending energy of the membrane, and the second term is the nonlocal elastic energy due to the deviation of the geometrical monolayer area difference, ΔA, from the preferred value, ΔA_0. The shape of a vesicle with the surface area, A, and the volume, V, is determined by two geometrical parameters, the reduced volume, $v = 3V/4\pi R_0^3$ ($R_0 = \sqrt{A/4\pi}$) (Eq. (5.3)), and the normalized preferred area difference of the two monolayers given by:

$$\Delta a_0 = \frac{\Delta A_0}{8\pi R_0 d} \tag{5.12}$$

When a vesicle incorporates additional amphiphiles from the external solution into the outer leaflet of the vesicle membrane, the amphiphiles in the outer monolayer undergo flip-flop motions to relax the elastic energy. Then, the growing vesicle changes the normalized preferred area difference, Δa_0, and the reduced volume, v, which causes vesicle deformation if the equilibration of the water molecules across the vesicle bilayer

is slow.

Here, we map the observed vesicle growth trajectory by using two geometrical parameters, the reduced volume, v, and the normalized preferred area difference, Δa. The reduced volume and the normalized area difference were calculated from the reproduced vesicle images using the Surface Evolver software package [Brakke 1992; Jimbo et al. 2016] (**Fig.5-3-5**). The observed vesicle growth trajectory in the $(v, \Delta a)$ plane with the stable vesicle shape types for oblates (line O), prolates (line P), and budded limiting shapes (line L) (called "vesicle branches") is shown in **Fig.5-3-6**, whereby the minimum of the ADE energy determines the location of each branch. The observed growth trajectory (*pathway **1, 2*** in **Fig.5-3-6**) agrees with the stable prolate branch, indicating that the ADE model describes the vesicle growth well. In the vesicle growth stage, AOT molecules in the external solution incorporate into the outer monolayer of the vesicle, which increases the normalized preferred area difference, Eq. (5.12). Since in the region of $0.652 < v < 1.0$, the most stable vesicle branch is the prolate branch [Jimbo et al. 2016; Seifert 1997], AOT molecules in the outer monolayer undergo flip-flop motions to relax the vesicle shape to the stable prolate shape ($\Delta a_0(v) = \Delta a_{pro}(v)$, whereby $\Delta a_{pro}(v)$ is the normalized geometrical area difference of the stable prolate shape with reduced volume v). Thus, the observed growth trajectory indicates that AOT molecules in the bilayer readily undergo flip-flop motions from the outer to the inner monolayer of the AOT bilayer. This is in qualitative agreement with the high fluidity of AOT bilayers [Kashima et al. 2018; Iwasaki et al. 2017]. The observed deformation pathway strongly supports that the targeted vesicles are "giant unilamellar vesicles" and not "giant multi-lamellar vesicles." In this experiment, we supplied membrane molecules from the external solution, which means that the outermost bilayer shows growth with the aid of PANI-ES. If the targeted giant vesicle only consists of one single bilayer (*i.e.*, if it is a GUV), the deformation pathway is well described by the ADE model [Jimbo et al. 2016; Sakashita et al. 2012; Döbereiner et al. 1997] as shown in **Fig.5-3-6**. On the other hand, if the targeted giant vesicle is composed of multi-bilayers, all inner bilayers cannot grow due to the lack of PANI-ES. This geometrical constraint – growth of only the outermost membrane and constant vesicle volume – prevents the vesicle from transforming along the standard vesicle deformation pathway (*e.g.,* formation of a tubular membrane). The observed deformation pathway shown in **Fig.5-3-5(a)** and **Fig.5-3-6** supports that the targeted vesicles were unilamellar.

A simple way to attain AOT vesicle reproduction (deformation to the limiting shape and fission of the neck) is to add to the AOT vesicles a second amphiphile with a negative molecular spontaneous curvature. When the vesicle is composed of two types of

amphiphiles, *e.g.*, one amphiphile having a zero spontaneous curvature (AOT) and the second amphiphile having a negative spontaneous curvature, $H_{sp}^{n}(<0)$, the second amphiphile prefers to stay in the inner monolayer of the spherical vesicle due to simple geometrical preference. This asymmetric distribution of the second amphiphile in the bilayer causes spontaneous curvature of the binary membrane, $c_0 = H_{sp}^{n}\Delta\phi$ where $\Delta\phi = \phi^{out} - \phi^{in}$ is the difference in the second amphiphile's area fraction between outer leaflet ϕ^{out} and inner leaflet ϕ^{in}. This modifies the normalized preferred area difference. The renormalized preferred area difference modified by c_0 is given by:

$$\Delta\tilde{a}_0 = \Delta a_0 + \frac{\kappa\, R_0 c_0}{2\kappa_r} \tag{5.13}$$

which encourages the vesicle deformation to the limiting shape (**Fig.5-3-6**) [Jimbo et al. 2016; Sakashita et al. 2012]. In addition, the amphiphile geometry modifies the monolayer Gaussian curvature modulus, $\bar{\kappa}^m$, through a geometrical relationship,

$$2\,\bar{\kappa}^m = \bar{\kappa} + 4\,\kappa^m H_{sp} d \tag{5.14}$$

where $\bar{\kappa}$ is the bilayer Gaussian curvature modulus, κ^m is the monolayer bending modulus, and H_{sp} is the molecular spontaneous curvature of the amphiphile [Urakami et al. 2018; Siegel & Kozlov 2004]. The limiting shape vesicle consists of two spherical regions having a positive Gaussian curvature and a neck region having a negative Gaussian curvature. Then, if the second amphiphile with $H_{sp}^{n}(<0)$ has a smaller monolayer Gaussian curvature modulus than the one of AOT, *i.e.*, $\bar{\kappa}_n^m < \bar{\kappa}_{AOT}^m$, the second amphiphile will be excluded from the neck region. This segregation increases the free energy and destabilizes the neck, which results in vesicle division [Urakami et al. 2018; Chen et al. 1997]. In fact, the binary AOT/Chol (9/1) GUVs showed vesicle reproduction (**Fig.5-3-4** and **Fig.5-3-5(b)**). The observed vesicle reproduction pathway is illustrated with the $(v, \Delta a)$ phase diagram (*pathway **1, 3*** in **Fig.5-3-6**). The mother AOT GUV is initially deformed with an increase in Δa as v decreases, following line P, *i.e.*, the line for stable prolates (prolate branch). At v = 0.78, the GUV hopped to the limiting shape branch (line L) discontinuously through a pear-like intermediate shape, which agrees well with the prediction of the ADE model. When a mother GUV with initial surface area $A(0)$ and volume $V(0)$ deformed to the limiting shape, the limiting shape GUV had the surface area $\sim 1.30\, A(0)$ and the volume $\sim 1.05\, V(0)$. Thus, the reduced volume, v, decreased from 0.94 to 0.74. The limiting shape GUV spontaneously divided into two independent GUVs as predicted by the neck destabilization model.

a

AOT GUV

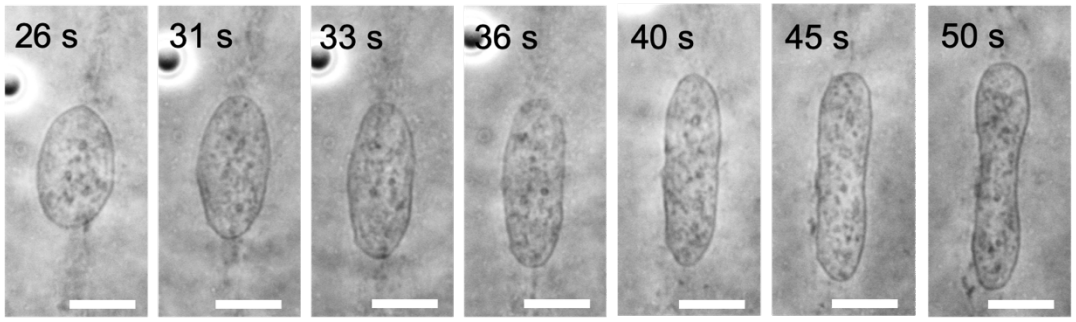

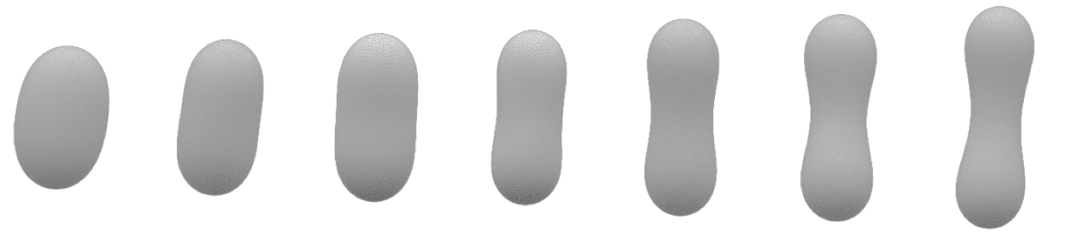

$v =$ 0.94	$v =$ 0.90	$v =$ 0.86	$v =$ 0.82	$v =$ 0.78	$v =$ 0.74	$v =$ 0.70
$\Delta a =$ 1.03	$\Delta a =$ 1.05	$\Delta a =$ 1.07	$\Delta a =$ 1.11	$\Delta a =$ 1.15	$\Delta a =$ 1.19	$\Delta a =$ 1.24

b

AOT/Chol (9/1) GUV

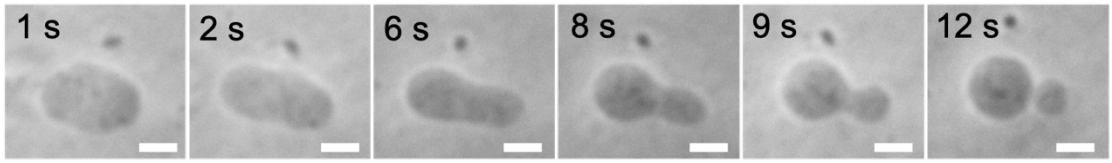

$v =$ 0.94	$v =$ 0.86	$v =$ 0.78	$v =$ 0.78	$v =$ 0.78	$v =$ 0.78
$\Delta a =$ 1.03	$\Delta a =$ 1.07	$\Delta a =$ 1.15	$\Delta a =$ 1.20	$\Delta a =$ 1.24	$\Delta a =$ 1.35

Figure 5-3-5. Phase-contrast microscopy images and reconstructed vesicle shapes during GUV growth coupled with PANI-ES synthesis. For each figure, the upper line shows the experimental microscopy images, the middle line shows the reconstructed images using the Surface Evolver software package [Brakke 1992], and the bottom line shows the reduced volumes, v (see Eq. (5.3)), and the normalized geometrical area differences, $\Delta a = \oint dA\, H/(4\pi R_0)$ (H: local mean curvature), calculated from the reconstructed images.

a, Growth of an AOT GUV in "reference condition" (identical to the data shown in **Fig.2-5-2(b)**) induced by micro-injection of H_2O_2 (2.0 M) and AOT micelles (20 mM, prepared in pure water). The GUV suspension (3.0 mM AOT in 20 mM NaH_2PO_4, pH = 4.3) contained aniline (4.0 mM) and HRPC (0.92 μM). The length of the scale bar: 20 μm.

b, Growth of an AOT/Chol (9/1) binary GUV in "reference condition" (entry #2 in **Table 5-3-1**) induced by micro-injection of H_2O_2 (2.0 M) and AOT micelles (20 mM, prepared in pure water). The GUV suspension (3.0 mM total amphiphile, 9:1 molar ratio, in 20 mM NaH_2PO_4, pH = 4.3) contained aniline (4.0 mM) and HRPC (0.92 μM). The length of the scale bar corresponds to 5 μm.

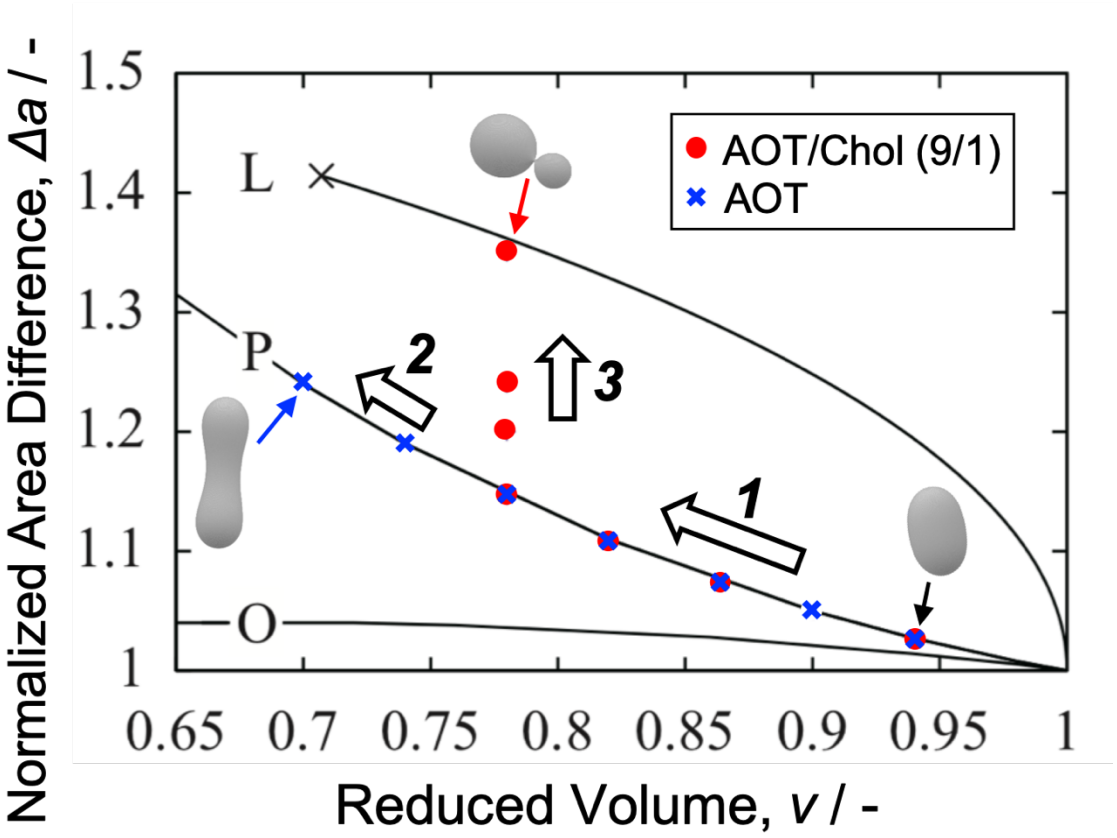

Figure 5-3-6. Pathways for the growth of AOT GUVs plotted in $(v, \Delta a)$ space. Pathway indicated with hollow arrows (**1** and **2**) is for the AOT vesicles coupled with the synthesis of PANI-ES *without* cholesterol system (**Fig.5-3-5(a)**). Pathway indicated with hollow arrows (**1** and **3**) is for the reproduction of binary AOT/Chol (9/1) GUVs coupled with the synthesis of PANI-ES (**Fig.5-3-5(b)**). Lines O, P, and L represent the oblate, prolate, and limiting shape (L^{pear}) branches, respectively.

Tube formation of AOT GUVs supplied with SDBS/Chol micelles, entry #3 in Table 5-3-1.

In the AOT/Chol (9/1) binary GUV system, we showed that Chol having a small polar head and a bulky hydrocarbon part works as the second component of the membrane molecule to attain the deformation and division of vesicle. When we supplied AOT micelles to binary GUVs, GUVs showed deformation to the limiting shape, and then the neck was spontaneously broken to form completely separated two daughters GUVs. However, the reproduction of vesicles ceases after the division due to the dilution of initially contained Chol. To attain the recursive vesicle growth and division, Chol must be externally supplied to the vesicle membrane.

Here, we adopted SDBS micelles as the Chol carrier since SDBS molecules have sulfonate head group and can be incorporated into AOT membrane. When we supplied 2.0 M H_2O_2 solution containing 20 mM AOT micelles from one side, and SDBS/Chol mixed micelles from another side to an AOT single component GUV under the reference reaction condition (entry #3 in **Table 5-3-1**), the GUV showed protrusion and then divided into the spherical mother vesicle and a prolate daughter vesicle (**Fig.5-3-7**). This observation contrasts with the GUV growth without Chol (**Fig.5-3-5(a)**). Thus, the supplied Chol was incorporated into the AOT GUV membrane and induced the vesicle division, although the target AOT GUV with no initial content of Chol in the bilayer does not show the nice reproduction pathway as observed by using GUV containing Chol from the beginning (**Fig.5-3-5(b)**). Then, we tested this Chol carrier SDBS micelles to the AOT/Chol (9/1) binary GUV under the "cascade system" to realize the reproduction of vesicles under the condition of artificial metabolism.

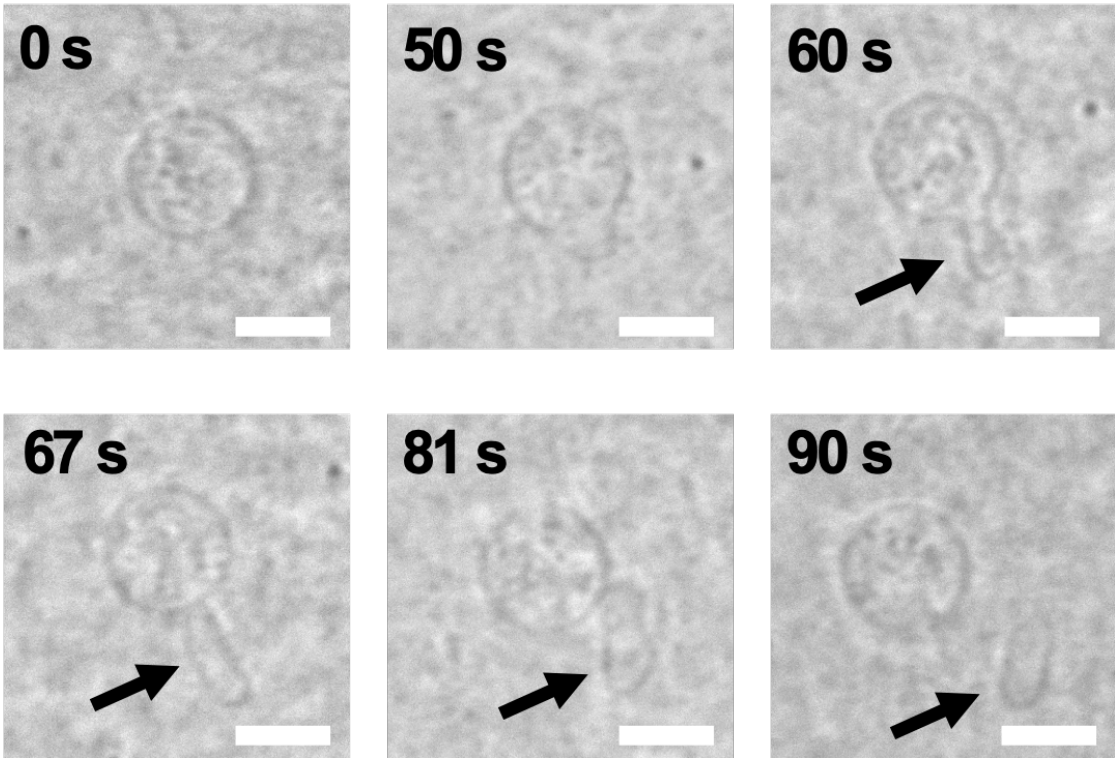

Figure 5-3-7. Phase-contrast light microscopy images AOT GUVs, taken in the "reference condition" with the supply of 100 mM SDBS/0.5 mM Chol micelles (entry #3 in **Table 5-3-1**), coupled with PANI-ES synthesis. The time-dependent changes are shown after starting the micro-injection for t = 0, 50, 60, 67, 81, and 90 sec. The initially spherical AOT GUV showed growth and formation of a tubular structure (at *"60 s"*), and the tubular structure is spontaneously cut from the mother AOT GUV (at *"81 s"* and *"90 s"*). The length of the scale bar: 10 μm.

5.3.5 Result 2: Growth and Division of Vesicles Coupled with Artificial Metabolism System

Recursive reproduction of AOT/Chol binary GUVs, entry #4 in Table 5-3-1.

To realize recursive growth and division system, we adopted the Chol carrier system, shown above, to the AOT/Chol (9/1) binary GUV which can grow and divide once, rarely twice, with the feeding of AOT micelles. To test this, we prepared binary GUVs composed of AOT and cholesterol (at a molar ratio of 9:1, 2.7 mM AOT, 0.3 mM cholesterol) in 20mM NaH_2PO_4 solution (pH = 4.3) containing 4.0 mM aniline and 0.92 μM HRPC, 1.0 μM GOD, and 100 mM sucrose, and then micro-injected to individual binary GUVs a micellar solution consisting of 20mM AOT and 100 mM D-glucose from one side, and 100 mM SDBS/0.5 mM Chol and 100 mM D-glucose from the other side (see entry #4 in **Table 5-3-1.**).

When we supplied AOT micelles and SDBS/Chol mixed micelles to binary GUVs composed of AOT/Chol (9/1), the GUVs repeated the growth and division cycles as shown in **Fig.5-3-8**. Here, the GUV started growth and deformation just after starting micro-injections, then completed the first cycle at *"28 s"* (black arrows: formation of 2nd generation). A similar growth and division cycle is achieved at *"58 s"* (red arrows: formation of 3rd generation), but as we can see, the size of vesicles becomes smaller by generation, especially in the 4th generation (blue arrows) at *"67 s"*. In the end, multiple small vesicles are observed (at *"83 s"*). It should be noted that the total surface area of vesicles increased with time, whereas the total volume of vesicles kept constant (**Fig.5-3-9**), which seems to be one of the leading causes of the decrease in size by generations. Thus, finally, the size of offspring GUVs should be recovered to the size of their parent GUV by coupling the vesicle volume growth mechanism.

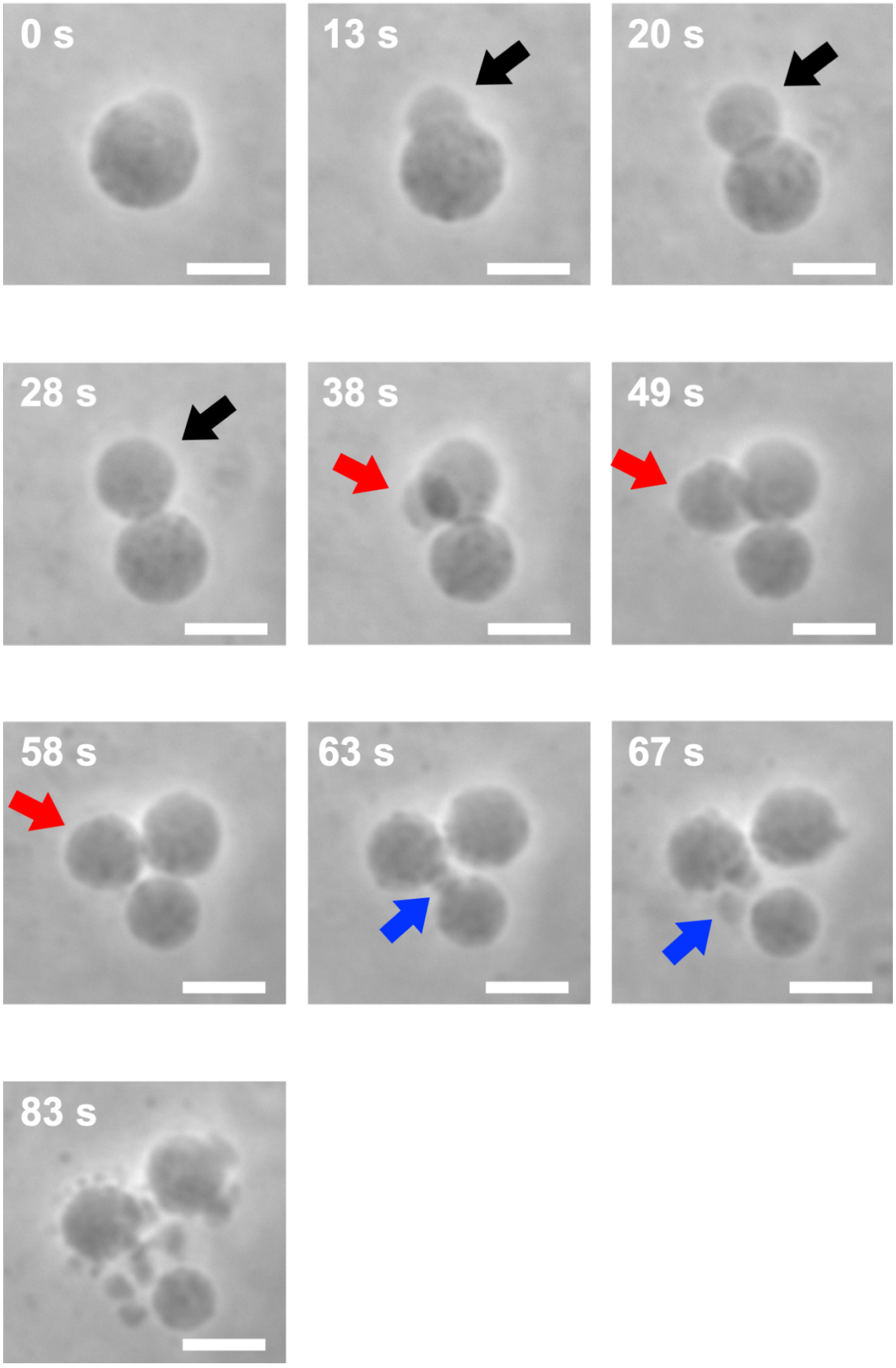
0 s
13 s
20 s
28 s
38 s
49 s
58 s
63 s
67 s
83 s

Figure 5-3-8. Phase-contrast light microscopy images AOT/Chol (9/1) binary GUVs, taken in the "cascade condition" with the supply of 20 mM AOT micelles and 100 mM SDBS/0.5 mM Chol micelles (entry #4 in **Table 5-3-1**), coupled with PANI-ES synthesis. The time-dependent changes are shown after starting the micro-injection for t = 0, 13, 20, 28, 38, 49, 58, 63, 67, and 83 sec. The initially spherical AOT/Chol GUV showed growth, deformation to limiting shape, and then the division (the first cycle, indicated by black arrows, from *″0 s″* to *″28 s″*). Then, the vesicle showed the second cycle (indicated by red arrows, from *″28 s″* to *″58 s″*), the third cycle (indicated by blue arrows, from *″58 s″* to *″67 s″*), and the further growth and divisions to form multiple small vesicles (from *″67 s″* to *″83 s″*). The length of the scale bar: 10 μm.

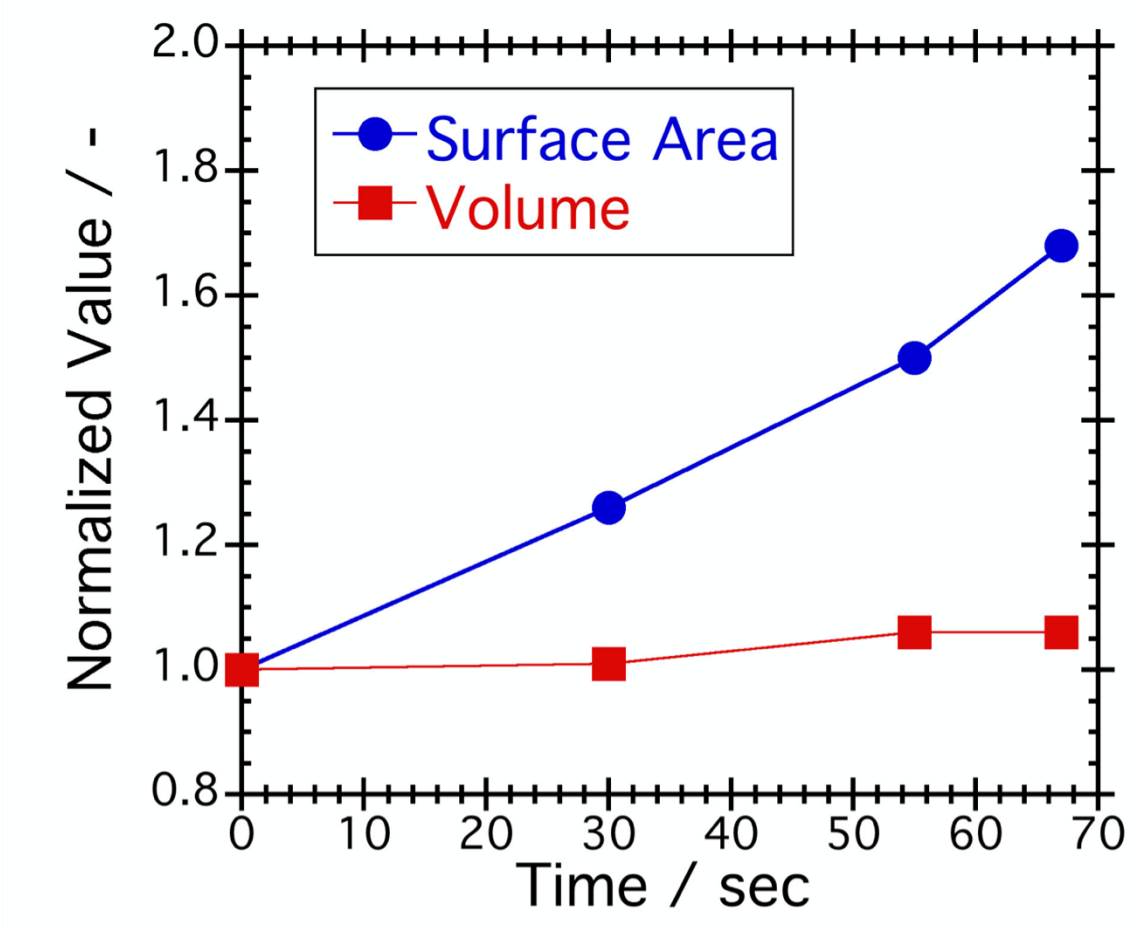

Figure 5-3-9. Changes in total normalized surface area (blue circles) and volume (red squares) of all vesicles originated from the initial mother GUV observed in **Figure 5-3-8** above. The lines between the data points are drawn for guiding the eyes.

5.3.6 Result 3: Osmotic Inflation of Vesicles

Osmotic inflation of AOT GUV.

To achieve a recursive reproduction system with volume recovery, we firstly test the simple osmotic inflation system of AOT GUVs where AOT GUV encapsulating 100 mM sucrose prepared in 20 mM NaH_2PO_4 solution (pH=4.3) containing 3.0 mM AOT (cvc~1.5 mM) are transferred into the 20 mM NaH_2PO_4 solution (pH=4.3) containing 100 mM D-fructose and 3.0 mM AOT (cvc~1.5 mM) (**Fig.5-3-2(a) and (b)**). No chemical reaction and other reaction components are added.

The phase-contrast microscopy image of an AOT GUV immediately after the transfer ("+ 0 sec") is compared with that after 600 sec in **Fig.5-3-10(a)**, which clearly shows the volume increase of the AOT GUV. The volume increase of three AOT GUVs with initial diameters of 14.6±0.1 μm is plotted in **Fig.5-3-10(b)**. The volume of AOT GUVs increased almost linearly with time up to ~700 sec (which is enough to realize the recursive vesicle reproductions) while keeping their spherical shapes and the volume at 600 sec is approximately 1.7V(0), where V(0) is the initial GUV volume. The observed volume increase of the AOT GUVs is described by the simultaneous differential equations as follows:

$$\frac{dn_f(t)}{dt} = P_f A(t)\left(c_{f,ext} - \frac{n_f(t)}{V(t)}\right) \tag{5.15}$$

$$\frac{dV(t)}{dt} = v_w \frac{dn_w(t)}{dt} = P_w A(t) v_w \left(\frac{n_f(t) + n_s}{V(t)} - c_{f,ext}\right) \tag{5.16}$$

where we assume that AOT molecules in the external solution are instantly incorporated into the vesicle membrane to relax the membrane tension. Here $n_f, n_w,$ and n_s are the concentrations of D-fructose (permeable), water (permeable), and sucrose (*impermeable*) molecules encapsulated in the AOT GUV, respectively. P_f and P_w are the permeability of D-fructose and water against AOT membrane, A and V are the surface area and the volume of the spherical AOT GUV, $c_{f,ext}(= 0.100\ mol\ L^{-1})$ is the concentration of D-fructose in the external solution, and $v_w(= 1.8 * 10^{-2}\ L\ mol^{-1})$ is the molar volume of water molecules. The observed volume growth profile is fitted (red line) by the simultaneous differential equations Eq. (5.15) and (5.16) with the fitting parameters $P_w = 2.3 * 10^{-4}\ m\ s^{-1}$ and $P_f = 3.0 * 10^{-9}\ m\ s^{-1}$. These permeability values are considerably larger than those of phosphatidylcholine (PC) membranes, usually $P_w \sim 10^{-5}\ m\ s^{-1}$, and fructose is almost impermeable. One of the main reasons is the thin AOT membrane thickness (shorter hydrophobic path across the membrane) of ~2 nm, whereas the typical thickness of PC membranes is ~4-5 nm.

a

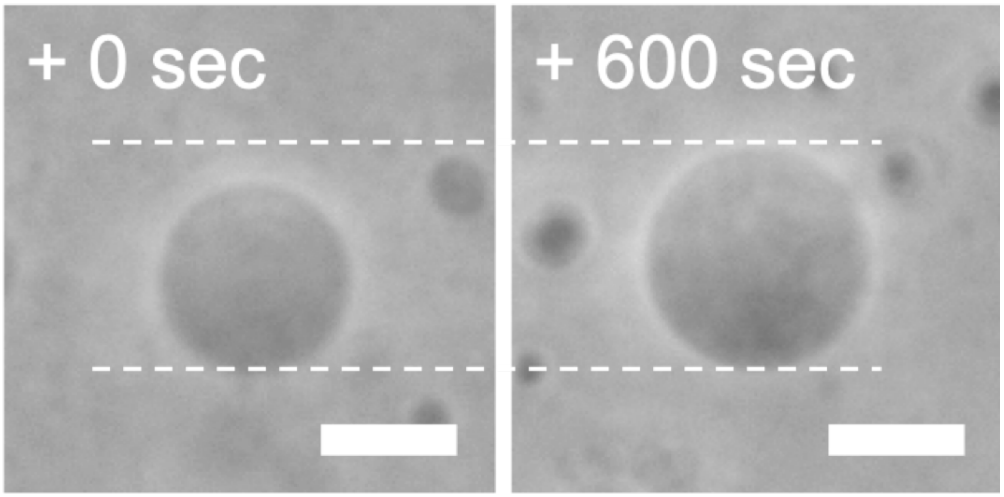
+ 0 sec
+ 600 sec

b

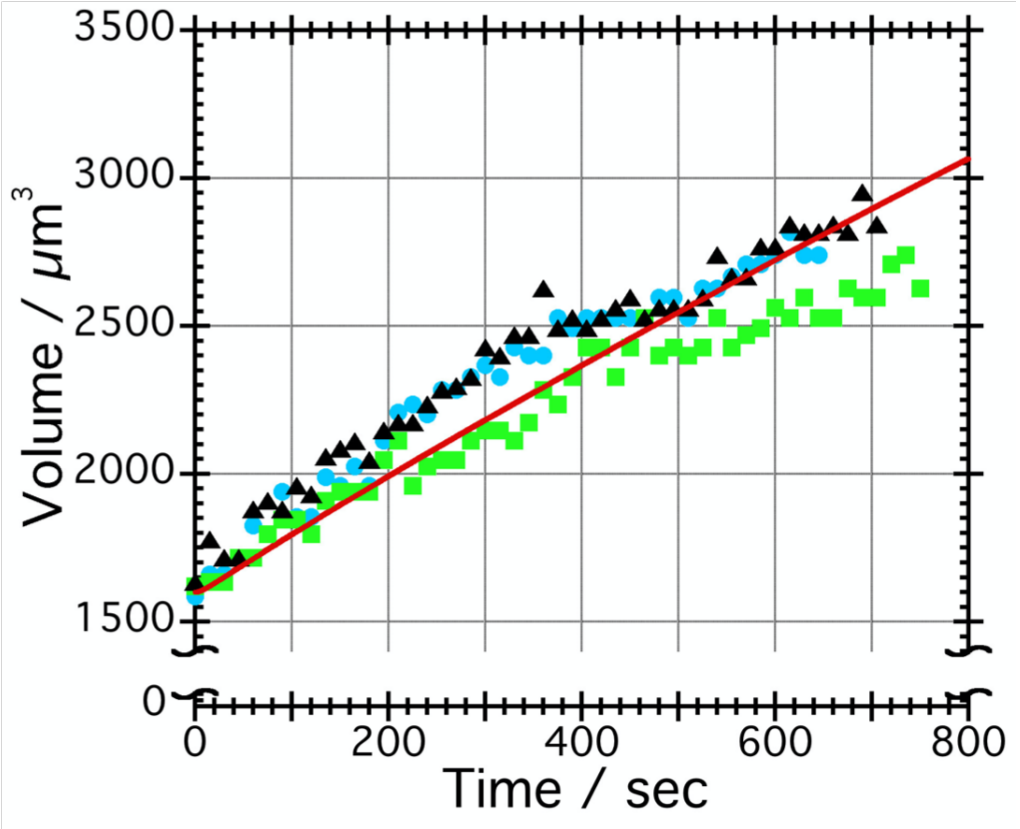
3500
3000
2500
2000
1500
0
Volume / μm3
0
200
400
600
800
Time / sec

Figure 5-3-10. Osmotic inflation of AOT GUVs encapsulating 20 mM NaH_2PO_4 solution (pH=4.3) containing 100 mM sucrose, surrounded by 20 mM NaH_2PO_4 solution (pH=4.3) containing 100 mM D-fructose. The experimental setup is shown as **Fig.5-3-2 (a) and (b)**.

a, Phase contrast light microscope images of an AOT GUV swollen by osmotic pressure difference, just after (0 sec) and 600 sec after the transfer. The initial composition of the internal and external solutions just after the transfer was as follows: (internal solution) 20 mM NaH_2PO_4 solution (pH=4.3) containing 100 mM sucrose and 3.0 mM AOT (cvc~1.5 mM), and (external solution) 20 mM NaH_2PO_4 solution (pH=4.3) containing 100 mM D-fructose and 3.0 mM AOT (cvc~1.5 mM). The elapsed time after starting the observation is indicated in each image. Length of the scale bars: 10 μm.

b, Time dependence of the volume of AOT GUVs caused by the asymmetric swelling, where AOT GUVs encapsulating 100 mM sucrose was transferred into the solution containing 100 mM D-fructose. The three plots represent the three independent observations. The initial diameter of the AOT GUVs was 14.6±0.1 μm. The red line is the fitting curve obtained from the simultaneous differential equations (4.15) and (4.16), yielding the permeability of water and D-fructose against the AOT membrane of $P_w = 2.3 * 10^{-4}\, m\, s^{-1}$ and $P_f = 3.0 * 10^{-9}\, m\, s^{-1}$, respectively.

5.3.7 Result 4: My Synthetic Minimal Cell.

Osmotic inflation-introduced recursive vesicle reproduction system coupled with artificial metabolism system.

The final experimental step for constructing our synthetic minimal cell is introducing a volume recovery mechanism (**Fig.5-3-10**) into the recursive growth and division vesicle system (**Fig.5-3-8**). We prepared AOT/Chol (9/1) binary GUVs in 20 mM NaH_2PO_4 solution (pH=4.3) containing 100 mM sucrose, then transferred a GUV into the reaction mixture in 20 mM NaH_2PO_4 solution (pH=4.3) which contains 100 mM D-fructose as osmolytes, 4.0 mM aniline, 0.92 μM HRPC, 1.0 μM GOD, and dissolved oxygen as reaction components. Towards the target GUV, we micro-injected two solutions: 100 mM D-glucose solutions containing 20 mM AOT micelles, and 100 mM D-glucose solutions containing 100 mM SDBS/0.5 mM mixed micelles. Then, the energy currency molecule, H_2O_2, is *in situ* formed in the reaction mixtures from D-glucose and dissolved oxygen with GOD (R1), which triggers the PANI-ES synthesis reaction domains (R2 – R8). The PANI-ES formed on the vesicle surface will promote the GUV growth (R9), then the GUV obeys the deformation pathway explained by the ADE model and show the spontaneous division. The daughter vesicles will recover their volume to their original mother's size by using osmotic difference continuously generated by asymmetric permeation of osmolytes inside/outside the membrane. This is the design principles of our synthetic minimal cell.

Phase-contrast light microscopy images of AOT/Chol (9/1) binary GUV after the transfer to induce osmotic difference and after starting the micro-injection to trigger the PANI-ES synthesis and to feed amphiphiles with GUVs are shown in **Fig.4-12**. Here, the GUV started growth and deformation after starting micro-injections (at *"+ 37 sec"*), deformed to limiting shape at around *"+ 44 sec"*, and then spontaneously divided into two daughter vesicles (at *"+ 70 sec"*). During deformation and division, the volume of two daughter vesicles continuously showed growth (from *"+ 44 sec"* to *"+ 100 sec"*) and finally recovered to (correctly, exceed) their mother's size in 100 sec. This is the complete reproduction cycle of vesicles that we designed initially (**Fig.1-2**). Unfortunately, this system has been realized only by a single cycle in the present stage. Since the membrane growth and volume growth are independent of each other in our system, we need to elaborate more detailed conditions to synchronize them, *i.e.*, no excess membrane growth and no excess volume growth.

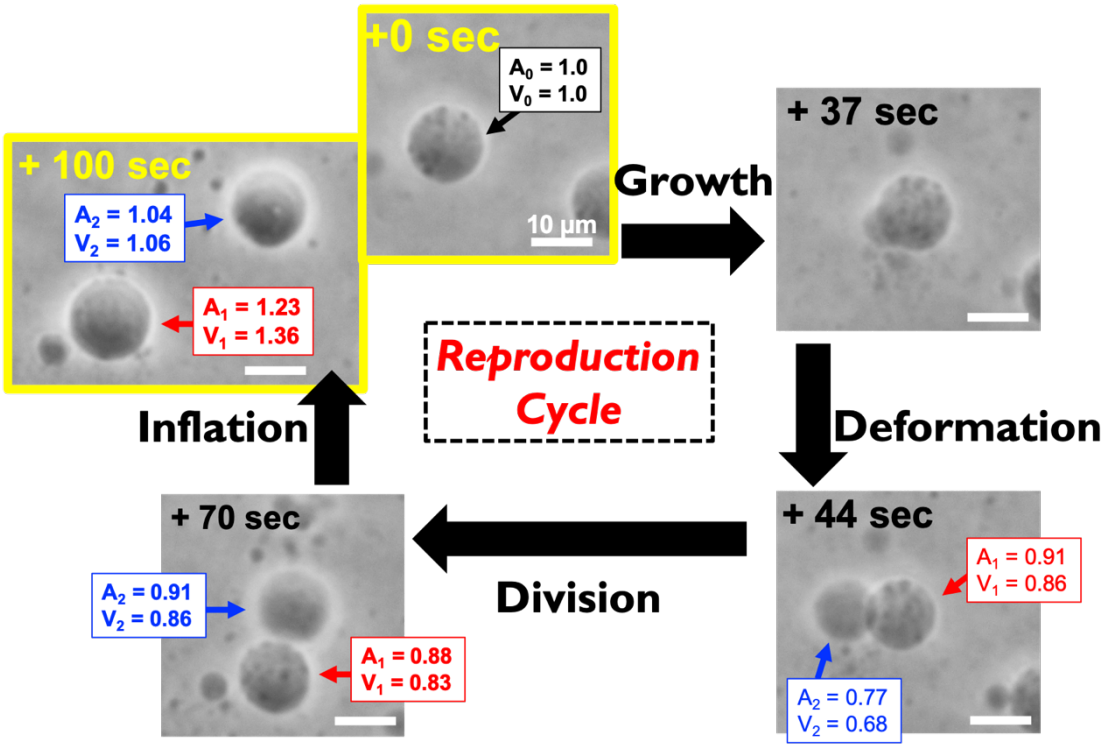

Figure 5-3-11. Experimental establishment of my synthetic minimal cell showing a complete reproduction cycle. Coupled with the artificial metabolism system (**Fig.3-2-1**) which realizes the coupling between vesicle surface-confined information polymer (PANI-ES) synthesis and vesicle membrane growth. The morphology of the AOT/Chol (9/1) binary GUV follows the deformation pathway (**Fig.5-3-6**) described by the membrane elasticity model. The "$A_{i=0,1,2}$" and "$V_{i=0,1,2}$" represent the normalized surface area and volume of mother vesicle ($i = 0$), and two daughter vesicles ($i = 1,2$).

5.4 Conclusion

This chapter focused on the morphological regulations on our synthetic minimal cell. Based on the membrane elasticity model, I demonstrated the control of the vesicle growth pathway; tubular growth, deformation to limiting shape, or spontaneous division. To attain these controls, there is no external mechanical force (*e.g.,* membrane contraction by using specific proteins). According to the molecular geometrical shapes and the asymmetry in the bilayer membrane, these pathways are spontaneously appeared, while I design the appropriate initial states and the surrounding conditions. In the course of morphological control of vesicles, I made clear the subsequent problem after recursive divisions: the volume growth problem. Finally, I experimentally realized the complete reproduction cycles of vesicles; membrane growth → deformation → division → volume recovery (**Fig.1-3-1**). To the best of the author's knowledge, this is the first example to realize the complete reproduction cycle.

To attain the single cycle of reproduction system starting from the very simple molecular assembly, not only the design principles on the chemical system, (R1 – R9) in **Fig. 3-2-1**, but also one another design principles related to soft matter physics, the control principle on the pathways to restrict the growth, was required. I should emphasize that, although I supply the specific molecules to the system with appropriate concentrations and chemical potential gradients, and although I prepare the ideal initial conditions, the experimental results I demonstrate in this chapter appear in the self-organization way coupling the chemical and soft matter physics aspects. These two aspects will be the wheels of a cart to investigate "What is Life?" from the standpoint of physical sciences.

The contents in this chapter are partially based on the following original paper:

Minoru Kurisu, Harutaka Aoki, Takehiro Jimbo, Yuka Sakuma, Masayuki Imai, Sandra Serrano-Luginbühl, and Peter Walde "Reproduction of vesicles coupled with a vesicle surface-confined enzymatic polymerization.", *Communications Chemistry*, **2**:117 (2019).

5.5 Appendix

5.5.1 Appendix 5-A: Neck Stability of Limiting Shape.

The neck of the limiting shape observed by feeding SDBS micelles with AOT GUVs (condition #1 in **Table 5-3-1**) was very stable (**Fig.5-5-1**). After the neck formation, even when we applied strong water flow by micro-injection, the tubes elongated and never showed division.

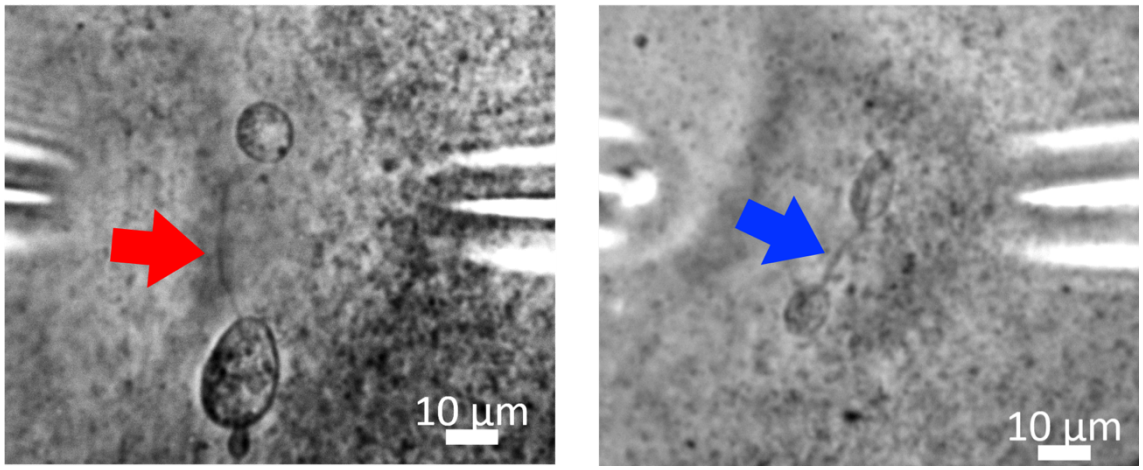

Figure 5-5-1. Phase-contrast light microscopy images of vesicles, obtained by a further supply of amphiphiles after the vesicle reaches the limiting shape. Both images were obtained in the condition of entry #1 in **Table 5-3-1**. Red and blue arrows indicate the stable neck structures connecting two vesicles. Please note that the contrast of both images were emphasized to make the presence of neck structures clear.

Chapter 6
Conclusion and Outlook

In this thesis, I firstly focused on the artificial information polymer in chapter 2. Based on the consideration to the essence of information polymer on the thermodynamical entropy loss and the enthalpy gain, I focused on the template polymerization system by using vesicle membrane as a template. Due to the specific interaction between vesicle forming molecules and monomers, the polymerization process was restricted to forn regular sequence structure of polyaniline, PANI-ES. PANI-ES encodes the property (sulfonated/sulfated polar head group) of vesicle forming molecules as its regular sequence structure, which selectively promote the incorporation of the corresponding membrane molecules, resulting in vesicle membrane growth (decode). Thus, PANI-ES was confirmed to work as information polymer for vesicles. In chapter 3, based on the knowledge of recent molecular biology and the well-known protocell model, I designed artificial metabolism system which conceptually mimics the three essential reaction domains for biological systems: energy currency production domain, information polymer synthesis domain, and membrane growth domain. Then, I introduced a new reaction domain to produce energy currency molecule, H_2O_2, from D-glucose and dissolved oxygen with enzyme GOD. After the optimization of the reaction condition, the synthesis of information polymer and vesicle membrane growth were successfully achieved with the artificial metabolism system involving energy currency production domain. In chapter 4, I constructed reduced model reaction system which extract the essence from the actual metabolism system, and then I developed the kinetic model to describe the system. Our artificial metabolism system has simple and clear reaction network, therefore, I could finally reproduces the experimental system without no adjustable parameters. That means the artificial metabolism system works well according to my design. For the synthetic minimal cell system, the vesicles should show not only membrane growth, but also show the deformation to the limiting shape, the division of the neck, and volume recovery to their original sizes. Biological systems adopted very complex molecular mechanism to attain this reproduction cycle, but such mechanism is not appropriate for the “minimal” cell system. Therefore, in chapter 5, I controlled the morphology of vesicles based on the knowledge of the membrane elasticity theory, and I also designed the sustainable osmotic inflation system. Then, finally, I succeeded in realizing complete vesicle reproduction cycle coupled with artificial metabolism system.

All in all, my synthetic minimal cell system conceptually the three major characteristics of biological system: gene, metabolism, and reproduction.

Comparing my synthetic minimal cell design and biological systems, there are some significant differences. First, while genetic information flows from DNA to proteins in one-way in biological systems, my synthetic minimal cell has the two-way genetic information flow, *i.e.*, I have called PANI-ES as information polymer for the sake of convenience, but the information of vesicles are encoded in PANI-ES, and at the same time, the sequential information of PANI-ES is also encoded as vesicle membranes. When we consider the very beginning stage of the emergence of living systems, such difference in the direction of genetic information flow may affect the stability and evolvability of the system. Second, the membrane molecules are not synthesized in my artificial metabolism design. In any biological systems, they synthesize membrane molecules and then incorporate them into cell membrane. When we consider the universal essence of any living systems, we will need to discuss the necessity of mechanisms to synthesize the compartment-consisting molecules. Finally, my synthetic minimal cell does not contain the reaction system inside the membrane, but exposes it on the outer surface of vesicle membrane. Here, we need to discuss the essence of compartment for living systems. My minimal cell can prevent dissociation of information polymer through the specific interaction between the membrane, so the minimal cell keeps reaction field on its surface. Recently many protocell / minimal cell model have been proposed, and some of them uses droplet or coacervate as template. When we will succeed in mimicking biological behavior by such membrane-less compartment, how can we define such systems? All in all, the bottom-up constructive approaches to understanding of universal essence of any possible living systems will have the possibility to capture the living systems from various field of science, including physical sciences. My synthetic minimal cell will be one of the pioneering systems to contribute to open up a new road for the physical understanding of living systems.

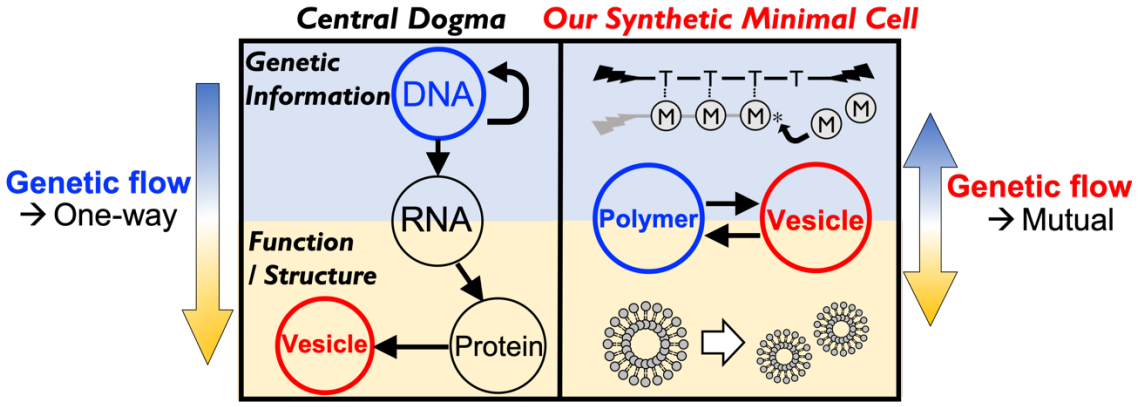

Figure 6-1-1. Comparison with the central dogma of molecular biology with our synthetic minimal cell.

7. References

(ABC order)

Adamala, K., & Szostak, J. W. “Competition between model protocells driven by an encapsulated catalyst.” *Nature Chemistry*, **5,** 495–501 (2013).

Araiso, T. & Dunford, H.B. “Horseradish peroxidase. XLI. Complex formation with nitrate and

its effect upon compound I formation.", *J. Chem. Inf. Model.,* **53**, 1689–1699 (1980).

Akashi, M. & Ajiro, H. "Template Polymerization (Molecular Templating)" in Encyclopedia of Polymeric Nanomaterials., Springer-Verlag Berlin Heidelberg, (2014). doi:10.1007/978-3-642-36199-9

Akashi, M. (*Japanese article*) "「テンプレート重合」-30 年後の解答とその先へ", *高分子*, **54**, 318-319 (2005).
https://www.jstage.jst.go.jp/article/kobunshi1952/54/5/54_5_318/_pdf

Alberts, B. et al. "Molecular Biology of the Cell" 6th ed., Garland Science, (2015).

Allen, W. V. & Ponnamperuma, C. "A possible prebiotic synthesis of monocarboxylic acids." *BioSystems* **1**, 24–28 (1967).

Athavale, S. S., Spicer, B. & Chen, I. A. "Experimental fitness landscapes to understand the molecular evolution of RNA-based life." *Curr. Opin. Chem. Biol.* **22**, 35–39 (2014).

Attwater, J., Wochner, A. & Holliger, P. "In-ice evolution of RNA polymerase ribozyme activity." *Nat. Chem.* **5**, 1011–1018 (2013).

Baaske, P. *et al.* "Extreme accumulation of nucleotides in simulated hydrothermal pore systems." *Proc. Natl. Acad. Sci.,* **104**, 9346–9351 (2007).

Bankar, S. B., Bule, M. V., Singhal, R. S. & Ananthanarayan, L. "Glucose oxidase - An overview.", *Biotechnol. Adv.,* **27**, 489–501 (2009).

Baxter, R. & Hu, P. "Insight into why the Langmuir-Hinshelwood mechanism is generally preferred.", *J. Chem. Phys.*, 116, 4379-4381 (2002).

Becker, S. *et al.* "Unified prebiotically plausible synthesis of pyrimidine and purine RNA ribonucleotides." *Science.* **366**, 76–82 (2019).

Bhattacharya, A., Brea, R. J., Niederholtmeyer, H. & Devaraj, N. K. "A minimal biochemical route towards de novo formation of synthetic phospholipid membranes." *Nat. Commun.* **10**, 1–8 (2019).

Bhattacharya, A., Cho, C. J., Brea, R. J. & Devaraj, N. K. “Expression of Fatty Acyl-CoA Ligase Drives One-Pot de Novo Synthesis of Membrane-Bound Vesicles in a Cell-Free Transcription-Translation System.” *J. Am. Chem. Soc.* **143**, 11235–11242 (2021).

Bich, L., & Green, S. “Is defining life pointless? Operational definitions at the frontiers of biology.”, *Synthese*, ***195***, 3919-3946 (2018).

Bilal, S., Gul, S., Holze, R. & Shah, A.A. “An impressive emulsion polymerization route for the synthesis of highly soluble and con- ducting polyaniline salts.”, *Synth. Met.*, **206**, 131–144 (2015).

Bissette, A. J., & Fletcher, S. P. “Mechanisms of autocatalysis.”, *Angew. Chem. Int.Ed.*, **52**, 12800–12826 (2013).

Black, R. A. *et al.* “Nucleobases bind to and stabilize aggregates of a prebiotic amphiphile, providing a viable mechanism for the emergence of protocells.” *Proc. Natl. Acad. Sci. U. S. A.* **110**, 13272–13276 (2013).

Black, R. A. & Blosser, M. C. “A self-assembled aggregate composed of a fatty acid membrane and the building blocks of biological polymers provides a first step in the emergence of protocells.” *Life* **6**, (2016).

Blain, J. C. & Szostak, J. W. “Progress toward synthetic cells.” *Annu. Rev. Biochem.* **83**, 615–640 (2014).

Blanken, D., Foschepoth, D., Serrão, A. C. & Danelon, C. “Genetically controlled membrane synthesis in liposomes.” *Nat. Commun.* **11**, 1–13 (2020).

Bozic, B., Svetina, S., Zeks, B. & Waugh, R. E. “Role of lamellar membrane structure in tether formation from bilayer vesicles.”, *Biophys. J.,* **61**, 963–973 (1992).

Brakke, K. A. “The surface evolver.”, *Exp. Math.,* **1**, 141–165 (1992).

Braun, D. & Libchaber, A. “Trapping of DNA by Thermophoretic Depletion and Convection.” *Phys. Rev. Lett.* **89**, 2–5 (2002).

Brea, R. J., Cole, C. M. & Devaraj, N. K. “In Situ Vesicle Formation by Native Chemical Ligation.” *Angew. Chemie* **126**, 14326–14329 (2014).

Brea, R. J., Bhattacharya, A. & Devaraj, N. K. “Spontaneous Phospholipid Membrane Formation by Histidine Ligation.” *Synlett* **28**, 108–112 (2017).

Breuer, M. *et al.* “Essential metabolism for a minimal cell.”, *Elife,* **8**, 1–77 (2019).

Bright, H. J. & Porter, D. J. T. P., D.Boyer (Ed.), “Flavoprotein oxidases”, in “The Enzymes: vol. 12” (3rd ed.). *NewYork: Academic Press.* (1975).

Bruckner, R. J., Mansy, S. S., Ricardo, A., Mahadevan, L. & Szostak, J. W. “Flip-flop-induced relaxation of bending energy: Implications for membrane remodeling.”, *Biophys. J.,* **97**, 3113–3122 (2009).

Caschera, F., Stano, P. & Luisi, P. L. “Reactivity and fusion between cationic vesicles and fatty acid anionic vesicles.” *J. Colloid Interface Sci.* **345**, 561–565 (2010).

Castro, J. M., Sugiyama, H. & Toyota, T. “Budding and Division of Giant Vesicles Linked to Phospholipid Production.” *Sci. Rep.* **9**, 1–9 (2019).

Cleland, W.W. (1963).

“The kinetics of enzyme-catalyzed reactions with two or more substrates or products: I. Nomenclature and rate equations.”, *Biochim. Biophys. Acta,* **67**, 104-137.

“The kinetics of enzyme-catalyzed reactions with two or more substrates or products: II. Inhibition: nomenclature and theory”, *Biochim. Biophys. Acta,* **67**, 173-187.

“The kinetics of enzyme-catalyzed reactions with two or more substrates or products: III. Prediction of initial velocity and inhibition patterns by inspection.”, *Biochim. Biophys. Acta,* **67**, 188-196.

Chen, C. M., Higgs, P. G. & Mac Kintosh, F. C. “Theory of fission for two-component lipid vesicles.”, *Phys. Rev. Lett.,* **79**, 1579–1582 (1997).

Chen, I. A., & Szostak, J. W. (2004).

(a) “A kinetic study of the growth of fatty acid vesicles.” *Biophysical Journal*, **87,** 988–998.

(b) “Membrane growth can generate a transmembrane pH gradient in fatty acid vesicles.”,

Proc. Natl. Acad. Sci., **101**, 7965–7970.

Chen, I. A. & Walde, P. "From self-assembled vesicles to protocells." *Cold Spring Harb. Perspect. Biol.* **2**, 1–14 (2010).

Cherney, D. P., Bridges, T. E. & Harris, J. M. "Optical trapping of unilamellar phospholipid vesicles: Investigation of the effect of optical forces on the lipid membrane shape by confocal-Raman microscopy.", *Anal. Chem.,* **76**, 4920–4928 (2004).

Chibowski, E. & Szcześ, A. "Zeta potential and surface charge of DPPC and DOPC liposomes in the presence of PLC enzyme." *Adsorption* **22**, 755–765 (2016).

Childs, R. E. & Bardsley, W. G. "The steady-state kinetics of peroxidase with 2,2′-azino-di-(3-ethyl-benzthiazoline-6-sulphonic acid) as chromogen.", *Biochem. J.,* **145**, 93–103 (1975).

Cochet, M., Louarn, G., Quillard, S., Buisson, J.P., and Lefrant, S. "Theoretical and experimental vibrational study of emeraldine in salt form. Part II", J. *Raman Spectrosc.*, **31**, 1041–1049 (2000).

Cordomí, A., Edholm, O. & Perez, J. J. "Effect of ions on a dipalmitoyl phosphatidylcholine bilayer. A molecular dynamics simulation study." *J. Phys. Chem. B* **112**, 1397–1408 (2008).

Cornell, C. E. *et al.* "Prebiotic amino acids bind to and stabilize prebiotic fatty acid membranes." *Proc. Natl. Acad. Sci.* **116**, 17239–17244 (2019).

Crick, F.H. "The origin of the genetic code." *J. Mol. Biol., **38,*** 367–379 (1968).

Crick, F.H. "Central dogma of molecular biology." *Nature*, **227**, 561-563 (1970).

Ćirić-Marjanović, G., Trchová, M., and Stejskal, J. "The chemical oxidative polymerization of aniline in water: Raman spectroscopy", *J. Raman Spectrosc*., **39**, 1375– 1387 (2008).

Ćirić-Marjanović, G., Milojević-Rakić, M., Janošević-Ležaić, A., Luginbühl, S. & Walde, P. "Enzymatic oligomerization and polymerization of arylamines: State of the art and perspectives.", *Chem. Pap.,* **71**, 199–242 (2017).

Derganc, J. "Curvature-driven lateral segregation of membrane constituents in Golgi cisternae.",

Phys. Biol., **4**, 317–324 (2007).

Deshpande, S., Wunnava, S., Hueting, D. & Dekker, C. "Membrane Tension–Mediated Growth of Liposomes." *Small* **15**, 1–10 (2019).

Ding, Y., Padias, A.B., and Hall, H.K. "Chemical Trapping Experiments Support a Cation-Radical Mechanism for the Oxidative Polymerization of Aniline.", *J. Polym. Sci. Part A: Polym. Chem.,* **37**, 2569-1579 (1999).

Deamer, D. W. "Boundary structures are formed by organic components of the Murchison carbonaceous chondrite." *Nature* **317**, 792–794 (1985).

Deamer, D. "The Role of Lipid Membranes in Life's Origin". *Life* **7**, 5 (2017).

de Lange, N., Kleijn, J. M. & Leermakers, F. "Structural and mechanical parameters of lipid bilayer membranes using a lattice refined self-consistent field theory.", *Phys. Chem. Chem. Phys., **23,*** 5152–5175 (2021).

Dennany, L., Innis, P. C., McGovern, S. T., Wallace, G. G. & Forster, R. J. "Electronic interactions within composites of polyanilines formed under acidic and alkaline conditions. Conductivity, ESR, Raman, UV-vis and fluorescence studies." *Phys. Chem. Chem. Phys.* **13**, 3303–3310 (2011).

Dervaux, J., Noireaux, V. & Libchaber, A. J. "Growth and instability of a phospholipid vesicle in a bath of fatty acids." *Eur. Phys. J. Plus,* **132**, 1–10 (2017).

Desjonquères, M.C. & Spanjaard, D. "Concepts in Surface Physics", 2nd ed., Springer-Verlag, Berlin, 2002.

De Visser, J. A. G. M. & Krug, J. "Empirical fitness landscapes and the predictability of evolution." *Nat. Rev. Genet.* **15**, 480–490 (2014).

Dimitrieva, E. & Dunsch, L. "How linear is "linear" polyaniline?", *J Phys Chem B*, **115**, 6401–6411 (2011).

Ding, Y., Padias, A.B., & Hall, H.K. "Chemical Trapping Experiments Support a Cation-Radical Mechanism for the Oxidative Polymerization of Aniline.", *J. Polym. Sci. Part A: Polym. Chem.,*

37, 2569-1579 (1999).

Do Carmo, M. P. “Differential geometry of curves and surfaces: revised and updated second edition.”, Courier Dover Publications, (2016).

do Nascimento, G. M. & de Souza, M. A. In “Nanostructured Conductive Polymers.” ed. Eftekhari, A., John Wiley & Sons, Chichester, (2015).

Dreher, Y., Jahnke, K., Bobkova, E., Spatz, J. P. & Göpfrich, K. “Division and regrowth of phase-separated giant unilamellar vesicles.” *Angew. Chemie* **133**, 2–11 (2021).

Dunford, H.B. & Stillman, J.S. “On the function and mechanism of action of peroxidases.”, *Coord. Chem. Rev.*, **19**, 187–251 (1976).

Dunford, H. B., Hewson, W. D. & Steiner, H. “Horseradish peroxidase. XXIX. Reactions in water and deuterium oxide: cyanide binding, compound I formation, and reactions of compounds I and II with ferrocyanide.”, *Can. J. Chem.,* **56**, 2844–2852 (1978).

Dunford, H.B. Chapter 1 (pp.1-24) in “Peroxidases in Chemistry and Biology” Vol. II, CRC Press, (1991).

Dunford, H.B. “Heme Peroxidases.”, John Wiley & Sons (1999).

Döbereiner, H. G., Evans, E., Kraus, M., Seifert, U. & Wortis, M. “Mapping vesicle shapes into the phase diagram: A comparison of experiment and theory.”, *Phys. Rev. E,* **55**, 4458–4474 (1997).

Eigen, M. & Schuster, P. “The Hypercycle. A Principle of Natural Self-Organization Part A: Emergence of the Hypercycle.” *Naturwissenschafte* **64**, 541–565 (1977).

Eigen, M. & Schuster, P.

(a) “The Hypercycle. A principle of Natural Self-Organization. Part B: The Abstract Hypercycle.” *Naturwissenschaften,* **65**, 7–41 (1978).

(b) “The Hypercycle. A Principle of Natural Self-Organization. Part C: The Realistic Hypercycle.” *Naturwissenschaften* **65**, 341–369 (1978).

Eigen, M. & Schuster, P. “The Hypercycle: a principle of natural self-organization”, Springer

Science & Business Media (2012).

Edwards, H. G. M., Brown, D. R., Dale, J. A., and Plant, S. “Raman spectroscopy of sulfonated polystyrene resins”, *Vib. Spectrosc*., **24**, 213–224 (2000).

Exterkate, M., Caforio, A., Stuart, M. C. A. & Driessen, A. J. M. “Growing Membranes in Vitro by Continuous Phospholipid Biosynthesis from Free Fatty Acids.” *ACS Synth. Biol.* **7**, 153–165 (2018).

Ferguson, J. & Shah, A. O. “Further studies on polymerization in interacting polymer systems.”, *Eur. Polym. J.* **4**, 611–619 (1968).

Ferris, J. P. “Montmorillonite catalysis of 30-50 mer oligonucleotides: Laboratory demonstration of potential steps in the origin of the RNA world.” *Orig. Life Evol. Biosph.* **32**, 311–332 (2002).

Field, R. J., Koros, E. & Noyes, R. M. “Oscillations in Chemical Systems. II. Thorough Analysis of Temporal Oscillation in the Bromate-Cerium-Malonic Acid System.”, *J. Am. Chem. Soc.,* **381**, 8649–8664 (1972).

Field, R. J. & Noyes, R. M. “Oscillations in chemical systems. IV. Limit cycle behavior in a model of a real chemical reaction.” *J. Chem. Phys.,* **60**, 1877–1884 (1974).

Foreman, J. P. & Monkman, A. P. “Theoretical investigations into the structural and electronic influences on the hydrogen bonding in doped polyaniline.”, *Synth. Met.*, **107**, 7604–7610 (2003).

Fourcade, B., Miao, L., Pao, M. & Wortis, M. “Scaling analysis of narrow necks in curvature models of fluid-bilayer vesicles.”, *Phys. Rev. E,* **49**, 5276–5287 (1994).

Fujisaki, T. *et al.* “Effect of template type on the preparation of the emeraldine salt form of polyaniline (PANI-ES) with horseradish peroxidase isoenzyme C (HRPC) and hydrogen peroxide.”, *RSC Adv.,* **9**, 33080–33095 (2019).

Gaut, N. J. & Adamala, K. P. “Reconstituting Natural Cell Elements in Synthetic Cells.” *Adv. Biol.* **5**, 1–20 (2021).

Gánti, T. “Organization of chemical reactions into dividing and metabolizing units: The

chemotons.", *BioSystems*, *7*, 15 – 21 (1975).

Gánti, T. "On the early evolutionary origin of biological periodicity.", *Cell Biol. Int.,* **26**, 729–735 (2002).

Gánti, T., "*The Principles of Life*.", Száthmary, E., & Griesemer, J. (eds.), Oxford University Press, (2003).

Genies, E. M. & Tsintavis, C. "Redox mechanism and electrochemical polyaniline deposits behaviour of polyaniline deposits.", *J. Electroanal. Chem.,* **195**, 109–128 (1985).

Ghosh, B., Bose, R. & Tang, T. Y. D. "Can coacervation unify disparate hypotheses in the origin of cellular life?" *Curr. Opin. Colloid Interface Sci.* **52**, 101415 (2021).

Gilbert, W. "Origin of Life - the RNA World." *Nature, **319**,* 618–618. (1986).

Grafmüller, A., Shillcock, J. & Lipowsky, R. "The fusion of membranes and vesicles: Pathway and energy barriers from dissipative particle dynamics." *Biophys. J.* **96**, 2658–2675 (2009).

Griesemer, J. "The enduring value of Gánti's chemoton model and life criteria: Heuristic pursuit of exact theoretical biology.", *Journal of theoretical biology*, ***381***, 23-28 (2015).

Grillo, I., Levitz, P. & Zemb, T. "Insertion of small anionic particles in negatively charged lamellar phases.", *Langmuir,* **16**, 4830–4839 (2000).

Grillo, I., Kats, E. I. & Muratov, A. R. "Formation and Growth of Anionic Vesicles Followed by Small-Angle Neutron Scattering Formation and Growth of Anionic Vesicles Followed by Small-Angle Neutron Scattering.", *Langmuir*, **19**, 4573–4581 (2003).

Guo, Z. *et al.* "Vesicles as soft templates for the enzymatic polymerization of aniline.", *Langmuir,* **25**, 11390–11405 (2009).

Guo, Z., Hauser, N., Moreno, A., Ishikawa, T. & Walde, P. "AOT vesicles as templates for the horseradish peroxidase-triggered polymerization of aniline.", *Soft Matter,* **7**, 180–193 (2011).

Haines, T. H. "Anionic lipid headgroups as a proton-conducting pathway along the surface of

membranes: a hypothesis." *Proc. Natl. Acad. Sci. U. S. A.* **80**, 160–164 (1983).

Haluska, C. K. *et al.* "Time scale of membrane fusion revealed by direct imaging of vesicle fusion with high temporal resolution." *Proc. Natl. Acad. Sci.* **103**, 15841–15846 (2006).

Hamilton, J. A. "Fast flip-flop of cholesterol and fatty acids in membranes: implications for membrane transport proteins.", *Curr. Opin. Lipidol.,* **14**, 263–271 (2003).

Hanczyc, M. M., Fujikawa, S. M., & Szostak, J. W. "Experimental Models of Primitive Cellular Compartments: Encapsulation, Growth, and Division.", *Science*, **302**, 618–622 (2003).

Hanczyc, M. M. & Monnard, P. A. "The origin of life and the potential role of soaps." *Lipid Technol.* **28**, 88–92 (2016).

Hardy, M. D. *et al.* "Self-reproducing catalyst drives repeated phospholipid synthesis and membrane growth." *Proc. Natl. Acad. Sci.* **112**, 8187–8192 (2015).

Hayden, E. J., von Kiedrowski, G. & Lehman, N. "Systems Chemistry on Ribozyme Self-Construction: Evidence for Anabolic Autocatalysis in a Recombination Network." *Angew. Chemie* **120**, 8552–8556 (2008).

Hengen, P. N., Bartram, S. L., Stewart, L. E. & Schneider, T. D. "Information analysis of Fis binding sites.", *Nucleic Acids Res.* **25**, 4994–5002 (1997).

Heinrich, V., Svetina, S. & Ek, B. "Nonaxisymmetric vesicle shapes in a generalized bilayer-couple model and the transition between oblate and prolate axisymmetric shapes.", *Phys. Rev. E,* **48**, 3112–3123 (1993).

Helfrich, W. "Elastic properties of lipid bilayers: theory and possible experiments.", *Zeitschrift für Naturforschung c*, **28**, 693-703 (1973).
Helfrich, W. and Harbich, W. In "*Physics of Amphiphilic Layers"*, Springer, Berlin (1987).

Helfrich, W. In "Giant Vesicles", Luisi, P.L. and Walde, P. Eds., John Wiley & Sons, Chichester (2000).

Heuvingh, J., Pincet, F. & Cribier, S. "Hemifusion and fusion of giant vesicles induced by

reduction of inter-membrane distance." *Eur. Phys. J. E* **14**, 269–276 (2004).

Higgs, P.G. and Lehman N. "The RNA World: molecular cooperation at the origins of life." *Nature Reviews Genetics, **16***, 7 – 17. (2015).

Hordijk, W. & Steel, M. "Detecting autocatalytic, self-sustaining sets in chemical reaction systems." *J. Theor. Biol.* **227**, 451–461 (2004).

Hu, M., Briguglio, J. J. & Deserno, M. "Determining the Gaussian curvature modulus of lipid membranes in simulations.", *Biophys. J.,* **102**, 1403–1410 (2012).

Huang, W. S. & MacDiarmid, A. G. "Optical properties of polyaniline.", *Polymer*, **34,** 1833–1845 (1993).

Hutchison, C. A. *et al.* "Design and synthesis of a minimal bacterial genome.", *Science,* **351**, aad6253 (2016).

Ikari, K. *et al.* "Dynamics of fatty acid vesicles in response to pH stimuli." *Soft Matter* **11**, 6327–6334 (2015).

Ikkala, O. "Functional Materials Based on Self-Assembly of Polymeric Supramolecules.", *Science.,* **295**, 2407 (2010).

Imai, M. & Walde, P. In *The Giant Vesicle Book*, R. Dimova, and C. Marques, Eds., CRC Press, Boca Raton, (2019).

International Human Genome Sequencing Consortium, "Initial sequencing and analysis of the human genome", *Nature*, **409**, 860-921 (2001).

Israelachvili, J.N. "Intermolecular and surface forces" 3rd ed., Elsevier Inc., (2011).

Ivanov, I. *et al.* "Directed Growth of Biomimetic Microcompartments." *Adv. Biosyst.* **3**, 1–9 (2019).

Iwasaki, F., Luginbühl, S., Suga, K., Walde, P. & Umakoshi, H. "Fluorescent Probe Study of AOT Vesicle Membranes and Their Alteration upon Addition of Aniline or the Aniline Dimer p-

Aminodiphenylamine (PADPA).", *Langmuir,* **33**, 1984–1994 (2017).

Jahn, R. & Grubmüller, H. "Membrane fusion." *Curr. Opin. Cell Biol.* **14**, 488–495 (2002).

Jimbo, T., Sakuma, Y., Urakami, N., Ziherl, P. & Imai, M. "Role of Inverse-Cone-Shape Lipids in Temperature-Controlled Self-Reproduction of Binary Vesicles.", *Biophys. J.,* **110**, 1551–1562 (2016).

Job, D. & Dundord, H. B. "Substituent Effect on the Oxidation of Phenols and Aromatic Amines by Horseradish Peroxidase Compound I.", *Eur. J. Biochem.,* **66**, 607–614 (1976).

Johnston, W.K., Unrau, P.J., Lawrence, M.S., Glasner, M.E., and Bartel, D.P. "RNA-catalyzed RNA polymerization: accurate and general RNA-templated primer extension." *Science*, **292**, 1319–1325 (2001).

Joshi, M. P., Sawant, A. A. & Rajamani, S. "Spontaneous emergence of membrane-forming protoamphiphiles from a lipid-amino acid mixture under wet-dry cycles." *Chem. Sci.* **12**, 2970–2978 (2021).

Joyce, G. F. & Szostak, J. W. "Protocells and RNA self-replication." *Cold Spring Harb. Perspect. Biol.* **10**, a034801 (2018).

Junker, K. et al. "Mechanistic aspects of the horseradish peroxidase-catalysed polymerisation of aniline in the presence of AOT vesicles as templates.", *RSC Adv.*, **2**, 6478–6495 (2012).

Junker, K., Gitsov, I., Quade, N. & Walde, P. "Preparation of aqueous polyaniline-vesicle suspensions with class III peroxidases. Comparison between horseradish peroxidase isoenzyme C and soybean peroxidase.", *Chem. Pap.,* **67**, 1028–1047 (2013).

Junker, K. *et al.* "Efficient polymerization of the aniline dimer p -aminodiphenylamine (PADPA) with trametes versicolor laccase/O2 as catalyst and oxidant and AOT vesicles as templates.", *ACS Catal.,* **4**, 3421–3434 (2014).

Junker, K., Zandomeneghi, G., Schuler, L. D., Kissner, R. & Walde, P. "Enzymatic polymerization of pyrrole with Trametes versicolor laccase and dioxygen in the presence of vesicles formed from AOT (sodium bis-(2-ethylhexyl) sulfosuccinate) as templates.", *Synth. Met.,* **200**, 123–134 (2015).

Kaasgaard, T., Mouritsen, O. G. & Jørgensen, K. “Freeze/thaw effects on lipid-bilayer vesicles investigated by differential scanning calorimetry.”, *Biochim. Biophys. Acta - Biomembr.,* **1615**, 77–83 (2003).

Kamal, M. M., Mills, D., Grzybek, M. & Howard, J. “Measurement of the membrane curvature preference of phospholipids reveals only weak coupling between lipid shape and leaflet curvature.”, *Proc. Natl. Acad. Sci.,* **106**, 22245–22250 (2009).

Karafiloglou, P. & Launay, J. P. “Electron pair (De)coupling in aniline radical cation and its implications for organic ‘mixed valence’ systems.”, *J. Phys. Chem. A,* **102**, 8004–8012 (1998).

Kauffman, S. A. “Autocatalytic sets of proteins.”, *J. Theor. Biol.,* **119,** 1–24 (1986).

Kauffman, S. & Levin, S. “Towards a General Theory of Adaptive Walks on Rugged Landscapes.” *J. Theor. Biol.* **128**, 11–45 (1987).

Kauffman, S. A. & Weinberger, E. D. “The NK model of rugged fitness landscapes and its application to maturation of the immune response.” *J. Theor. Biol.* **141**, 211–245 (1989).

Kauffman, S. A. “Origins of Order: Self Organization and Selection in Evolution”, Oxford University Press, New York (1993).

Kaneko, K. & Yomo, T. “On a kinetic origin of heredity: Minority control in a replicating system with mutually catalytic molecules.”, *J. Theor. Biol.,* **214,** 563–576 (2002).

Kaneko, K. (金子邦彦) “普遍生物学”, 東京大学出版会, (2019). (*Japanese edition only*)

Kashima, K. *et al.* “How experimental details matter. The case of a laccase-catalysed oligomerisation reaction.”, *RSC Adv.,* **8**, 33229–33242 (2018).

Kim, S. C., Sandman, D., Kumar, J., Bruno, F. F. & Samuelson, L. A. “Self-doped polyaniline/poly (diallyldimethyl ammonium chloride) complex: N-type doping with high stability.”, *Chem. Mater.* **18**, 2201–2204 (2006).

Kim, S. C. *et al.* “Template-assisted synthesis of self-doped polyaniline: Morphological effects

of templates on the conductivity.", *Macromol. Rapid Commun.,* **28**, 1356–1360 (2007).

Kim, S. C. *et al.* "A Model for the Emergence of RNA from a Prebiotically Plausible Mixture of Ribonucleotides, Arabinonucleotides, and 2′-Deoxynucleotides." *J. Am. Chem. Soc.* **142**, 2317–2326 (2020).

Kim, S. C., O'Flaherty, D. K., Giurgiu, C., Zhou, L. & Szostak, J. W. "The Emergence of RNA from the Heterogeneous Products of Prebiotic Nucleotide Synthesis." *J. Am. Chem. Soc.* **143**, 3267–3279 (2021).

Kolasinski, K. W. "Surface Science: Foundations of Catalysis and Nanoscience", 3rd ed., John Wiley & Sons, 2012.

Koonin, E. V. "How many genes can make a cell: The Minimal-Gene-Set Concept.", *Annu. Rev. Genomics Hum. Genet.,* **01,** 99–116 (2000).

Kreysing, M., Keil, L., Lanzmich, S. & Braun, D. "Heat flux across an open pore enables the continuous replication and selection of oligonucleotides towards increasing length." *Nat. Chem.* **7**, 203–208 (2015).

Kruger, K., Grabowski, P. J., Zaug, A. J., Sands, J., Gottschling, D. E., & Cech, T. R. "Self-splicing RNA: autoexcision and autocyclization of the ribosomal RNA intervening sequence of Tetrahymena." *Cell*, **31**, 147-157 (1982).

Kuipers, E. W., Vardi, A., Danon, A., & Amirav, A. "Surface-Molecule Proton Transfer: A Demonstration of the Eley-Rideal Mechanism", *Phys. Rev. Lett.*, **66**, 116-119 (1991).

Kurihara, K. *et al.* "Self-reproduction of supramolecular giant vesicles combined with the amplification of encapsulated DNA." *Nat. Chem.* **3**, 775–781 (2011).

Kurihara, K. *et al.* "A recursive vesicle-based model protocell with a primitive model cell cycle." *Nat. Commun.* **6**: 8352 (2015).

Kurisu, M. et al. "Reproduction of vesicles coupled with a vesicle surface-confined enzymatic polymerisation.", *Commun. Chem.*, **2**:117 (2019).

Kurisu, M., Kissner, R., Imai, M. & Walde, P. “Application of an enzymatic cascade reaction for the synthesis of the emeraldine salt form of polyaniline.”, *Chem. Pap.,* **75**, 5071–5085 (2021).

Kuruma, Y., Stano, P., Ueda, T. & Luisi, P. L. “A synthetic biology approach to the construction of membrane proteins in semi-synthetic minimal cells.” *Biochim. Biophys. Acta - Biomembr.* **1788**, 567–574 (2009).

Kuzmin, P. I., Zimmerberg, J., Chizmadzhev, Y. A. & Cohen, F. S. “A quantitative model for membrane fusion based on low-energy intermediates.” *Proc. Natl. Acad. Sci. U. S. A.* **98**, 7235–7240 (2001).

Lancet, D., Zidovetzki, R. & Markovitch, O. Systems protobiology: Origin of life in lipid catalytic networks. *J. R. Soc. Interface* **15**: 20180159 (2018).

Landau, L. D., Lifshitz, E. M., Kosevich, A. M., & Pitaevski, L. P. “*Theory of Elasticity”*, 3rd ed. Elsevier, New York (1986).

Lee, N., Bessho, Y., Wei, K., Szostak, J. W. & Suga, H. “Ribozyme-catalyzed tRNA aminoacylation.” *Nat. Struct. Biol.* **7**, 28–33 (2000).

Leskovac, V., Trivić, S., Wohlfahrt, G., Kandrač, J. & Peričin, D. “Glucose oxidase from Aspergillus niger: The mechanism of action with molecular oxygen, quinones, and one-electron acceptors.”, *Int. J. Biochem. Cell Biol.,* **37**, 731–750 (2005).

Leslie E, O. “Prebiotic chemistry and the origin of the RNA world.”, *Critical reviews in biochemistry and molecular biology*, ***39*,** 99-123. (2004).

Letelier, J. C., Cárdenas, M. L. & Cornish-Bowden, A. “From L’Homme Machine to metabolic closure: Steps towards understanding life.”, *J. Theor. Biol.,* **286**, 100–113 (2011).

Lira, R. B., Robinson, T., Dimova, R. & Riske, K. A. “Highly Efficient Protein-free Membrane Fusion: A Giant Vesicle Study.” *Biophys. J.* **116**, 79–91 (2019).

Lincoln, T.A., and Joyce, G.F. “Self-sustained replication of an RNA enzyme.” *Science*, **323**, 1229–1232 (2009).

Lipowsky, R. In "*The Giant Vesicle Book"*, R. Dimova, and C. Marques, Eds., CRC Press, Taylor & Francis: Boca Raton (2020).

Liu, J. M., Sun, L., Hwang, J.-H. & Yang, S. C. "Novel template guided synthesis of polyaniline.", *Mat. Res. Soc. Symp. Proc.*, **247**, 601–606 (1992).

Liu, W., et al. (1999).
(a) "Enzymatically synthesized conducting polyaniline.", *J. Am. Chem. Soc.*, **121**,71–78.
(b) "The role of template in the enzymatic synthesis of conducting polyaniline.", *J. Am. Chem. Soc.,* **121**, 11345–11355.

Liu, Z. *et al.* "In Vitro Reconstitution and Optimization of the Entire Pathway to Convert Glucose into Fatty Acid." *ACS Synth. Biol.* **6**, 701–709 (2017).

Liu, Z. *et al.* "Harnessing chemical energy for the activation and joining of prebiotic building blocks." *Nat. Chem.* **12**, 3–10 (2020).

Luginbühl, S., Bertschi, L., Willeke, M., Schuler, L. D. & Walde, P. "How anionic vesicles steer the oligomerization of enzymatically oxidized p-aminodiphenylamine (PADPA) toward a polyaniline emeraldine salt (PANI-ES)-type product." *Langmuir,* **32**, 9765–9779 (2016).

Luginbühl, S. et al.
(a) "The influence of anionic vesicles on the oligomerization of p-aminodiphenylamine catalyzed by horseradish peroxidase and hydrogen peroxide.", *Synth. Met.*, **226**,89–103 (2017).
(b) "Novel Role of Vesicles as Templates for the Oxidation and Oligomerization of p-Aminodiphenylamine by Cytochrome c.", *Helv. Chim. Acta,* **100**, e1700027 (2017).

Luginbühl, S., Ruiz-Mirazo, K., Ostaszewski, R., Gallou, F. & Walde, P. "Soft and dispersed interface-rich aqueous systems that promote and guide chemical reactions." *Nat. Rev. Chem.,* **2**, 306–327 (2018).

Mally, M., Peterlin, P. & Svetina, S. "Partitioning of oleic acid into phosphatidylcholine membranes is amplified by strain.", *J. Phys. Chem. B,* **117**, 12086–12094 (2013).

Manghi, M. & Destainville, N. "Physics of base-pairing dynamics in DNA.", *Phys. Rep.,* **631**, 1–41 (2016).

Mansy, S. S. “Model protocells from single-chain lipids.”, *Int. J. Mol. Sci.,* **10**, 835–843 (2009).

Marangoni, A.G. “Enzyme kinetics: a modern approach”, John Wiley & Sons, Inc., USA (2003).

Marsh, D. “Lateral pressure profile, spontaneous curvature frustration, and the incorporation and conformation of proteins in membranes.”, *Biophys. J.* **93**, 3884–3899 (2007).

Martin, W., Baross, J., Kelley, D. & Russell, M. J. “Hydrothermal vents and the origin of life.” *Nat. Rev. Microbiol.* **6**, 805–814 (2008).

Matsubara, C., Kawamoto, N. & Takamura, K. “Oxo [5, 10, 15, 20-tetra (4-pyridyl) porphyrinato] titanium(IV): An ultra-high sensitivity spectrophotometric reagent for hydrogen peroxide.”, *Analyst,* **117**, 1781–1784 (1992).

Matsuo, M. *et al.* “DNA Length-dependent Division of a Giant Vesicle-based Model Protocell.” *Sci. Rep.* **9**, 1–11 (2019).

Matsusaki, M., Ajiro, H., Kida, T., Serizawa, T. & Akashi, M. “Layer-by-layer assembly through weak interactions and their biomedical applications.” *Adv. Mater.,* **24**, 454–474 (2012).

Mayor, S., Presley, J. F. & Maxfield, F. R. “Sorting of membrane components from endosomes and subsequent recycling to the cell surface occurs by a bulk flow process.”, *J. Cell Biol.,* **121**, 1257–1269 (1993).

Mccollom, T. M., Ritter, G. & Simoneit, B. R. T. “Lipid synthesis under hydrothermal conditions by Fischer-Tropsch-type reactions.” *Orig. Life Evol. Biosph.* **29**, 153–166 (1999).

Mendel, J.G. "Versuche über Pflanzenhybriden", *Verhandlungen des naturforschenden Vereines in Brünn*, Bd. IV für das Jahr, 1865, Abhandlungen: 3–47 (1866).

Miao, L., Seifert, U., Wortis, M. & Döbereiner, H. G. “Budding transitions of fluid-bilayer vesicles: The effect of area-difference elasticity.”, *Phys. Rev. E*, **49**, 5389–5407 (1994).

Michal, G. “Roche Biochemical Pathways 4th ed.”, Roche Diacnostics (2014).

Millero, F. J., Huang, F. & Laferiere, A. L. “The solubility of oxygen in the major sea salts and their mixtures at 25°C.”, *Geochim. Cosmochim. Acta,* **66**, 2349–2359 (2002).

Mißbach, H. *et al.* “Assessing the diversity of lipids formed via Fischer-Tropsch-type reactions.” *Org. Geochem.* **119**, 110–121 (2018).

Moitzi, C., Freiberger, N. & Glatter, O. “Viscoelastic wormlike micellar solutions made from nonionic surfactants: structural investigations by SANS and DLS.”, *J. Phys. Chem. B*, **109,** 16161–16168 (2005).

Monnard, P. A. & Deamer, D. W. “Membrane self-assembly processes: Steps toward the first cellular life.” *Anat. Rec.* **268**, 196–207 (2002).

Morigaki, K., Walde, P., Misran, M. & Robinson, B. H. “Thermodynamic and kinetic stability. Properties of micelles and v esicles formed by the decanoic acid / decanoate system.”, *Colloids Surfaces A Physicochem. Eng. Asp.,* **213**, 37–44 (2003).

Morigaki, K. & Walde, P. “Fatty acid vesicles.” *Curr. Opin. Colloid Interface Sci.* **12**, 75–80 (2007).

Morini, M. A. *et al.* “Influence of temperature, anions and size distribution on the zeta potential of DMPC, DPPC and DMPE lipid vesicles.” *Colloids Surfaces B Biointerfaces* **131**, 54–58 (2015).

Nabid, M. R. & Entezami, A. A. “Enzymatic synthesis and characterization of a water-soluble, conducting poly(o-toluidine).”, *Eur. Polym. J.,* **39**, 1169–1175 (2003).

Nabid, M. R. & Entezami, A. A. “A novel method for synthesis of water-soluble polypyrrole with horseradish peroxidase enzyme.”, *J. Appl. Polym. Sci.,* **94**, 254–258 (2004).

Nagarajan, R. *et al.* “Manipulating DNA conformation using intertwined conducting polymer chains.” *Macromolecules,* **34**, 3921–3927 (2001).

Nakano, M., Fukuda, M., Kudo, T., Endo, H. & Handa, T. “Determination of interbilayer and transbilayer lipid transfers by time-resolved small-angle neutron scattering.”, *Phys. Rev. Lett.,* **98**, 30–33 (2007).

Nakagawa, K. M. & Noguchi, H. “Nonuniqueness of local stress of three-body potentials in molecular simulations.” *Phys. Rev. E.* **94**, 1–11 (2016).

Namsheer, K. & Rout, C. S. “Conducting polymers : a comprehensive review on recent advances in synthesis, properties and applications.”, *RSC Adv.,* **11,** 5659–5697 (2021).

Nave, S., Eastoe, J. & Penfold, J. “What Is So Special about Aerosol-OT? 1. Aqueous Systems.”, *Langmuir,* **16,** 8733–8740 (2000).

Nekrasov, A.V., Ivanov, V.F., Vannikov, A.V. “Effect of pH on the structure of absorption spectra of highly protonated polyani- line analyzed by the Alentsev－Fock method.”, *Electrochim Acta,* **46**, 4051–4056 (2001).

Neveu, M., Kim, H.-J. & Benner, S. A. The “Strong” RNA World Hypothesis: Fifty Years Old. *Astrobiology* **13**, 391–403 (2013).

Ngola, S. M., Kearney, P. C., Mecozzi, S., Russell, K. & Dougherty, D. A. “A selective receptor for arginine derivatives in aqueous media. Energetic consequences of salt bridges that are highly exposed to water.” *J. Am. Chem. Soc.,* **121**, 1192–1201 (1999).

Noireaux, V., Maeda, Y. T. & Libchaber, A. “Development of an artificial cell, from self-organization to computation and self-reproduction.” *Proc. Natl. Acad. Sci.* **108**, 3473–3480 (2011).

Noller, H. F. “Evolution of protein synthesis from an RNAworld.” *Cold Spring Harb. Perspect. Biol.* **4**, a003681 (2012).

Noyes, R. M., Field, R. J. & Koros, E. “Oscillations in Chemical Systems. I. Detailed Mechanism in a System Showing Temporal Oscillations.”, *J. Am. Chem. Soc.,* **7315**, 1971–1972 (1972).

Pašti, I. *et al.* “Superior capacitive properties of polyaniline produced by a one-pot peroxidase/H2O2-triggered polymerization of aniline in the presence of AOT vesicles.”, *Electrochim. Acta,* **258**, 834–841 (2017).

Pan, A., Rakshit, S., Sahu, S., Bhattacharya, S. C. & Moulik, S. P. “Synergism between anionic double tail and zwitterionic single tail surfactants in the formation of mixed micelles and vesicles,

and use of the micelle templates for the synthesis of nano-structured gold particles.", *Colloids Surfaces A Physicochem. Eng. Asp.,* **481**, 644–654 (2015).

Parker, E. T. *et al.* "Primordial synthesis of amines and amino acids in a 1958 Miller H 2S-rich spark discharge experiment." *Proc. Natl. Acad. Sci. U. S. A.* **108**, 5526–5531 (2011).

Pascal, R. & Chen, I. A. "From soup to peptides." *Nat. Chem.* **11**, 763–764 (2019).

Patel, B. H., Percivalle, C., Ritson, D. J., Duffy, C. D. & Sutherland, J. D. "Common origins of RNA, protein and lipid precursors in a cyanosulfidic protometabolism." *Nat. Chem.* **7**, 301–307 (2015).

Pauling, L. "The Origin of Life on Earth." Oparin, A. I. ed. New York: MacMillan, (1938).

Pasti, I. et al. "Superior capacitive properties of polyaniline produced by a one-pot peroxidase / H2O2 -triggered polymerization of aniline in the presence of AOT vesicles", *Electrochimica Acta*, ***258*,** 834–841, (2017).

Podolsky, K. A. & Devaraj, N. K. "Synthesis of lipid membranes for artificial cells." *Nat. Rev. Chem.* **5**, 676–694 (2021).

Połowiński, S. "Template polymerisation and co-polymerisation.", *Prog. Polym. Sci.,* **27**, 537–577 (2002).

Praprotnik, M., Site, L. D. & Kremer, K. "Multiscale simulation of soft matter: From scale bridging to adaptive resolution." *Annu. Rev. Phys. Chem.,* **59**, 545–571 (2008).

Pressman, A., Blanco, C. & Chen, I. A. "The RNA world as a model system to study the origin of life." *Curr. Biol.* **25**, R953–R963 (2015).

Pressman, A. D. *et al.* "Mapping a Systematic Ribozyme Fitness Landscape Reveals a Frustrated Evolutionary Network for Self-Aminoacylating RNA." *J. Am. Chem. Soc.* **141**, 6213–6223 (2019).

Rajendiran, N. & Swaminathan, M. "Luminescence characteristics of 4,4'-diaminodiphenyl methane in different solvents and at various pH.", *Spectrochim. Acta Part A,* **52**, 1785–1792 (1996).

Rasmussen, S., Constantinescu, A. & Svaneborg, C. “Generating minimal living systems from non-living materials and increasing their evolutionary abilities.” *Philos. Trans. R. Soc. B Biol. Sci.* **371**, (2016).

Reeves, J. P. & Dowben, R. M. “Formation and properties of thin-walled phospholipid vesicles.”, *J. Cell. Physiol.*, **73**, 49–60 (1969).

Rettner, C. T. “Dynamics of the Direct Reaction of Hydrogen Atoms Adsorbed on Cu(111) with Hydrogen Atoms Incident from the Gas Phase”, *Phys. Rev. Lett.,* 69, 383-386 (1992).

Reynafarje, B., Costa, L. E. & Lehninger, A. L. “O2 solubility in aqueous media determined by a kinetic method.”, *Anal. Biochem.,* **145**, 406–418 (1985).

Rodriguez-Garcia, M. *et al.* “Formation of oligopeptides in high yield under simple programmable conditions.” *Nat. Commun.* **6**, (2015).

Rowlett, V. W., & Margolin, W. “The Min system and other nucleoid-independent regulators of Z ring positioning.”, *Frontiers in Microbiology*, **6,** 478 (2015).

Rushdi, A. I. & Simoneit, B. R. T. “Lipid formation by aqueous Fischer-Tropsch-type synthesis over a temperature range of 100 to 400 °C.” *Orig. Life Evol. Biosph.* **31**, 103–118 (2001).

Sakashita, A., Urakami, N., Ziherl, P. & Imai, M. “Three-dimensional analysis of lipid vesicle transformations.”, *Soft Matter,* **8**, 8569–8581 (2012).

Sakuma, Y., Imai, M., Yanagisawa, M. & Komura, S. “Adhesion of binary giant vesicles containing negative spontaneous curvature lipids induced by phase separation.”, *Eur. Phys. J. E,* **25**, 403–413 (2008).

Sakuma, Y., Taniguchi, T. & Imai, M. “Pore formation in a binary giant vesicle induced by cone-shaped lipids.” *Biophys. J.,* **99**, 472–479 (2010).

Sakuma, Y. & Imai, M. “Model system of self-reproducing vesicles.” *Phys. Rev. Lett.,* **107**, 1–5 (2011).

Sakurada, J., Sekiguchi, R., Sato, K. & Hosoya, T. “Kinetic and Molecular Orbital Studies on the Rate of Oxidation of Monosubstituted Phenols and Anilines by Horseradish Peroxidase Compound II.”, *J. Biol. Phys.,* **29**, 4093–4098 (1990).

Samuelson, L. A., Anagnostopoulos, A., Alva, K. S., Kumar, J. & Tripathy, S. K. “Biologically Derived Conducting and Water Soluble Polyaniline.”, *Macromolecules* **31**, 4376–4378 (1998).

Sapurina, I., Riede, A. & Stejskal, J. “In-situ polymerized polyaniline films - 3. Film formation.”, *Synth. Met.,* **123**, 503–507 (2001).

Schmidli, P. K., Schurtenberger, P. & Luisi, P. L. “Liposome-Mediated Enzymatic.” **113**, 8127–8130 (1991).

Schneider, H. J., Schiestel, T. & Zimmermann, P. “The Incremental Approach to Noncovalent Interactions: Coulomb and van der Waals Effects in Organic Ion Pairs.”, *J. Am. Chem. Soc.,* **114**, 7698–7703 (1992).

Schneider, T. D. “A brief review of molecular information theory.”, *Nano Commun. Netw.* **1**, 173–180 (2010).

Schrödinger, E. “What Is Life? The Physical Aspect of the Living Cell.”, Cambridge University Press, UK, (1944).

Schwille, P. *et al.* “MaxSynBio: Avenues Towards Creating Cells from the Bottom Up.” *Angew. Chemie - Int. Ed.* **57**, 13382–13392 (2018).

Scott, A. *et al.* “Cell-free phospholipid biosynthesis by gene-encoded enzymes reconstituted in liposomes.” *PLoS One* **11**, 1–23 (2016).

Segré, D., Ben-Eli, D., Deamer, D. W. & Lancet, D. *Orig. Life Evol. Biosph.*, 2001, **31,** 119-145.

Seifert, U., Berndl, K. & Lipowsky, R. “Shape transformations of vesicles: Phase diagram for spontaneouscurvature and bilayer-coupling models.”, *Phys. Rev. A,* **44**, 1182–1202 (1991).

Seifert, U., Miao, L., Döbereiner, H.-G. & Wortis, M. “Budding Transition for Bilayer Fluid Vesicles with Area-Difference Elasticity.”, *Springer Proc. Phys.,* **66**, 93–96 (1992).

Seifert, U. “Configurations of fluid membranes and vesicles.”, *Adv. Phys.*, **46**, 13–137 (1997).

Serizawa, T., Hamada, K. & Akashi, M. “Polymerization within a molecular-scale stereoregular template.” *Nature,* **429**, 52–55 (2004).

Shillcock, J. C. & Lipowsky, R. “Tension-induced fusion of bilayer membranes and vesicles.” *Nat. Mater.* **4**, 225–228 (2005).

Shimizu, Y. *et al.* “Supplemental Material for ‘Cell-free translation reconstituted with purified components.” *Nat. Biotechnol.* **19**, 751–755 (2001).

Siegel, D. P. & Kozlov, M. M. “The Gaussian curvature elastic modulus of N-monomethylated dioleoylphosphatidylethanolamine: Relevance to membrane fusion and lipid phase behavior.”, *Biophys. J.,* **87**, 366–374 (2004).

Smith, R. & Tanford, C. “Hydrophobicity of Long Chain n-Alkyl Carboxylic Acids, as Measured by Their Distribution Between Heptane and Aqueous Solutions.” *Proc. Natl. Acad. Sci.* **70**, 289–293 (1973).

Socrates, G. “Infrared and Raman Characteristic Group Frequencies”, John Wiley & Sons, New York, p. 220 (2001).

Stampfl, C., & Scheffler, M. “Anomalous Behavior of Ru for Catalytic Oxidation: A Theoretical Study of the Catalytic Reaction CO + 1/2 O2 → CO2.”, *Phys. Rev. Lett.,* **78**, 1500-1503 (1997).

Stano, P. & Luisi, P. L. “Achievements and open questions in the self-reproduction of vesicles and synthetic minimal cells.” *Chem. Commun.* **46**, 3639–3653 (2010).

Stano, P., Carrara, P., Kuruma, Y., Pereira De Souza, T. & Luisi, P. L. “Compartmentalized reactions as a case of soft-matter biotechnology: Synthesis of proteins and nucleic acids inside lipid vesicles.” *J. Mater. Chem.* **21**, 18887–18902 (2011).

Stelzl, U. *et al.* “A human protein-protein interaction network: A resource for annotating the proteome.”, *Cell,* **122**, 957–968 (2005).

Steinkühler, J. *et al.* “Controlled division of cell-sized vesicles by low densities of membrane-bound proteins.” *Nat. Commun.,* **11**: 905 (2020).

Stella, S., Cascio, D. & Johnson, R. C. “The shape of the DNA minor groove directs binding by the DNA-bending protein Fis.”, *Genes Dev.* **24**, 814–826 (2010).

Sun, L., Liu, H., Clark, R. & Yang, S. “Double-strand polyaniline.” *Synth. Met.,* **84**, 67–68 (1997).

Sun, L., Cui, Z., Gottlieb, R. L. & Zhang, B. “A selected ribozyme catalyzing diverse dipeptide synthesis.” *Chem. Biol.* **9**, 619–628 (2002).

Sunami, T. *et al.* “Detection of association and fusion of giant vesicles using a fluorescence-activated cell sorter.” *Langmuir* **26**, 15098–15103 (2010).

Suzuki, K., Aboshi, R., Kurihara, K. & Sugawara, T. “Adhesion and fusion of two kinds of phospholipid hybrid vesicles controlled by surface charges of vesicular membranes.” *Chem. Lett.* **41**, 789–791 (2012).

Swoboda, B.E.P. & Massey, V. “Purification and properties of the glucose oxidase from Aspergillus niger.”, *J. Biol. Chem.*, **240**, 2209–2215 (1965).

Szostak, J. W., Bartel, D. P. & Luisi, P. L. “Synthesizing life.” *Nature,* **409**, 387–390 (2001).

Takamura, K. & Matsubara, C. “Versatility of the Titanium(IV)–Porphyrin Reagent for Determining Hydrogen Peroxide.”, *Bull. Chem. Soc. Jpn.,* **76**, 1873–1888 (2003).

Takamura, K. & Matsumoto, T. “Ultraviolet–Visible Spectral Analysis for the Reaction of Hydrogen Peroxide with a Titanium(IV)-Porphyrin Reagent”, *Appl. Spectrosc.*, **63**, 579–584 (2009).

Takakura, K., Toyota, T. & Sugawara, T. “A novel system of self-reproducing giant vesicles.” *J. Am. Chem. Soc.* **125**, 8134–8140 (2003).

Takakura, K., & Sugawara, T. “Membrane dynamics of a myelin-like giant multilamellar vesicle applicable to a self-reproducing system.” *Langmuir*, **20**, 3832–3834, (2004).

Tanaka, H. (田中博) “生命と複雑系”, 培風館, (2002). (*Japanese edition only*)

Tanaka, T., Sano, R., Yamagami, A. & Yamazaki, M. “Membrane fusion of giant liposomes of neutral phospholipid membranes induced by La3+ and Gd3+.” *AIP Conf. Proc.* **708**, 316–317 (2004).

Tamm, L. K., Crane, J. & Kiessling, V. Membrane fusion: A structural perspective on the interplay of lipids and proteins. *Curr. Opin. Struct. Biol.* **13**, 453–466 (2003).

Tatulian, S. A. “Effect of lipid phase transition on the binding of anions to dimyristoylphosphatidylcholine liposomes.” *BBA - Biomembr.* **736**, 189–195 (1983).

Tian, A. & Baumgart, T. “Sorting of lipids and proteins in membrane curvature gradients.”, *Biophys. J.,* **96**, 2676–2688 (2009).

Toyobo Enzymes, Product Information, “PEO-131・301・302 PEROXIDASE from Horseradish” https://www.toyobo-global.com/seihin/xr/enzyme/pdf_files/201707/PEO_131_301_302.pdf

Toyota, T., Takakura, K., Kageyama, Y., Kurihara, K., Maru, N., Ohnuma, K., Kaneko, K., Sugawara, T. “Population study of sizes and components of self-reproducing giant multilamellar vesicles.” *Langmuir*, 24: 3037–3044 (2008).

Traïkia, M., Warschawski, D. E., Recouvreur, M., Cartaud, J. & Devaux, P. F. “Formation of unilamellar vesicles by repetitive freeze-thaw cycles: Characterization by electron microscopy and 31P-nuclear magnetic resonance.”, *Eur. Biophys. J.,* **29**, 184–195 (2000).

Tominaga, K. (富永慶伊) “反応速度論” 3rd ed., 東京化学同人, 2001.

Toyabe, S. & Braun, D. “Cooperative Ligation Breaks Sequence Symmetry and Stabilizes Early Molecular Replication.” *Phys. Rev. X,* **9**, 11056 (2019).

Tsai, M. Y., Zhang, B., Zheng, W. & Wolynes, P. G. “Molecular Mechanism of Facilitated Dissociation of Fis Protein from DNA.”, *J. Am. Chem. Soc.* **138**, 13497–13500 (2016).

Urakami, N., Jimbo, T., Sakuma, Y. & Imai, M. “Molecular mechanism of vesicle division induced by coupling between lipid geometry and membrane curvatures.”, *Soft Matter,* **14**, 3018–

3027 (2018).

Urakami, N., Sakuma, Y., Chiba, T. & Imai, M. “Vesicle deformation and division induced by flip-flops of lipid molecules.” *Soft Matter,* **17**, 8434-8445 (2021).

Vance, J. A. & Devaraj, N. K. “Membrane Mimetic Chemistry in Artificial Cells.” *J. Am. Chem. Soc.* **143**, 8223–8231 (2021).

Vasas, V., Fernando, C., Santos, M., Kauffman, S. & Szathmáry, E. “Evolution before genes.”, *Biol. Direct,* **7**, 1–14 (2012).

van der Gulik, P., Massar, S., Gilis, D., Buhrman, H. & Rooman, M. “The first peptides: The evolutionary transition between prebiotic amino acids and early proteins.” *J. Theor. Biol.* **261**, 531–539 (2009).

Venter J. C. et al. “The sequence of the human genome”, *Science*, **291**, 1304-1351 (2001).

Von Neumann, J., In *The Hixon Symposium*, Jeffress, L.A. Ed., Wiley, New York (1951).

Walde, P., Wick, R., Fresta, M., Mangone, A., & Luisi, P. L. “Autopoietic Self-Reproduction of Fatty Acid Vesicles.”, *Journal of the American Chemical Society*, **116**, 11649–11654 (1994).

Walde, P. “Surfactant assemblies and their various possible roles for the origin(s) of life.” *Origins of Life and Evolution of the Biosphere* **36**, 109 – 150 (2006).

Walde, P., Umakoshi, H., Stano, P. & Mavelli, F. “Emergent properties arising from the assembly of amphiphiles. Artificial vesicle membranes as reaction promoters and regulators.” *Chem. Commun.* **50**, 10177–10197 (2014).

Wallace, G.G., Spinks, G.M., Kane-Maguire, L.A.P., Tesdale, P.R. “Conductive electroactive polymers, Intelligent polymer systems”, 3rd edn. CRC Press, Boca Raton, pp 179–196, (2009).

Wang, P., Meyer, T. A., Pan, V., Dutta, P. K. & Ke, Y. “The Beauty and Utility of DNA Origami.”, *Chem,* **2**, 359–382 (2017).

Wang, Z. G., Zhan, P. & Ding, B. “Self-assembled catalytic DNA nanostructures for synthesis of

para-directed polyaniline." *ACS Nano,* **7**, 1591–1598 (2013).

Waugh, R. E., Song, J., Svetina, S. & Zeks, B. "Local and nonlocal curvature elasticity in bilayer membranes by tether formation from lecithin vesicles.", *Biophys. J.,* **61**, 974–982 (1992).

Wächtershäuser, G. "Before Enzymes and Templates: Theory of Surface Metabolism." **52**, 452–484 (1988).

Weibel, M. K. & Bright, H. J. "The glucose oxidase mechanism. Interpretation of the pH dependence.", *J. Biol. Chem.,* **246**, 2734–2744 (1971).

Weiss, D. S. "Bacterial cell division and the septal ring.", *Mol. Microbiol.* **54**, 588–597 (2004).

Wick, R., Walde, P. & Luisi, P. L. "Light Microscopic Investigations of the Autocatalytic Self-Reproduction of Giant Vesicles." *J. Am. Chem. Soc.* **117**, 1435–1436 (1995).

Wiese, W., Harbich, W. & Helfrich, W. "Budding of lipid bilayer vesicles and flat membranes.", *J. Phys. Condens. Matter,* **4**, 1647–1657 (1992).

World Book Encyclopedia., "Life.", Chicago: World Book, 1983.

Wu, Q., Xue, Z., Qi, Z. & Wang, F. "Synthesis and characterization of PAn/clay nanocomposite with extended chain conformation of polyaniline.", *Polymer.,* **41**, 2029–2032 (2000).

Xavier, J. C., Hordijk, W., Kauffman, S., Steel, M., & Martin, W. F. "Autocatalytic chemical networks at the origin of metabolism.", *Proc. R. Soc. B,* **287**: 20192377 (2020).

Xu, P. *et al.* "Genome-wide essential gene identification in Streptococcus sanguinis." *Sci. Rep.,* **1**, 1–9 (2011).

Yu, X., Liu, T., Zhu, F. & Khosla, C. "In vitro reconstitution and steady-state analysis of the fatty acid synthase from Escherichia coli." *Proc. Natl. Acad. Sci. U. S. A.* **108**, 18643–18648 (2011).

Zhu, T. F., & Szostak, J. W. "Coupled growth and division of model protocell membranes.", *Journal of the American Chemical Society*, **131**, 5705–5713 (2009).

Zubay, G. “Origins of Life on the Earth and in the Cosmos”, Academic Press, San Diego (2000).

Zuckerman, D. M. “Statistical physics of biomolecules: an introduction.”, CRC press (2010).

List of Publications and Awards

Publications

1. **Minoru Kurisu**, Harutaka Aoki, Takehiro Jimbo, Yuka Sakuma, Masayuki Imai, Sandra Serrano-Luginbühl, and Peter Walde, “Reproduction of vesicles coupled with a vesicle surface-confined enzymatic polymerisation.” *Communications Chemistry,* **2**:117 (2019).

DOI: 10.1038/s42004-019-0218-0. **(*original paper*)**

2. **Minoru Kurisu**, Reinhard Kissner, Masayuki Imai, and Peter Walde, "Application of an enzymatic cascade reaction for the synthesis of the emeraldine salt form of polyaniline." *Chemical Papers,* 75: 5071-5085 (2021). DOI: 10.1007/s11696-021-01620-z. **(*original paper*)**
3. **Minoru Kurisu**, Peter Walde, and Masayuki Imai, "情報高分子の連携によるベシクルの成長と分裂. (Growth and Division of Vesicles Coupled with Information Molecules.)" *「生物物理」誌* (*SEIBUTSU BUTSURI*), **61** (6), 001-004 (2021). DOI: 10.2142/biophys.61.001. (***review article in Japanese***)
4. **Minoru Kurisu**, Ryosuke Katayama, Yuka Sakuma, Masayuki Imai, and Peter Walde, *manuscript in preparation*, (***original paper***)

Oral Presentations

1. **栗栖実**, 青木春隆, 佐久間由香, 今井正幸, Sandra Luginbühl, Peter Walde：「ベシクルと情報高分子の連携による自己複製システム」*日本物理学会２０１８年春季大会*、2018.3.23（千葉）.
2. **Minoru Kurisu**, "Sustainable reproduction of vesicles coupled with surface confined template polymerization" *From Soft Matter to Protocell 2020*, 2020.10.29 (Online).
3. **Minoru Kurisu**, "Sustainable reproduction of vesicles coupled with surface confined template polymerization" *The 4th Symposium for The Core Research Cluster for Materials Science and the 3rd Symposium on International Joint Graduate Program in Materials Science*, 2020.11.16 (Online).
4. **Minoru Kurisu**, Ryosuke Katayama, Yuka Sakuma, Peter Walde, Masayuki Imai, "Reproduction cycles of vesicle coupled with template polymerization: toward autonomous synthetic protocell." *The 59th Annual Meeting of the Biophysical Society of Japan*, 2021.11.26 (Online).

Poster Presentations

1. **栗栖実**, 青木春隆, 佐久間由香, 今井正幸, Peter Walde, "鋳型重合と連携したベシクルの成長", *日本物理学会２０１７年秋季大会*, 2017.9.24（岩手）.
2. **栗栖実**, 青木春隆, 佐久間由香, 今井正幸, Sandra Luginbühl, Peter Walde, "鋳型重合と連携したベシクルの成長・分裂", *第７回ソフトマター研究会*, 2017.9.25（京都）.
3. **Minoru Kurisu**, Harutaka Aoki, Yuka Sakuma, Masayuki Imai, Peter Walde, "Growth of

Vesicle Coupled with Template Polymerization.", *International Symposium on Fluctuation and Structure out of Equilibrium 2017*, 2017.11.20 (Sendai, Japan).

4. **栗栖実**, 青木春隆, 佐久間由香, 今井正幸, Sandra Luginbühl, Peter Walde, "鋳型重合と連携した脂質膜の自己生産～分子集合系からプロトセルへ～", *東北大学学際高等研究教育院・第 4 回全領域合同研究交流会*, 2019.1.11（仙台）.
5. **栗栖実**, 青木春隆, 神保岳大, 佐久間由香, 今井正幸, Sandra Luginbühl, Peter Walde, "Reproduction of Vesicles coupled with Template Polymerization.", *第 57 回生物物理学会年会*, 2019.9.24（宮崎）.
6. **栗栖実**, 青木春隆, 神保岳大, 佐久間由香, 今井正幸, Sandra Luginbühl, Peter Walde,"膜面上での高分子合成と連携したベシクルの自己生産",*「細胞を創る」研究会 12.0*, 2019.10.17（愛媛）.
7. **Minoru Kurisu**, Peter Walde, Masayuki Imai, "Reproduction of Microscale Membrane-Bounded Compartments coupled with Synthesis of Conductive Polymer.", *The 3rd Symposium for The Core Research Clusters for Materials Science and Spintronics*, 2020.2.10 (Sendai, Japan).
8. **Minoru Kurisu**, Harutaka Aoki, Takehiro Jimno, Yuka Sakuma, Sandra Luginbühl, Peter Walde, Masayuki Imai, "Reproduction of Vesicles coupled with a Membrane Surface-Confined Template Polymerization.", *Molecular Origins of Life 2020*, 2020.7.8 (Online).
9. **栗栖実**, 青木春隆, 神保岳大, 佐久間由香, 今井正幸, Sandra Luginbühl, Peter Walde, "Sustainable Reproduction of Vesicles coupled with a Surface- Confined Template Polymerization.", *第 58 回生物物理学会年会*, 2020.9.16（online）.
10. **栗栖実**, Peter Walde, 今井 正幸, "膜成長と高分子合成が相互触媒的に連携した持続的自己生産系の構築", *「細胞を創る」研究会 13.0*, 2020.11.12（online）.
11. **Minoru Kurisu**, Ryosuke Katayama, Yuya Takashima, Peter Walde, Masayuki Imai, "Giant Vesicle of AOT: New Material for Soft Microscale Compartment and its Dynamic Property", *The 4th Symposium for The Core Research Cluster for Materials Science and the 3rd Symposium on International Joint Graduate Program in Materials Science*, 2020.11.16 (Online).
12. **Minoru Kurisu,** Ryosuke Katayama, Yuka Sakuma, Peter Walde, Masayuki Imai, "Recursive vesicle reproduction system coupled with template polymerization of aniline: toward synthetic minimal cell.", *Cell Synth 14.0 meeting,* 2021.11.4 (Online).

Awards and Grants

1. Division for Interdisciplinary Advanced Research and Education (DIARE), *Tohoku University*, 2018.4.1 – 2019.3.31.

2. International Joint Graduate Program in Materials Science (GP-MS), *Tohoku University*, 2019.4.1 – 2022.3.31.
3. **Best Poster Award**, *The 3rd Symposium for The Core Research Clusters for Materials Science and Spintronics*, 2020.2.10 (Sendai).
4. **Student Presentation Award**, *The 58th Annual Meeting of Biophysical Society of Japan,* 2020.9.16 (Online).
5. **Poster Award**, *The 4th Symposium for The Core Research Cluster for Materials Science and the 3rd Symposium on International Joint Graduate Program in Materials Science*, 2020.11.16 (Online).
6. Research Fellowship for Young Scientists (DC2), *Japan Society for the Promotion of Science,* 2021.4.1 – 2022.3.31.
7. **Student Presentation Award**, *The 59th Annual Meeting of Biophysical Society of Japan,* 2021.11.26 (Online).

Other Activities

1. Visiting Student, ETH Zürich, Switzerland, 2018.10 – 2018. 12.
2. Academic Guest, ETH Zürich, Switzerland, 2019.7 – 2019. 9.
3. Member of organizing committee, *International workshop "From Soft Matter to Protocell 2020"*, 2020.10.29 (Online).
4. 分野別専門委員（E-02: 非平衡・自己組織化分野）, *日本生物物理学会*, 2021.1.1 – 2021.12.31.
5. 分野別専門委員（E-02: 非平衡・自己組織化分野）, *日本生物物理学会*, 2022.1.1 – 2022.12.31.

Acknowledgements

First of all, I am deeply grateful to my supervisor Prof. Masayuki Imai. I joined his group five years ago, and I still remember well that I started my work described in this thesis from considering how to prepare large and nice AOT vesicles. Nobody has known such a fundamental thing in this thesis before us! I experienced many twists and turns, but many discussions with him allowed me to cut my way through a jungle to the magnificent

scenery.

I am greatly indebted to Prof. Peter Walde for instructing me in chemical techniques. My research is highly interdisciplinary work, however, I was educated in physics and a complete laymen in chemistry when I started my research. He is gentle in communication and strict in science. His lectures and discussions with him always gave me deep insights. I would like to thank him also for my many visits and twice two-month stays in his laboratory (Oct – Dec in 2019 and Jul – Sep in 2020). ***Danke Vielmals!***

I appreciate the supports and the encouragement from past and present member of our laboratory. Mr. Harutaka Aoki supported the initial stage of my experimental trials. Mr. Ryosuke Katayama supported the late stage of my experiments and gave me insights into the theoretical points. Dr. Takehiro Jimbo helped me with the theoretical analysis on deformation of vesicles. Thanks to Dr. Yuka Sakuma, I could learn the fundamental techniques on vesicles. Ms. Akiko Baba took care of our experimental environments, and especially I would like to thank her for refilling our pipette tips. As a senior PhD student in our lab, Dr. Akihiro Morohashi always gave me critical comments on my work and guided me in many stages of graduate school. I sometimes felt depression, anxiety, irritation, and loneliness during my research life, but each time I was helped by many friends. I am thankful to Dr. Atsuji Kodama, Mr. Kazuki Yokoyama, Mr. Ryuta Ebihara, Mr. Kei Murakami, Mr. Noboru Nagata, Mr. Seiji Hatano, Mr. Yoshiaki Miyahira, Mr. Keidai Sato, Mr. Masayuki Toyoda, Mr. Toshikaze Chiba, and Mr. Yuto Hachiya.

最後に、博士課程在学中に遠くからいつも励まし、期待し、心配し、頻繁に電話してくれ支えてくれた出雲の両親に感謝します。*(Lastly, I would like to thank my parents. They always encouraged me, expected me, worried about me, supported me, and frequently called me during my PhD studies from Izumo, far away from Sendai.)*

December 6th, 2021
Minoru KURISU
栗栖　実